Final Report

ARB Contract #08-322

Integrated Physical and Chemical Measurements of Heavy-duty Diesel Emissions in the WVU Full-Scale Wind Tunnel

Prepared for:

Seungju Yoon

California Air Resources Board

1001 I Street

Sacramento, CA 95812

March
2013

Submitted by:

Anthony S. Wexler (PI), University of California – Davis

K. Max Zhang (co-PI), Jonathan Steffens, and Yan Wang, Cornell University

Daniele Littera, Dan Carder and Mridul Gautam, West Virginia University

Anthony Strawa (co-PI), NASA Ames Research Center

Disclaimer

The statements and conclusions in this report are those of the contractor and not necessarily those of California Air Resources Board. The mention of commercial products, their source, or their use in connection with material reported herein is not to be construed as actual or implied endorsement of such products.

Acknowledgement

We would like to thank Drs. Seungju Yoon, John Collins, Harry Dwyer, Shaohua Hu and Tao Huai at California Air Resources Board for their consistent guidance on this project. We would also like to thank Drs. Jorn Herner and Alberto Ayala for their valuable advices to this project.

Contents

Disclaimer ……..……..……..……..2
Acknowledgement ……..……..……..……..2
Contents ……..…….. ……...……..……..3
List of Figures ……..……...……..……..……..5
List of Tables ……..……..……..……..7
Executive Summary ……..……..,,……..……..8
1. Introduction ……..……..……..……..……..9
2. Wind Tunnel Facility ……..……..……..……..10
2.1 Background ……..……..……..……...10
2.2 Comparison between the NFAC and WVU wind tunnel designs ……...11
2.3 Wind tunnel operations ……...……...……...……..13
3. Measurements ……...……...……...……...……...……..14
3.1 Test matrix and engine specifications …...……...……...……...14
3.2 Overall sampling design …...……...……...……....16
3.3 Wind tunnel measurements …...……...……...……16
3.3.1 Instruments …...……...……...……....16
3.3.2 Plume mapping protocol …...……...……...……...18
3.3.3 Examples of wind tunnel measurement results ……...19
3.4 Dilution tunnel measurements ……...……...21
3.4.1 Two-stage dilution system ……...21
3.4.2 Instruments ……...21
3.5 QA/QC ……...…….....22
4. Wind tunnel modeling ……...…….....25
4.1 Computational mesh and geometry …….....25
4.2 Velocity field……...……...26
4.3 CO_2 ……...……...……28
4.4 Aerosol dynamics …….....28
5. Results and Discussions ……..29
5.1 Dilution ratios and dilution-corrected NOx and BC concentrations ……29
5.2 Evolution of particle size distributions ……..32
5.2.1 Pre2007 Idle ……...…….....32
5.2.2 Pre2007 20MPH ……...…….....34
5.2.3 Pre2007 35MPH ……...…….....36
5.2.4 Post2007 Idle ……...……..38
5.2.5 Post2007 20MPH ……...…….....39
5.2.6 Post2007 35MPH ……...…….....40
5.2.7 Post2010 Idle ……...……...41
5.2.8 Post2010 20MPH ……....…….....41

5.2.9 Post2010 35MPH ……...…….....42
6. Summary and Conclusions ……...…….....43
7. Recommendations ……...…….....44
8. References ……...…….....45
Appendix ……...……...……..46

List of Figures

Figure 1-1: Dilution-corrected number size distributions measured during two diesel intercomparison experiments between a T-mixing dilutor (the dash line) and a coaxial mixing dilutor (the solid line) (Lipsky and Robinson, 2005). Note that linear scale is used for particle concentrations.

Figure 1-2: Comparison of dilution-corrected size distributions measured at on-road conditions and in the laboratory with three different primary dilution ratios (Ronkko et al., 2006)

Figure 2-1: Wind Tunnel in "Pulling" configuration: (a) Side View; (b) Inlet View

Figure 2-2: Wind Tunnel, Chassis Dynamometer and TREL setup

Figure 3-1: Sketch of the overall sampling design

Figure 3-2: Initial identification of the plume sampling points. The vertical lines indicate different sampling planes.

Figure 3-3: Illustrations of sampling point locations on Plane 1 and 7.

Figure 3-4: Pre2007 vehicle, 20mph Test, Plane 1

Figure 3-5: Pre2007 vehicle, 20mph Test, Plane 4

Figure 3-6: WVU Transportable Raw Emissions Laboratory (TREL)

Figure 4-1: Geometries in Solidworks (a): Cabin and wind tunnel; (b) Cabin

Figure 4-2: Mesh of cabin in ANSYS Workbench

Figure 4-3: Velocity (m s^{-1}) contours near cabin (left) and magnified at the stack exit (right)

Figure 4-4: Comparison of predicted and measured centerline velocity for Pre2007 20 MPH case. Both RANS and LES models are employed to solve the turbulence flow fields.

Figure 4-5: Comparisons between predicted and measured centerline CO_2 profiles for (a) Pre2007 Truck, (b) Post2007 Truck and (c) Post2010 Truck.

Figure 5-1: Dilution-corrected (a) NOx and (b) BC concentrations for Pre2007 cases

Figure 5-2: Dilution-corrected NOx and BC concentrations for Post2007 cases

Figure 5-3: Dilution-corrected NOx and BC concentrations for Post2010 cases

Figure 5-4: The CO_2 and non-dilution-corrected NOx concentrations for (a) Post2007 Idle and (b) Post2010 Idle

Figure 5-5: Dilution-corrected particle size distributions for Pre2007 Idle case; (a): linear scale; (b): logarithm scale

Figure 5-6: Dilution-corrected particle size distributions for Pre2007 20 MPH case; (a): linear scale; (b): logarithm scale

Figure 5-7: Dilution-corrected particle size distributions for Pre2007 20 MPH case at sampling points surrounding the center point

Figure 5-8: Dilution-corrected particle size distributions for Pre2007 35 MPH case; (a): linear scale; (b): logarithm scale

Figure 5-9: Size distributions at different planes for Pre2007 35 MPH case

Figure 5-10: Dilution-corrected particle size distributions for Post2007 Idle case; (a): linear scale; (b): logarithm scale

Figure 5-11: Dilution-corrected particle size distributions for Post2007 20 MPH case; (a): linear scale; (b): logarithm scale

Figure 5-12: Dilution-corrected particle size distributions for Post2007 35 MPH case; (a): linear scale; (b): logarithm scale

Figure 5-13: Particle size distributions for Post2010 Idle case

Figure 5-14: Dilution-corrected particle size distributions for Post2010 20 MPH case; (a): linear scale; (b): logarithm scale

Figure 5-15: Particle size distributions for Post2010 35 MPH case

List of Tables

Table 1: Wind Tunnel Parameters

Table 3-1. Descriptions of different wind speed and road load conditions and different aftertreatment technologies

Table 3-2: Vehicle and engine specifications

Table 4-1: Descriptions of modeling tools

Executive Summary

Understanding the health and climatic impacts of mobile sources and developing corresponding control technologies require the laboratory measurements of vehicle emissions to represent their real world conditions. However, there exists a disconnect between the particulate emissions measured on road and in the laboratory. This discrepancy is particularly pronounced for ultrafine particles (<100 nm). Further, the introduction of a Diesel Particulate Filter (DPF) as a retrofit technology in the state of California complicates the formation of ultrafine particles since it removes nearly all solid soot particles in the accumulation mode (0.3 to 1 μm, diameter).

In this report, we describe our measurement and analysis in characterizing the evolution of diesel plumes in a full-scale wind tunnel. This wind tunnel emission test marries the advantages of both the laboratory (repeatable driving cycles and well-characterized diluent properties) and on-road (natural dilution) emission tests, while avoiding the main shortcomings in either method. We tested nine configurations, combining three heavy-duty diesel engines, i.e., Pre-2007, 2007-compliant (Post2007) and 2010-compliant (Post2010) and three operating conditions, i.e., idle, 20 mile per hour and 35 mile per hour conditions. In each case, the plume was mapped and characterized by 130 sampling points in 10 planes at various downwind distances.

We have the following preliminary findings:

- Particle concentrations in the plumes of Post2010 truck are comparable to the ambient background levels, given the uncertainties in the aerosol instrumentation.
- No distinguishable nucleation modes were observed for Post2010 trucks, likely due to storage of sulfur in the DPF during the testing.
- A DPF regeneration event was observed during the test of Post2007 truck, leading to highly elevated nucleation-mode and accumulation-mode particle concentration.
- The sulfuric acid-induced nucleation mode particles from Pre2007 truck experienced formation, growth and shrinking processes as plumes disperse in the wind tunnel.

However, there are several observed phenomena that are currently unexplainable:

- Most notably, we observed unusually volatile behaviors for accumulation mode particles, which were supposed to remain unchanged after dilution correction given their large mass and the short residence time in the wind tunnel. Those volatile behaviors pose a major challenge in analyzing nucleation-mode particles.
- Similarly, dilution-corrected NOx and Black Carbon concentrations, which were supposed to remain unchanged, fluctuate significantly for a majority of test cases.

The large amounts of data generated from this study provide valuable information on the evolution of particle size distributions, which cannot be easily observed in laboratory dilution tunnel testing. Thus we have the following recommendations.

- Further analysis and modeling of the datasets are needed to verify whether the unexplainable behaviors are due to instrumentation errors/limitations, weakness in sampling designs, or are true physical phenomena. Due to the time constrain, the datasets have not been fully investigated. The additional efforts will help reveal the nature of diesel particulate matter in the atmosphere.
- A review of lessons learned from the wind tunnel experiment is needed after the further

analysis and modeling described above. Even though the wind tunnel measurement holds great promise in advancing our understanding of diesel particle matter, this study also suggest a need to improve the sampling plan and instruments employed in the measurement to make sure the wind tunnel measurement will deliver the promise.

1. Introduction

Dilution tunnel-based sampling systems play a critical role in regulatory and certification processes. Over the years, researchers have identified several limitations in the current laboratory dilution systems for representing atmospheric conditions and those limitations are pronounced for measuring the semi-volatile composition and the ultrafine range (<100 nm) of the particulate emissions (Wang et al., 2013). For example, Lipsky and Robinson (2005) compared the performance of two different types of dilution tunnels, one with coaxial mixing and the other with T-mixing between raw exhaust and dilution air. They observed good agreement between the two dilution systems for $PM_{2.5}$ mass measured with filters. However, the large differences in the total particle number and particle size distributions were observed using a real-time instrument, as shown in Figure 1-1.

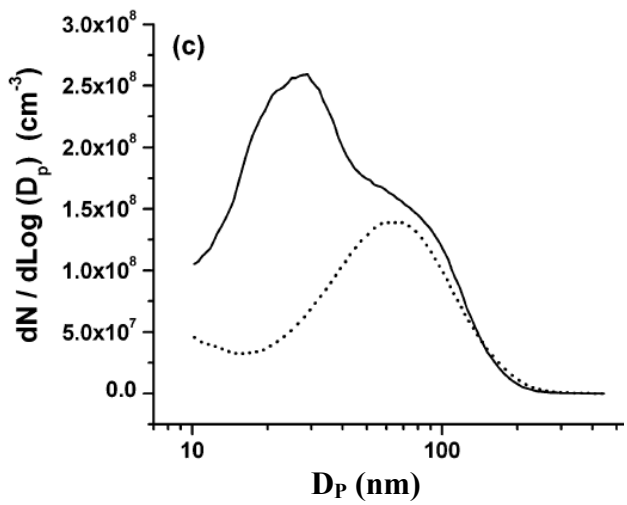

Figure 1-1: Dilution-corrected number size distributions measured during two diesel intercomparison experiments between a T-mixing dilutor (the dash line) and a coaxial mixing dilutor (the solid line) (Lipsky and Robinson, 2005). *Note that linear scale is used for particle concentrations*.

The limitations in laboratory measurements constitute a major uncertainty in predicting future climate change, protecting public health (especially regarding to human exposure to near-source air pollution) and evaluating the benefits of low-carbon fuels. Those limitations also pose a major challenge to policy makers on how to regulate particulate emissions in the future. Therefore, there is an urgent need to improve the laboratory dilution systems given their wide utilization of for emissions testing at present and in the future.

On the other hand, on-road measurements of vehicular emissions using mobile platforms have show promise in quantifying real-world emissions (Park et al., 2011). Ronkko et al. (2006) studied exhaust particle-size distribution of a heavy-duty diesel vehicle in the laboratory and on

road. Laboratory measurements of emissions were performed on a heavy-duty chassis dynamometer, where a porous-tube-type diluter followed by an ageing chamber and an ejector-type diluter was used to dilute the exhaust sample. Illustrated in Figure 1-2, the nucleation mode is found to be sensitive to sampling conditions and thus the laboratory measurements may differ considerably from on-road emissions depending on chosen dilution parameters.

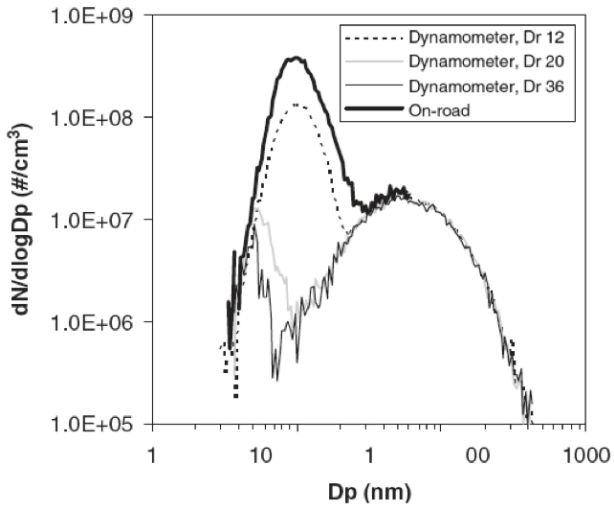

Figure 1-2: Comparison of dilution-corrected size distributions measured at on-road conditions and in the laboratory with three different primary dilution ratios (Ronkko et al., 2006)

Nevertheless, on-road measurements also have limitations such as uncontrollable environmental factors (e.g., wind speed, direction, temperature and relative humidity) and the difficulty in capturing a wide range of vehicle operation conditions. Furthermore, neither on-road nor laboratory measurements can easily executed to reveal the plume evolution process.

This project is designed to bridge the gaps between on-road and laboratory measurements. The wind tunnel emission test marries the advantages of both the laboratory (repeatable driving cycles and well-characterized diluent properties) and on-road (natural dilution) emission tests, while avoiding the main shortcomings in either method. By measuring plume properties at different downwind distances, we are able to characterize the initial plume evolution process that is very challenging to do in the field measurement.

Finally, it is worth pointing out that both Lipsky and Robinson (2005) and Ronkko et al., (2006) indicate that dilution-corrected accumulation mode particles remained unchanged among different conditions, which has a significant implication on the analysis of the wind tunnel data.

2. Wind Tunnel Facility

2.1 Background

We originally proposed to characterize the physical and chemical evolutions of the exhaust plumes in the National Full-Scale Aerodynamics Complex (NFAC) in NASA Ames Research Center. However, NFAC had not been able to confirm the test dates. Without the confirmed test dates, the experiment could be canceled with a last-minute notice from NFAC and Department of

Defense, which manages the NFAC facilities. It was deemed too risky to use the NFAC wind tunnel for this project, and decided in June 2010 to seek alternative facilities to continue the project. Since then, several full-scale wind tunnels across the U.S. were evaluated, but were eventually deemed unsuitable, due either to design/performance characteristics or availability. Two prime criteria were identified: the tunnel needed to be an open-circuit configuration and it must provide for a minimum of 100 feet of sampling zone downstream of the test section, for plume measurement. The length criterion was based upon work conducted by in the NASA Langley Wind Tunnel facility. These results indicated that CO_2 concentration, temperature, and dilution ratio in the plume of a heavy-duty truck emitted in a 55 mph wind speed stabilized at a distance of approximately 40 feet from the vehicle exhaust stack. Neither of the two criteria was met by any of the tunnels that were investigated. The final solution was reached in October that a wind tunnel would be constructed at West Virginia University (WVU) for this project. At the same time, the modeling component was added to the scope of work in order to augment the analysis from the limited experimental data.

2.2 Comparison between the NFAC and WVU wind tunnel designs

There were significant advantages, as listed below, to building the new tunnel and conducting tests at WVU:

a. Full access to the tunnel and the equipment at all hours of the day
b. No restriction on personnel who can work on the facility at WVU due to immigration status.
c. Less stringent requirements on our equipment (size, weight, power requirements, data cables, etc.) than the NFAC facility demanded. In fact, in order to satisfy their requirements we would have had to drop some of the experiments we were planning on conducting because we would be unable to meet their demands or the costs of meeting the requirements were prohibitive.

The NFAC wind tunnel is an open circuit type with a closed, rectangular test section, which is 24 m high and 37 m wide. Test section speed in the tunnel is continuously variable from nearly 0 to 50 m s^{-1} (or about 110 mph). The tunnel would have afforded us a 115ft downwind distance to measure the plume evolution.

The WVU wind tunnel is also an open-circuit type with a closed, rectangular test section, which is 4.9 m (16ft) high and 4.9 m (16ft) wide and will house the cab (and the wind cowl) of a heavy-duty truck. This tunnel employs a 1,170 HP suction fan to provide up to 15.75 m s^{-1} (or 35 mph) flow rate. The WVU design is a "pulling" tunnel, where the truck is located upstream near the inlet, and the air is pulled inward into the test section and then pulled out through a suction fan at the far end of the tunnel (illustrated in Figures 2-1). A small convergent section, as well as a flow straightener, is positioned upstream of the test cell in order to stabilize the flow field. The flow straightener removes any swirl and axial fluctuations. A convergent lofted surface connects the test cell to the fan section. The geometry and operating parameters are described in Table 2-1. The detailed description on the wind tunnel design, structural analysis, and construction can be found in the Appendix.

(a)

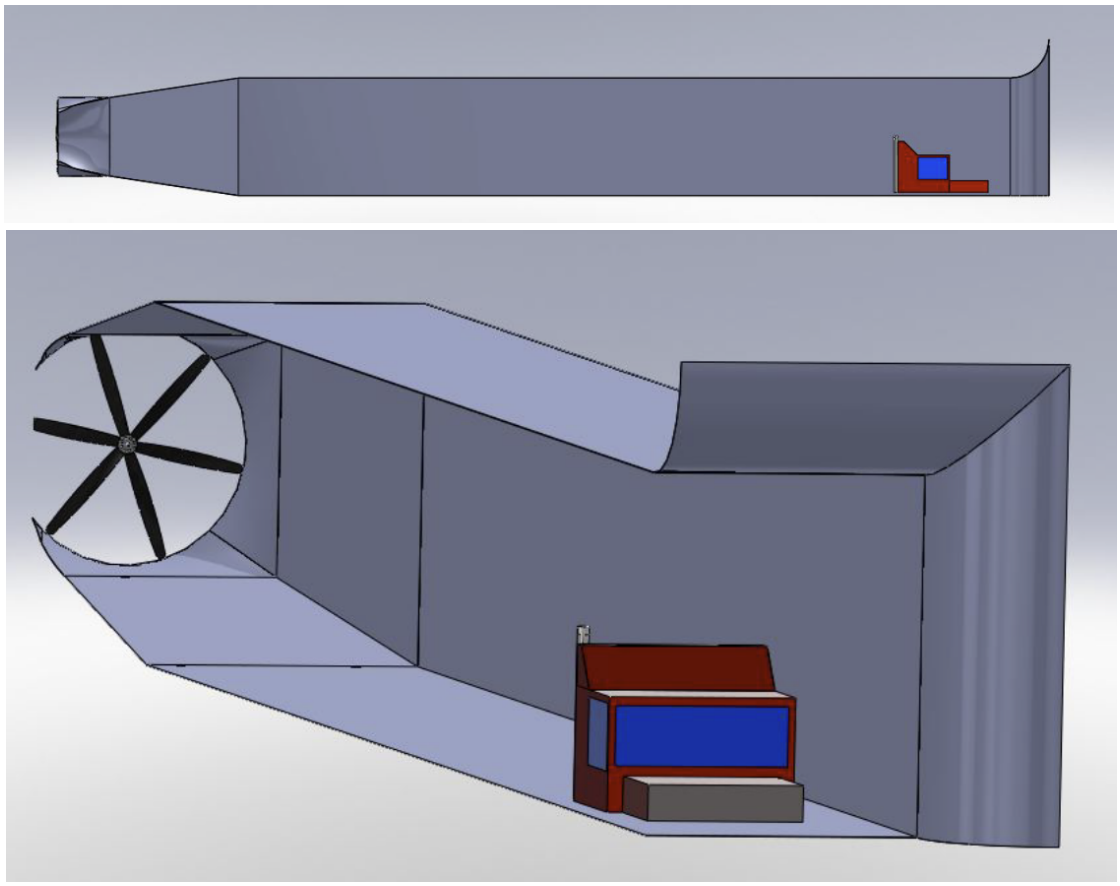

(b)

Figure 2-1: Wind Tunnel in "Pulling" configuration: (a) Side View; (b) Inlet View

Table 2: Wind Tunnel Parameters

Parameter	Value	Unit
Test Cell Width	16	ft.
Test Cell Height	16	ft.
Truck Width	2.5	m
Truck Height	2	m
Blockage Model Area	20.0	%
Velocity	15.75	$m\ s^{-1}$
	35.02	mph
Flow Rate	393.75	$m^3 s^{-1}$
	834,309	CFM
	1,417,500	$m^3\ hr^{-1}$
Pressure Drop (truck only)	1000	Pa
Pressure Drop (screen only)	200	Pa
Pressure Drop	100	Pa

(accelerate)		
Total Pressure Drop	1300	
Propeller efficiency	0.7	-
Total Power	878	kW
	1170	HP

2.3 Wind Tunnel Operations

In order to supply a continuous stream of exhaust for the exhaust plume simulation within the wind tunnel, the truck to be tested is installed on a heavy-duty chassis-dynamometer, located outside the wind tunnel, and operated at idle, 20 mph and 35 mph. The exhaust stack is connected to a 5 in (diameter) transfer pipe and ducted through an underground channel to a mock-up tractor cabin located inside the wind tunnel (Figure 2-2). The position of the chassis-dynamometer outside the wind tunnel, in close proximity to the position of exhaust introduction to the air flow in the tunnel and the thermal insulation of the transfer pipe guarantees a minimal temperature loss of the exhaust stream. This solution was chosen to avoid the logistical and structural problems of placing the chassis-dynamometer inside the wind tunnel.

Figure 2-2: Wind Tunnel, Chassis Dynamometer and TREL (described in Section 4) setup

The heavy-duty chassis-dynamometer employed during the present study is part of WVU's Transportable Emissions Measurement System (TEMS). The chassis-dynamometer consists of two sets of 12.6in diameter rollers, two flywheel assemblies, two air cooled eddy current power absorbers (Model CC300, Mustang) capable of absorbing peak power up to 1000hp, and two electrical motors to balance frictional losses within the dynamometer system, one for each side (hub) of the vehicle's drive axle. The flywheel assembly simulates the inertia of the test vehicle and is capable of simulating a vehicle weight of up to 110,000lbs.

In order to achieve similar turbulent mixing conditions among the different engine technologies, the same tractor cabin is used inside the wind tunnel for every test, referred to as the mockup cabin. A Volvo day-cabin was selected as average representation of typical fleet cabins.

3. Measurements

3.1 Test Matrix and Engine Specifications

The test matrix consists of nine configurations, combing three wind speeds and three trucks with and without aftertreatment technologies (as described in Table 3-1). Tables 3-2 list the specifications for the trucks and their engines.

Table 3-1. Descriptions of different wind speed and road load conditions and different aftertreatment technologies

Wind Speed	Description
Idle	The vehicle is in idling condition and a wind of 5mph is generated.
20 MPH	The vehicle was at 20mph in steady state conditions and a wind of 20mph was generated inside the wind tunnel. This test represents a vehicle cruising on a flat road at 20mph in calm air.
35 MPH	The vehicle was at 35mph in steady state conditions and a wind of 35mph was generated inside the wind tunnel. This test represents a vehicle cruising on a flat road at 35mph in calm air.
Truck	**Description**
Pre2007	The pre-2007 vehicle is not equipped with any aftertreatment devices. The vehicle is part of the CAFEE fleet.
Post2007	The Post-2007 vehicle is equipped with DOC/DPF to meet the 2007 US EPA regulations. The vehicle was rented from FYDA Freightliner Inc. in Canonsburg, PA.
Post2010	The Post-2010 vehicle is equipped with urea-based SCR and DOC/DPF assembly to meet the 2010 US EPA regulations. The vehicle was rented from Worldwide Equipment Inc. in Prestonsburg, KY.

It should be noted that the normal highway cruise speed, 55 mph, was not tested due to the limitation of the wind tunnel. The suction fan does not have sufficient power to provide 55 mph wind speed.

Table 3-2: Vehicle and engine specifications

Pre2007		Post2007		Post2010	
Chassis Manufacturer / Model	Mack Trucks Inc / CH613	**Chassis Manufacturer / Model**	Freightliner Cl120	**Chassis Manufacturer / Model**	Mack Trucks Inc. / CXU613
VIN	1M1AA13Y95WO54437	**VIN**	1FUJA6CK89DAE7405	**VIN**	1M1AW07Y1CM017126
Class	8	**Class**	8	**Class**	8
Vehicle Model Year (MY)	1995	**Vehicle Model Year (MY)**	2008	**Vehicle Model Year (MY)**	2011
Aftertreatment System	-	**Aftertreatment System**	DOC/DPF	**Aftertreatment System**	DOC / DPF / urea-SCR
Fuel	Standard ULSD (<15ppm)	**Fuel**	Standard ULSD (<15ppm)	**Fuel**	Standard ULSD (<15ppm)
Emission Family	SMK728EJDARA (45)	**Emission Family**	8DDXH14.0ELC	**Emission Family**	BVPTH12.8S01
Curb Weight [lbs]	15'000	**Curb Weight [lbs]**	23,587	**Curb Weight [lbs]**	15'000
Engine Manufacturer	Mack Trucks Inc.	**Engine Manufacturer**	Detroit Diesel	**Engine Manufacturer**	Mack Trucks Inc.
Engine Model	E7-400	**Engine Model**	SERIES 60 S/N 06R1012772	**Engine Model**	MP8-445C
Engine Model Year	1995	**Engine Model Year**	2008	**Engine Model Year**	2011
Displacement [L]	11.93	**Displacement [L]**	14.0 L	**Displacement [L]**	12.8
Configuration / # of Cylinders	In-line / 6 cylinder	**Configuration / # of Cylinders**	In-line / 6 cylinder	**Configuration / # of Cylinders**	In-line / 6 cylinder
Rated Power [hp]	400@ 1800rpm	**Rated Power [hp]**	515@1800	**Rated Power [hp]**	445 @ 1500rpm
NOx [g/bhp-hr]	4.5*	**NOx [g/bhp-hr]**	1.07*	**NOx [g/bhp-hr]**	0.12*
PM [g/bhp-hr]	0.09*	**PM [g/bhp-hr]**	0.003*	**PM [g/bhp-hr]**	0.003*

*Certification values

3.2 Overall sampling design

Figure 3-1 illustrates the overall sampling design. There are two sets of concurrent measurements, the wind tunnel measurement and a dilution tunnel measurement. In the wind tunnel measurement, raw exhaust was diluted in the wind tunnel, and sampled by a suite of instruments mounted on a mobile platform (described in Section 3.3). In the dilution tunnel measurements, raw exhaust was diluted by 6.5:1 to 23:1 using a customized Double Dilution System (DDS), and subsequently sampled by a number of instruments (described in Section 3.4).

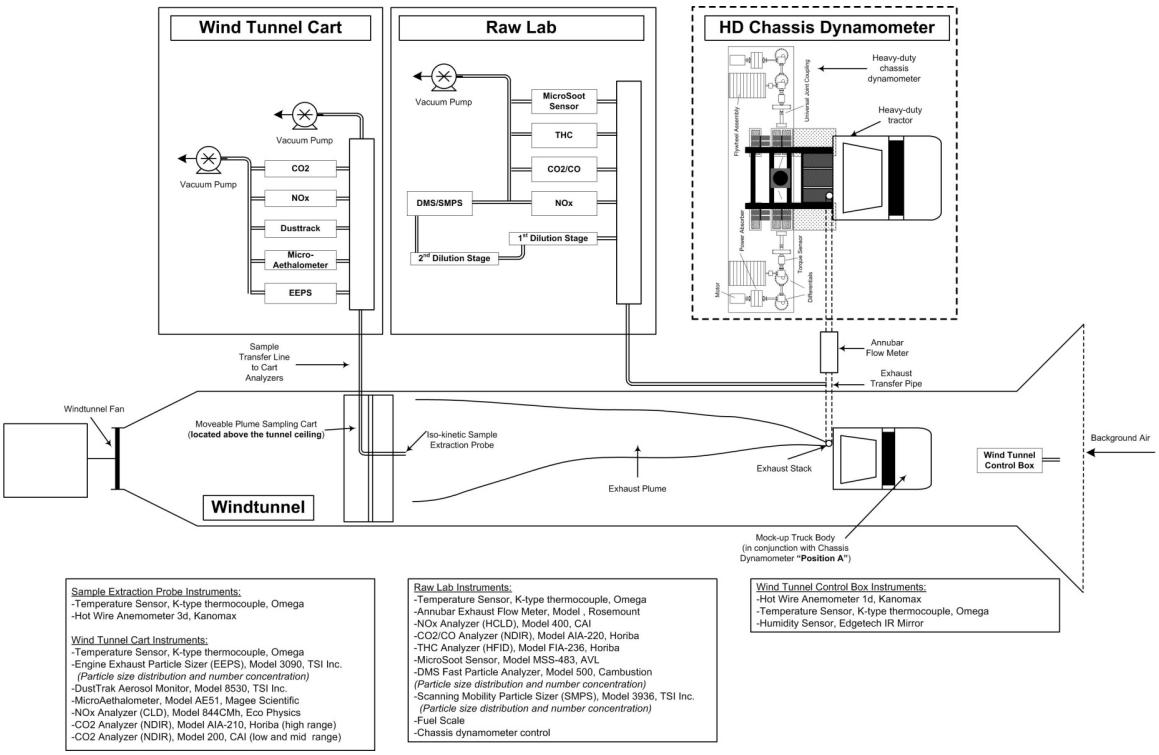

Figure 3-1: Sketch of the overall sampling design

3.3 Wind Tunnel Measurements

3.3.1 Instruments

Mobile Platform

A mobile platform was designed to carry the entire suite of instruments on a cart, moving longitudinally along the ceiling of the wind tunnel. Underneath the cart, a gantry system moves the probe vertically and horizontally. Position of the probe is monitored with 3 laser distance meters, capable of 1mm accuracy over the entire wind tunnel test cell. This configuration allows sampling throughout the cross-sectional area of the test cell, and for efficiently moving the sampling probe around the truck model placed within tunnel.

Sample Extraction Probe Instruments:

- Temperature Sensor, K-type thermocouple, Omega
- Wind speed sensor Hot Wire Anemometer 3D, Kanomax

Wind Tunnel Sampling Cart Instruments:

- Temperature Sensor, K-type thermocouple, Omega
- Engine Exhaust Particle Sizer (EEPS), Model 3090, TSI Inc.
- DustTrak Aerosol Monitor, Model 8530, TSI Inc.
- MicroAethalometer, Model AE51, Magee Scientific
- NOx Analyzer (CLD), Model 844CMh, Eco Physics
- NOx+amines Analyzer (CLD), Model 844CMh, Eco Physics
- CO_2 Analyzer (NDIR), Model AIA-210, Horiba (high-range)
- CO_2 Analyzer (NDIR), Model 200, CAI (low- and mid-range)

Carbon dioxide (CO_2) concentrations (low-, mid- and high-range) are measured on a dry basis using a non-dispersive infrared (NDIR) analyzer (Model AIA-220, Horiba and Model 200, CAI). A solution with a combination of three different CO2 analyzers was chosen to better cover the wide range of measurements, from 450ppm in the background air to 8% in the core of the plume. The ranges of the three instruments overlap, thus careful attention needs to be put in place to evaluate the most reasonable local value of CO_2. Nitrogen oxides (NOx) are measured on a dry basis using a Chemiluminescence detector (CLD) (Model 844CMh, Eco Physics). All analyzers are calibrated and operated according to recommendations outlined in Code of Federal Regulations (CFR), title 40, subpart 1065. An Amines converter with using a Chemiluminescence detector (CLD) (Model 844CMh, Eco Physics) provides the combination signal of NOx and Ammonia. Ammonia can be evaluated by subtracting the NOx signal from the NOx-amines. The flow in the sample extraction probe is managed according to the local wind speed (hot wire anemometer right in front of the probe tip), achieving in all the points an isokinetic sampling probe. This solution was chosen to reduce the particles losses and a sample the region as big as the probe tip, avoiding averaging measurements. The sample flow had no effects on the wind speed measurements obtained by the hot wire anemometer.

Measurements of PM concentrations and size distributions are performed with an Engine Exhaust Particle Sizer (EEPS™) spectrometer, model 3090, from TSI Inc. (Minnesota, USA) within the exhaust plume and the background air. Spectrometers classify particles based upon differential electrical mobility classification principle at a frequency of 10 Hz, making it best suited for transient PM characterization. Particles between 7 nm and 500 nm are measured with a resolution of 16 channels per decade; hence a total of 32 channels. DustTrak Aerosol Monitor (Model 8530, TSI Inc.) is a light-scattering laser photometer capable of measuring suspended aerosol mass corresponding to $PM_{2.5}$. The DustTrak came already calibrated for CARB (owner of the instruments). Prior to any tests, the instruments were cleaned and zeroed with the procedure indicated in the manual. The linear response of the instruments and the zerowere checked prior to testing. The MicroAethalometer (Model AE51, Magee Scientific) is a laser absorption photometer capable of measuring black carbon concentration. Engine Exhaust Particle Sizer (EEPS) (Model 3090, TSI Inc.), DustTrak Aerosol Monitor (Model 8530, TSI Inc.) and MicroAethalometer (Model AE51, Magee Scientific) are operated according to the manual and periodic cleaning is enforced prior to any test. The transfer line from the probe to the analyzers is a Tygon™ tube and kept and thermally isolated at 60°C to reduce thermophoretic losses and not influence the PM particle and size distribution.

3.3.2 Plume mapping protocol

The adopted plume mapping protocol consists of 130 sampling points divided into 10 planes. The sampling planes are not evenly spaced along the wind tunnel. They are more densely spaced near the stack to capture the new particle formation and other dynamical processes (illustrated in Figure 3-2). The stack is 2.87 m from origin of the wind tunnel reference system. The downwind distances from origin of the wind tunnel reference system are: 2.97 m (Plane1), 3.17m (Plane2), 3.42m (Plane3), 3.67m (Plane4), 4.17m (Plane5), 4.67m (Plane6), 5.67m (Plane7), 7.67m (Plane8), 9.67 m (Plane9) and 15.67 m (Plane10), respectively. The corresponding downwind distances from the stack are: 0.1 m (Plane1), 0.3 m (Plane2), 0.55 m (Plane3), 0.8 m (Plane4), 1.3 m (Plane5), 1.8 m (Plane6), 2.8 m (Plane7), 4.8 m (Plane8), 6.8 m (Plane9) and 11.8 m (Plane10), respectively.

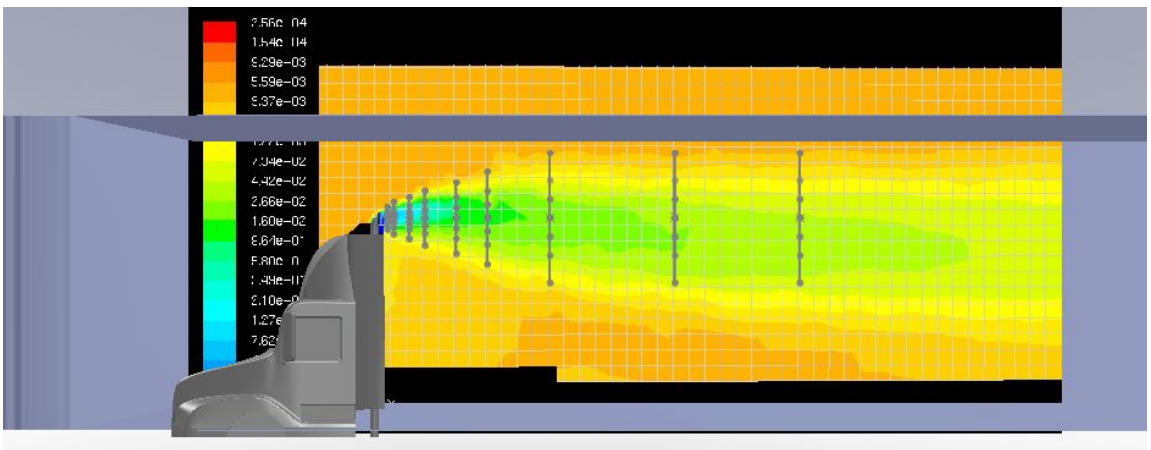

Figure 3-2: Initial identification of the plume sampling points. The vertical lines indicate different sampling planes.

All the planes share the same sampling pattern, but each plane has different vertical dimension and position, designed to capture the plume shape and evolution. The mapping pattern is composed of 2 nested hexagons, rotated by 90°, and an additional center point, i.e., 13 points per plane (Figure 3-3). In addition, Point 0 (p0) is added right at the stack exhaust, intended to compare drifts or shifts of the sampling cart analyzers with the ones of the TREL. So there are totally 131 sampling points. The first 65 points and p0 take 100 s in sampling time (1000 data points at 10 Hz), and the remaining points 50 s (500 data points at 10 Hz). Prior to any sampling, 30s of non-sampling stabilization time is observed once the probe reached the desired position, accounting for the inertia of the measurement system.

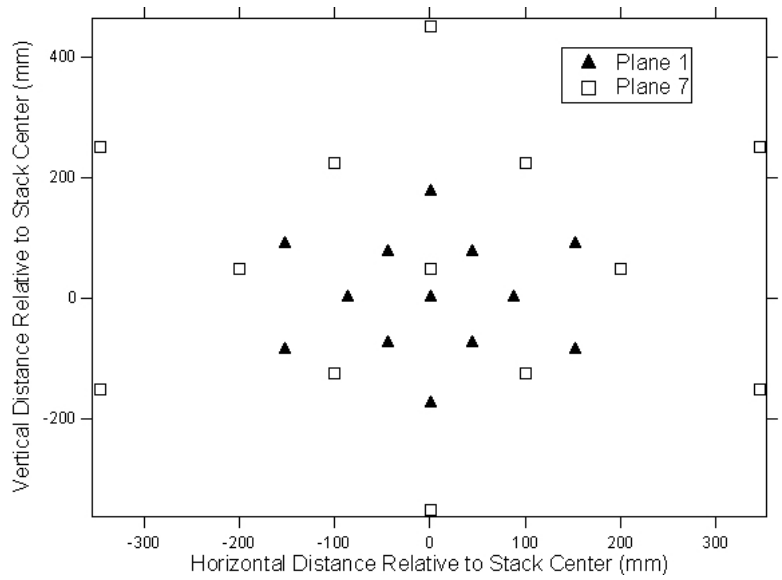

Figure 3-3: Illustrations of sampling point locations on Plane 1 and 7.

3.3.3 Examples of wind tunnel measurement results

The plume mapping in the wind tunnel measurements resulted in a large set of data describing the evolution of the plumes spatially and temporally. Figures 3-4 and 3-5 depict the contours of nine different plume parameters on two different planes (Plane 1 and Plane 4) for Pre2007 20 MPH case. The contour files were generated through linear interpolation/extrapolation of the measured values at 13 sampling points. The parameters represented are:

- NOx
- Micro Aethalometer
- DustTrak
- CO_2 low-range (CO2l)
- CO_2 mid-range (CO2m)
- CO_2 high-range (CO2h)
- Temperature
- Air Speed
- Turbulence Intensity (TI)

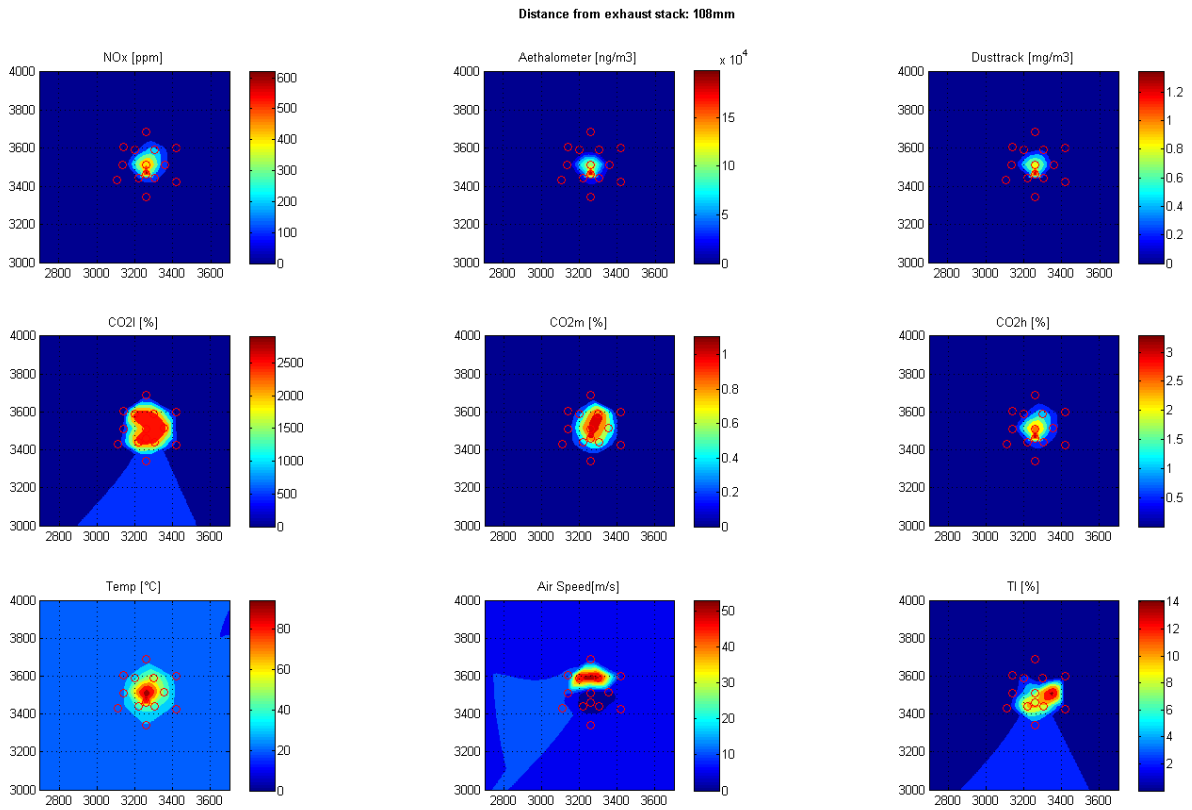

Figure 3-4: Pre2007 vehicle, 20mph Test, Plane 1

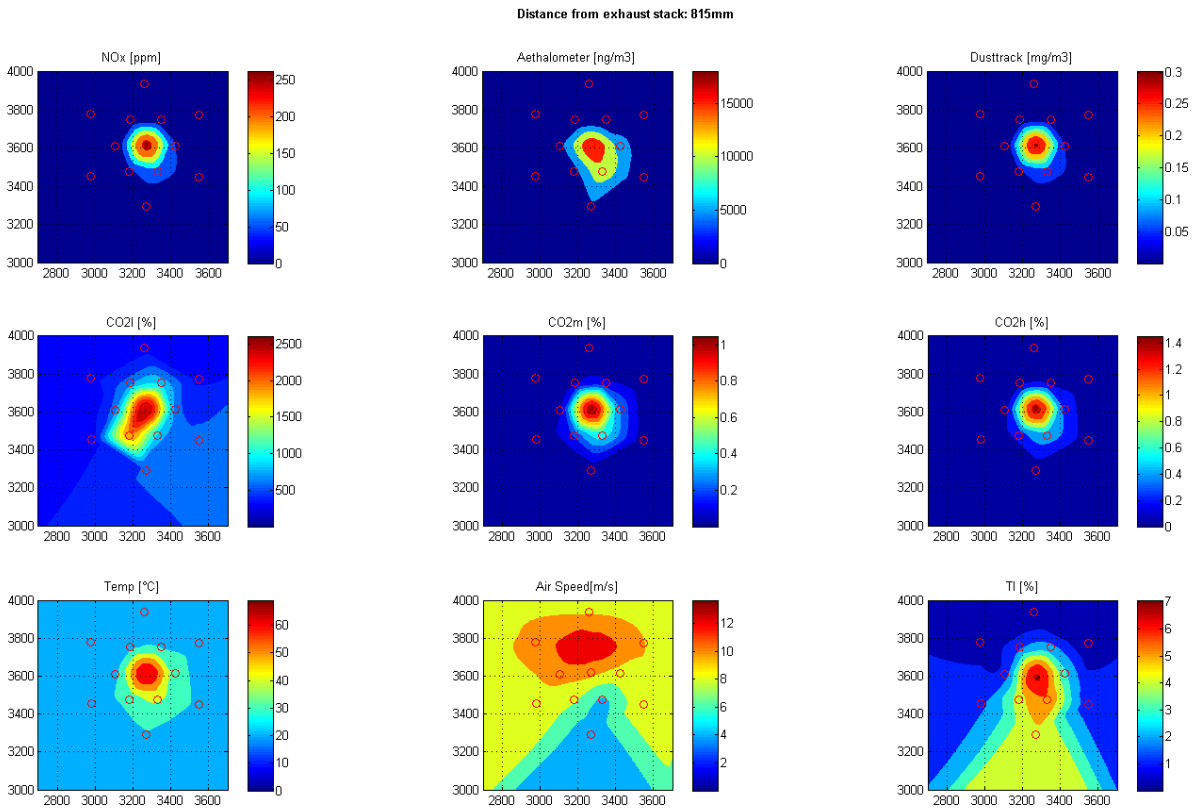

Figure 3-5: Pre2007 vehicle, 20mph Test, Plane 4

3.4 Dilution Tunnel Measurements

3.4.1 Two-stage dilution system

In the dilution tunnel measurements, raw PM emissions were sampled from the exhaust transfer pipe by means of a customized Double Dilution System (DDS). The apparatus was composed by two mini-dilution tunnels equipped with two ejector diluters that allow for variable Dilution Ratio (DR) settings.

The first stage dilution was performed using hot air (~150°C) that was previously filtered and dried by means of a HEPA filter and a dryer. The second stage dilution was, on the contrary, obtained by supplying cold air (~20°C) in order to obtain a gas mixture with a temperature low enough to satisfy the requirements of the PM instruments used in this study.

3.4.2 Instruments

Transportable Raw Emissions Laboratory (TREL) as depicted in Figure 3-6:

- Temperature Sensor, K-type thermocouple, Omega
- Annubar Exhaust Flow Meter, Rosemount
- NOx Analyzer (HCLD), Model 400, CAI
- CO_2/CO Analyzer (NDIR), Model AIA-220, Horiba

- THC Analyzer (HFID), Model FIA-236, Horiba
- MicroSoot Sensor, Model MSS-483, AVL
- DMS Fast Particle Analyzer, Model 500, Cambustion
  (Particle size distribution and number concentration from 5 nm to 2.5 µm)
- Scanning Mobility Particle Sizer (SMPS), Model 3080, TSI Inc. consisting of a long DMA (TSI, Model 3081) and an Ultrafine Condensation Particle Counter (TSI, Model 3025) for particle size distribution and number concentration from 6 nm to 200 nm
- Fuel Scale
- Chassis dynamometer control

Figure 3-6: WVU Transportable Raw Emissions Laboratory (TREL)

Gaseous emissions of CO_2, CO, NOx, NO as well as THC are measured directly from raw (undiluted) exhaust. NOx and NO are measured on a dry basis using a dual-channel CLD (Model 844CMh, Eco Physics) with the possibility to calculate NO2 through subtraction of NO from NOx, CO_2 and CO on a dry basis using an NDIR analyzer (Model AIA-220, Horiba) as well as THC on a wet basis using a HFID analyzer (Model FIA-236, Horiba). The analytical bench further houses sampling conditioning units (dryers), flow meters, and heated sampling pumps and filters that are controlled by electronic micro-controllers and maintained at 112°C for CO, CO_2 and NOx and 191°C for THC sample trains.

PM measurements are conducted for the diluted exhaust. DMS was employed to measured particle size distribution for all Pre2007 cases except 35 MPH and all Post2007 cases. SMPS was used for the rest of the cases. A micro-soot sensor (MSS-483) from AVL is being employed in order to measure continuous soot (solid carbon only) emissions.

3.5 QA/QC

Quality control and quality assurance procedures adopted by the WVU Wind Tunnel and the WVU Transportable Heavy-Duty Vehicle Emissions Laboratory are given below. The laboratories are capable of measuring regulated and non-regulated engine or vehicle emissions such as carbon monoxide (CO), oxides of nitrogen (NOx), total hydrocarbons (THC), total particulate matter (TPM), carbon dioxide (CO_2). Reliable sampling is assured through system design, periodic system inspection, and scheduled instrument calibration as described below.

Sampling Lines and Probes

The sampling streams use separate sampling probes and lines with their own pumps (heated in the case of NOx, THC, and also CO/CO_2 to avoid condensation of moisture in the lines). This design feature ensures reliable operation of the THC and NOx analyzers. Great care is taken in verifying that emissions measurement equipment is in order before commencement of emissions testing. Prior to the performance of a test schedule, supervisory personnel verify that all sample probes in the raw exhaust are properly placed (all probes sample at equidistant locations from the center of the tunnel and oriented with their sample inlets facing upstream) and that the integrity of the sampling systems has been maintained. The sampling lines are leak checked (by pressurization) and back-flushed with high pressure air in order to clean the lines of residual particulate matter. Heated sampling lines and their associated control systems (PID temperature controllers and associated thermocouples) are checked to ensure continuity between the controller, heater elements, and thermocouples. The temperature settings also are verified (THC sampling probes and lines are maintained at 375°F while NOx lines and probes are maintained at 250°F). Sample line temperatures, at various locations, are displayed on the sampling cabinet for monitoring by the operator.

Thermocouples and Pressure transducers

Thermocouples K are used for temperature measurements and calibrated by a certified signal generator from 0 to 100% of their range in 10% increments. The thermocouple readings are allowed to stabilize at each measurement point and a computer averaged (100 points) reading of the instrument is recorded. The eleven data points and their corresponding temperature are recorded and a fifth degree polynomial is fitted to the data to complete the calibration data file. Pressure transducers are calibrated with a certified pressure analyzer from 0 to 100% of their range in 10% increments. The pressure readings are allowed to stabilize at each measurement point and a computer averaged (100 points) reading of the instrument is recorded. The eleven data points and their corresponding temperature are recorded and a linear polynomial is fitted to the data to complete the calibration data file.

Exhaust Transfer Tube

The exhaust transfer tube, which routes exhaust from the engine exhaust system to the wind tunnel, is checked for leaks after assembly. Joints in the tube are sealed using a high-temperature aluminum tape and periodically checked to ensure integrity. The exhaust transfer tube is insulated to minimize errors in PM measurement due to thermophoretic effects.

Calibration and Calibration Gases

The gases used to calibrate the emissions measurement instruments are certified by the supplier to have an accuracy of 1% traceable to NIST. The laboratory uses the same gases for calibration, span and zero gases. All span and calibration gases have concentrations equal to approximately 85% to 95% of full scale. All emissions measurement instruments are calibrated using appropriate ranges of calibration gas for the engine or vehicle being tested. These calibrations are performed before each series of tests and after any instrument maintenance has been performed. HC, CO, NOX, and CO_2 instruments are calibrated by sampling a varying mixture of zero air and span gas (calibration gas) through a gas divider from 0 to 100% of their range in 10% increments. The instrument readings are allowed to stabilize at each measurement point and a computer averaged (100 points) reading of the instrument is recorded. The eleven data points and their corresponding gas concentrations are recorded and a second degree (third degree in

case of NDIRs) polynomial is fitted to the data to complete the calibration data file. The calibration file overwrites the previous calibration file on the main computer (each test data disk contains the calibration files from that test) to prevent using incorrect calibration files for testing. No gas cylinder is used if the pressure drops below 200 psig.

Additional Calibration and Maintenance Procedures

In addition to the calibration procedures, each analyzer is subjected to a range of checks and maintenance procedures as described below.

Hydrocarbon Analyzer

The THC analyzer is subjected to the 'FID burner peaking process' to get the highest flame ionization detector (FID) response. This process involves measuring and recording the response of the instrument to 100% span gas and zero air with various settings of FID burner fuel and air. Upon completion of the FID burner peaking process, the fuel and air settings of the FID are placed at the setting which produced the highest instrument response, and the analyzer is calibrated. A HC hang-up check, following the procedures outlined in 40 CFR, Part 86, Subpart N, is also performed on the heated FID. If the differences in the responses are more than two percent, the sampling probe is backflushed (direct injection of zero air into the analyzer and through the 'overflow' sampling probe) and steps are taken to rectify the problem.

NOx Analyzers

On a monthly basis, a NOx efficiency test is performed on the NOx analyzers. This test is performed to ensure that the analyzer converter (which converts NO_2 to NO) is performing satisfactorily. A conversion efficiency of less than 90% is considered a failure and maintenance is performed to rectify the situation. Filters in the NOx sampling are visually inspected and replaced after analyzer maintenance has been performed and whenever necessary.

CO/CO_2 Analyzers

Since moisture can affect the operation of the NDIR analyzers used for carbon monoxide and carbon dioxide, a water interference check is performed. The sample flow is passed through a refrigerator dryer to lower the dew point of the sample stream before it reaches the NDIR.

Particulate Sampling

PM sampling is obtained with 3 different spectrometer (SMPS, EEPS, DMS) and 3 soot analyzers (DustTrak, MicroAethalometer and MSS). All instruments operated, cleaned and zeroed according to their respective manuals and common procedure, applied as extension of CFR 1065 indications on quality measurements.

Data Analysis and Reporting

Quality assurance for data reported from testing is achieved using multiple checks. First, the operators of the laboratory, including the senior supervisory personnel as well as technicians, have a vast amount of experience in testing a multitude of different vehicle/engine/fuel combinations. This experience is valuable in quality assurance since it allows the laboratory operators to identify problems at the test site.

As a test is performed, data is logged to a local hard disk on the data acquisition computer. After the test is completed, data is transferred to a media storage device as well as separate backup optical drive. A data reduction program is used to extract emissions data from a binary data file

and translate it into the appropriate units using calibration files. On-site examination of the data is done by supervisory personnel to determine the accuracy of the data in order that equipment malfunctions can be identified and promptly corrected.

4. Wind tunnel modeling

The original objective of the wind tunnel modeling effort is to test the capability of simulating plume dispersion and aerosol dynamics in the wind tunnel environment. The procedure usually starts with flow field simulations, followed by tracer gas simulations, and completed by aerosol dynamics simulations. Before introducing the wind tunnel modeling effort, we briefly describe the different modeling tools that we employed in this project, listed in Table 4-1.

Table 4-1: Descriptions of modeling tools

Modeling Tool	Descriptions
SolidWorks	A 3D mechanical CAD (computer-aided design) program, used in this project to create the geometry of the mock cabin.
ANSYS Workbench	An integrated software environment, used in this project to create computational mesh for CTAG simulations
ANSYS Fluent	A computational fluid dynamics (CFD) program, used in this project to simulate velocity field and gas transport.
Reynolds-averaged Navier–Stokes (RANS) model	A type of models to simulate the average flow fields, which is generally less computationally expensive and less accurate
Large-Eddy Simulation (LES) model	A type of models to simulate the average flow fields, which is generally more computationally expensive and more accurate
CTAG	A CFD-based aerosol dynamics and gas chemistry model

4.1 Computational Mesh and Geometry

The geometry of the truck cabin and wind tunnel was reproduced in SolidWorks. The geometry, shown in Figure 4-1a, represents the most accurate digital version of the experimental geometry while still being simple enough to mesh. A magnified view of the truck cabin is shown in Figure 4-1b.

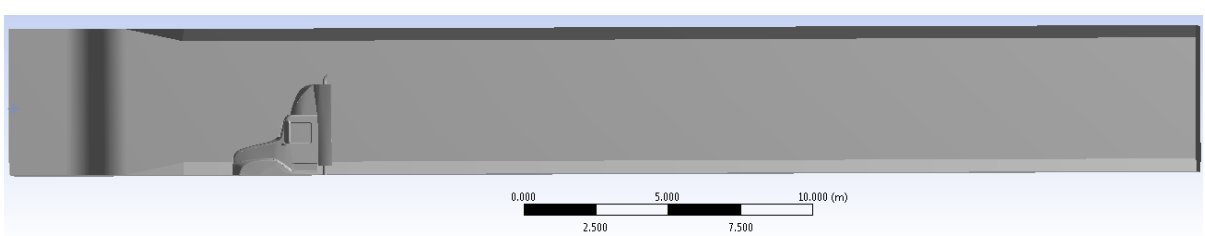

(a)

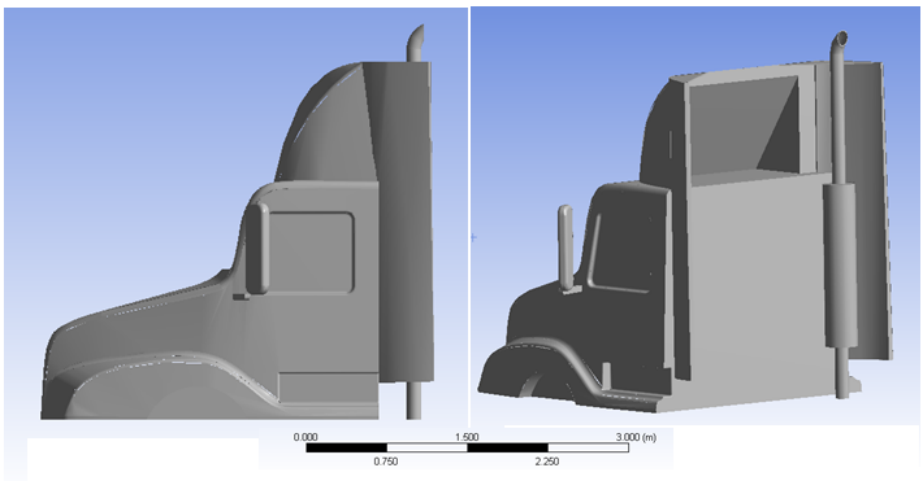

(b)

Figure 4-1: Geometries in Solidworks (a): Cabin and wind tunnel; (b) Cabin

For the purposes of the simulation, the air space of the geometry is meshed in ANSYS Workbench 14. The mesh is more refined near the wind tunnel boundaries, the truck cabin, and especially near the stack outlet. The total computational mesh consists of 1,909,860 unstructured elements. The mesh around the cabin can be seen in Figure 4-2.

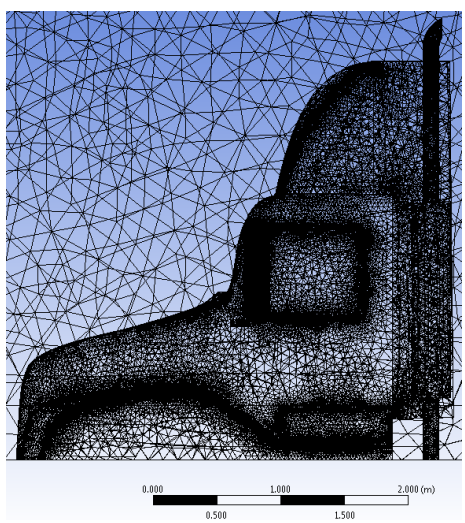

Figure 4-2: Mesh of cabin in ANSYS Workbench.

4.2 Velocity Field

Simulation velocity downwind of the stack was recorded and compared with experiment. Simulated velocity contours are shown in Figure 4-3. The velocity moving over and around the cabin accelerates. Behind the cabin, a complex flow recirculation zone is formed.

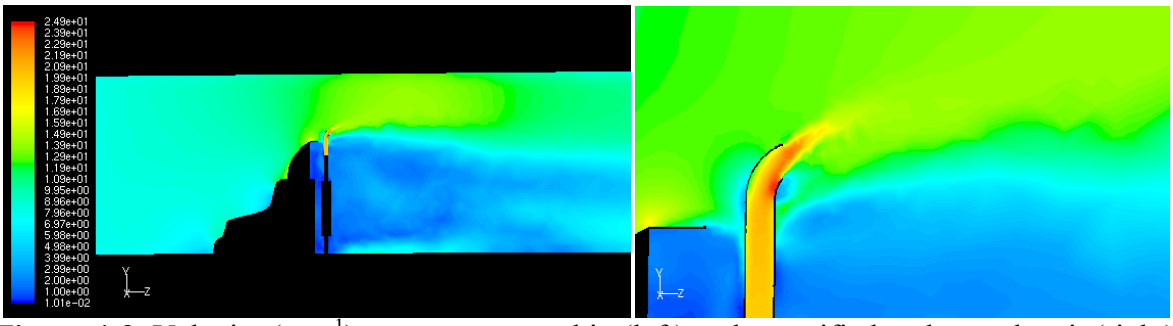

Figure 4-3: Velocity (m s^{-1}) contours near cabin (left) and magnified at the stack exit (right)

As a simple first order analysis, a Reynolds-averaged Navier–Stokes (RANS) model was employed. However, RANS models typically perform poorly in areas of complex flow regimes, such as the wake behind a bluff body. As such, we expect the RANS model to be insufficient to capture the aerodynamic trends that will limit its usefulness in the full aerosol dynamics model. Therefore, a more complex, but computationally expensive Large-Eddy Simulation (LES) model is employed. Figure 4-4 shows the comparison of centerline velocity downwind of the stack between the RANS, LES, and the experiment. Both models capture the general trend of the velocity profile. However, the RANS model has trouble capturing the velocity in the vicinity immediately downwind of the stack outlet. This is the area where the greatest amount of aerosol chemistry will occur. Therefore, the full model will be performed using the LES flow solver. Both models overpredict the velocities further downwind, which is indicative of the model underpredicting the amount of mixing that occurs away from the cabin.

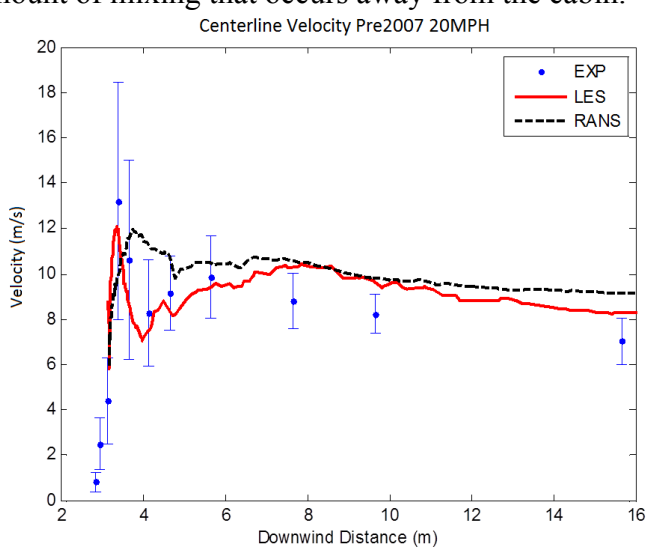

Figure 4-4: Comparison of predicted and measured centerline velocity for Pre2007 20 MPH case. Both RANS and LES models are employed to solve the turbulence flow fields.

Figures 4-4 suggests that the model cannot fully capture the relatively low velocity on the first three data points, corresponding to Point 0, Plane 1 and Plane 2. One reason is related to the large gradients in velocity near the stack. The contour plots presented in Figure 4-3 show that moving even a few centimeters up or down near the stack exit will lead to significant change in velocity (e.g., from 10 m/s to 25 m/s). In other words, there are sharp velocity gradients in the region where Point 0, Plane 1 and Plane 2 reside. The model performs adequately for the rest of

the planes, though the model tends to overestimate the velocity. There are a couple of ways to further improve the velocity results. The wind tunnel inlet turbulence is uncertain and is not well characterized, which we can adjust to improve the results in the last 3 planes. The stack geometry can be further refined to improve the results on Point 0 and the first 2 planes, as the predicted velocity is highly sensitive to stack geometry. The proposed efforts were not carried out due to the time constrain to complete the project.

4.3 CO_2

Tracer gas, in this case CO_2, was measured downwind of the stack. Figure 4-5 illustrates the centerline CO_2 profiles for the Pre2007, Post2007 and Post2010 trucks, which show that the model systemically overpredicts the dilution rates for all three cases. Overall, the LES model (i.e., CTAG's flow solver) preforms much better in predicting CO_2 concentrations than velocities for Point 0, Plane 1 and Plane 2. The main reason is that those CO_2 concentrations are still heavily influenced by the inlet condition, i.e., the stack-level CO_2 concentration. Nevertheless, the overpredicted velocities may have led to overpredicted dilution rates (i.e., lower CO_2 concentrations) shown here.

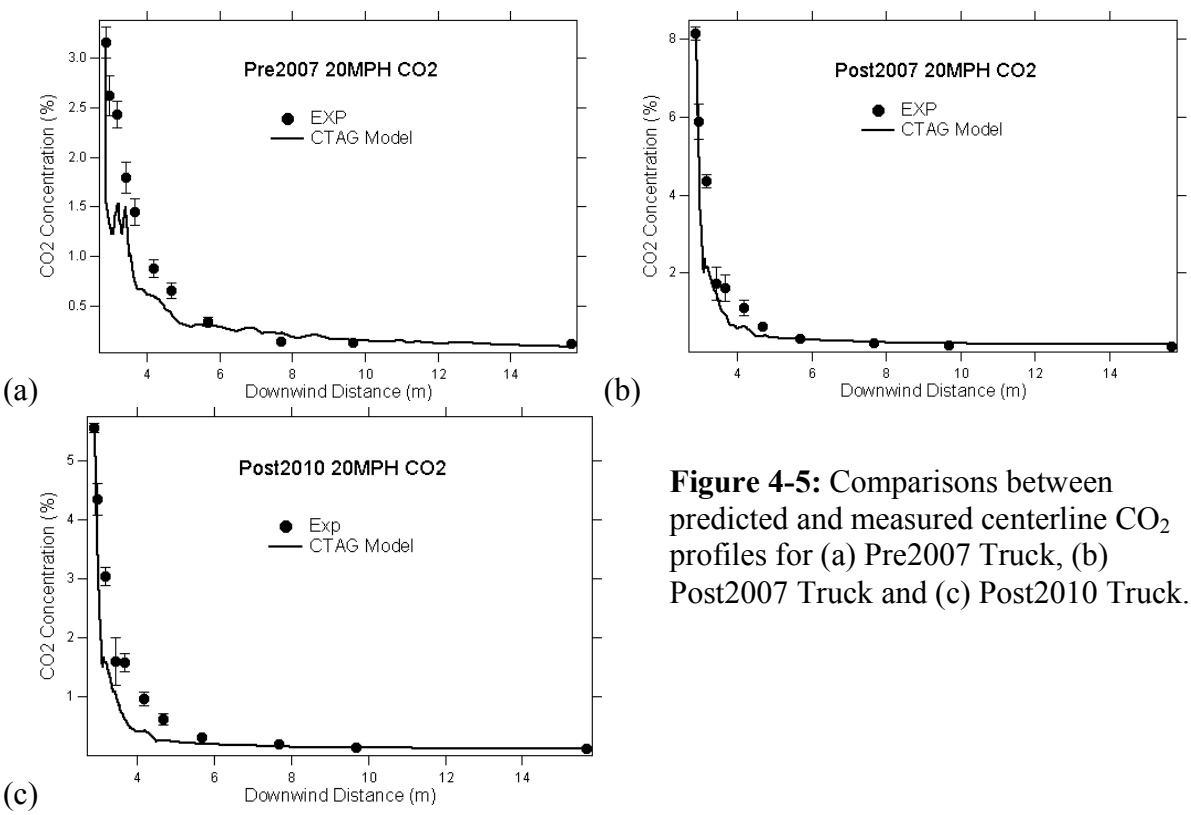

Figure 4-5: Comparisons between predicted and measured centerline CO_2 profiles for (a) Pre2007 Truck, (b) Post2007 Truck and (c) Post2010 Truck.

4.4 Aerosol dynamics

We decided not to proceed with aerosol dynamics simulations for the following reasons. *First*, the unusually volatile behaviors of the accumulation-mode particles have been observed, to be

discussed in Section 5, though the accumulation-mode particles were expected to experience little change other than dilution, as shown in (Lipsky and Robinson, 2005) and(Ronkko et al., 2006). There are no mechanisms currently incorporated in the CTAG model that are able to explain those behaviors. Simulating new particle formation has been the strength for the CTAG model and was the original area of interest for this project. However, the large uncertainties in simulating accumulation-mode particles will lead to large uncertainties in simulating nucleation-mode particles. The volatile behaviors of the accumulation-mode particles could be due to sampling errors or new physical process unknown to the research community. But until we can identify the cause(s) for those behaviors, aerosol dynamics simulations will reveal little new information. *Second*, the Post2007 truck was found to have a cracked DPF, which makes the comparison between Pre2007 and Post2007 trucks less meaningful. *Third*, the results from the Post2010 truck appear to be indistinguishable from the background conditions. Thus, modeling aerosol dynamics and the interpretations of the results for the Post2007 and Post2010 trucks will have very large uncertainties without identifying exactly how a cracked DFF in the Post2007 truck affected the oxidations of hydrocarbon, SO_2 and soot particles and without identifying the plume signals for the Post2010 truck.

5. Results and Discussions

All data reported here, otherwise specified, are average values at individual sampling locations. For example, EEPS has a 10 Hz time resolution. Each sampling location takes either 100 s (for the first five planes) or 50 s (for the rest of the planes). Therefore, the EEPS data are reported as the average of either 1000 or 500 data points for each sampling location.

In addition, the positions of the sampling planes vary with downwind distances. As depicted in Figures 3-4 and 3-5 (the CO2% panel), the center of the plane approximately captures the center of the plume. Thus, the results that we present in this section are for the plane centers, unless noted otherwise.

5.1 Dilution correction and dilution-corrected NOx and BC concentrations

The evolution of exhaust particles in the wind tunnel is governed by turbulent mixing (resulting in dilution) and aerosol dynamical processes (e.g., condensation, evaporation, coagulation, etc). To better understand the effects of aerosol dynamic processes on particle size distributions, we introduce a dilution correction method to account from the dilution effect. In other words, if particles experiences no aerosol dynamic processes at all, the dilution-corrected particle size distributions measured at any given point on any given plane should be the same.

Dilution ratio (DR) is defined as:

$$DR = \frac{[CO2]_0 - [CO2]_B}{[CO2] - [CO2]_B}$$

where $[CO2]_0$ is the stack-level CO_2 concentration (i.e., from point0); [CO2] is the CO_2 concentration at each sampling point; $[CO2]_B$ is the background CO_2 concentration.

Dilution correction is given by multiplying the pollutant concentration at a sampling point by the DR.

We first test whether the dilution correction works by plotting the downwind profiles of NOx and Black Carbon (BC) concentration (following the center point of each plane), adjusted for dilution of CO_2 tracer along the same trajectory (Figure 5-1).

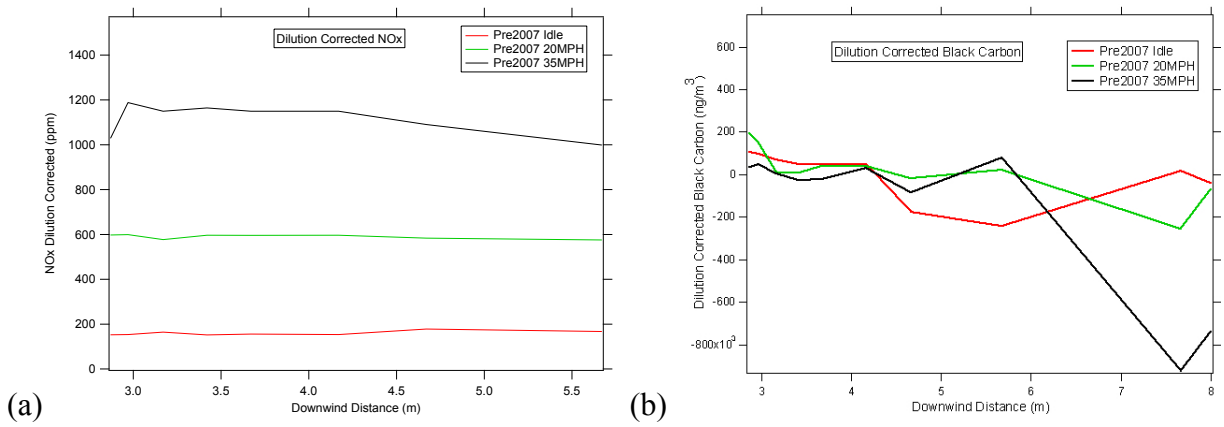

(a) (b)

Figure 5-1: Dilution-corrected (a) NOx and (b) BC concentrations for Pre2007 cases

If the dilution correction works well, the dilution-corrected NOx concentrations should stay the same at any given sampling point. For both Idle and 20 MPH cases, we can see that the dilution-corrected NOx concentrations stay close to a horizontal line, indicating that dilution correction worked well. For the 35 MPH case, the dilution-corrected NOx concentration increases from ~1000 ppm to ~1200 ppm in the first 3 meters, and then it decreases gradually back to 1000 ppm, for a maximum deviation of a little less than 20%. There are two potential causes for the initial increase of dilution-corrected NOx concentrations. First, the diesel engine may have experienced some unsteady condition, even though the intention was to keep it at the steady state. However, the corresponding dilution tunnel measurement did not reveal the similar trend. Second, the NOx and/or CO_2 instrument may not have worked properly when sampling the first two planes (2.87 m and 2.97 m).

Dilution-corrected BC concentrations were expected to behave like an inert gaseous species. However, the MicroAethalometer reported a large number of negative values (Figure 5-1b).

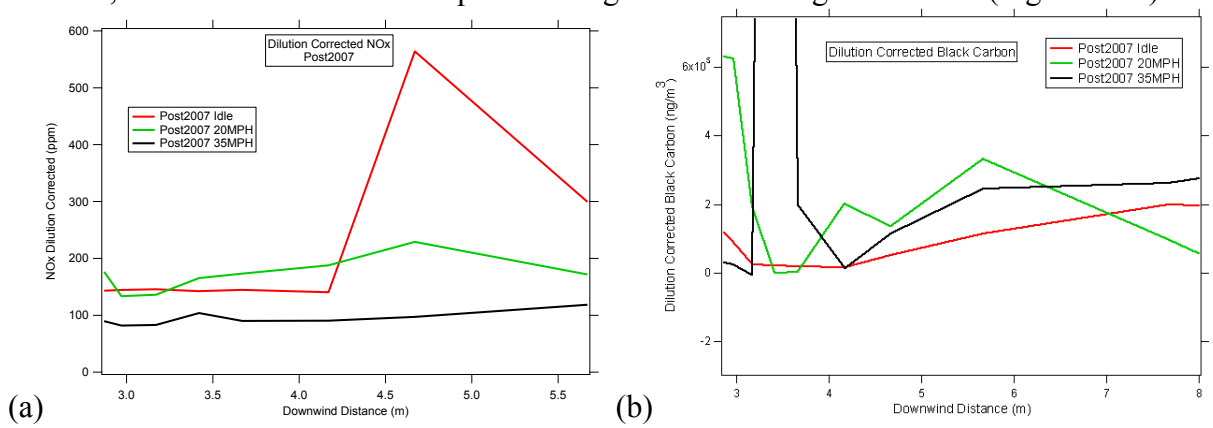

(a) (b)

Figure 5-2: Dilution-corrected NOx and BC concentrations for Post2007 cases

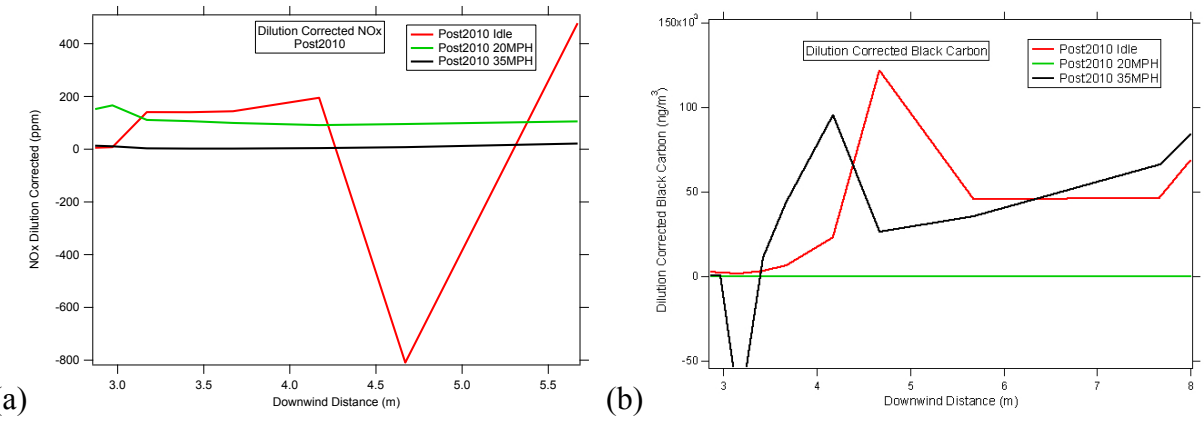

Figure 5-3: Dilution-corrected NOx and BC concentrations for Post2010 cases

We did the same analysis for the Post2007 cases (Figure 5-2) and Post2010 cases (Figure 5-3). There is clearly some problem with NOx and CO_2 measurement for the two Idle cases, as the dilution-corrected NOx undergoes large changes in concentration. To further illustrate this problem, we plot the CO_2 and non-dilution-corrected NOx concentrations side by side for the two cases, as depicted in Figures 5-4.

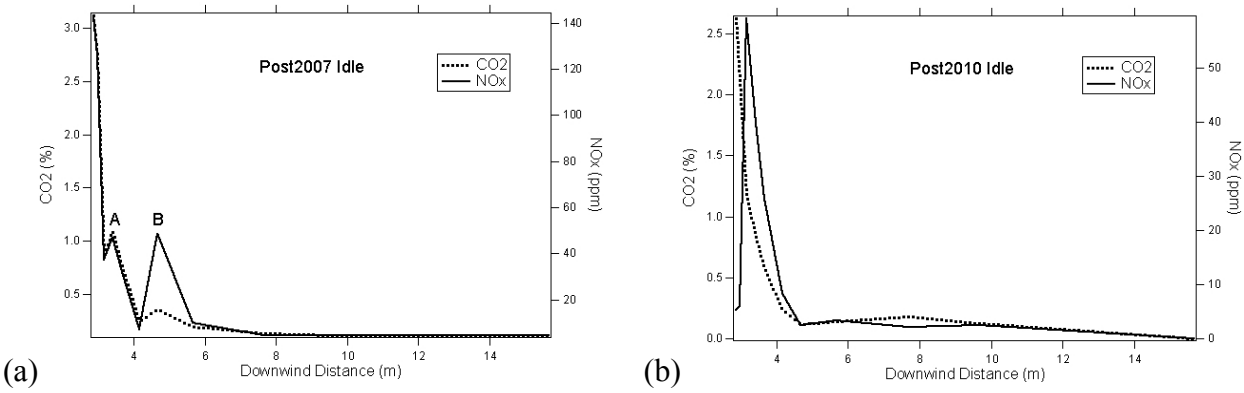

Figure 5-4: The CO_2 and non-dilution-corrected NOx concentrations for (a) Post2007 Idle and (b) Post2010 Idle

Figure 5-4a shows that the CO_2 and NOx profiles almost perfectly match each other for most of the planes except Plane 6 (4.67 m), marked as "B", which causes the sudden drop in dilution-corrected NOx at the same plane illustrated in Figure 5-3a. Figure 5a also shows that both CO_2 and NOx concentrations increase at Plane 3, marked as "A". Our analysis indicates that the increases are due to the changing inlet condition. Because CO_2 and NOx are being affected by the inlet condition in the same manner, their profiles still match at Plane 3, and the dilution-corrected NOx remain approximately constant (Figure 5-3a). In contrast, the profiles of CO_2 and NOx do not match at Plane 6. Considering the continuous dilution tunnel measurement does not show any significant drift in either CO_2 or NOx, it is strongly suggested that one of or both CO_2 and NOx instruments may have encountered some problem at Plane 6 during the wind tunnel experiment for Post2007 Idle case.

Figure 5-4b shows that the NOx concentration starts at low concentrations, reaches the maximum at 3.17 m (Plane 2), and then decays. The NOx profile is very different from the CO2 profile, which presents a typical decaying shape. Thus, it is very likely that the NOx instrument may have some problem during the wind tunnel experiment for Post2010 Idle case.

The dilution-corrected NOx concentrations for Post2010 20 MPH case behaves as expected. The dilution-corrected NOx concentrations for Post2010 35 MPH case are almost zero, indicative of more effective SCR operations at higher speed (35 MPH) than lower speed (20 MPH). There are still some larger than expected variations for both Post2007 and Post2010 20 MPH cases.

The dilution-corrected BC concentrations for both Post2007 and Post2010 cases change significantly at different sampling planes, which suggests that MicroAethalometer may not have worked reliably at all during the wind tunnel measurements.

5.2 Evolution of particle size distributions (PSD)

5.2.1 Pre2007 - Idle

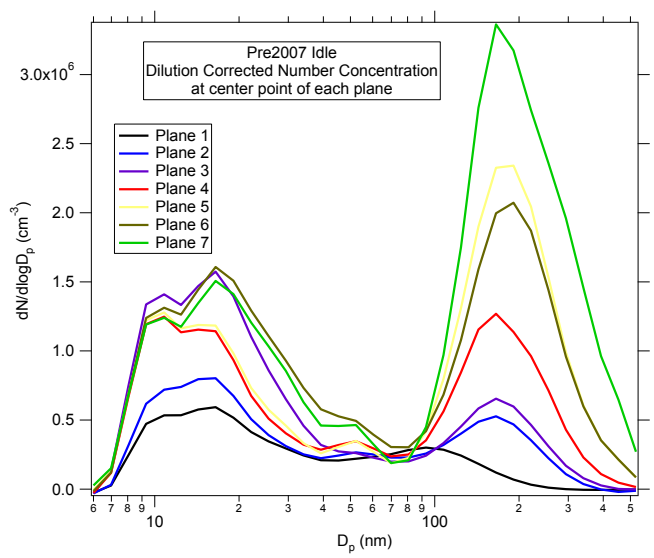

(a)

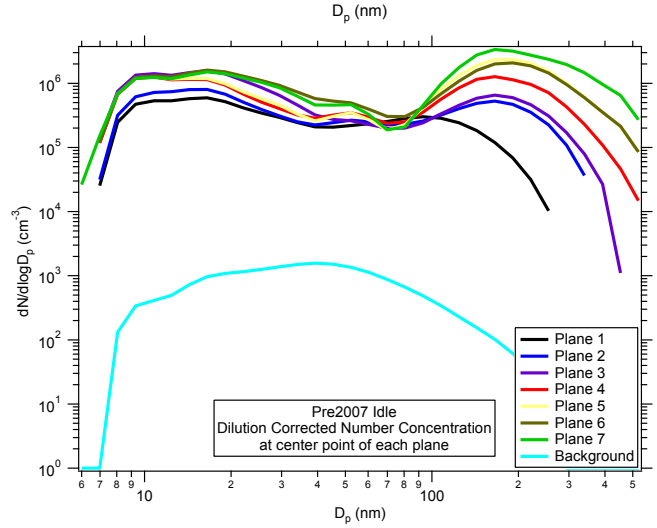

(b)

Figure 5-5: Dilution-corrected particle size distributions for Pre2007 Idle case; (a): linear scale; (b): logarithm scale

Figure 5-5 illustrates the dilution-corrected PSDs at different planes for Pre2007 Idle case. It should be noted that the dilution correction works very well for NOx for this case so that we should have confidence in the dilution-corrected PSDs. Pre2007 case has a relatively small nucleation mode, likely due to the presence of a relatively large accumulation model serving as a sink for nucleating and condensing materials.

We see the accumulation mode actually increase in concentrations after accounting for dilution. It should be noted that the background particle size distribution has very little impact on the overall analysis, as the background particle concentrations is nearly two orders of magnitudes lower than that on Plane 7. It is unclear what would cause such a large increase. There are only a couple physical processes that could cause such a behavior:

- PM emissions at the stack level drift toward higher values during the sampling even at steady state operations.
- Particles are not following the streamlines of the flow the way a tracer would, and the accumulation mode is diluting slower than the tracer. This would be a reasonable explanation for much larger particles, but it is highly unlikely that this is the case for 200 nm particles and smaller;
- Condensation of smaller particles is causing a growth in the larger size range. However, we do not see any significant shift in size for either nucleation mode (centering around 12 nm) or accumulation mode (centering around 200 nm). One exception is that the median diameter for the accumulation grows from 100 nm in Plane 1 to 200 nm in Plane 2. Additionally, the time scale is very short for this type of process to take place (on the order of 1 second or less).

.

5.2.2 Pre2007 – 20 MPH

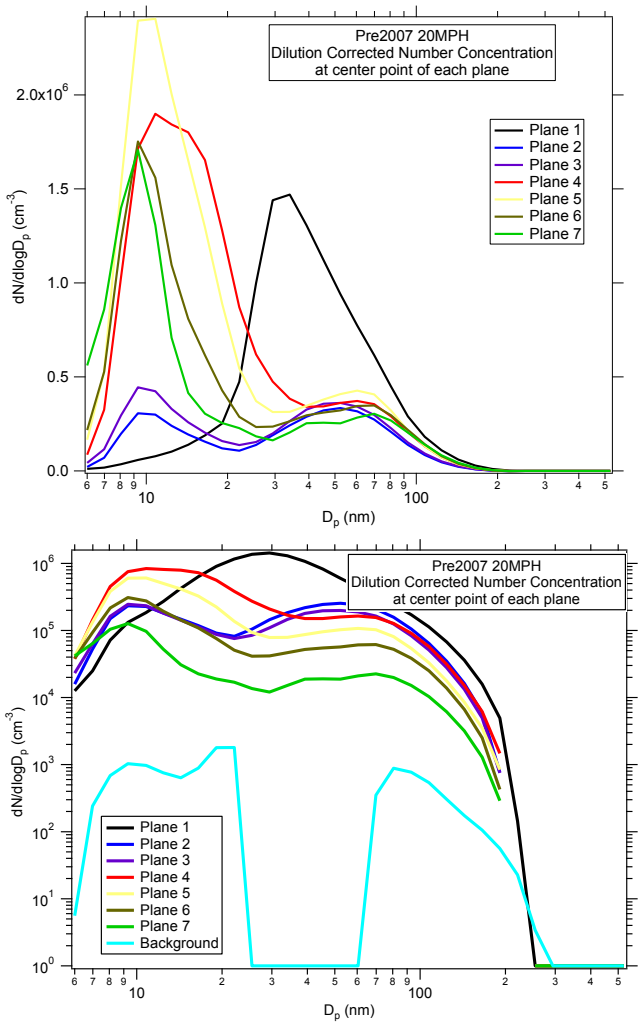

Figure 5-6: Dilution-corrected particle size distributions for Pre2007 20 MPH case; (a): linear scale; (b): logarithm scale

Figure 5-6 shows the PSDs at the center point of each plane corrected for the dilution of CO_2 at the same point for the Pre2007-20MPH case. Once again, accumulation mode particles are expected to dilute at the same rate as the tracer, and this is actually observed (Figure 5-6a) except for the Plane 1, where the PSD is unusually high. We observe a much stronger nucleation for the 20 MPH case than the Idle case. The nucleation mode particles can be seen growing, reaching a maximum around Plane 4 and then diluting with the tracer. Overall, this data behaves generally how we expect it to.

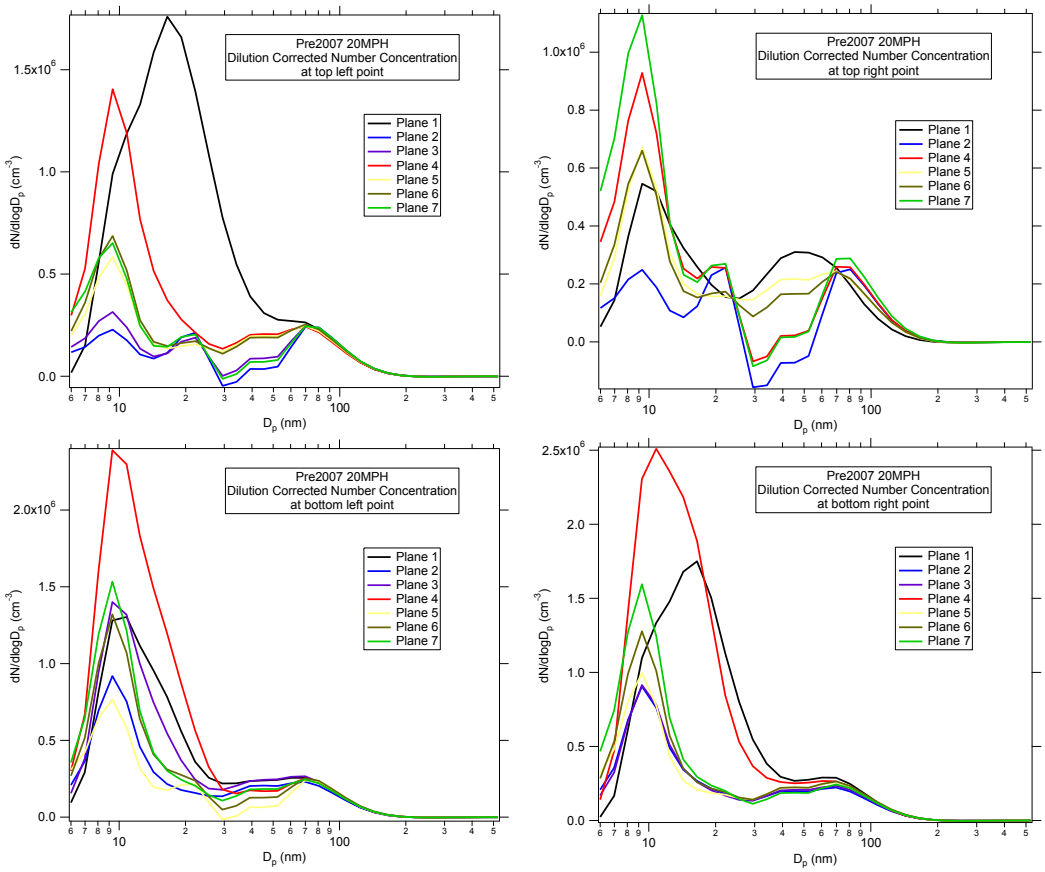

Figure 5-7: Dilution-corrected particle size distributions for Pre2007 20 MPH case at sampling points surrounding the center point

To further verify whether the accumulation mode particles dilute as tracer gases, we plotted the dilution-corrected PSDs for some points off the center (Figure 5-7) to verify the hypothesis that dilution-corrected accumulation mode particles should remain more or less unchanged regardless the spatial locations. The four subplots show a trajectory following the 4 points immediately surrounding the center point. In all of these figures, we can see that the accumulation mode is roughly constant over all planes. We also see the general trend in the nucleation mode where it initially grows and then shrinks slightly.

5.2.3 Pre2007 – 35 MPH

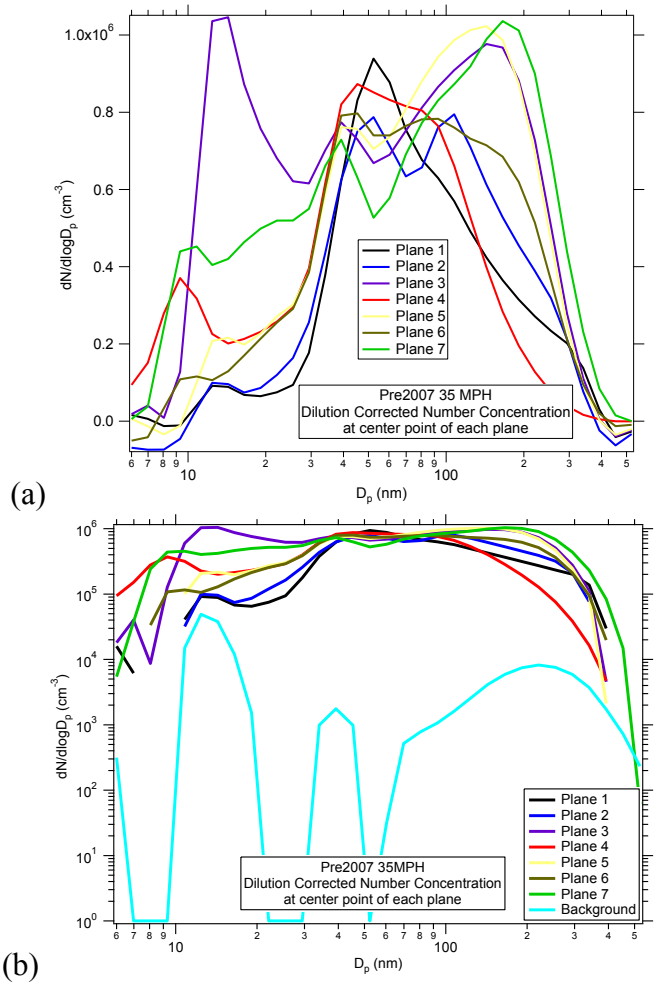

Figure 5-8: Dilution-corrected particle size distributions for Pre2007 35 MPH case; (a): linear scale; (b): logarithm scale

Figure 5-8 shows the PSD for the Pre2007-35MPH case. The background particle concentrations are noticeably higher, and the shape of the background PSD is unusual. It is difficult to distinguish different planes in Figure 5-8, so Figure 5-9 shows a few of the individual planes plotted at the center points and two nearby points.

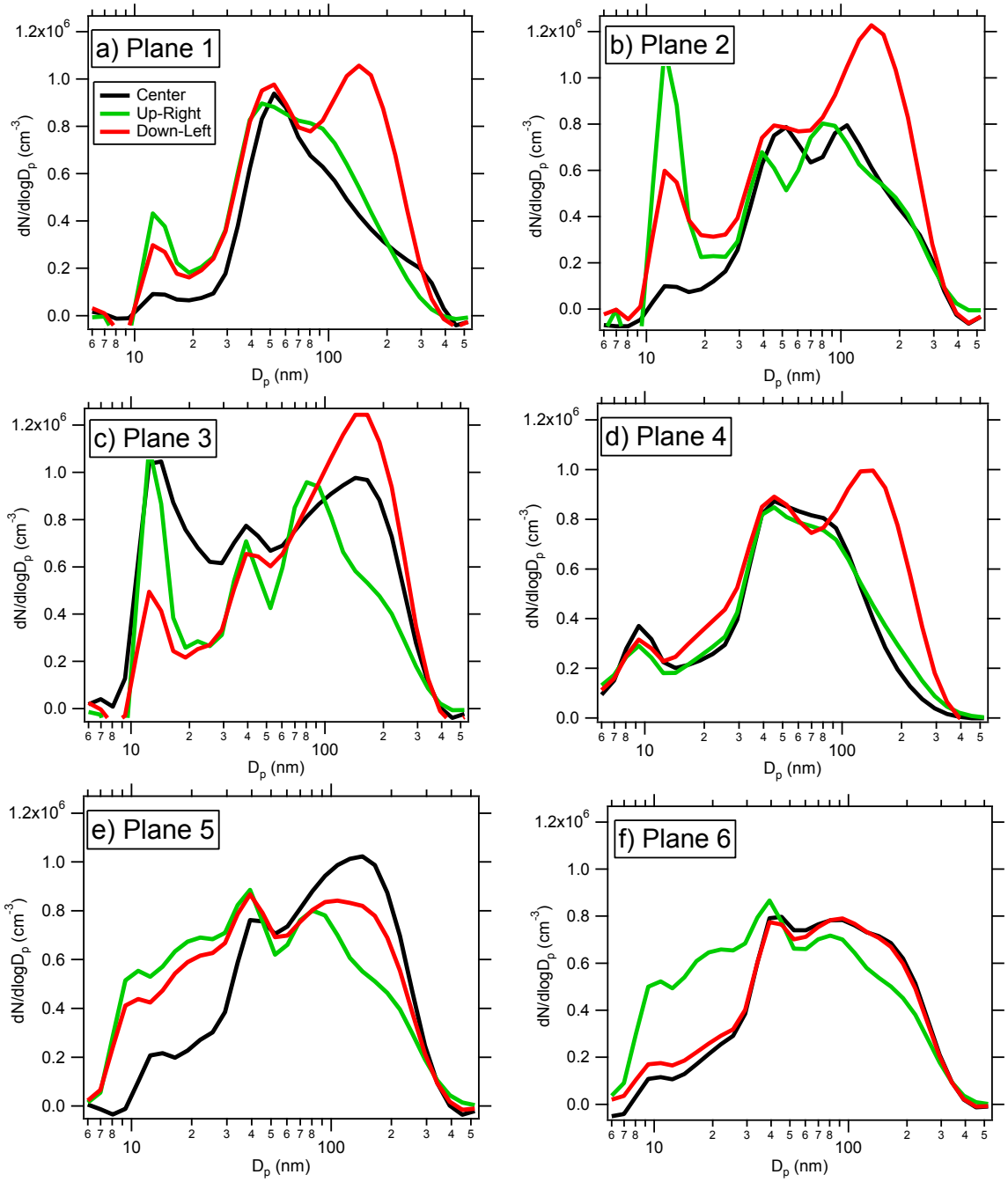

Figure 5-9: Size distributions at different planes for Pre2007 35 MPH case

First, a three-mode distribution (12 nm, 40 nm and 200 nm) starts appearing at Plane 2, persists on Plane 3, disappears on Plane 4, and reappears on Plane 5. This three-mode distribution is actually already present in an off center point on Plane 1. The nucleation mode grows as expected in the early planes, but then shrinks rapidly between Plane 3 and Plane 4.

5.2.4 Post2007 – Idle

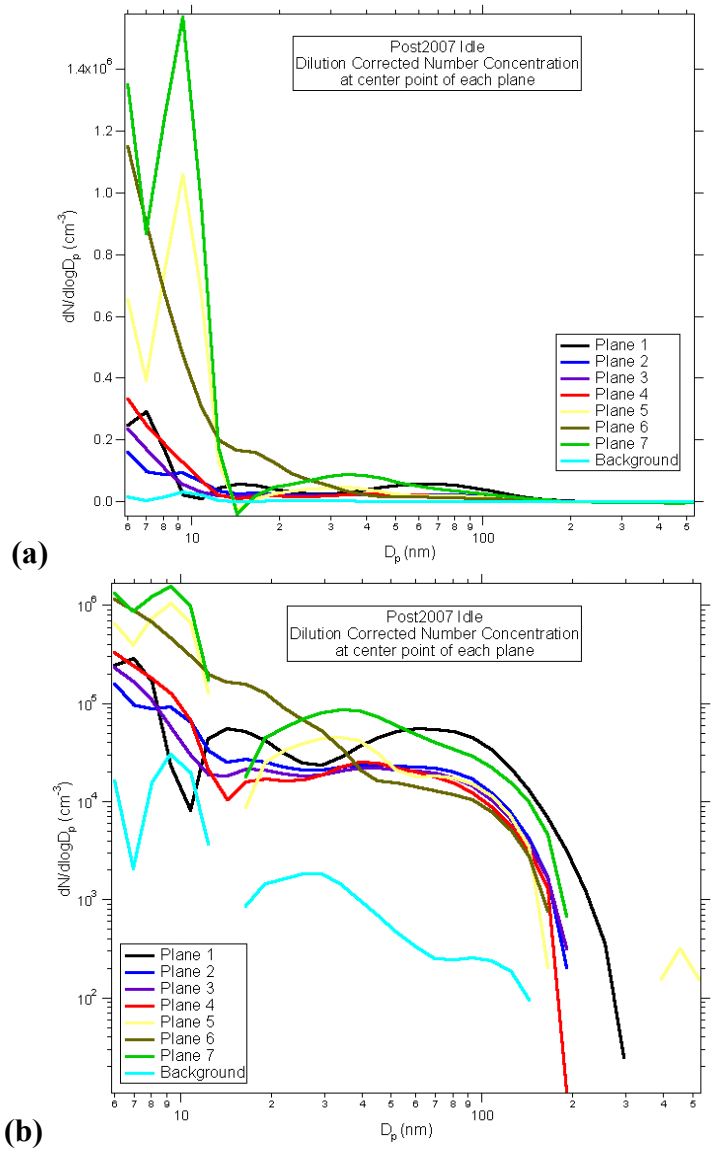

Figure 5-10: Dilution-corrected particle size distributions for Post2007 Idle case; (a): linear scale; (b): logarithm scale

The Post2007 truck has a cracked DPF so that the accumulation mode particles are higher than expected for a truck with a working DPF. The main challenge for analyzing the Post2007 data is that it is not clear how the cracked DPF affected the emission characteristics, since we do not have another Post2007 truck with a working DPF to compare against. Clearly, a nucleation event takes place for the Idle case.

5.2.5 Post2007 – 20MPH

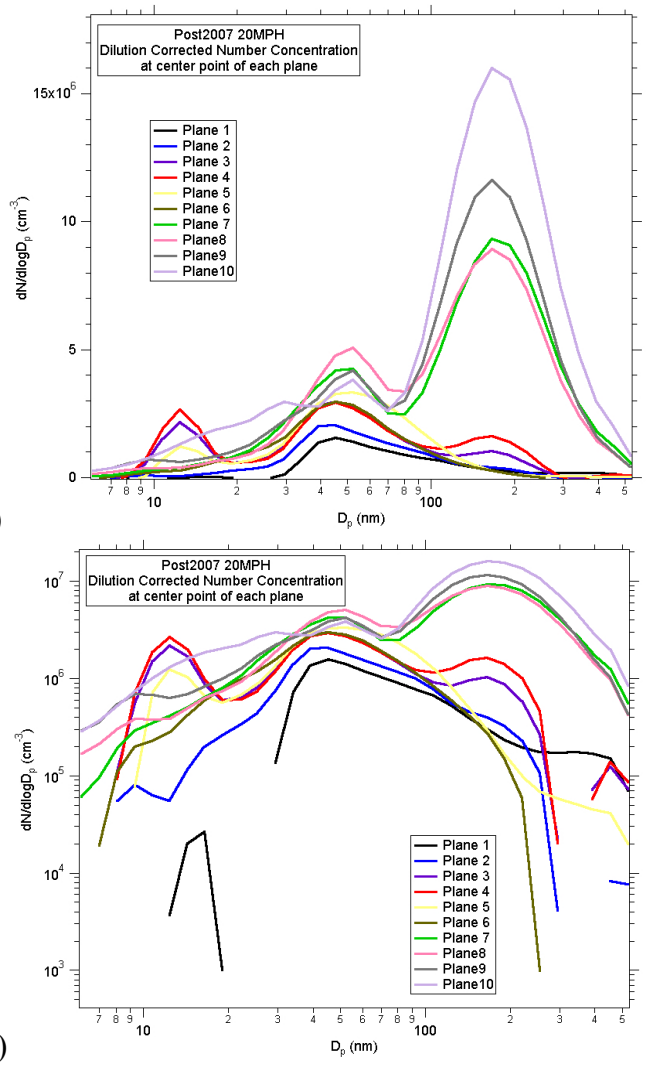

Figure 5-11: Dilution-corrected particle size distributions for Post2007 20 MPH case; (a): linear scale; (b): logarithm scale

In the Post2007 20MPH case (Figure 5-11) we see the growth of the accumulation mode further from the stack. Additionally there is a third mode centered around ~200nm which grows, disappears, and then grows extremely large by Plane 7. There are three important points that need to be emphasized. First, the relatively high accumulation mode concentrations for this Post2007 truck is due to a crack in the DPF. Therefore, the Post2007 and Pre2007 trucks have similar accumulation model concentrations. Second, the usually high accumulation mode particle concentration on Plane 7 is likely due to a DPF regeneration event. The high particle concentrations persist on Planes 8, 9 and 10. Third, the regeneration event changes the general trend observed for nucleation mode particles. As mentioned earlier, the general trend is that nucleation model particles first grow and then shrink. This trend is observed from Plane 1 to 6. The regeneration event starting from Plane 7 leads to increase in nucleation-mode particle concentrations, thus making a grow-shrink-grow phenomenon.

5.2.6 Post2007 – 35 MPH

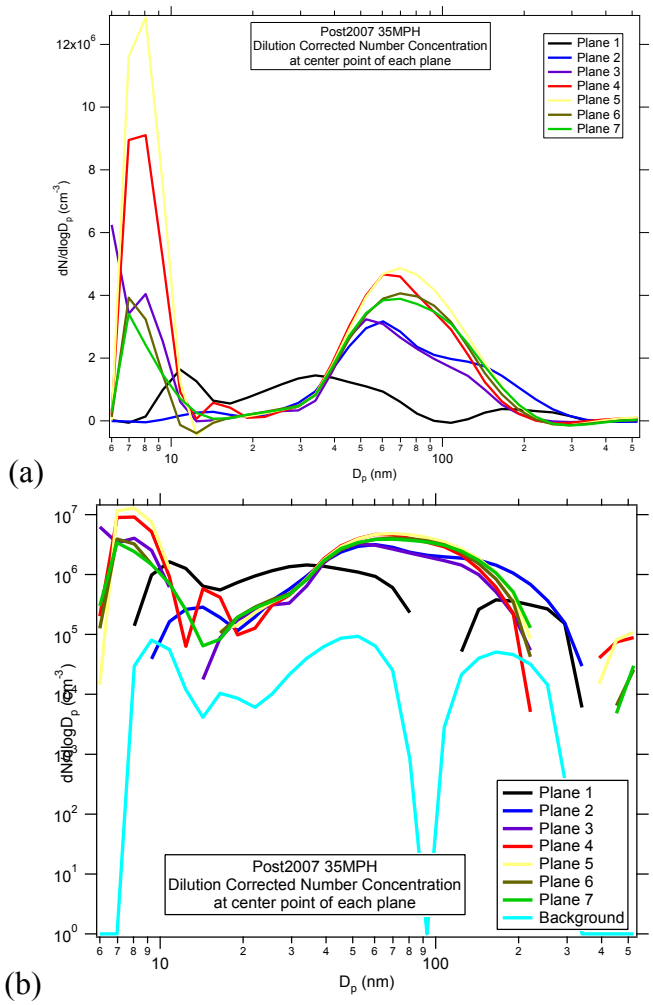

Figure 5-12: Dilution-corrected particle size distributions for Post2007 35 MPH case; (a): linear scale; (b): logarithm scale

For this case, the researchers conducted the experiments observed a regeneration event prior to the testing. Therefore, the 35mph Test started with a newly regenerated DPF. The researchers who conducted the measurements believe that the DPF would initially has a lower efficiency (due to lack of PM buildup above the filter walls), and then gains the efficiency back around half way through the test. If this were indeed the case, we would have observed a higher dilution-corrected accumulation mode when the DPF has a lower efficiency, and a lower dilution-corrected accumulation mode when the DPF has a higher efficiency. But this is not what Figure 5-12 indicates. The accumulation mode concentration on Plane1 is relative low compared to those on the rest of the planes. Figure 5-12a suggests that dilution-corrected accumulation mode keeps an increasing trend throughout the test. It indicates that the cracked DPF is still not working properly.

5.2.7 Post2010 - Idle

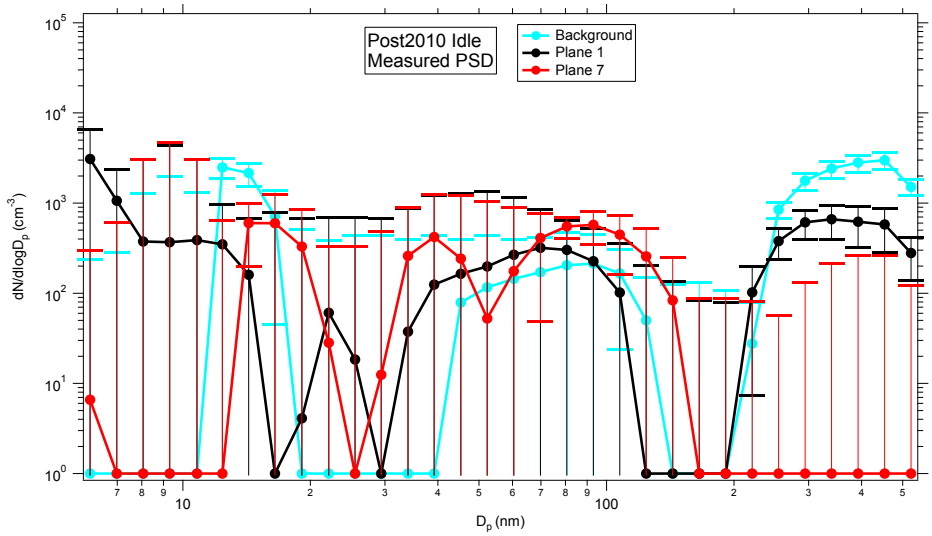

Figure 5-13: Particle size distributions for Post2010 Idle case

Recall that dilution-corrected NOx for Post2010 Idle case shows unstable behavior (Figure 5-3). Thus, we only plot the non-corrected PSDs in Figure 5-13. In general, the particle concentrations are close to the background level.

5.2.8 Post2010 – 20 MPH

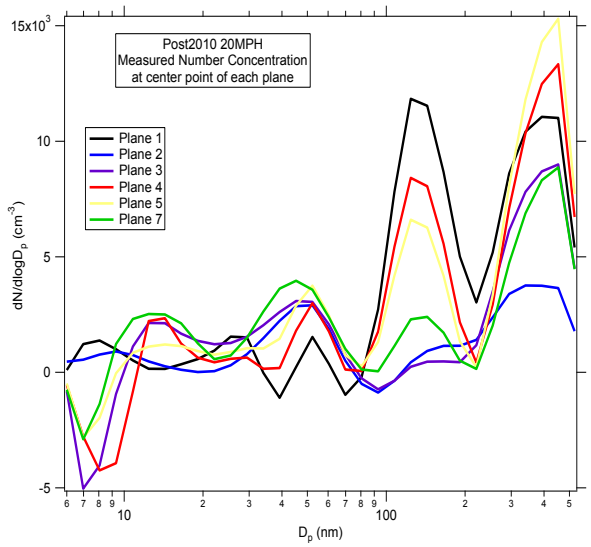

(a)

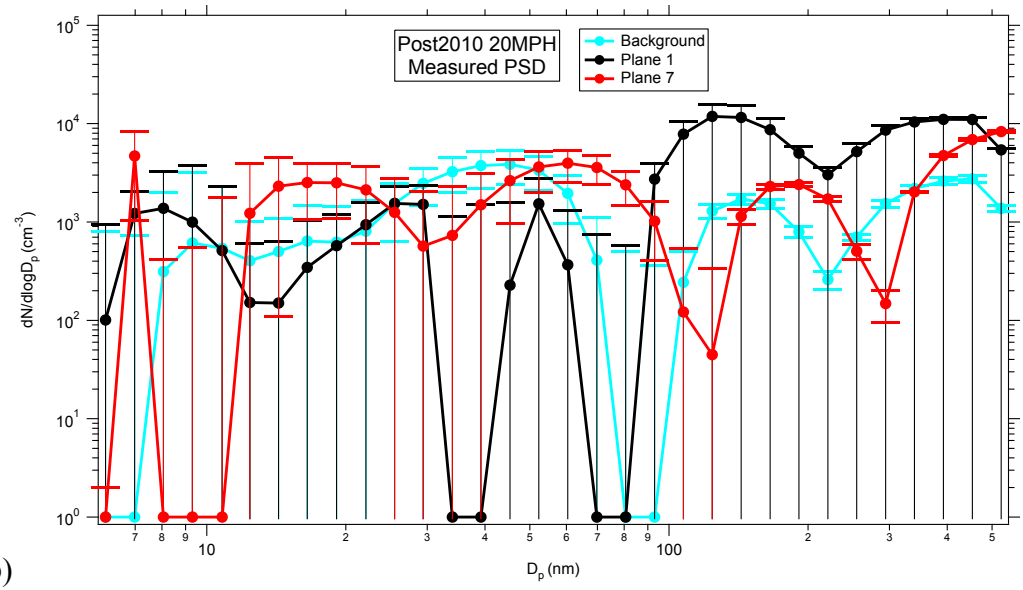

(b)

Figure 5-14: Dilution-corrected particle size distributions for Post2010 20 MPH case; (a): linear scale; (b): logarithm scale

The post2010-20MPH data recorded the lowest particle number concentrations among all cases during the entire wind tunnel experiment (Figure 5-14). In general, the particle concentrations are close to the background level except for particles larger than 100 nm. Additionally, there are a number of negative values seen in these data (not shown in Figure 5-14).

5.2.9 Post2010 – 35 MPH

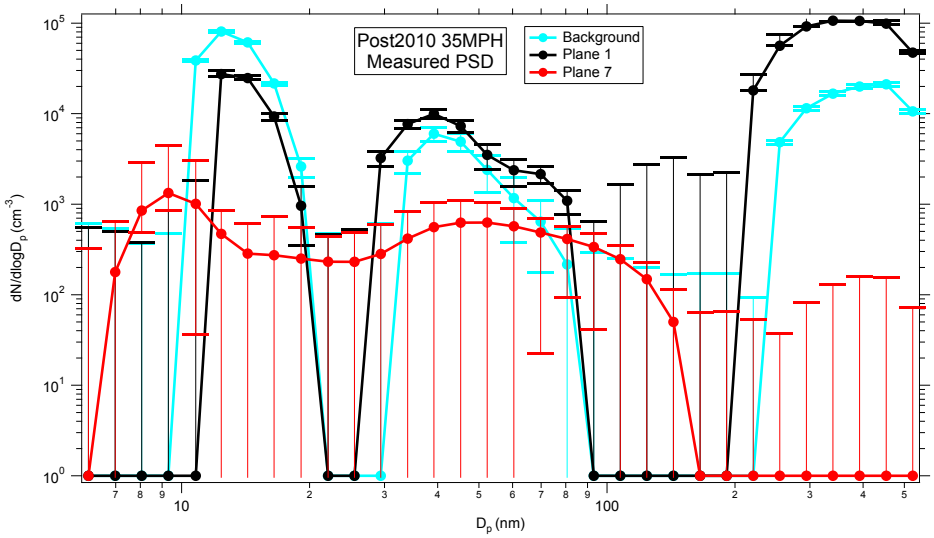

Figure 5-15: Particle size distributions for Post2010 35 MPH case

Once again, for the Post2010 35 MPH case, the particle concentrations are close to the background level except for particles larger than 200 nm (Figure 5-15).

6. Summary and Conclusion

The main research objective of this project was to advance our understanding on how dilution conditions affect the measurement of diesel particulate matter. To bridge the laboratory dilution tunnel testing and on-road mobile platform sampling (with atmospheric dilution), we measured and analyzed the evolution of three types of diesel engines (Pre2007, Post2007 and Post2010) under three different speeds (Idle, 20 mph and 35 mph) in a wind tunnel.

The plume properties including temperature, velocity, CO_2 and NOx concentrations, black carbon concentration, and particle size distributions were measured at 130 sampling points divided into 10 planes. In parallel to the wind tunnel experiment, the same engine exhaust was also measured using a two stage dilution systems at the same time.

Our data analysis indicate the following preliminary results:

- Based on Pre2007 truck results, we have observed a qualitatively consistent trend for nucleation mode particles. First, nucleation takes place; Then, nucleation mode particle grow in size and their concentrations increase; Next, at further distance, they shrink in size and their concentrations decrease. This general behavior is analogous to what has been observed near roadways.
- Compared to pre-2007 trucks, the number concentrations in post-2010 trucks have been greatly reduced. Particle concentrations in the plumes of Post2010 truck are comparable to the ambient background levels, given the uncertainties in the aerosol instrumentation.
- A DPF regeneration event was observed during the test of Post2007 truck, leading to highly elevated accumulation mode and nucleation mode particle concentration.

There are still a number of uncertainties and unexplainable behaviors in the datasets.

- The unusually volatile behaviors of the accumulation-mode particles in very short residence time (~1-2 seconds) have been observed, though the accumulation-mode particles were expected to experience little change other than dilution, as shown in Lipsky and Robinson (2005) and Ronkko et al., (2006). In many cases, dilution-corrected accumulation mode particles were shown to grow in concentrations substantially. In some cases, there are three modes of particles instead of classical two-mode distribution. We originally planned to employ the CTAG model to simulate the wind tunnel experiment. However, there are no mechanisms currently incorporated in the CTAG model that are able to explain the volatile behaviors of the accumulation-mode particles given the short residence time. Simulating new particle formation has been the strength for the CTAG model and was the original area of interest for this project. However, the large uncertainties in simulating accumulation-mode particles will lead to large uncertainties in simulating nucleation-mode particles. The volatile behaviors of the accumulation-mode particles could be due to sampling errors or new physical process unknown to the research community. But until we can identify the cause(s) for those behaviors, aerosol dynamics simulations will reveal little new information.

- *Second*, the Post2007 truck was found to have a cracked DPF, which makes the comparison between Pre2007 and Post2007 trucks less meaningful. Furthermore, the actual impact of the cracked DPF is complicated by several DFP regeneration events.
- *Third*, the results from the Post2010 truck appear to be indistinguishable from the background conditions, even though quantitative uncertainty analysis has not been conducted due to incomplete datasets.

This project shows both promises and risks associated with wind tunnel measurements of diesel exhaust. On one hand, large amounts of data have been generated from this study, which provide valuable information on the evolution of particle size distributions, which cannot be easily observed in laboratory dilution tunnel testing or on-road sampling. On the other hand, the wind tunnel experiments and corresponding modeling efforts have to be carefully designed and executed to yield reliable data, which then motivates us to provide the recommendations about the future of this type of studies.

7. Recommendations

The objectives of the recommendations describe are twofold: 1) to fully take advantage of the existing wind tunnel experimental data given the limited time spent on data analysis due to project completion; and 2) to provide guidance for future wind tunnel studies.

First, follow-up analysis and modeling of the datasets are needed to verify whether the unexplainable behaviors are due to instrumentation errors/limitations, weakness in sampling designs, or are true physical phenomena. For example, the analysis described in Section 5.1 identified the malfunctions of NOx or CO_2 sensors. In terms of modeling, the analysis suggests that time-varying inlet boundary conditions are required for the non-circulating wind tunnels. Due to the time constrain, the datasets have not been fully investigated and modeled. The additional efforts will help reveal the nature of diesel particulate matter in the atmosphere.

Second, after the further analysis and modeling described above, a review of lessons learned from the wind tunnel experiment is necessary. Even though the wind tunnel measurement holds great promise in advancing our understanding of diesel particle matter, this study also suggest a need to improve the sampling plan and instrument reliability to make sure the wind tunnel measurement will deliver the promise.

8. References

Herner, J. D.; Hu, S.; Robertson, W. H.; Huai, T.; Chang, M.-C. O.; Rieger, P.; Ayala, A. Effect of advanced aftertreatment for PM and NOx reduction on heavy-duty diesel engine ultrafine particle emissions. *Environmental Science & Technology* **2011**, *45*, 2413–9.

Lipsky, E. M.; Robinson, A. L. Design and evaluation of a portable dilution sampling system for measuring fine particle emissions from combustion systems. *Aerosol Science and Technology* **2005**, *39*, 542–553.

Park, S. S.; Kozawa, K.; Fruin, S.; Mara, S.; Hsu, Y.-K.; Jakober, C.; Winer, A.; Herner, J. Emission Factors for High-Emitting Vehicles Based on On-Road Measurements of Individual Vehicle Exhaust with a Mobile Measurement Platform. *JOURNAL OF THE AIR & WASTE MANAGEMENT ASSOCIATION* **2011**, *61*, 1046–1056.

Rönkkö, T.; Virtanen, A.; Vaaraslahti, K.; Keskinen, J.; Pirjola, L.; Lappi, M.; Ronkko, T. Effect of dilution conditions and driving parameters on nucleation mode particles in diesel exhaust: Laboratory and on-road study. *Atmospheric Environment* **2006**, *40*, 2893–2901.

Appendix

2. Wind Tunnel Facility

2.1. Design

We originally proposed to characterize the physical and chemical evolutions of the exhaust plumes in the National Full-Scale Aerodynamics Complex (NFAC) in NASA Ames Research Center. However, NFAC had not been able to confirm the test dates. Without the confirmed test dates, the experiment could be canceled with a last-minute notice from NFAC and Department of Defense, which manages the NFAC facilities. It was deemed too risky to use the NFAC wind tunnel for this project, and decided in June 2010 to seek alternative facilities to continue the project. Since then, several full-scale wind tunnels across the U.S. were evaluated, but were inevitably deemed unsuitable, due either to design/performance characteristics or availability. Two prime criteria were identified: the tunnel needed to be an open-circuit configuration and it must provide for a minimum of 100 feet of sampling zone downstream of the test section, for plume interrogation. The length criterion was based upon work conducted by in the NASA Langley Wind Tunnel facility. These results indicated that CO_2 concentration, temperature, and dilution ratio in the plume of a heavy-duty truck emitted in a 55 mph wind speed stabilized at a distance of approximately 40 feet from the vehicle exhaust stack. Neither of the two criteria was met by any of the tunnels that were investigated. The final solution was reached in October that a full-scale wind tunnel would be constructed at West Virginia University (WVU) for this project. At the same time, the aerosol dynamics modeling component was added to the scope of work in order to augment the analysis from the limited experimental data.

There are significant advantages, as listed below, to building the new tunnel and conducting tests at WVU:

a. There will be full access to the tunnel and the equipment at all hours of the day
b. There will be no restriction on personnel who can work on the facility at WVU.
c. The logistics and time factors of traveling to NFAC would have been a major drain on the budget of this study.
d. The project team does not have to satisfy the stringent requirements on our equipment (size, weight, power requirements, data cables, etc.) that the NFAC facility demanded. In fact, in order to satisfy their requirements we would have had to drop some of the experiments we were planning on conducting because we would be unable to meet their demands or the costs of meeting the requirements were prohibitive.
e. As a result of the flexibility and reduced size, more arbitrary control of dilution air conditions could be afforded, thus providing increased parametrics.

2.1.1. Comparison between the NFAC and WVU wind tunnel designs

The NFAC wind tunnel is an open circuit type with a closed, rectangular test section, which is 24 m high and 37 m wide. Test section speed in the tunnel is continuously variable from nearly 0 to 50 m s^{-1} (or about 110 mph). The tunnel would have afforded us a 115ft downwind distance to measure the plume evolution.

The WVU wind tunnel is also a full-scale, open-circuit, suction tunnel. The test section is 16ft high and 16ft wide and will house the cab (and the wind cowl) of a heavy-duty truck. This tunnel will employ a 2,200 HP suction fan to provide up to 14 m s^{-1} (or 32 mph) flow rate. The preliminary computational fluid dynamics (CFD) simulations on the flow fields inside the proposed wind tunnel design show that the main mixing events behind the truck agree with the actual turbulent flow field measurements reported by Gautam et al. (2003) [1].

2.1.2. Wind tunnel geometry and aerodynamics

2.1.2.1. Design target and constraints

The target is the identification of a Wind Tunnel capable to accommodate a full scale mock-up truck, guarantee a wind speed of 35 mph with a plume aging of 2s over the entire length of the wind tunnel test section, and comply with turbulence and quality flow standard identified for this project. In addition, a system containing the instruments needs to able to move in three dimensions in the tunnel in order to identify the plume characteristics. These target and constraints bring several structural aerodynamic and structural challenges.

2.1.2.2. Design main parameters

The target and constraints allows the project team to identify and define the main parameters of this Wind Tunnel, mainly related to its dimension and velocity field. SolidWorks© has been chosen as CAD software for the design process. An illustration of the design is shown in Figure 1.

Figure 1: Wind Tunnel in "Pulling" configuration

The WVU design is a classic "pulling" tunnel, where the truck is located upstream near the inlet, and the air is pulled inward into the test section and then pulled out through a suction fan at the far end of the tunnel (illustrated in Figures 2 and 3). A small convergent section, as well as a flow straightener, is positioned upstream of the test cell in order to stabilize the flow field. The flow straightener removes any swirl and axial fluctuations. A convergent loft surface connects the test cell to the fan section.

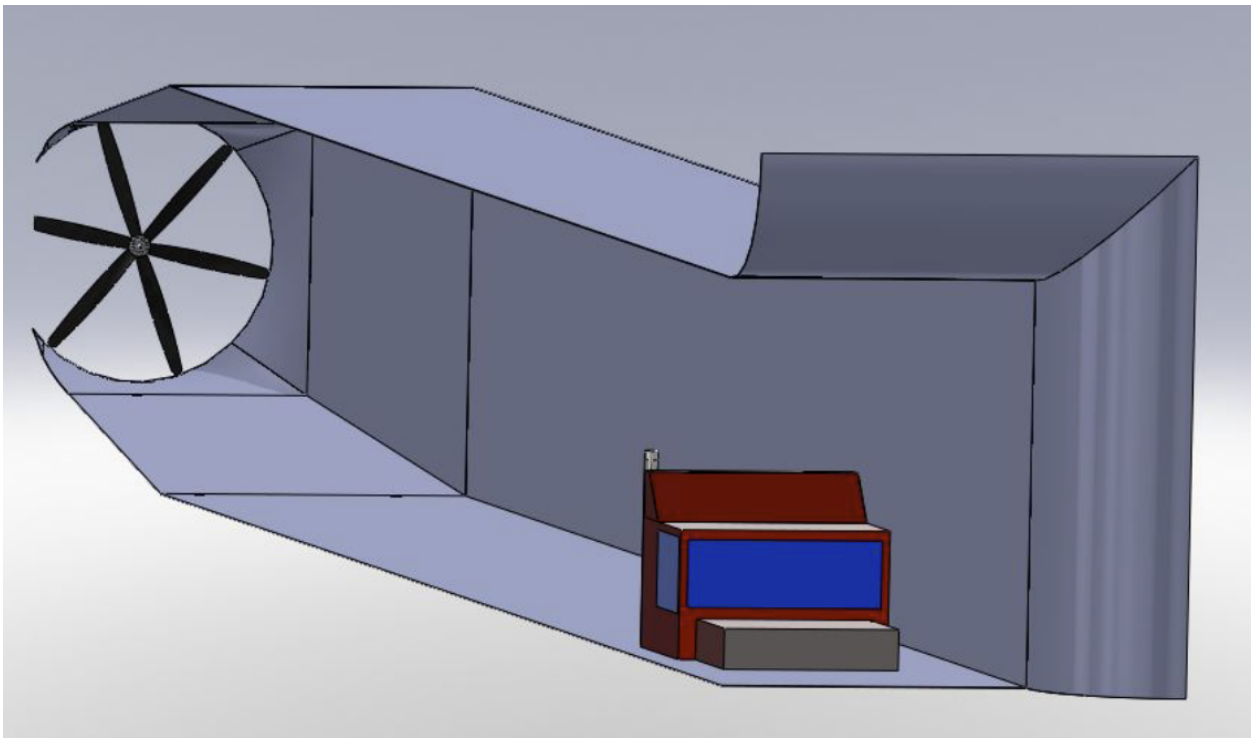

Figure 2: Wind Tunnel Inlet View

With a fixed budget, the "pulling" tunnel design is able to achieve better flow properties and longer sampling distances than a "pushing" design, since the "pushing" design would require a divergent and convergent section (which will increase the cost) to remove the swirling caused by the upstream fan. The preliminary computational fluid dynamics (CFD) simulations on the flow fields inside the wind tunnel design show that the main mixing events behind the truck agree with turbulent flow field measurements presented by Gautam et al. (2003).

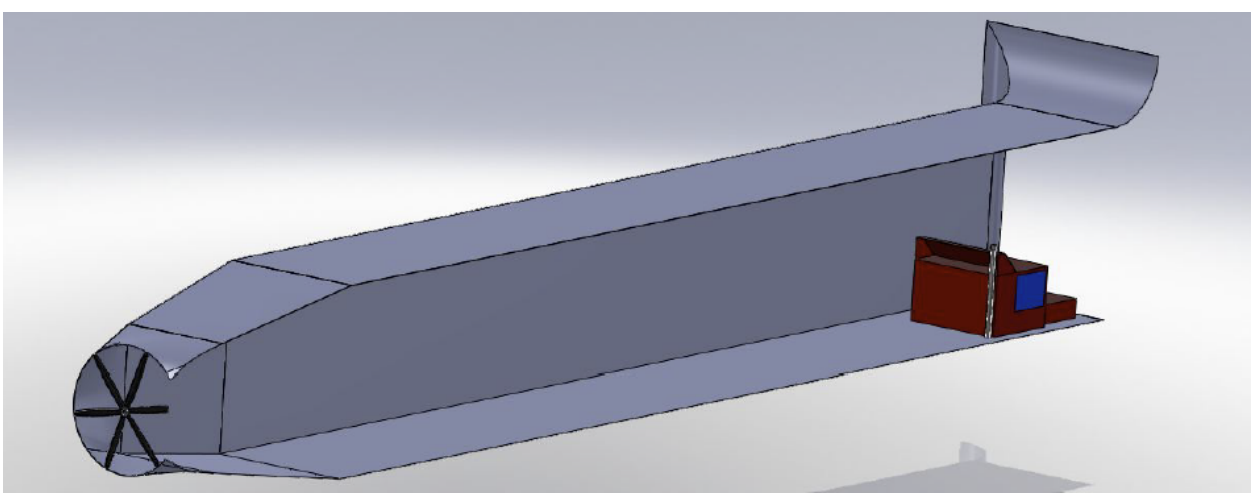

Figure 3: Wind Tunnel Outlet View

Considering that minimum dimensions of 5m x 5m were chosen to satisfy a maximum blockage of 20%, the tunnel section should be at least 30m long in order to give a 2 second plume residence time. Detailed CFD data are shown in Table 1.

Table 1: Wind Tunnel Computational Fluid Dynamics (CFD) Simulation Data

Parameter	Value	Unit
Test Cell Width	16	ft.
Test Cell Height	16	ft.
Truck Width	2.5	m
Truck Height	2	m
Blockage Model Area	20.0	%
Velocity	15.75	m/s
	35.02	mph
Flow Rate	393.75	m^3s^{-1}
	834,309	CFM
	1,417,500	$m^3\ hr^{-1}$
Pressure Drop (truck only)	1000	Pa
Pressure Drop (screen only)	200	Pa
Pressure Drop (accelerate)	100	Pa
Total Pressure Drop	1300	
DP Amp factor	1.2	-
Propeller efficiency	0.7	-
Total Power	878	Kw
	1170	HP

The wind tunnel structure was built of wood and steel construction. All internal surfaces were sanded, and plywood joints were massaged so as to minimize flow disturbance. The entire structure is covered with paint to protect outside and reduce drag inside the wind tunnel. A loft connection from the circular section of the propeller to the square section of the diffuser was constructed.

2.1.2.3. Aerodynamics Simulations and Analyses

As described in the previous paragraph CFD simulations have been executed to identify the plume evolution.

The following images (Figure 4: Wind Tunnel Aerodynamics Blockage Effect Image and Figure 5: Wind Tunnel Aerodynamics Blockage Effect Image) clearly show that the blockage effect of the truck corresponds to the limits defined by the project. The edgy version of the mock-up was defined intentionally to maximize the aerodynamics effects of a general truck.

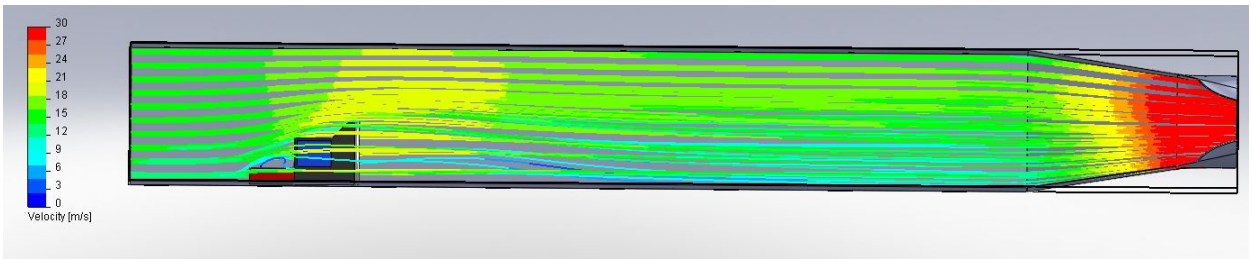

Figure 4: Wind Tunnel Aerodynamics Blockage Effect Image

Because of the simplicity of these analyses, CosmosFlow© was used as part of the feature of SolidWorks©.

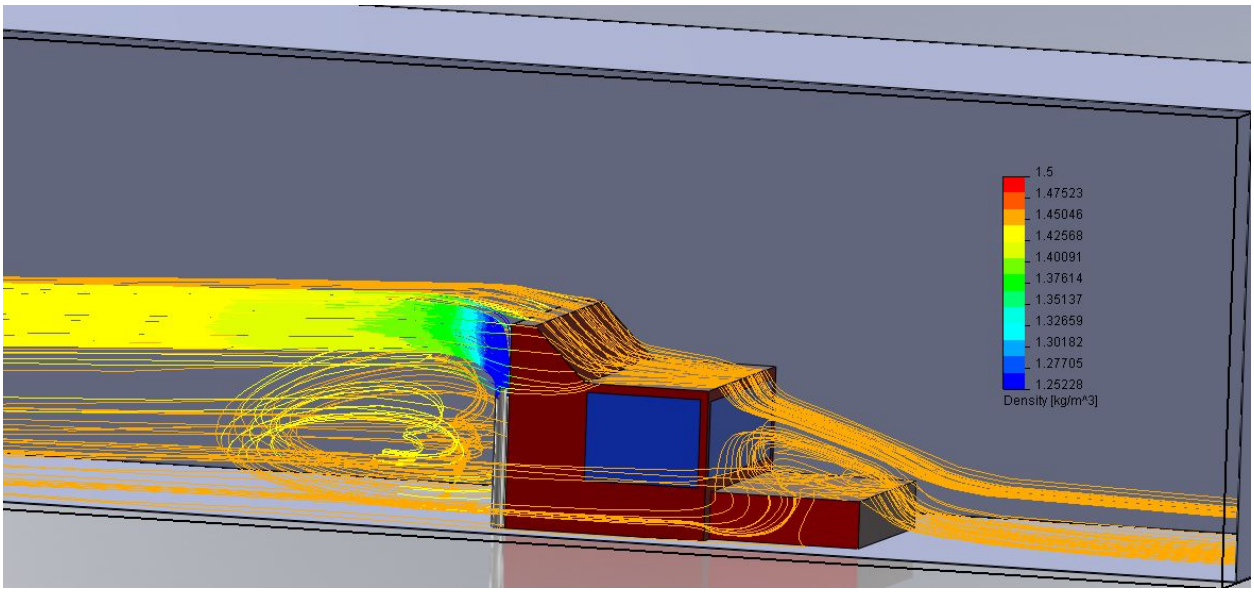

Figure 5: Wind Tunnel Aerodynamics Blockage Effect Image

The following image (Figure 6: Wind Tunnel Aerodynamics Plume Velocity Image) indicates that the plume reaches the wind velocity in few meters.

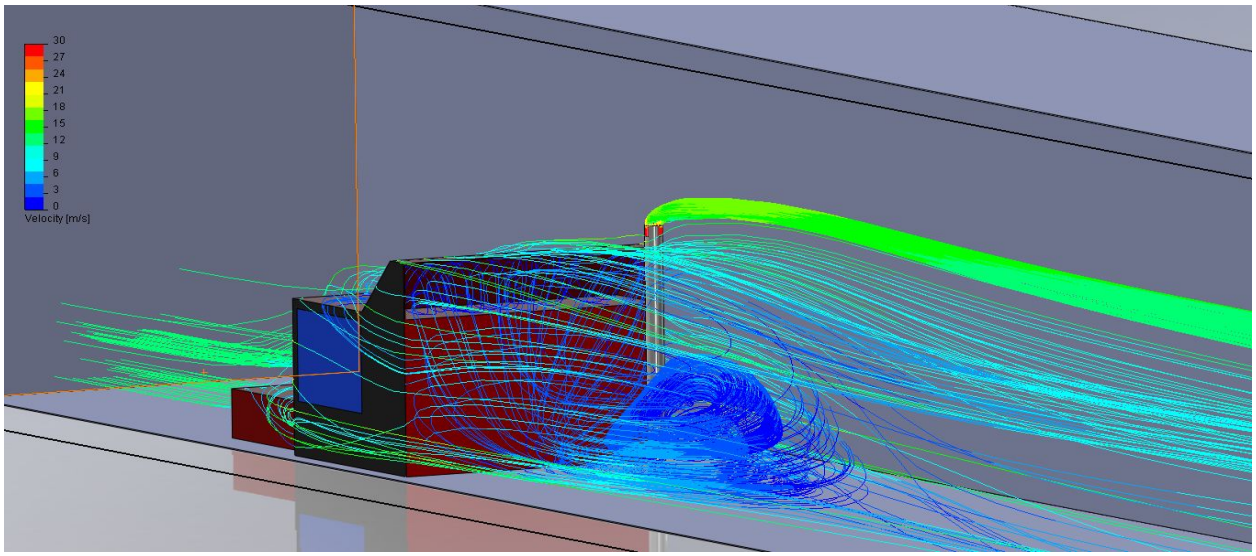

Figure 6: Wind Tunnel Aerodynamics Plume Velocity Image

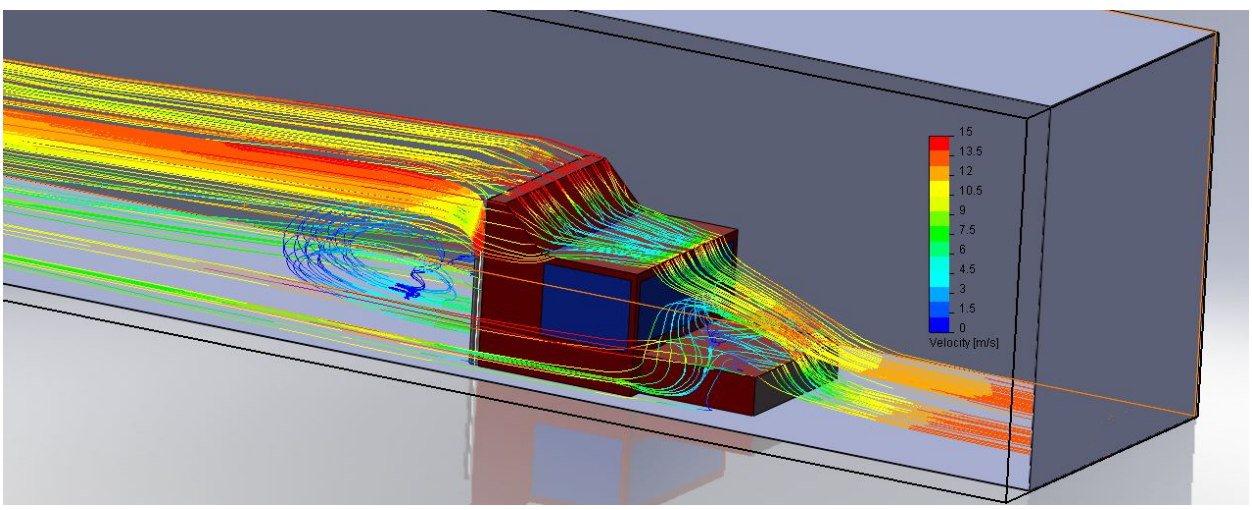

Figure 7: Wind Tunnel Aerodynamics

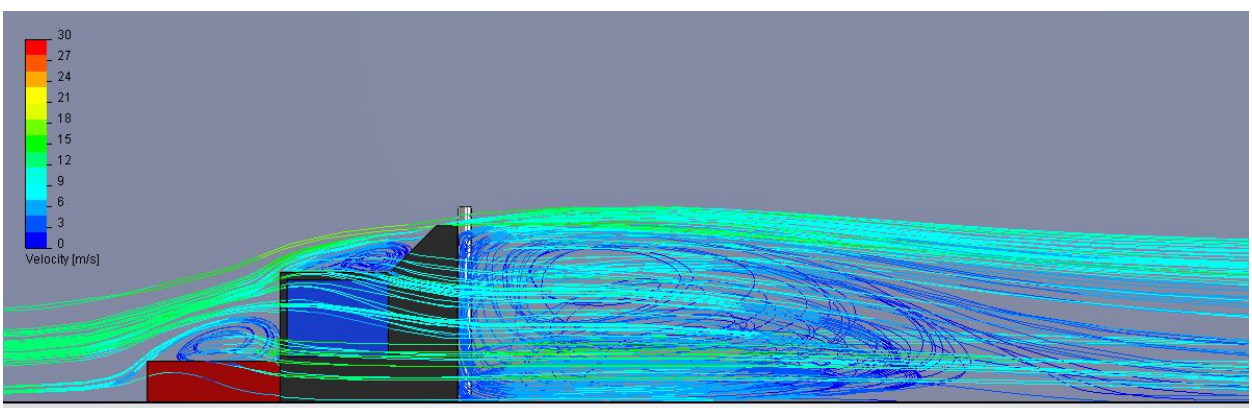

Figure 8: Wind Tunnel Aerodynamics

It results interesting the different exhaust and background air mixing occurring with the two

stack exhaust configurations in Figure 6: Wind Tunnel Aerodynamics Plume Velocity Image and Figure 7: Wind Tunnel Aerodynamics. In the first one the exhaust stack is higher than the wind fairing and the plume assume tubular shape. Instead, in Figure 7: Wind Tunnel Aerodynamics a lower exhaust stack generate a more rapid and effective mixing, thus with a potential influence on the volatile compound of the PM and the particle size distribution.

The growth of the boundary layer over a long Wind Tunnel could provoke an increase in the average velocity (for the region outside the boundary layer) [3]. In addition, this leads to a decrement of static pressure and the formation of floating force in the longitudinal direction of the Wind Tunnel. The solution is to diverge the section of wind tunnel with the value of the Displacement Thickness, which is defined as the theoretical distance by which a surface has to be moved parallel to itself (towards the reference plane) in-order to yield the same mass rate for an inviscid fluid as would be realized by a viscid fluid in the original geometry. Assuming the flow to be incompressible, we can then substitute the mass flow with volumetric flow to get the velocity profile. The Reynolds number for this Wind Tunnel, at the given conditions, indicates it is operating with turbulent flow. Applying the formula for a duct flow in turbulent conditions, it is possible to obtain the following plots. The first plot (Figure 9: Wind Tunnel Boundary Layer and Displacement Thickness Growth) indicates the Boundary Layer and Displacement Thickness growth over the length of the wind tunnel.

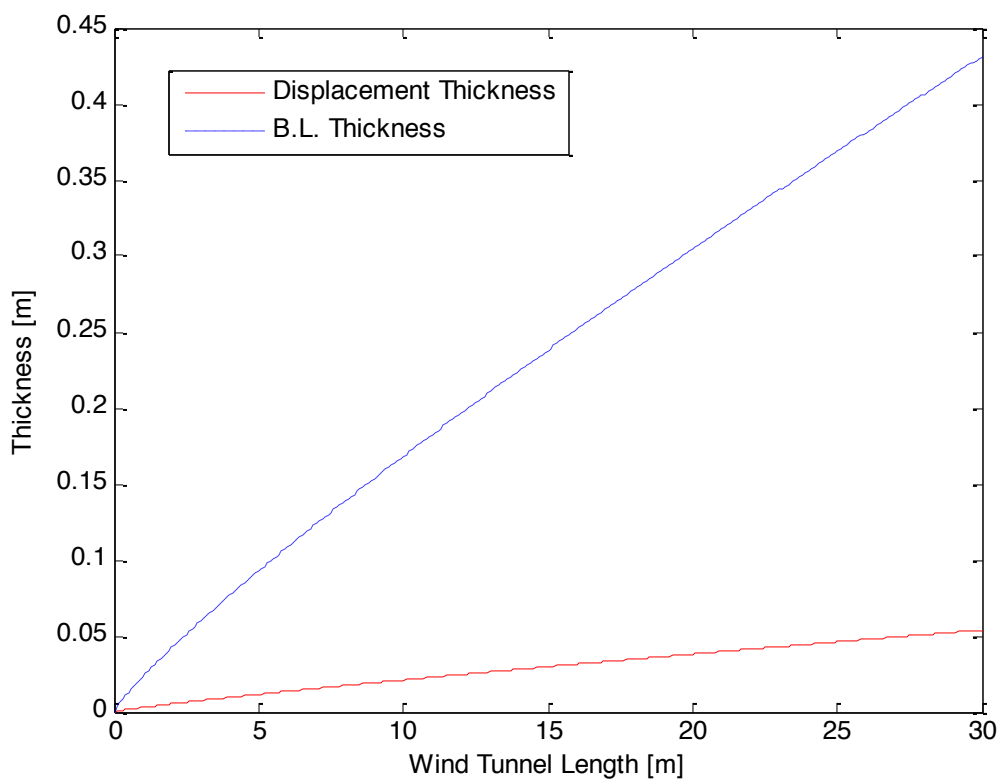

Figure 9: Wind Tunnel Boundary Layer and Displacement Thickness Growth

The previous plot clearly indicates that, in order to compensate the boundary layer growth, a 5cm diverge over 30m needs to be applied. Obviously, phenomena at this level could be neglected.

The effect for a range of wind speed centered on the 14 m/s designed speed was also modeled. In this case, the plot (Figure 10: Wind Tunnel Boundary Layer and Displacement Thickness at 30 m) shows the value of Boundary Layer and Displacement Thickness at 30 m distance. The Displacement Thickness remains almost the same for this range of velocity, thus the effect can be neglected for any conditions within the operating range.

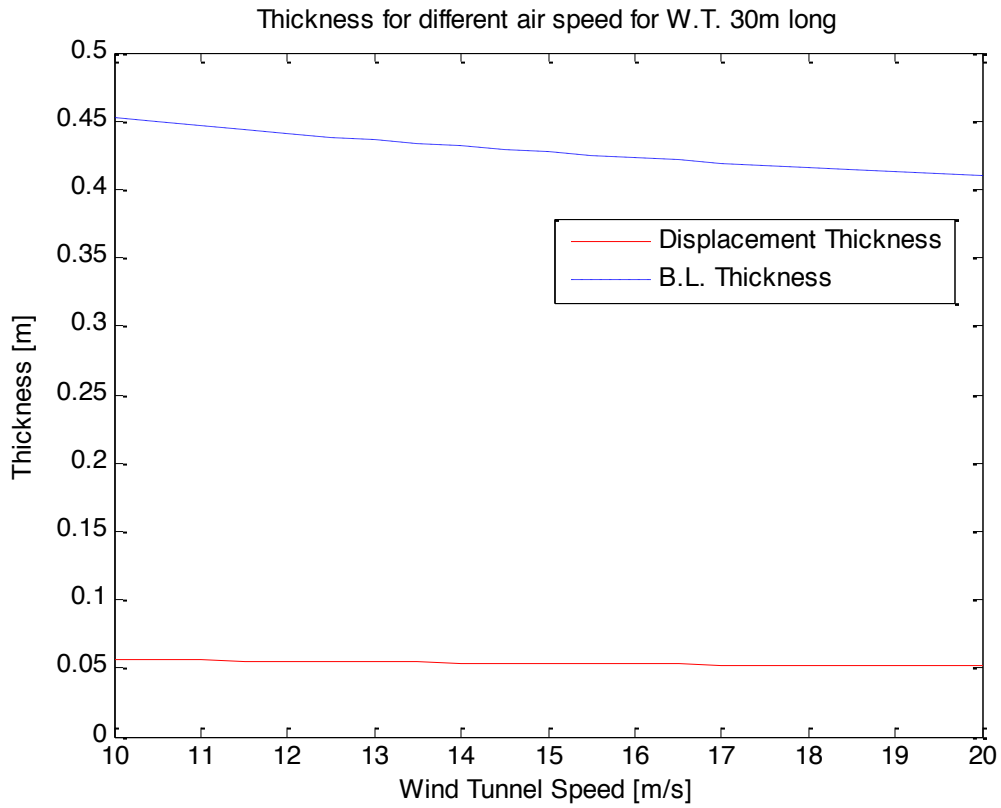

Figure 10: Wind Tunnel Boundary Layer and Displacement Thickness at 30 m

2.1.3. Structural Analysis

The needs of a specifically design Wind Tunnel for plume investigation arose several technical and structural problems. The detailed descriptions of the structural analysis can be found in the Appendix A.

2.1.4. Sampling Platform

2.1.4.1. Sampling Cart

Detailed plume analysis requires a system able to sample throughout the entire test cell, without affecting the dynamics of the flow itself. The instrumentation required to characterize the exhaust plume could not be placed within the flow field without strongly influencing it. However a single sampling probe could extract a localized fraction of the plume and redirect the sample to the instruments. In order to minimize the length of the transfer line connecting sampling probe and instrumentation and hence, the PM losses, a novel solution has been adopted by implementing a cart carrying the entire suite of instruments and moving longitudinally within the ceiling of the tunnel. Underneath the cart, and within the test cell, a gantry system spans the probe vertically and horizontally as depicted in Figure 11 and Figure 12. This configuration allows to sample throughout the cross-sectional area of the test cell, and to proficiently move the sampling probe around the truck model placed within tunnel. Position of the probe is monitored with 3 laser distance meters, capable of 1mm accuracy over the entire wind tunnel test cell.

Figure 11: Movable Platform during the installation

Figure 12: Sampling probe during velocity measurements

2.1.4.2. Wind Tunnel Reference System

The wind tunnel is defined as 3d Cartesian grid, where the origin sits on the lower left corner at the entrance facing the wind (Figure 13). In this way X represents the transverse coordinate, Y the vertical and Z the longitudinal ones. With this configuration, the exhaust reference coordinates are X=3263mm, Y=3415mm and Z=2845mm. All the points in the data file present the absolute coordinates.

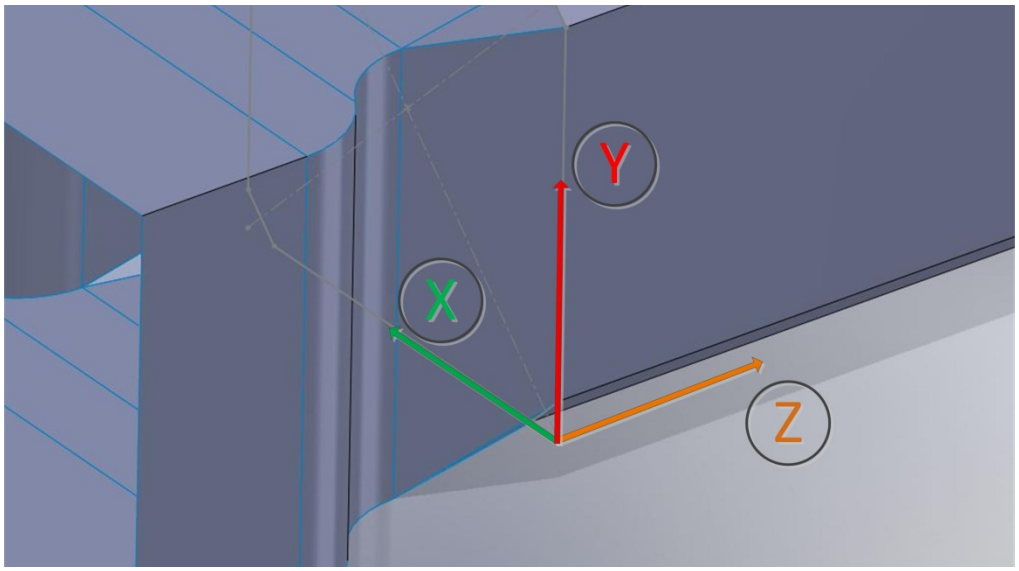

Figure 13: Wind Tunnel 3D Cartesian Reference System

2.1.5. Tractor cabin

In order to guarantee consistency of data among different tested trucks, the same cabin will be used inside the wind tunnel, as called mockup cabin. Guaranteeing the same aerodynamic mixing conditions between different engine technologies will better evidentiate their effect on PM. A Volvo day-cabin was selected as average representation of typical fleet cabins (Figure 14).

Figure 14: Mockup cabin during the installation in the Wind Tunnel test cell

With 3D camera recording and further surface refinement a CAD model of the cabin is obtained (Figure 15) as crucial component of the CFD model described in the following chapter.

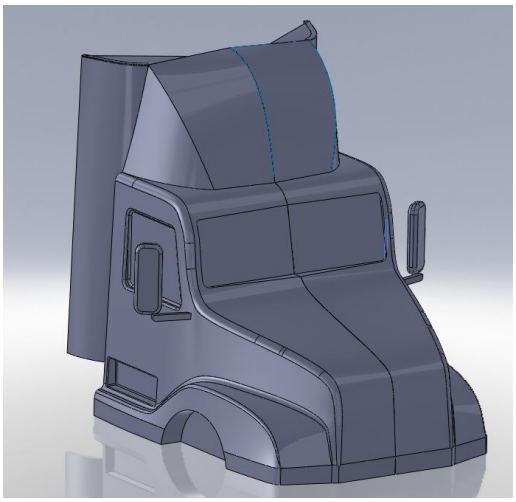

Figure 15: CAD model of the mockup cabin

3. Experiments

3.1. Instruments, sampling procedures and QA/QC

3.1.1. Wind Tunnel

In order to supply a continuous stream of exhaust for the exhaust plume simulation within the tunnel, a vehicle is installed on a heavy-duty chassis-dynamometer, located outside the wind tunnel, and operated at a pre-defined vehicle speed. The vehicles exhaust stack is connected to a 5in (diameter) transfer pipe and ducted through an underground channel to a mock-up tractor cabin located inside the wind tunnel. The position of the chassis-dynamometer outside the wind tunnel, in close proximity to the position of exhaust introduction to the air flow in the tunnel and the thermal insulation of the transfer pipe guarantees a minimal temperature loss of the exhaust stream. This solution was chosen to avoid the logistical and structural problems of placing the chassis-dynamometer inside the wind tunnel. It has to be noted that this specific issue only arises for plume studies within the WVU wind tunnel.

The heavy-duty chassis-dynamometer employed during the presented study is part of WVU's Transportable Emissions Measurement System (TEMS). The chassis-dynamometer, custom built by West Virginia University, consist of two sets of 12.6in diameter rollers, two flywheel assemblies, two air cooled eddy current power absorbers (Model CC300, Mustang) capable of absorbing peak power up to 1000hp, and two electrical motors to balance frictional losses within the dynamometer system, one for each side (hub) of the vehicle's drive axle. The flywheel assembly simulates the inertia of the test vehicle and is capable of simulating a vehicle weight of up to 110,000lbs.

Figure 16: Wind Tunnel, Chassis Dynamometer and TREL setup

Recalling the concept of flexibility, which the WVU wind tunnel has been designed upon, the authors, would like to highlight a possible setup configuration allowing for studying the impact of aerodynamic effects onto exhaust emissions. For such scenario, the WVU wind tunnel would be transformed into a “pushing” configuration by simply reversing the tunnel flow. A concrete platform located at a slightly lower level just in front and of the regular wind tunnel inlet would accommodate the chassis-dynamometer, so that the installed test vehicle will be flush with the floor of the wind tunnel itself. This kind of study could aid in understanding how external aerodynamics of a vehicle will affect its emissions.

The instrumentation setup during a primary exhaust plume study is composed of three different sampling stations able to identify the three main flows involved. Continuous data from all three sampling stations is acquired at a sampling rate of 10Hz using a custom designed data acquisition system. Furthermore, the acquisition system is linked to an integrated system command computer, allowing for real-time control of the propeller (via DDC engine control), instrumentation cart and sampling probe as well as the chassis-dynamometer.

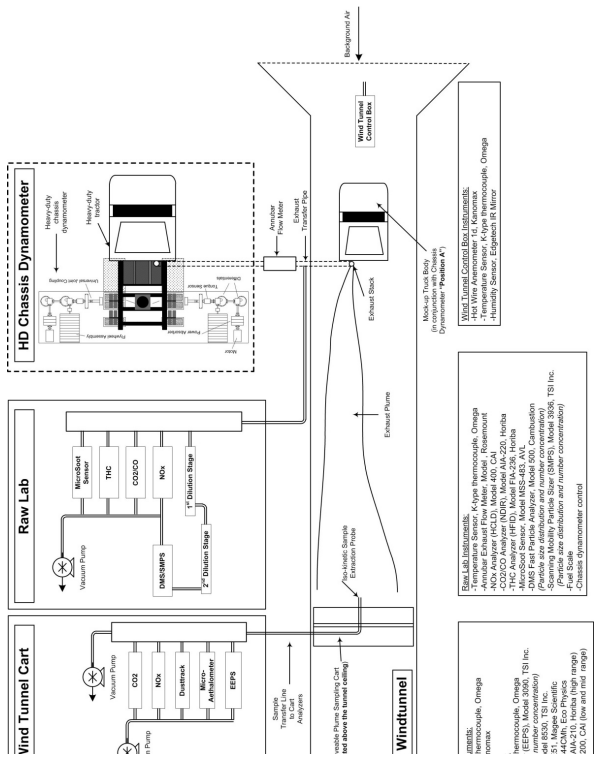

Figure 17: Wind Tunnel Experimental Setup

3.1.1.1. Plume instruments

The one of most importance to this particular study is the mobile platform, termed "instrumentation cart" for the reminder of the report, which analyzes the exhaust plume. The instrumentation cart is equipped with following analytical instruments:

Sample Extraction Probe Instruments:

- Temperature Sensor, K-type thermocouple, Omega
- Hot Wire Anemometer 3d, Kanomax

Wind Tunnel Sampling Cart Instruments:

- Temperature Sensor, K-type thermocouple, Omega
- Engine Exhaust Particle Sizer (EEPS), Model 3090, TSI Inc. (Particle size distribution and number concentration)
- DustTrak Aerosol Monitor, Model 8530, TSI Inc.
- MicroAethalometer, Model AE51, Magee Scientific
- NOx Analyzer (CLD), Model 844CMh, Eco Physics
- NOx-amines Analyzer (CLD), Model 844CMh, Eco Physics
- CO2 Analyzer (NDIR), Model AIA-210, Horiba (high-range)
- CO2 Analyzer (NDIR), Model 200, CAI (low- and mid-range)

Carbon dioxide (CO2) (low-, mid- and high-range) is measured on a dry basis using a non-dispersive infrared (NDIR) analyzer (Model AIA-220, Horiba and Model 200, CAI). A solution with a combination of three different CO2 analyzers was chosen to better cover the wide range of measurements, from 450ppm in the background air to 8% in the core of the plume. The ranges of the three instruments overlap, thus careful attention needs to be put in place to evaluate the most reasonable local value of CO2. Oxides of nitrogen (NOx) on a dry basis using a Chemiluminescence detector (CLD) (Model 844CMh, Eco Physics). All analyzers are calibrated and operated according to recommendations outlined in Code of Federal Regulations (CFR), title 40, subpart 1065. An Amines converter with using a Chemiluminescence detector (CLD) (Model 844CMh, Eco Physics) provides the combination signal of NOx and Ammonia. Ammonia can be evaluated by subtracting the NOx signal from the NOx-amines. The flow in the sample extraction probe is managed according to the local wind speed (hot wire anemometer right in front of the probe tip), achieving in all the points an isokinetic sampling probe. This solution was chosen to reduce the particles losses and a sample the region as big as the probe tip, avoiding averaging measurements. The sample flow had no effects on the wind speed measurements obtained by the hot wire anemometer. The span calibration gaseous utilized conforms to the following.

Pre-2007 and Post-2007 Truck:

Table 2: Span Calibration Gases for the Sampling Cart gaseous instruments for Pre-2007 and Post-2007 Truck

Gaseous Analyzer	Span Calibration Gas
CO2 low-range Analyzer	0.25%
CO2 mid-range Analyzer	1%
CO2 high-range Analyzer	8.139%
NOx Analyzer	1000ppm
Tot-amines Analyzer	1000ppm

Post-2010 Truck:

Table 3: Span Calibration Gases for the Sampling Cart gaseous instruments for Post-2010 Truck

Gaseous Analyzer	Span Calibration Gas
CO2 low-range Analyzer	0.25%
C02 mid-range Analyzer	1%
CO2 high-range Analyzer	8.139%
NOx Analyzer	148.9ppm
Tot-amines Analyzer	148.9ppm

Measurements of PM concentrations and size distributions are performed with an Engine Exhaust Particle Sizer (EEPS™) spectrometer, model 3090, from TSI Inc. (Minnesota, USA) within the exhaust plume and the background air. Spectrometers classify particles based upon differential electrical mobility classification principle at a frequency of 1Hz, making it best suited for transient PM characterization. Particles between 6.04nm and 523.3nm are measured with a resolution of 16 channels per decade; hence a total of 32 channels. DustTrak Aerosol Monitor (Model 8530, TSI Inc.) is a light-scattering laser photometer capable of measuring suspended aerosol mass corresponding to $PM_{2.5}$. The DustTrak came already calibrated for CARB (owner of the instruments). Prior to any tests, the instruments was cleaned and zeroed with the procedure indicated in the manual. The linear response of the instruments and the zeroing performed prior of any tests, guarantee quality results. MicroAethalometer (Model AE51, Magee Scientific) is a laser absorption photometer capable of measuring black carbon concentration. Engine Exhaust Particle Sizer (EEPS) (Model 3090, TSI Inc.), DustTrak Aerosol Monitor (Model 8530, TSI Inc.) and MicroAethalometer (Model AE51, Magee Scientific) are operated according to the manual and periodic cleaning is enforced prior to any test. The transfer line from the probe to the analyzers is a Tygon™ tube and kept and thermally isolated at 60°C to reduce thermophoretic losses and not influence the PM particle and size distribution.

3.1.1.2. Raw Exhaust instruments

The second sampling station measures the raw exhaust directly from the truck's exhaust stack.

Transportable Raw Emissions Laboratory (TREL):

- Temperature Sensor, K-type thermocouple, Omega
- Annubar Exhaust Flow Meter, Rosemount
- NOx Analyzer (HCLD), Model 400, CAI
- CO2/CO Analyzer (NDIR), Model AIA-220, Horiba
- THC Analyzer (HFID), Model FIA-236, Horiba
- MicroSoot Sensor, Model MSS-483, AVL
- DMS Fast Particle Analyzer, Model 500, Cambustion
  (Particle size distribution and number concentration)
- Scanning Mobility Particle Sizer (SMPS), Model 3080, TSI Inc.
  (Particle size distribution and number concentration)
- Fuel Scale
- Chassis dynamometer control

The raw exhaust platform comprises WVU's Transportable Raw Emissions Laboratory (TREL) shown in Figure 18, which was designed and constructed according to requirements outline in CFR, title 40, subparts 1033 and 1065, and capable of characterizing gaseous emissions of CO2, CO, NOx, NO as well as THC from raw (undiluted) exhaust. NOx and NO are measured on a dry basis using a dual-channel CLD (Model 844CMh, Eco Physics) with the possibility to calculate NO2 through subtraction of NO from NOx, CO2 and CO on a dry basis using an NDIR analyzer (Model AIA-220, Horiba) as well as THC on a wet basis using a HFID analyzer (Model FIA-236, Horiba). The analytical bench further houses sampling conditioning units (dryers), flow meters, and heated sampling pumps and filters that are controlled by electronic micro-controllers and maintained at 112°C for CO, CO2 and NOx and 191°C for THC sample trains. Furthermore, TREL includes a partial-flow PM sampling system, not used for this test campaign, BG-3 from Sierra, allowing for PM sample collection on filter media (TX40, Pallflex®) for subsequent gravimetric weighing or EC/OC analysis (using pre-fired quartz fiber filters).

Figure 18: WVU Transportable Raw Emissions Laboratory (TREL)

Different after-treatment technologies present sensible differences in terms of emissions, leading to different calibration span values for the analyzers.

Pre-2007 Truck

Table 4: Span Calibration Gases for the TREL gaseous instruments for Pre-2007 Truck

Gaseous Analyzer	Span Calibration Gas
CO2	8.139%
CO	1002ppm
THC	150.6ppm
NOx	1000ppm

Post-2007 Truck

Table 5: Span Calibration Gases for the TREL gaseous instruments for Post-2007 Truck

Gaseous Analyzer	Span Calibration Gas
CO2	8.139%
CO	100ppm
THC	25.6ppm
NOx	1000ppm

Post-2010 Truck

Table 6: Span Calibration Gases for the TREL gaseous instruments for Post-2010 Truck

Gaseous Analyzer	Span Calibration Gas
CO2	8.139%
CO	100ppm
THC	25.6ppm
NOx	148.9ppm

Raw PM emissions were sampled from the exhaust transfer pipe by means of a customized Double Dilution System (DDS). The apparatus was composed by two mini-dilution tunnels equipped with two ejector diluters that allow for variable Dilution Ratio (DR) settings.

The first stage dilution was performed using hot air (~150°C) which was previously filtered and dried by means of a HEPA filter and a dryer. The second stage dilution was, on the contrary, obtained by supplying cold air (~20°C) in order to obtain a gas mixture with a temperature low enough to satisfy the requirements of the spectrometers used in this study.

A double dilution composed by a first stage hot dilution and a subsequent second stage cold dilution should prevent the volatile organic fraction (VOF) of PM to reach supersaturation conditions during the dilution process, hence limiting the amount of particles due to nucleation of VOF (nucleation mode).

The PM spectrometers employed for particle count and size characterizations were:

- DMS Fast Particle Analyzer, Model 500, Cambustion
  (Particle size distribution and number concentration)
- Scanning Mobility Particle Sizer (SMPS), Model 3080, TSI Inc.
  (Particle size distribution and number concentration)

The DMS can measure aerosols ranging from 5 nm to 2.5 µm. The fast response time, 200 ms T10-90, of the differential mobility classifier allows capture of fast changing spectra such as combustion emissions during transient engine conditions

The SMPS measures the size distribution engaging electrical mobility detection technique. Particles, after passing through a charge neutralizer, enter an electric field where they are classified according to their electrical mobility. This classification occurs in the Differential Mobility Analyzer (DMA). For this study a long DMA (TSI, Model 3081) was used and particles were counted by an Ultrafine Condensation Particle Counter (UCPC) from TSI (Model 3025), set to the high flow mode. The SMPS sampling flow rate (1.5 lpm) was controlled with a critical orifice. The sheet flow rate was set 10 times higher (15 lpm) and was provided by the internal dual blower. The SMPS was programmed to scan particles over a size range of 5.73 to 216 nm across 64 channels per decade. Sampling time for the entire size range was 135 sec, with an up and down-scan time of 120 and 15 sec, respectively. Several analyses confirmed the consistency of the data of the two instruments, over a wide range of operation.

Table 7: PM spectrometer used for the different tests

Truck	Test	PM spectrometer
Pre 2007	Idle	DMS
	20mph	DMS
	35mph	SMPS
Post 2007	Idle	DMS
	20mph	DMS
	35mph	DMS
Post 2010	Idle	SMPS
	20mph	SMPS
	35mph	SMPS

Additionally, a micro-soot sensor (MSS-483) from AVL is being employed in order to measure continuous soot (solid carbon only) emissions from the raw exhaust stack.

3.1.1.3. Background Air instruments

The third sampling station is placed at the inlet of the WVU wind tunnel, continuously monitoring background air properties, thus, allowing for subsequent correction of background contamination within the wind tunnel test section.

<u>Wind Tunnel Control Box Instruments:</u>

- Hot Wire Anemometer 1d, Kanomax
- Temperature Sensor, K-type thermocouple, Omega
- Humidity Sensor, Edgetech IR Mirror
- Weather station

PM and Gaseous components measurements of the Background Air are obtained with samplings outside the plume.

3.1.1.4. Plume sampling pattern

The will of a detailed plume investigation and the guarantee almost constant boundary conditions during the test made the team decide to not exceed 6 hours for each combination of truck and wind speed. The adopted solution comprise of 130 sampling points divided into 10 planes. Each plane presents the same sampling pattern, with different vertical dimension and position, better focusing on the plume shape and dimension evolution. The pattern is composed of 2 nested hexagons, rotated by 90°, and an additional center point. This configuration presents the best trade off in terms of matching the plume with a low number of sampling points per plane. To the original 130 points and additional p0 (point 0) is added right at the stack exhaust, intended to compare drifts or shifts of the sampling cart analyzers with the ones of the TREL. The first 65 points and p0 present 100s sampling time (1000 data points), and the remaining points 50s (500 data points). This solution allows to better investigate turbulence in the area close to the stack exhaust, where the high turbulent kinetic energy of the flow represents the predominant driver for the plume mixing and evolution. Far away from the exhaust stack turbulent mixing has lost most of its energy, and a slow gas diffusion process take place. Prior to any sampling, 30s of non-sampling stabilization time is observed once the probe reached the desired position, accounting for the inertia of the measurement system.

The definition process for the points coordinate started with Figure 19, a preliminary plume simulation, overlapped with the wind tunnel CAD model. Preliminary tests further refined the sampling point coordinates. In the end, 3 different sampling patterns are identified, one per each wind speed.

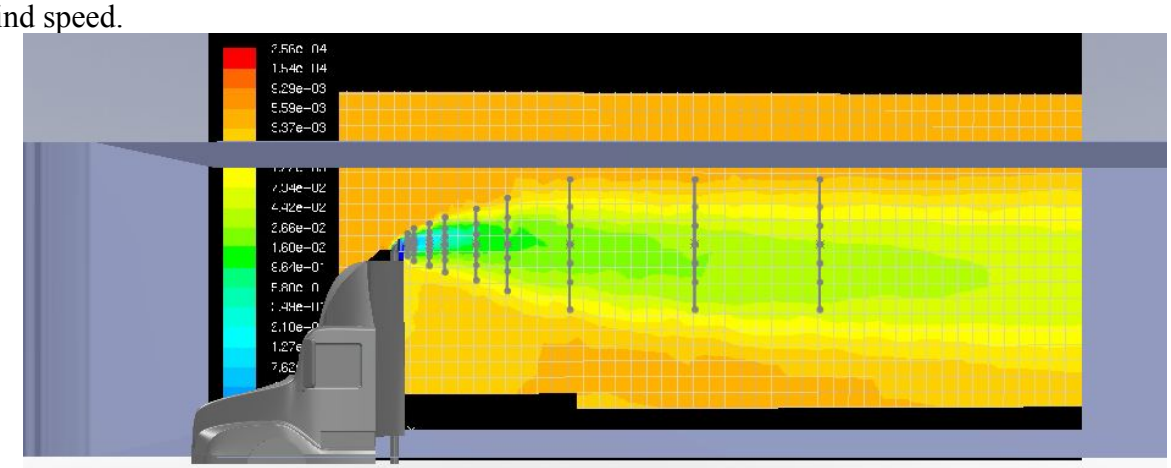

Figure 19: Initial identification of the plume sampling points

3.1.1.5. Data File Dictionary

The collected and untreated data are presented in and Excel worksheet (.xlsx), one file per each combination of truck and wind speed. In each Excel worksheet, each tab collects the channels recorded for all the points of a plane. The channels of each point are defined as a block, and the blocks are appended one under the other, as the points are sampled. Each block is composed of 69 channels, listed and described below.

Table 8: Data File Dictionary

	Channel Name	Unit of Measure	Description	Sampling Station
1	X	[mm]	X position of the probe	Sampling Cart
2	Y	[mm]	Y position of the probe	Sampling Cart
3	Z	[mm]	Z position of the probe	Sampling Cart
4	CO2l_probe	[ppm]	CO2 low-range Analyzer	Sampling Cart
5	CO2m_probe	[%]	CO2 mid-range Analyzer	Sampling Cart
6	CO2h_probe	[%]	CO2 high-range Analyzer	Sampling Cart
7	CO2_probe	[%]	Proposed CO2 combined signal	Sampling Cart
8	NOx_probe	[ppm]	NOx Analyzer	Sampling Cart
9	tot_amine_probe	[ppm]	NOX-Amines Analyzer	Sampling Cart
10	DustTrak	[mg/m3]	DustTrak Analyzer	Sampling Cart
11	aeth	[ng/m3]	MicroAethalometer Analyzer	Sampling Cart
12	eeps	[dn/dlog(Dp)]	Particle Concentration @ 6.04 nm	Sampling Cart
13	eeps	[dn/dlog(Dp)]	Particle Concentration @ 6.98nm	Sampling Cart
14	eeps	[dn/dlog(Dp)]	Particle Concentration @ 8.06nm	Sampling Cart
15	eeps	[dn/dlog(Dp)]	Particle Concentration @ 9.31nm	Sampling Cart
16	eeps	[dn/dlog(Dp)]	Particle Concentration @ 10.8nm	Sampling Cart
17	eeps	[dn/dlog(Dp)]	Particle Concentration @ 12.4nm	Sampling Cart
18	eeps	[dn/dlog(Dp)]	Particle Concentration @ 14.3nm	Sampling Cart
19	eeps	[dn/dlog(Dp)]	Particle Concentration @ 16.5nm	Sampling Cart
20	eeps	[dn/dlog(Dp)]	Particle Concentration @ 19.1nm	Sampling Cart
21	eeps	[dn/dlog(Dp)]	Particle Concentration @ 22.1nm	Sampling Cart
22	eeps	[dn/dlog(Dp)]	Particle Concentration @ 25.5nm	Sampling Cart
23	eeps	[dn/dlog(Dp)]	Particle Concentration @ 29.4nm	Sampling Cart
24	eeps	[dn/dlog(Dp)]	Particle Concentration @ 34nm	Sampling Cart
25	eeps	[dn/dlog(Dp)]	Particle Concentration @ 39.2nm	Sampling Cart
26	eeps	[dn/dlog(Dp)]	Particle Concentration @ 45.3nm	Sampling Cart

27	eeps	[dn/dlog(Dp)]	Particle Concentration @ 52.3nm	Sampling Cart
28	eeps	[dn/dlog(Dp)]	Particle Concentration @ 60.4nm	Sampling Cart
29	eeps	[dn/dlog(Dp)]	Particle Concentration @ 69.8nm	Sampling Cart
30	eeps	[dn/dlog(Dp)]	Particle Concentration @ 80.6nm	Sampling Cart
31	eeps	[dn/dlog(Dp)]	Particle Concentration @ 93.1nm	Sampling Cart
32	eeps	[dn/dlog(Dp)]	Particle Concentration @ 107.5nm	Sampling Cart
33	eeps	[dn/dlog(Dp)]	Particle Concentration @ 124.1nm	Sampling Cart
34	eeps	[dn/dlog(Dp)]	Particle Concentration @ 143.3nm	Sampling Cart
35	eeps	[dn/dlog(Dp)]	Particle Concentration @ 165.5nm	Sampling Cart
36	eeps	[dn/dlog(Dp)]	Particle Concentration @ 191.1nm	Sampling Cart
37	eeps	[dn/dlog(Dp)]	Particle Concentration @ 220.7nm	Sampling Cart
38	eeps	[dn/dlog(Dp)]	Particle Concentration @ 254.8nm	Sampling Cart
39	eeps	[dn/dlog(Dp)]	Particle Concentration @ 294.3nm	Sampling Cart
40	eeps	[dn/dlog(Dp)]	Particle Concentration @ 339.8nm	Sampling Cart
41	eeps	[dn/dlog(Dp)]	Particle Concentration @ 392.4nm	Sampling Cart
42	eeps	[dn/dlog(Dp)]	Particle Concentration @ 453.2nm	Sampling Cart
43	eeps	[dn/dlog(Dp)]	Particle Concentration @ 523.3nm	Sampling Cart
44	temp_probe	[°C]	Plume temperature @ the probe	Sampling Cart
45	flow_probe	[scfm]	Flow rate @ the probe	Sampling Cart
46	HWA_probe	[m/s]	Wind speed @ the probe	Sampling Cart
47	CO2_raw	[%]	CO2 Analyzer	TREL
48	CO_raw	[ppm]	CO Analyzer	TREL
49	NOx_raw	[ppm]	NOx Analyzer	TREL
50	HC_raw	[ppm]	THC Analyzer	TREL
51	AVL_MSS_raw	[mg/m3]	AVL MSS Analyzer	TREL
52	ex_flow_raw	[scfm]	Exhaust flow rate	TREL
53	ex_annu_temp_raw	[°C]	Exhaust temperature @ raw sampling point	TREL

54	ex_stack_temp_raw	[°F]	Exhaust temperature @stack exit	TREL
55	dyno_speed	[rpm]	Chassis Dynamometer speed	TREL
56	dyno_torque	[ft-lb]	Chassis Dynamometer absorbed torque	TREL
57	dyno_power	[Hp]	Chassis Dynamometer absorbed power	TREL
58	vehicle_speed	[mph]	Vehicle speed	TREL
59	fuel_mass_raw	[lb]	Fuel scale measurements	TREL
60	fuel_temp_raw	[°C]	Fuel temperature	TREL
61	HWA_wt	[m/s]	Wind Tunnel wind speed	Background Air
62	temp_inlet	[°F]	Background Air inlet temperature	Background Air
63	dewpoint_inlet	[°C]	Background Air inlet dew point temperature	Background Air
64	temp_weather	[°C]	local temperature from weather station	Background Air
65	dewpoint_weather	[°C]	local dew point temperature from weather station	Background Air
66	wind_int_weather	[mph]	local wind from weather station	Background Air
67	wind_dir_weather	[°]	local wind from weather station	Background Air
68	barometer_weather	[Pa]	local barometric pressure from weather station	Background Air

Summarizing, each vehicle will present three Excel sheets, comprehensive of the three tests, plus a fourth which contains the PM size particle and distributions from the raw exhaust.

3.1.1.6. Test Matrix

In this test campaign it three different aftertreatment technologies were chosen, thus three different vehicles are going to be investigated. The first one will reflect pre 2007 US EPA aftertreatment technology, one compliant with 2007 US EPA regulation and finally a 2010 US EPA compliant. Those three vehicles and their aftertreatment technologies represent their legacy fleet.

Three different wind speed/road loads are chosen for this test campaign. The first one called **Idle Test**, is the typical configuration in which a truck is in a rest area with the engine in idling conditions with low wind (5mph). The second is the **20mph Test,** where is meant to simulate a truck cruising on a flat road in calm air. According to the Road Load equation a high roof cabin at 20mph generate 40hp. The last and third **35mph Test** simulate a truck cruising on a flat road in calm air. According to the Road Load equation a high roof cabin at 35mph generate 63hp.

Table 9: Test Campaign Matrix

	Idle Test	20mph Test	35mph Test
Pre-2007	**1**	**1**	**1**
Post-2007	**1**	**1**	**1**
Post-2010	**1**	**1**	**1**

Due to the time extensive nature of every single combination, only a repetition was conducted.

3.1.2. Transportable Heavy-Duty Vehicle Emissions Testing Laboratory (THDVETL)

3.1.2.1. Chassis Dynamometer

The vehicles were tested on an inertial based heavy-duty chassis dynamometer which is part of the West Virginia University's Transportable Heavy-Duty Vehicle Emissions Testing Laboratory (THDVETL). Built by WVU, the chassis dynamometer makes use of rotational inertia to reliable match actual transitional vehicle inertia at a wide range of speeds and Gross Vehicle Weights (GVW) up to 70'000lbs. The power output from the rear (or forward rear) drive axle of the vehicle is transferred to flywheels, simulating the vehicle inertia, eddy current power absorbers, simulating the road load and Alternative Current (AC) variable speed motors to simulate light grade motoring, through the drive train units from hub adapters connected to the outboard wheels. The vehicle wheels run on 12.6in idler rollers which also insure that the left and right wheel speeds are the same, by negating axle differential action. Direct load coupling between the vehicle hub and dynamometer eliminates tire-roller slippage and thereby possible errors in speed data as well as the highly variable frictional loading at the tire-roller interface due to heat generation. During the test cycle, torque cells and speed transducers in the power absorber drivetrain measured vehicle load and speed. A Dyn-Loc IV digital dynamometer controller was integrated with the test system software to control the operation of the chassis dynamometers.

3.1.3. WVU QC/QA Assurance Plan

Quality control and quality assurance procedures adopted by the WVU Wind Tunnel and the WVU Transportable Heavy-Duty Vehicle Emissions Laboratory are given below.

Emissions Testing

The laboratories are capable of measuring regulated and non-regulated engine or vehicle emissions such as carbon monoxide (CO), oxides of nitrogen (NOx), total hydrocarbons (THC), total particulate matter (TPM), carbon dioxide (CO_2). Reliable sampling is assured through system design, periodic system inspection, and scheduled instrument calibration.

Sampling Lines and Probes

The sampling streams use separate sampling probes and lines with their own pumps (heated in the case of NOx, THC, and also CO/CO_2 to avoid condensation of moisture in the lines). This design feature ensures reliable operation of the THC and NOx analyzers. Great care is taken in verifying that emissions measurement equipment is in order before commencement of emissions testing. Prior to the performance of a test schedule, supervisory personnel verify that all sample probes in the raw exhaust are properly placed (all probes sample at equidistant locations from the center of the tunnel and oriented with their sample inlets facing upstream) and that the integrity of the sampling systems has been maintained. The sampling lines are leak checked (by pressurization) and back-flushed with high pressure air in order to clean the lines of residual particulate matter. Heated sampling lines and their associated control systems (PID temperature controllers and associated thermocouples) are checked to ensure continuity between the controller, heater elements, and thermocouples. The temperature settings also are verified (THC sampling probes and lines are maintained at 375°F while NOx lines and probes are maintained at 250°F). Sample line temperatures, at various locations, are displayed on the sampling cabinet for monitoring by the operator.

Thermocouples and Pressure transducers

Thermocouples K are used for temperature measurements and calibrated by a certified signal generator from 0 to 100% of their range in 10% increments. The thermocouple readings are allowed to stabilize at each measurement point and a computer averaged (100 points) reading of the instrument is recorded. The eleven data points and their corresponding temperature are recorded and a fifth degree polynomial is fitted to the data to complete the calibration data file. Pressure transducers are calibrated with a certified pressure analyzer from 0 to 100% of their range in 10% increments. The pressure readings are allowed to stabilize at each measurement point and a computer averaged (100 points) reading of the instrument is recorded. The eleven data points and their corresponding temperature are recorded and a linear polynomial is fitted to the data to complete the calibration data file.

Exhaust Transfer Tube

The exhaust transfer tube, which routes exhaust from the engine exhaust system to the wind tunnel, is checked for leaks after assembly. Joints in the tube are sealed using a high-temperature aluminum tape and periodically checked to ensure integrity. The exhaust transfer tube is insulated to minimize errors in PM measurement due to thermophoretic effects.

Calibration and Calibration Gases

The gases used to calibrate the emissions measurement instruments are certified by the supplier to have an accuracy of 1% traceable to NIST. The laboratory uses the same gases for calibration, span and zero gases. All span and calibration gases have concentrations equal to approximately 85% to 95% of full scale. All emissions measurement instruments are calibrated using appropriate ranges of calibration gas for the engine or vehicle being tested. These calibrations are performed before each series of tests and after any instrument maintenance has been performed. HC, CO, NOX, and CO_2 instruments are calibrated by sampling a varying mixture of zero air and span gas (calibration gas) through a gas divider from 0 to 100% of their range in 10% increments. The instrument readings are allowed to stabilize at each measurement point and a computer averaged (100 points) reading of the instrument is recorded. The eleven data points and their corresponding gas concentrations are recorded and a second degree (third degree in case of NDIRs) polynomial is fitted to the data to complete the calibration data file. The calibration file overwrites the previous calibration file on the main computer (each test data disk contains the calibration files from that test) to prevent using incorrect calibration files for testing. No gas cylinder is used if the pressure drops below 200 psig.

Additional Calibration and Maintenance Procedures

In addition to the calibration procedures, each analyzer is subjected to a range of checks and maintenance procedures as described below.

Hydrocarbon Analyzer

The THC analyzer is subjected to the 'FID burner peaking process' to get the highest flame ionization detector (FID) response. This process involves measuring and recording the response of the instrument to 100% span gas and zero air with various settings of FID burner fuel and air. Upon completion of the FID burner peaking process, the fuel and air settings of the FID are placed at the setting which produced the highest instrument response, and the analyzer is calibrated. A HC hang-up check, following the procedures outlined in 40 CFR, Part 86, Subpart N, is also performed on the heated FID. If the differences in the responses are more than two percent, the sampling probe is backflushed (direct injection of zero air into the analyzer and through the 'overflow' sampling probe) and steps are taken to rectify the problem.

NOx Analyzers

On a monthly basis, a NOx efficiency test is performed on the NOx analyzers. This test is performed to ensure that the analyzer converter (which converts NO_2 to NO) is performing satisfactorily. A conversion efficiency of less than 90% is considered a failure and maintenance is performed to rectify the situation. Filters in the NOx sampling are visually inspected and replaced after analyzer maintenance has been performed and whenever necessary.

CO/CO_2 Analyzers

Since moisture can affect the operation of the NDIR analyzers used for carbon monoxide and carbon dioxide, a water interference check is performed. The sample flow is passed through a refrigerator dryer to lower the dew point of the sample stream before it reaches the NDIR.

Particulate Sampling

PM sampling is obtained with 3 different spectrometer (SMPS, EEPS, DMS) and 3 soot analyzers (DustTrak, MicroAethalometer and MSS). All instruments operated, cleaned and

zeroed according to their respective manuals and common procedure, applied as extension of CFR 1065 indications on quality measurements.

Data Analysis and Reporting

Quality assurance for data reported from testing is achieved using multiple checks. First, the operators of the laboratory, including the senior supervisory personnel as well as technicians, have a vast amount of experience in testing a multitude of different vehicle/engine/fuel combinations. This experience is valuable in quality assurance since it allows the laboratory operators to identify problems at the test site.

As a test is performed, data is logged to a local hard disk on the data acquisition computer. After the test is completed, data is transferred to a media storage device as well as separate backup optical drive. A data reduction program is used to extract emissions data from a binary data file and translate it into the appropriate units using calibration files. On-site examination of the data is done by supervisory personnel to determine the accuracy of the data in order that equipment malfunctions can be identified and promptly corrected.

3.2. Class-8 Heady duty vehicles

3.2.1. Pre-2007

The pre-2007 vehicle is not equipped with any after-treatment devices. The vehicle is part of the CAFEE fleet, and additional information is summarized in Table 10: Pre-2007 vehicle specification and

Table 11.

Table 10: Pre-2007 vehicle specification

Chassis Manufacturer / Model	Mack Trucks Inc / CH613
VIN	1M1AA13Y95WO54437
Class	8
Vehicle Model Year (MY)	1995
Aftertreatment System	-
Fuel	Standard ULSD (<15ppm)
Emission Family	SMK728EJDARA (45)
Curb Weight [lbs]	15'000

Table 11: Pre-2007 engine specification (*certification values)

Engine Manufacturer	Mack Trucks Inc.
Engine Model	E7-400
Engine Model Year	1995
Displacement [L]	11.93
Configuration / # of Cylinders	In-line / 6 cylinder
Rated Power [hp]	400@ 1800rpm
NOx [g/bhp-hr]	4.5*
PM [g/bhp-hr]	0.09*

3.2.2. Post-2007

The Post-2007 vehicle is equipped with DOC/DPF to meet the 2007 US EPA regulations. The vehicle was rented from FYDA Freightliner Inc. in Canonsburg, PA. Additional information are summarized in the following Table 12 and

Table 13.

Table 12: Post-2007 vehicle specification

Chassis Manufacturer / Model	Freightliner Cl120
VIN	1FUJA6CK89DAE7405
Class	8

Vehicle Model Year (MY)	08/2008
Aftertreatment System	DOC/DPF
Fuel	Standard ULSD (<15ppm)
Emission Family	8DDXH14.0ELC
Curb Weight [lbs]	23,587

Table 13: Post-2007 engine specification (*certification values)

Engine Manufacturer	Detroit Diesel
Engine Model	SERIES 60 S/N 06R1012772
Engine Model Year	2008
Displacement [L]	14.0 L
Configuration / # of Cylinders	In-line / 6 cylinder
Rated Power [hp]	515@1800
NOx [g/bhp-hr]	1.07*
PM [g/bhp-hr]	0.003*

3.2.3. Post-2010

The Post-2010 vehicle is equipped with urea-based SCR and DOC/DPF assembly to meet the 2010 US EPA regulations. The vehicle was rented from Worldwide Equipment Inc. in Prestonsburg, KY. Additional information is summarized in Table 14 and

Table 15.

Table 14: Post-2010 vehicle specifications

Chassis Manufacturer / Model	Mack Trucks Inc. / CXU613
VIN	1M1AW07Y1CM017126
Class	8
Vehicle Model Year (MY)	2011
Aftertreatment System	DOC / DPF / urea-SCR
Fuel	Standard ULSD (<15ppm)
Emission Family	BVPTH12.8S01
Curb Weight [lbs]	15’000

Table 15: Post-2010 engine specifications (*certification values)

Engine Manufacturer	Mack Trucks Inc.
Engine Model	MP8-445C
Engine Model Year	2011
Displacement [L]	12.8
Configuration / # of	In-line / 6 cylinder

Cylinders	
Rated Power [hp]	445 @ 1500rpm
NOx [g/bhp-hr]	0.12*
PM [g/bhp-hr]	0.003*

3.3. Wind Tunnel Measurements

In the following paragraphs contour plots of 9 major plume parameters are presented for each vehicles and each related test. Each test presents 10 different sampling planes; only 2 per combination of truck and wind speed are presented for an overall description of the results. All the plume panels are collected in APPENDIX C. The parameters represented are:

- NOx
- Micro Aethalometer
- DustTrak
- CO2 low-range
- CO2 mid-range
- CO2 high-range
- Temperature
- Air Speed
- Turbulence Intensity (T.I.)

3.3.1. Pre-2007

The results of first vehicle tested, the pre-2007, are presented in this paragraph.

3.3.1.1. Idle Test

As described previously in the Idle test, the vehicle is in idling condition and a wind of 5mph is generated. This test represents the emission of truck in a rest area. It is important to notice among the contour plots that different instrument shows a similar contour in terms of dimension, color ratio and shape. This instance indicates that the instruments are detecting the same phenomena, which ultimately results in the plume itself.

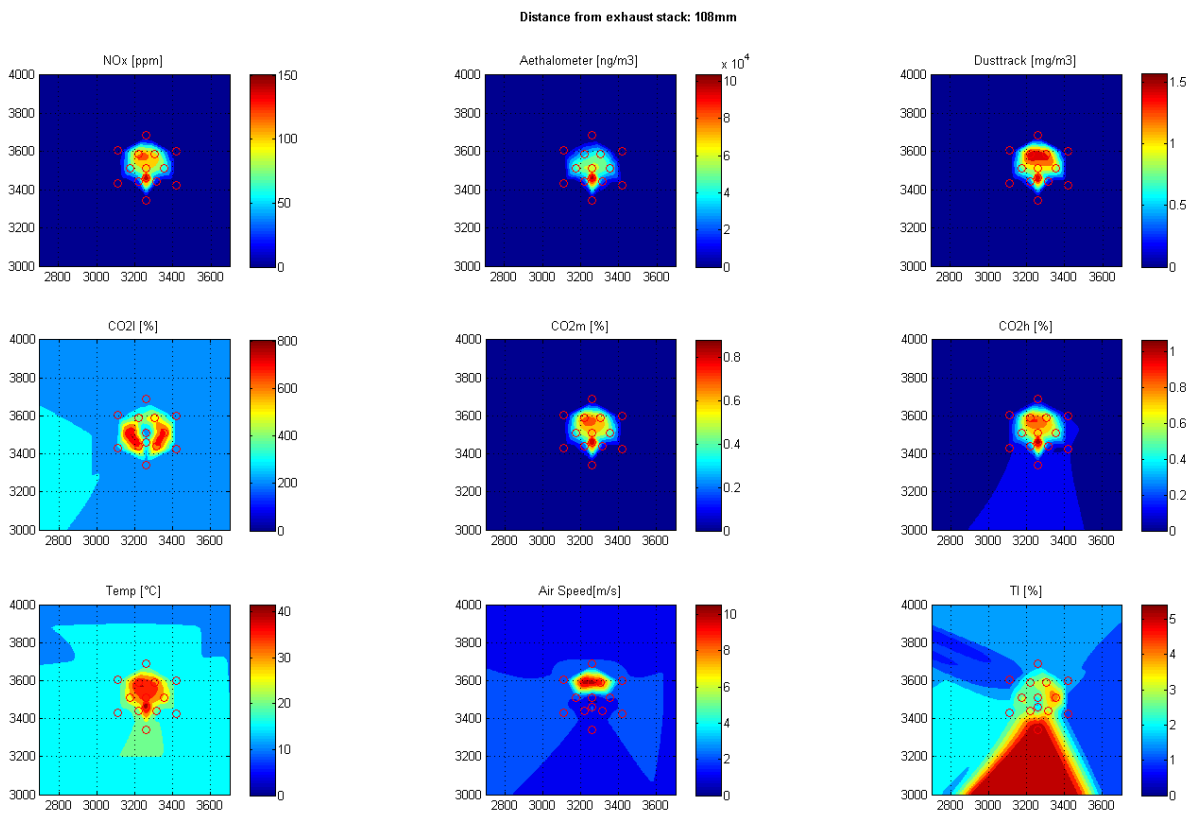

Figure 20: Pre2007 vehicle, Idle Test, Plane 1

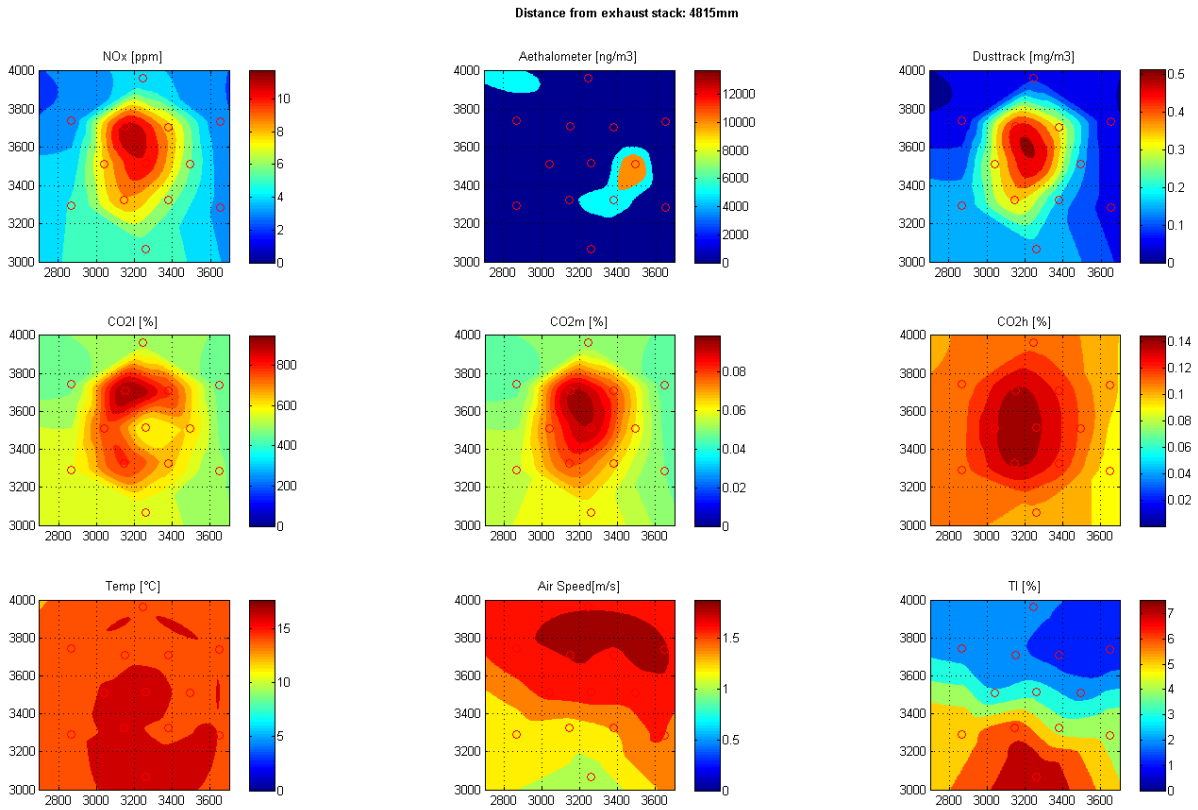

Figure 21: Pre-2007, Idle Test, Plane 8

The PM emissions indicated by the panels evidentiate a high value of solid particles from the DustTrak, up to 0.5mg/m3 from a distance of 5m from the exhaust stack. Unfortunately during this test the MicroAethalometer did not provide valuable additional information regarding the PM. The DustTrak measured right at the exit of the exhaust stack levels of soot in agreement with the raw emissions of the truck from the AVL MSS. This high level of soot emission is explained by the fact the vehicle is not equipped with any PM aftertreatment device. It is important to notice with the following figures that the longitudinal and vertical extension of the plume is influenced simultaneously by the wind in opposite ways, which ultimately balance themselves out. For this reason the plume has generally a similar shape and dimensions across different wind speeds. At low wind speed the plume has higher residence time, thus longer time to grow vertically and laterally, but the low turbulent mixing constraints the overall growth. At higher wind speed the plume tends to be stretched longitudinally, but a higher turbulent mixing make the plume expand more. In the end, at different wind speeds the plume present almost the same dimension, only the vertical position might be affected by the aerodynamics of the truck.

The confirmation of the high value of solid particle, or accumulation mode, is confirmed by the EEPS results in the plume.

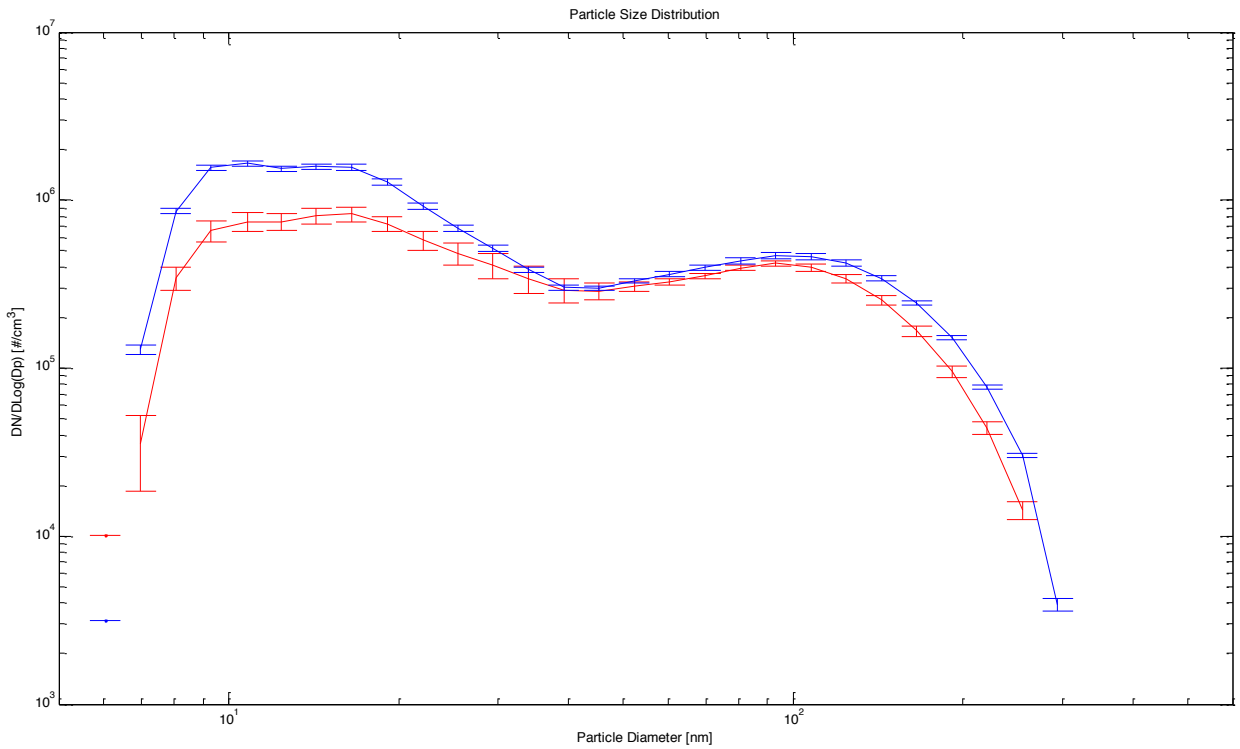

Figure 22: particle size distribution and concentration for point 1 and 10 at the plane 1

The results showed are tailpipe emissions. It is possible to notice how the point in the peripheral area of the plume (point10, blue line) undergoes a different dilution process and thus expressing a different nucleation mode if compared to a point of the of the plume (poin1, red line). This is related to a more rapid dilution and cooling process in the peripheral area than the core, enhancing the growth and nucleation of nanoparticles.

3.3.1.2. 20mph Test

The vehicle was at 20mph in steady state conditions and a wind of 20mph was generated inside the wind tunnel. This test represents a vehicle cruising on a flat road at 20mph in calm air. As well as the previous contour plots it is possible to observe among different instruments a similar shape and dimension of the identified plume. In this test the MicroAethalometer showed non-consistent behavior, alternating measurements in agreement and not with the DustTrak.

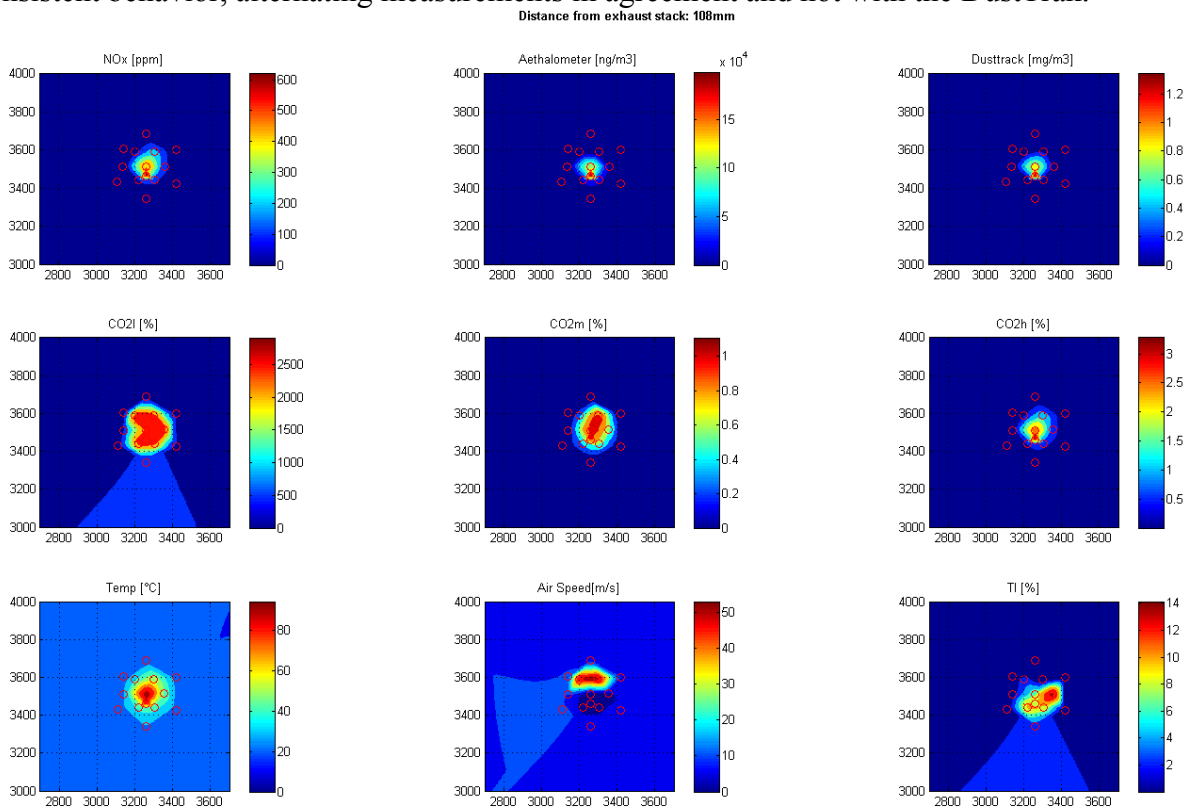

Figure 23: Pre2007 vehicle, 20mph Test, Plane 1

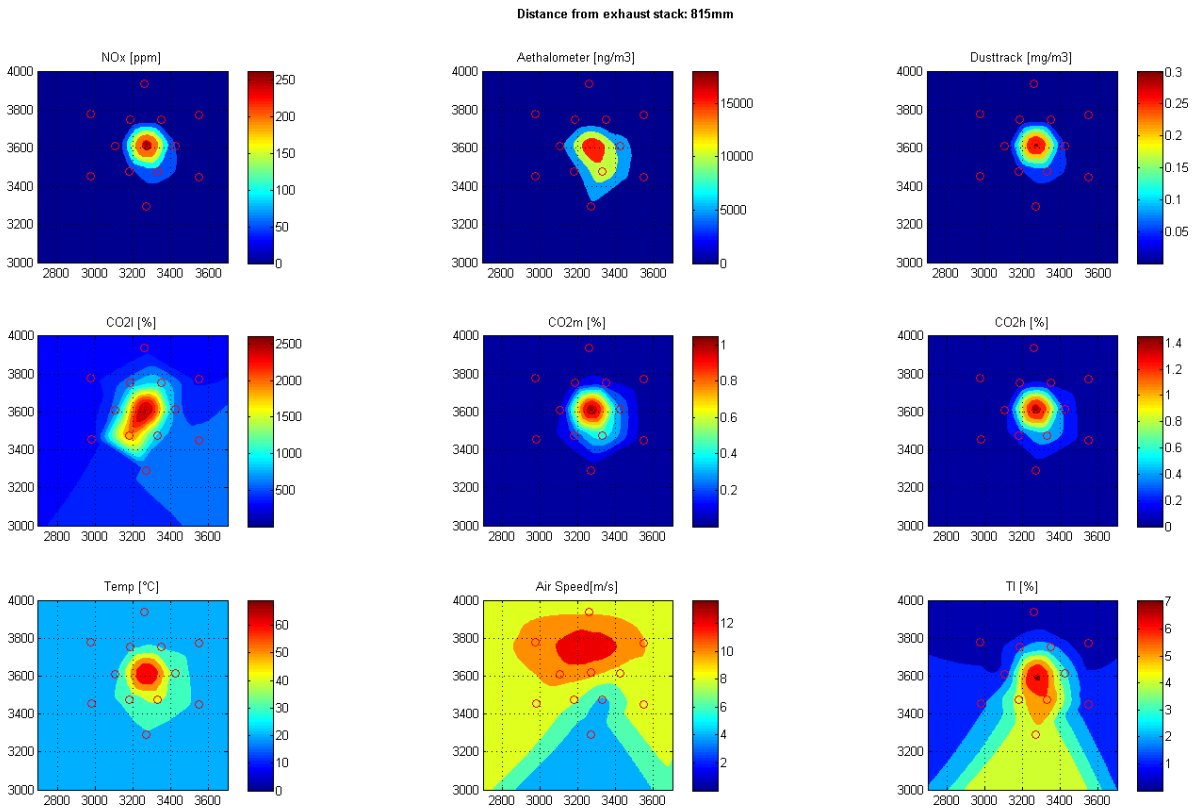

Figure 24: Pre2007 vehicle, 20mph Test, Plane 4

The higher speed compared to the Idle Test, shows a sensible increase of T.I. close to the exhaust area, this conduct to more effective cooling and mixing of the plume itself.

Observing the plots of the Air Speed, a bubble of air speed is present above and later in the superior part of the plume. This bubble of high speed and low TI is generated by the aerodynamics of the wind cowl and exhaust stack. This bubble at the beginning is above the plume, but with the plume growth and the diffusion of the bubble itself eventually it gets absorbed in the plume. This fact provokes a shear stress on the plume itself, which clarifies the vertical oval shape which the plume shows further from the exhaust stack.

3.3.1.3. 35mph Test

The vehicle was at 35mph in steady state conditions and a wind of 35mph was generated inside the wind tunnel. This test represents a vehicle cruising on a flat road at 35mph in calm air. As well as the previous contour plots it is possible to observe among different instruments a similar shape and dimension of the identified plume.

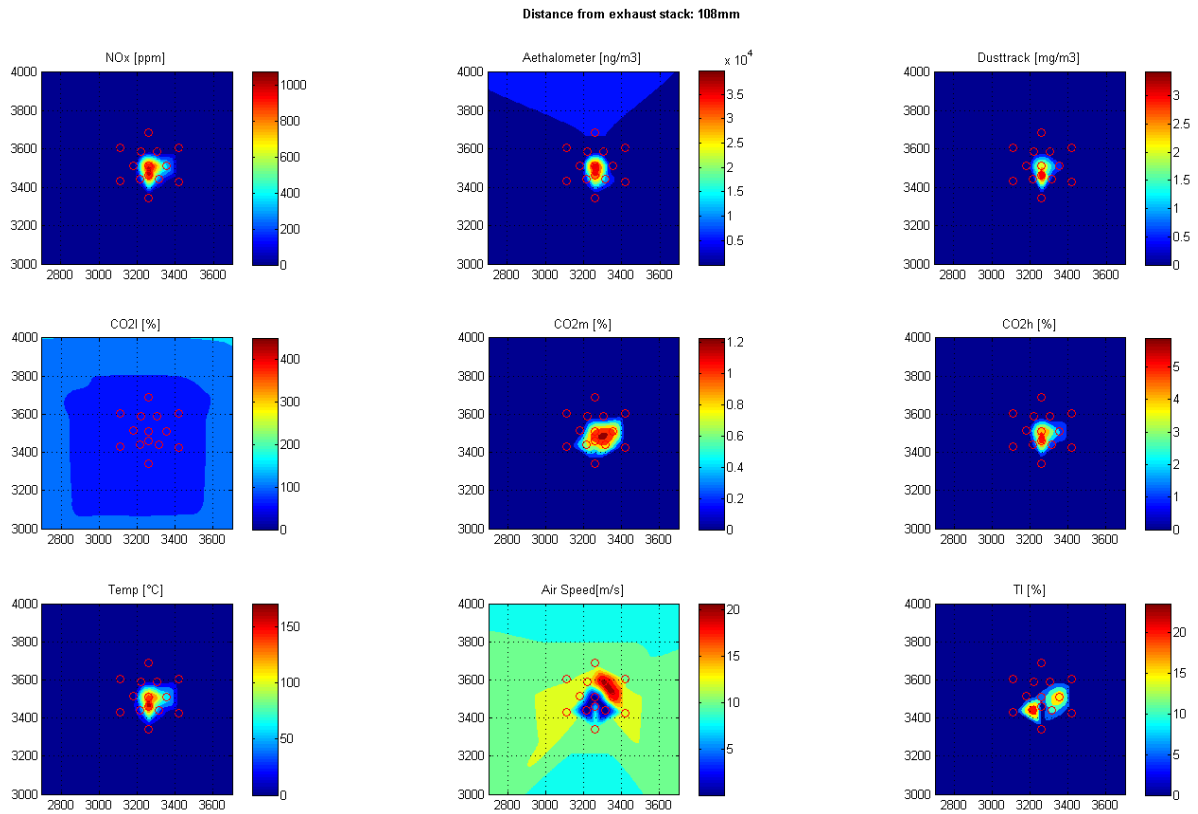

Figure 25: Pre-2007, 35mph Test, Plane1

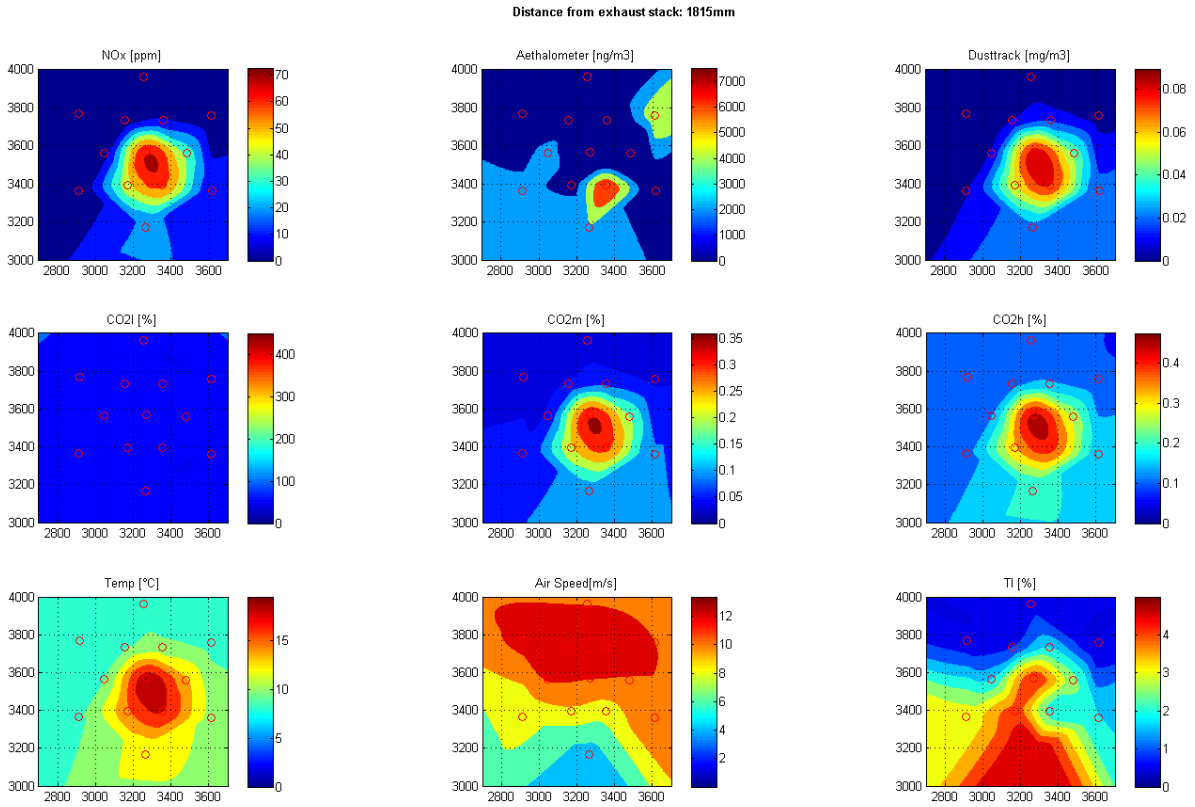

Figure 26: Pre-2007, 35mph Test, Plane 6

The higher turbulent kinetic energy present in the flow generates a more irregular shape of the plume if compared to the Idle and 20mph Test, which is observable in the extension of the turbulent region behind the cabin. But it is still possible to notice how the Pm and gaseous traces of the plume show similar shape, dimensions and gradient.

3.3.2. Post-2007

3.3.1.4. Idle test

As described previously in the Idle test, the vehicle is in idling condition and a wind of 5mph is generated. This test represents the emission of truck in a rest area. It is important to notice among the next 10 contour plots that different instrument shows a similar contour in terms of dimension, color ratio and shape.

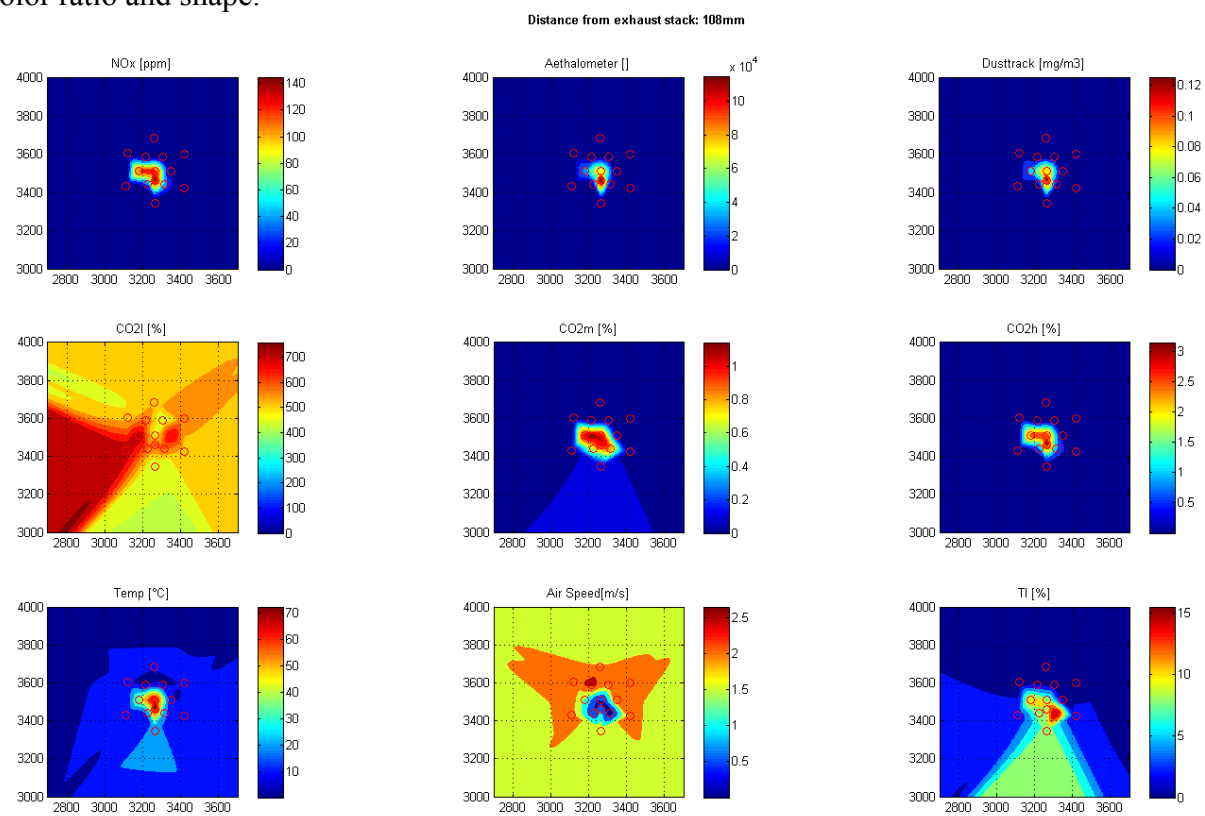

Figure 27: Post-2007, Idle Test, Plane 1

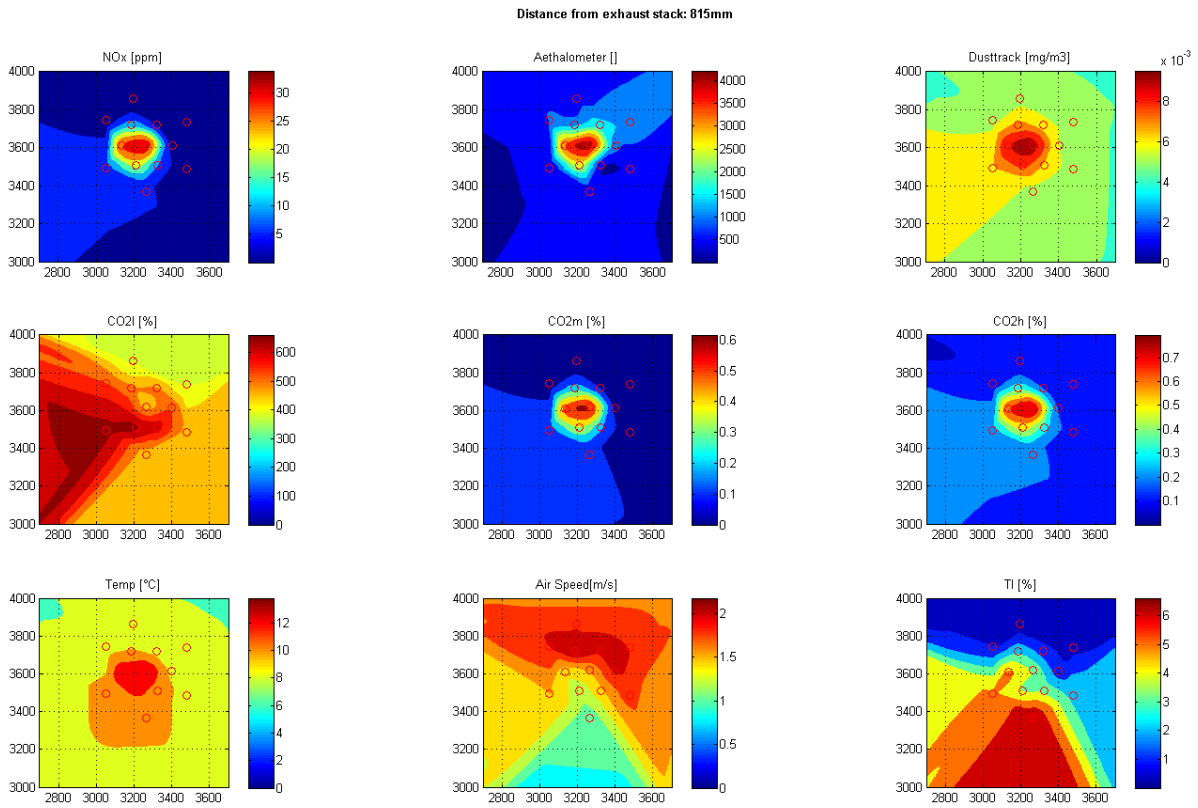

Figure 28: Post-2007, Idle Test, Plane 4

Similar analysis to the previous Idle Test can be conducted. The main differences are related to the levels of emission in the plume. Lower NOx and PM are explainable by the presence of a DOC-DPF aftertreatment system. The CO2 lower value might be explained by the better fuel efficiency of this engine, which is more than one decade younger than the Pre-2007 engine. The relatively high PM emissions for a DPF equipped truck raises some concerns better explained in the following paragraph.

3.3.1.5. 20mph Test

The vehicle was at 20mph in steady state conditions and a wind of 20mph was generated inside the wind tunnel. This test represents a vehicle cruising on a flat road at 20mph in calm air. As well as the previous contour plots it is possible to observe among different instruments a similar shape and dimension of the identified plume.

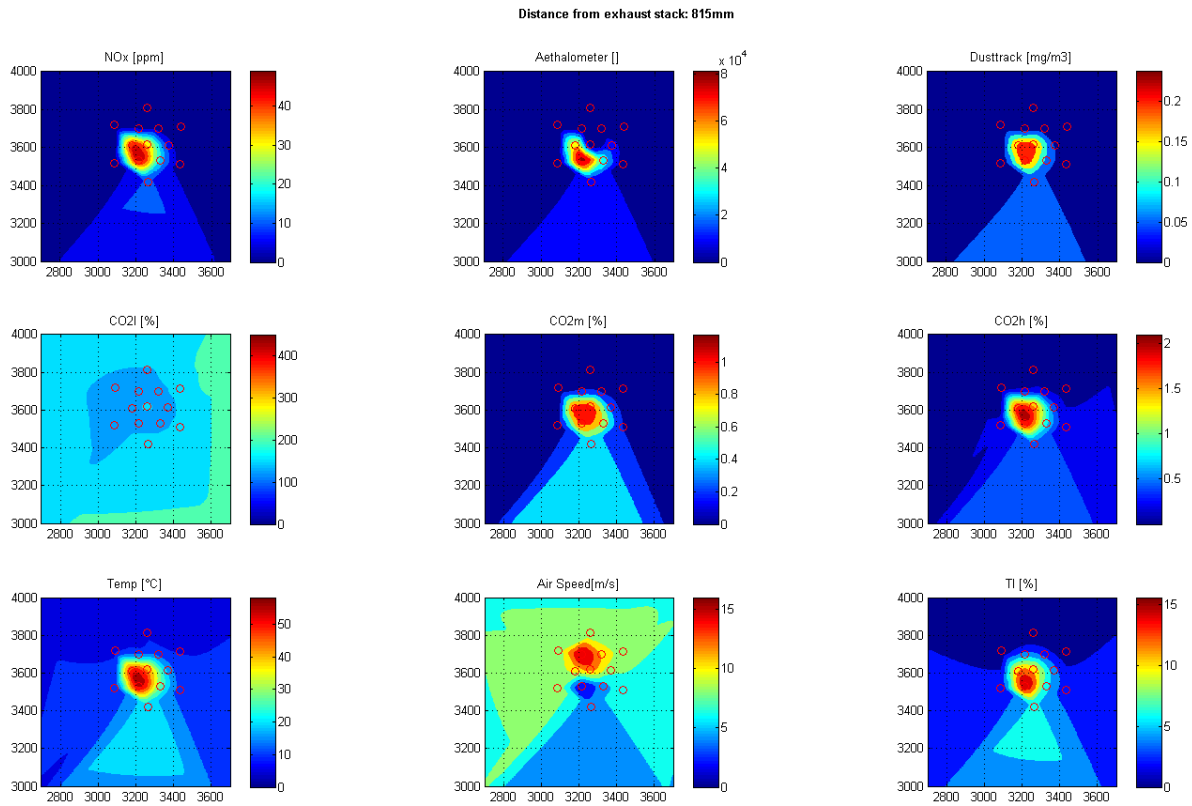

Figure 29: Post-2007, 20mph Test, Plane 4

The PM emissions resembles higher than what expected from a DPF equipped truck. Comparing the PM particle size distributions and AVL MSS between the post 2007 vehicle with the post 2010 (both equipped with DPF), we denoted a crack in the DPF, which was not observable by visual inspection, like many cracked DPF. The first indication and one of the strongest proofs is the presence of a strong accumulation mode and the absence of nucleation mode. This behavior is well expected for non DPF-equipped trucks or cracked DPF and not for healthy DPF equipped truck.

The extend of the crack didn't affect the regular loading of the DPF, which eventually experience the regular loading and regeneration events of a healthy DPF. But the crack has an extent large enough to substantially influence the PM emissions.

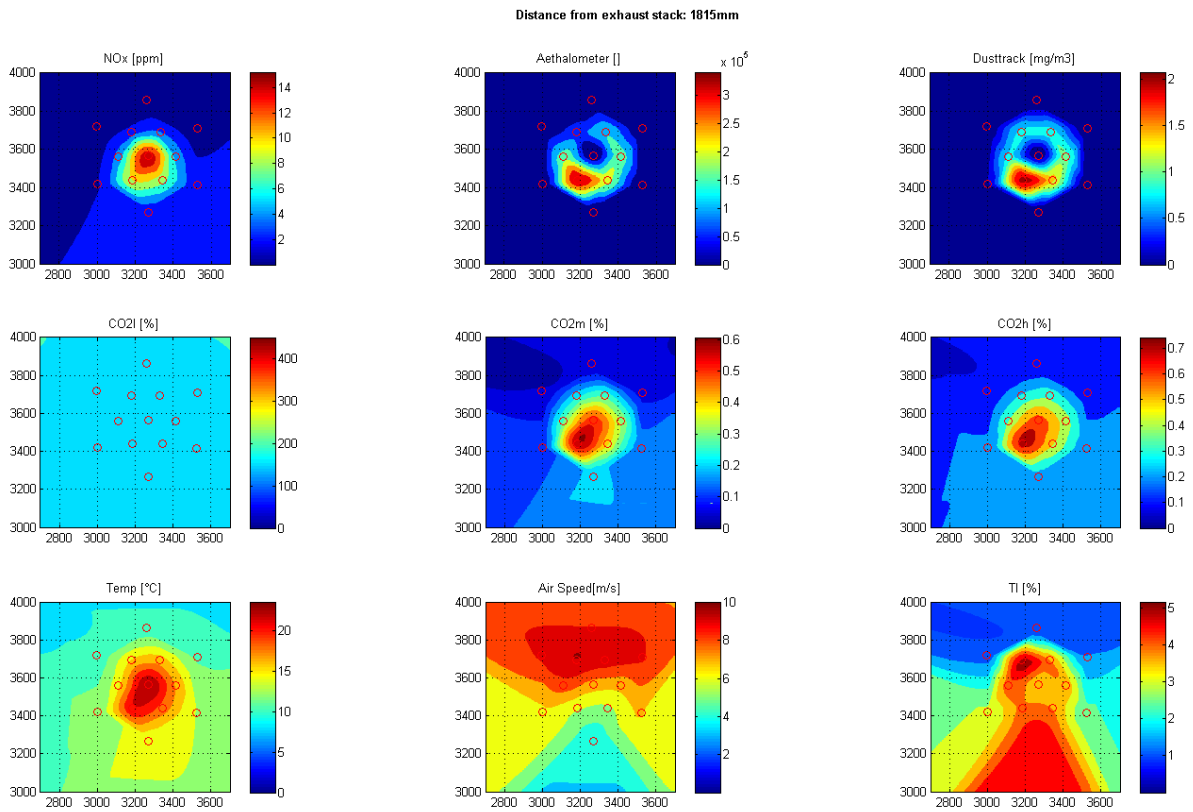

Figure 30: Post-2007, 20mph Test, Plane 6

In this Figure something extremely interesting was captured. The PM plots shows a donut shape plume, which has no evidence in any situations already examined. Looking at the values of PM emissions they results extremely high. The explanation is that the DPF entered into regeneration mode while the plume sampling already started. The 7th injector started to inject fuel into the exhaust increasing the temperature and activating the conversion of PM into CO and CO2. The regeneration was not complete and it lasted only 5 minutes. The presence of a crack in the DPF didn't influence the regular loading of the filter itself, mainly related to the high PM production of engine calibrations for US EPA 2007 regulations, in order to maintain low levels of NOx. The awareness of a regenerating event was denoted by the higher PM production, increase of exhaust temperature and higher fuel consumption.

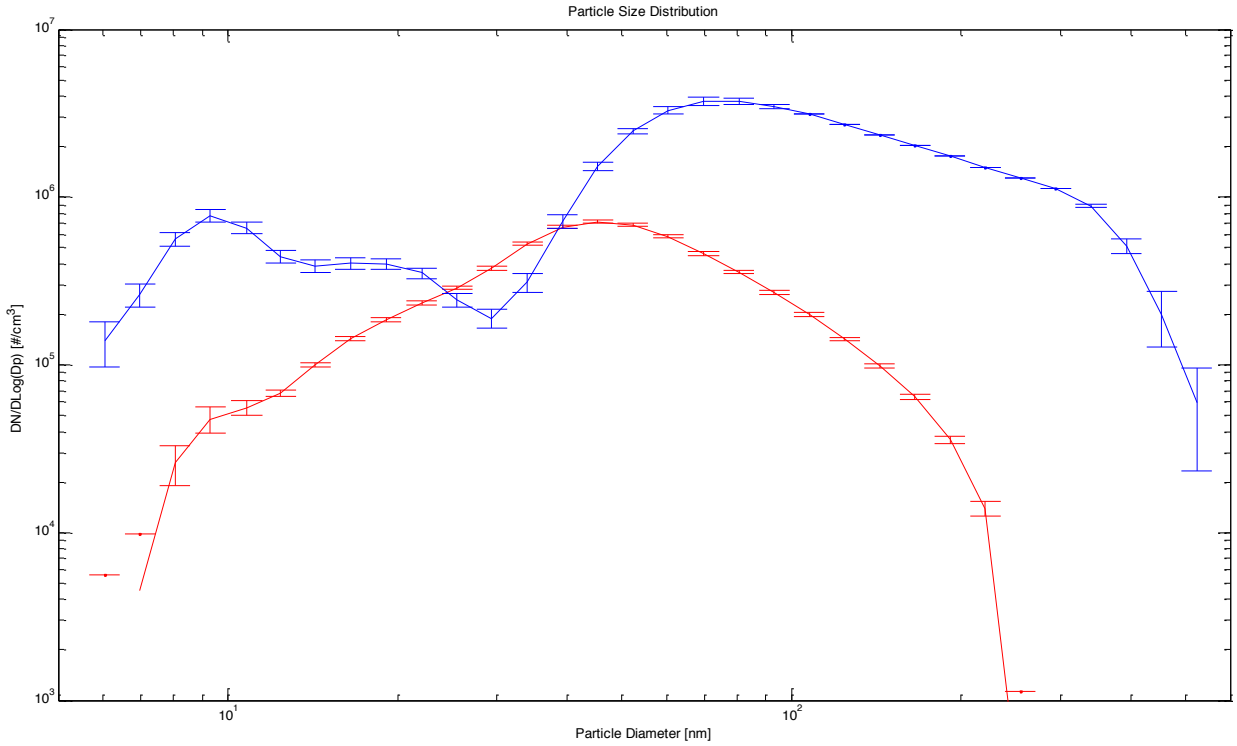

Figure 31: Particle Size Concentration and Distribution during DPF loading and regeneration events.

Is it interesting to notice how the regeneration event strongly influences the PM production. The red line represents the particle size distribution and concentration of a point prior the regeneration event, The blue line represents the particle size distribution and concentration during the regeneration event. The two points where these two particle size distribution and concentration were collected are in proximity of each other, thus they experience a similar dilution and cooling history. The regeneration event provokes the formation of a distinct nucleation mode and an increase from one to two orders of magnitude in the concentration of the accumulation mode. The formation of the nucleation mode is explained by the unburned HC after the injection in the exhaust, and the increase in the accumulation mode is mainly driven by the reduction of filtering efficiency of the DPF itself, by the conversion of carbon in CO2.

3.3.1.6. 35mph Test

The vehicle was at 35mph in steady state conditions and a wind of 35mph was generated inside the wind tunnel. This test represents a vehicle cruising on a flat road at 35mph in calm air. As well as the previous contour plots it is possible to observe among different instruments a similar shape and dimension of the identified plume.

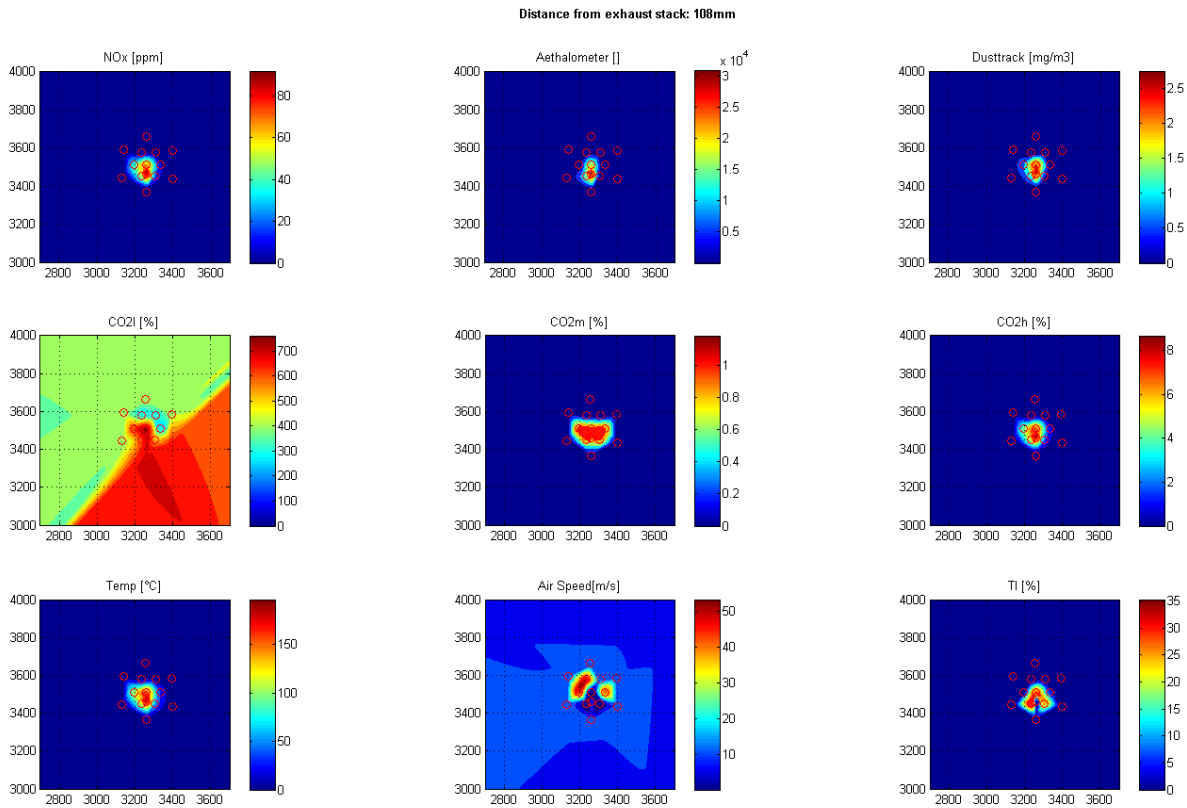

Figure 32: Post-2007, 35mph Test, Plane 1

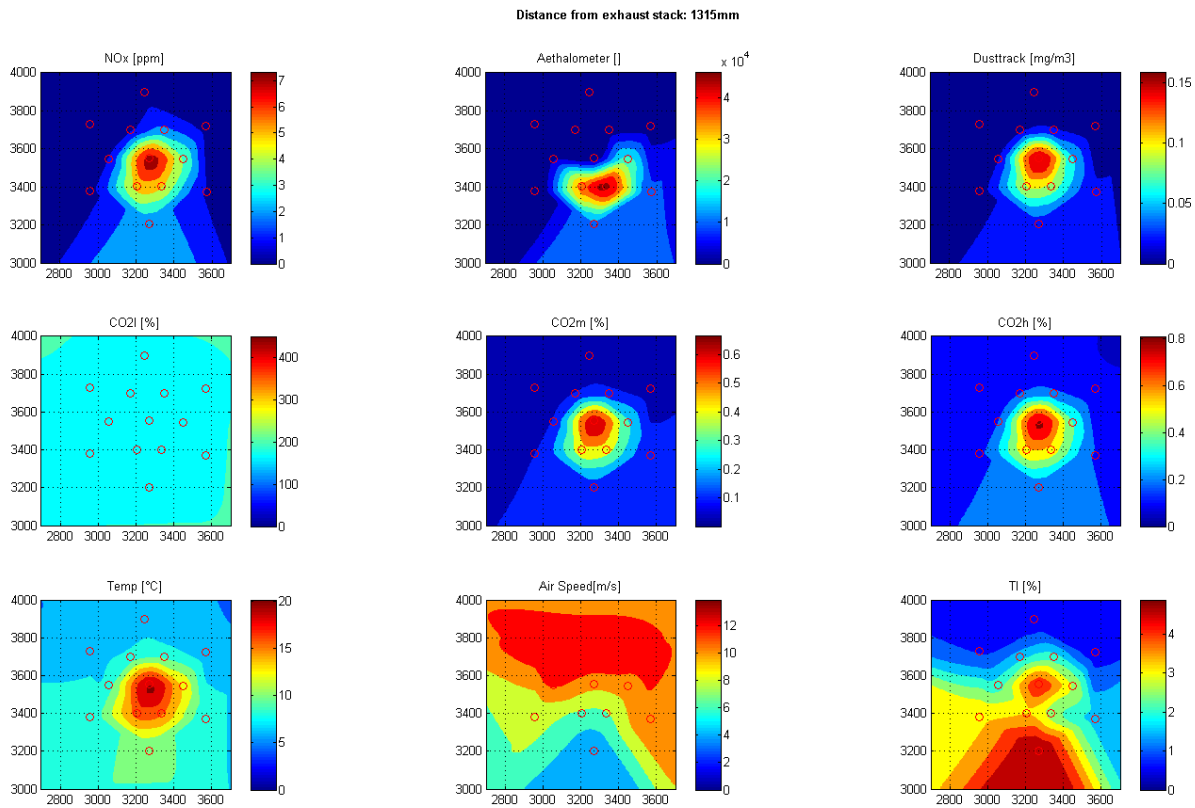

Figure 33: Post-2007, 35mph Test, Plane 5

During the morning warm up of the engine, prior the testing, the engine entered again in regeneration mode, which completed after 30minutes, the 35mph Test started with a newly regenerated DPF.As explained before, a newly regenerated DPF doesn't have a PM "cake" layer above the filter walls, this drastically reduce the filtering efficiency, thus higher PM emissions are observable In the first sampling plane, but at the same time the "cake layer" is building up again and the DPF gains efficiency; which was completed recovered by half way through the test.

3.3.3. Post-2010

3.3.3.1.Idle Test

As described previously in the Idle test, the vehicle is in idling condition and a wind of 5mph is generated. This test represents the emission of truck in a rest area. It is important to remark that among the next contour plots that different instrument shows a similar contour in terms of dimension, color ratio and shape. In addition, results are interesting that for this test the high efficiency of the aftertreatment system, where the PM emitted in the plume resembles lower than the one in the background air.

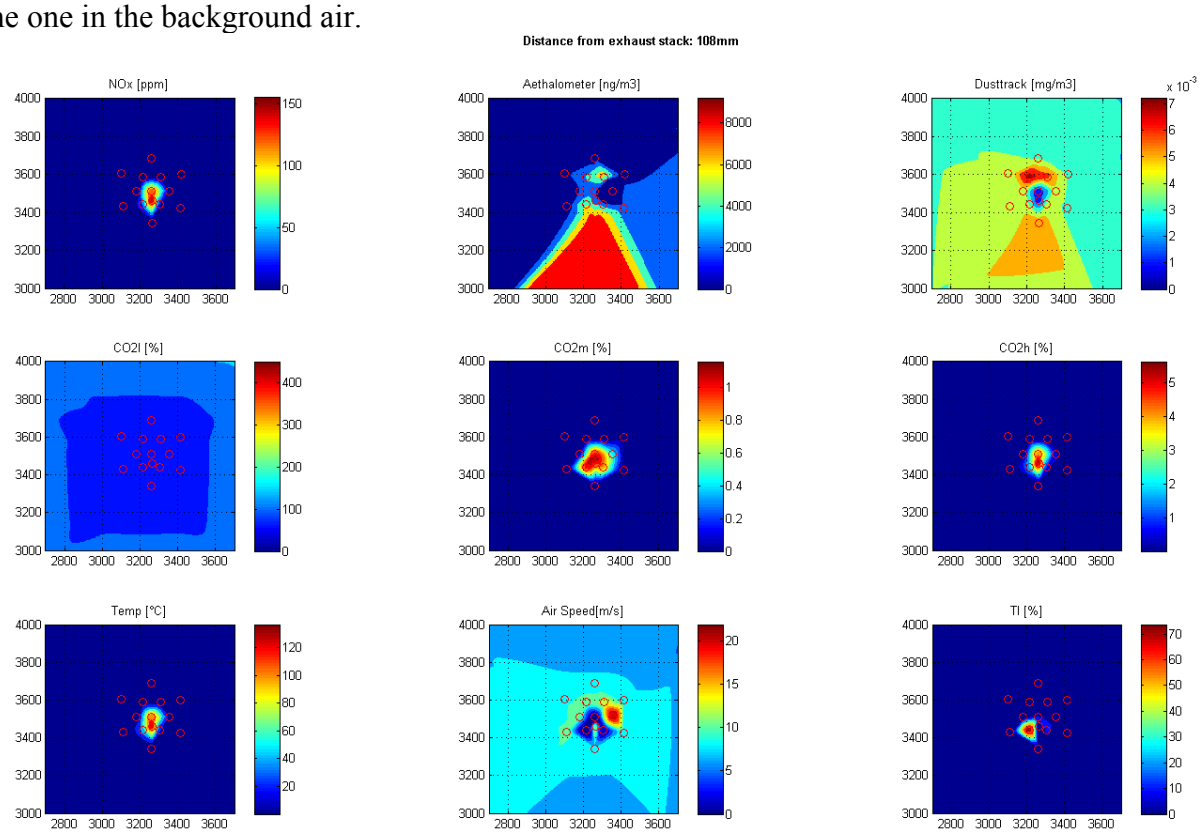

Figure 34: Post-2010, Idle test, Plane 1

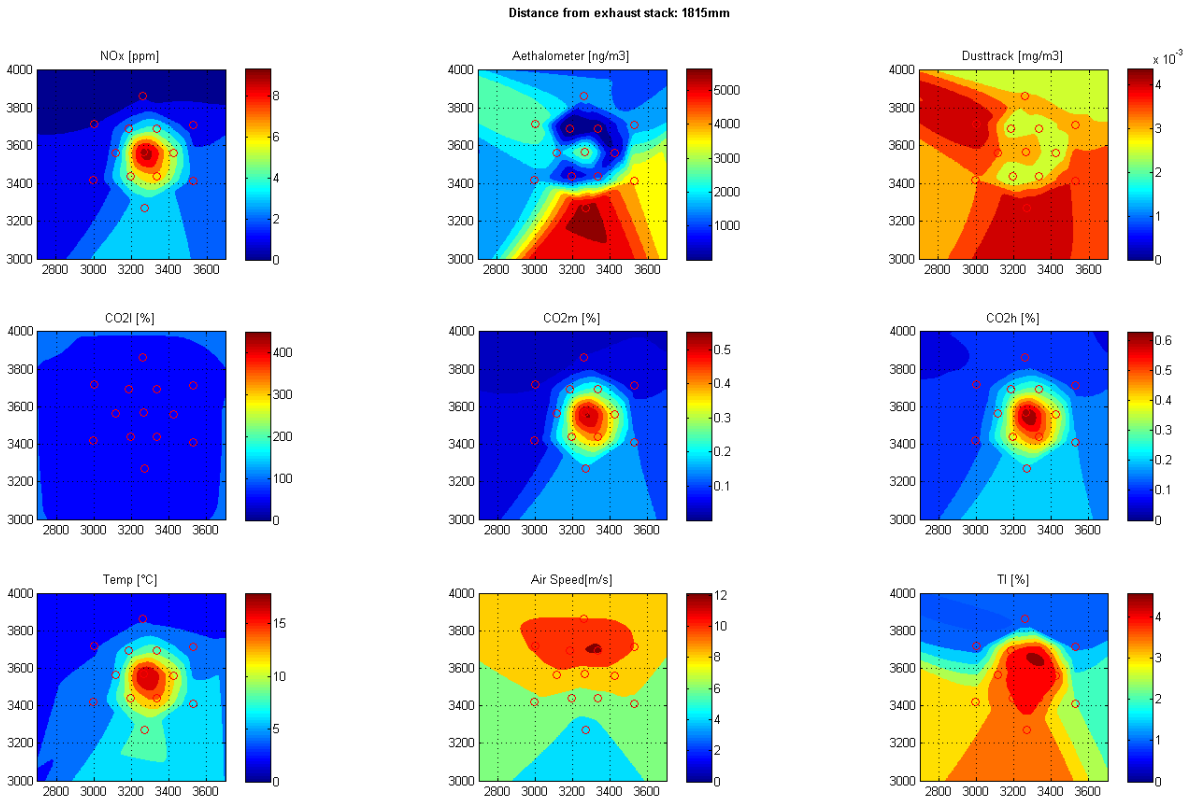

Figure 35: Post-2010, Idle test, Plane 6

This truck is equipped with a state-of-the-art aftertreatment device for on-road applications, which guarantee the compliancy with US EPA 2010 regulations. The raw emissions are extremely low, particularly in steady state operation, which represented a delicate challenge in the plume sampling. The CO2 in this case represents the only viable and reliable way to detect the plume. NOx are in the values of the accuracy of the instruments and more interestingly the PM emitted by the truck is lower than the background air, DustTrak and Aethalometer agree well in this case, the EEPS was in lower than the minimum measurable threshold and no additional information can be. The low NOx emissions are explained only by the fact the engine is idling and not thanks to the SCR. In fact, the exhaust temperature is too low to obtain a chemical activation.

3.3.3.2. 20mph Test

The vehicle was at 20mph in steady state conditions and a wind of 20mph was generated inside the wind tunnel. This test represents a vehicle cruising on a flat road at 20mph in calm air. As well as the previous contour plots it is possible to observe among different instruments a similar shape and dimension of the identified plume.

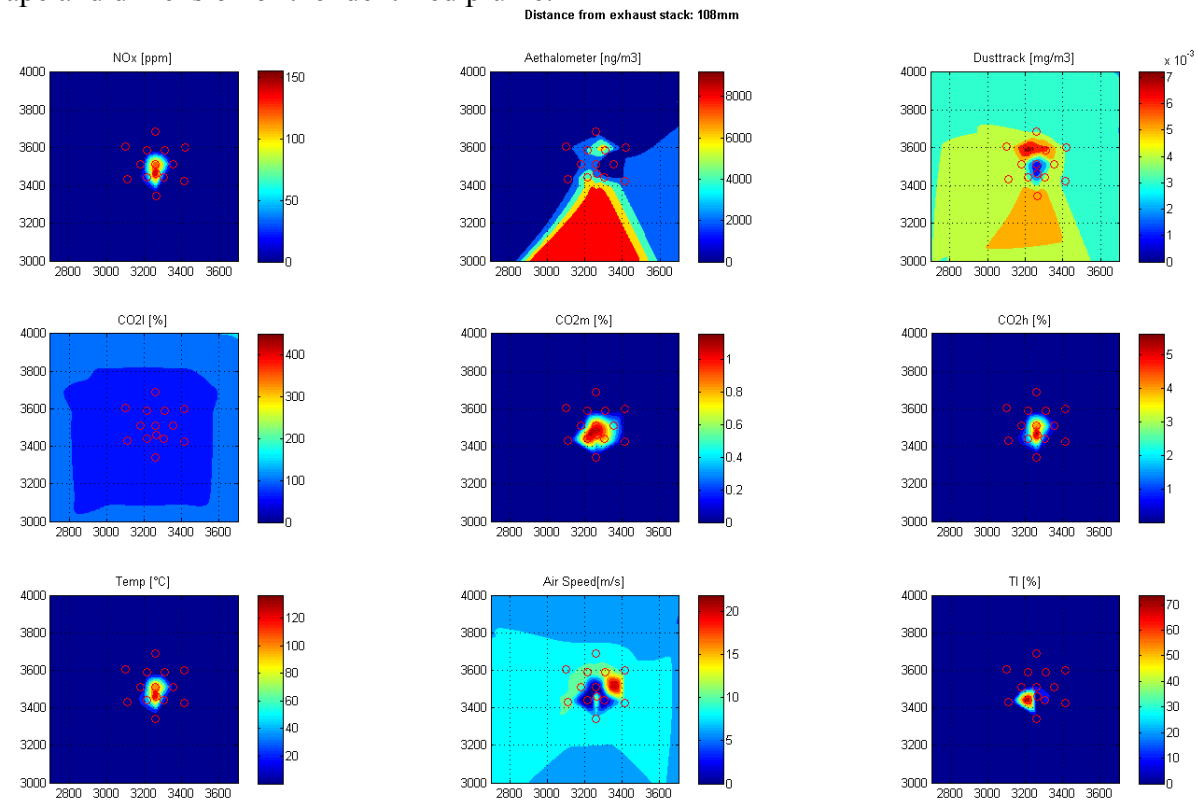

Figure 36: Post2010, 20mph Test, Plane 1

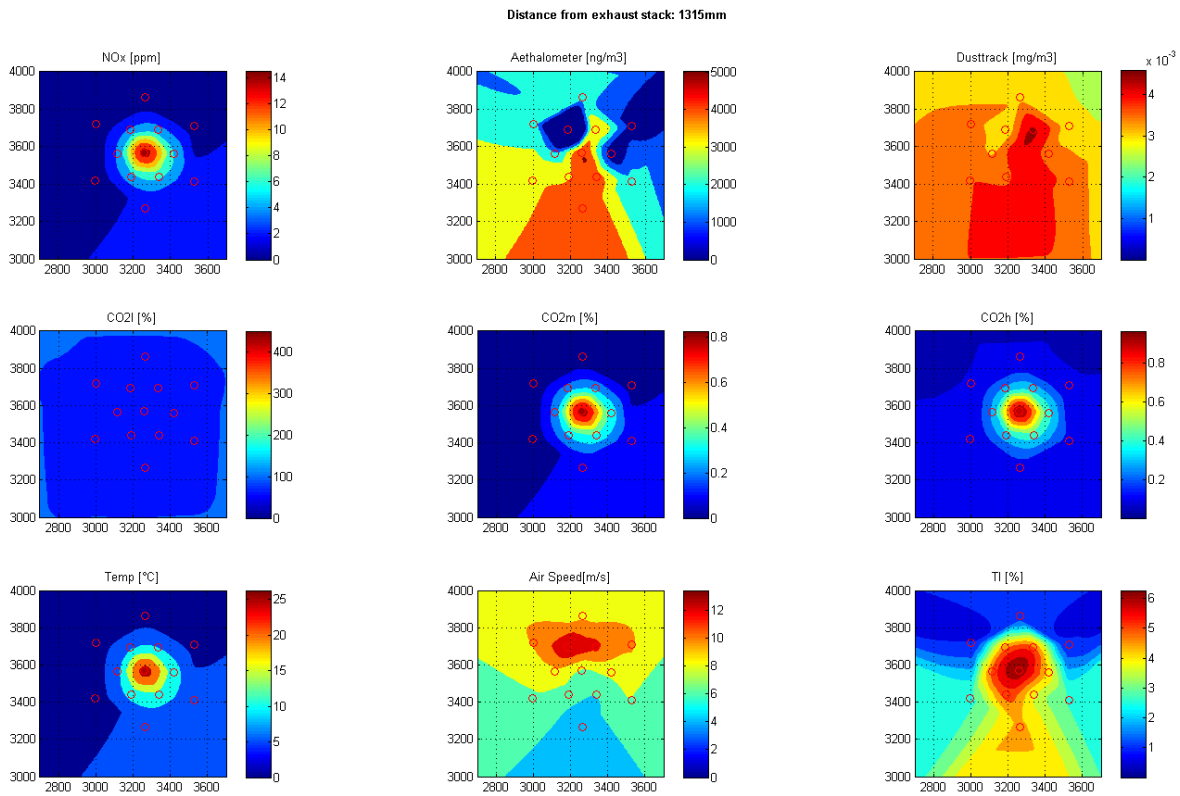

Figure 37: Post2010, 20mph Test, Plane 5

Like the previous test, the post-2010 truck still shows a PM production lower than the one in the background air, thanks to the high efficiency of the DPF. The NOx present a sensible increase, but still lower than the previous trucks. This increase is related to the higher power production from the engine which is not balanced by the SCR, which is still at a temperature too low to activate it.

3.3.3.3. 35mph Test

The vehicle was at 35mph in steady state conditions and a wind of 35mph was generated inside the wind tunnel. This test represents a vehicle cruising on a flat road at 35mph in calm air. As well as the previous contour plots it is possible to observe among different instruments a similar shape and dimension of the identified plume. The high temperature in the exhaust allows for better and more consistent urea-based SCR operations, lowering the NOx emission to value of 15ppm in the raw exhaust.

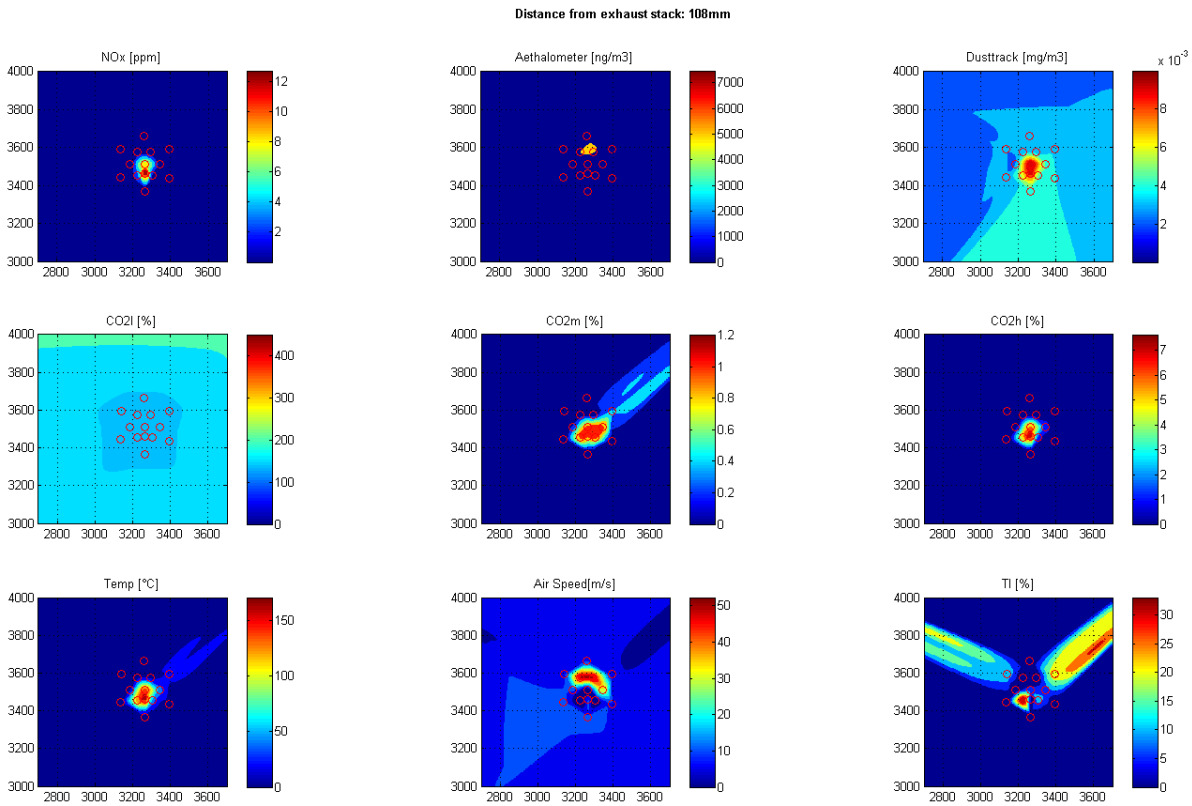

Figure 38: Post2010, 35mph Test, Plane 1

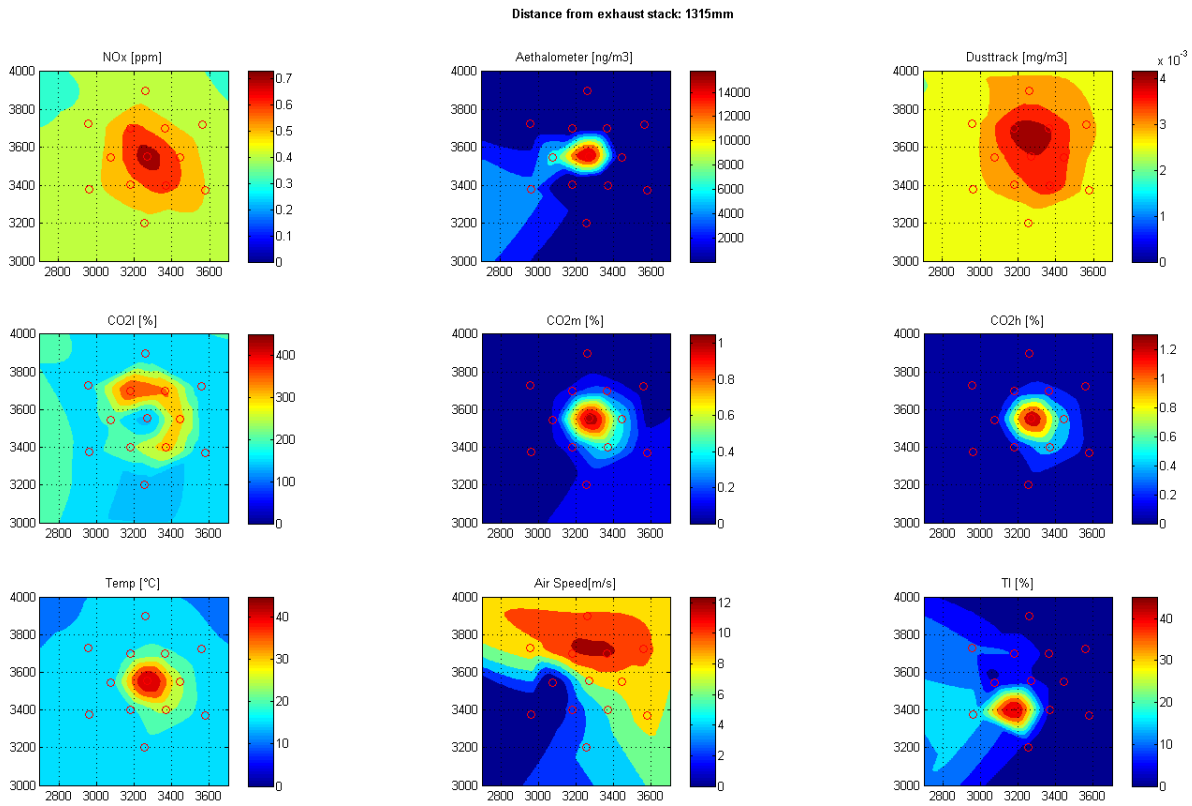

Figure 39: Post2010, 35mph Test, Plane 5

For this operation conditions the engine break the rules of the two previous tests and produce PM higher than the background air. At the same time an increase in the temperature exhaust brings the SCR to full capacity, lowering NOx to values barely traceable by the instruments.

3.4. Raw Exhaust Emissions

The emissions from the raw exhaust for each vehicle are collected in the following table, as averaged values among an entire test.

Truck	Test	CO2 [%]	CO [ppm]	NOx [ppm]	THC [ppm]	AVL MSS[mg/m^3]
Pre2007	Idle	1.357	84.907	214.458	127.782	0
	20mph	4.434	59.394	892.144	48.813	0.529
	35mph	6.261	37.034	1001.800	39.791	1.0726
Post2007	Idle	3.312	219.532	244.462	63.431	0
	20mph	8.736	0	56.888	8.027	0.260
	35mph	9.887	0	244.463	7.5395	0.251
Post2010	Idle	2.644	229.762	87.254	26.987	0
	20mph	5.625	0	125.998	1.095	0
	35mph	7.7792	0	1.232	0	0

The value of emissions for each vehicles fall within the literature values of their respective families of regulations. The same behavior on CO2 emissions are observed for the different vehicles at the same operating speed. A general trend of NOx, CO, THC and soot PM reduction is observed. Although, soot emissions of the post 2007 truck should be equal to the post 2010, but this doesn't happen due to the presence of the crack in the DPF, which is ultimately confirmed by these resuts.

It is important to remember that the PM size distribution and concentration from the raw exhaust are in Excel files.

APPENDIX A: Structural analysis

Geometry definition

SolidWorks© was used to define the final geometry of the Wind Tunnel. This geometry was exported to a FEM software. Femap© with Nastran© was used for the Structural Analysis. It is possible to observe in the following Figure 40: Wind Tunnel Geometry outside View and Figure 41: Wind Tunnel Geometry Direct Flow Path View the geometry generated with SolidWorks©.

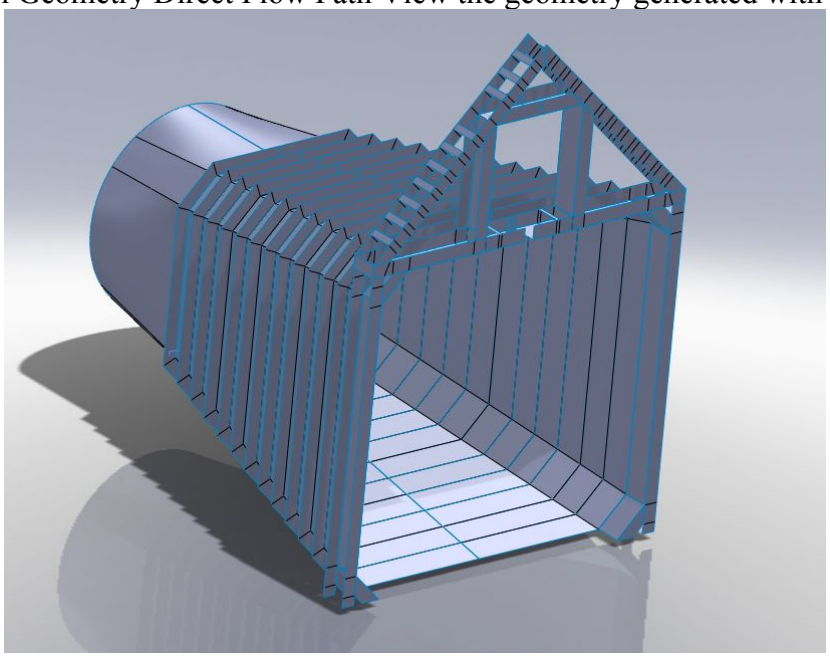

Figure 40: Wind Tunnel Geometry outside View

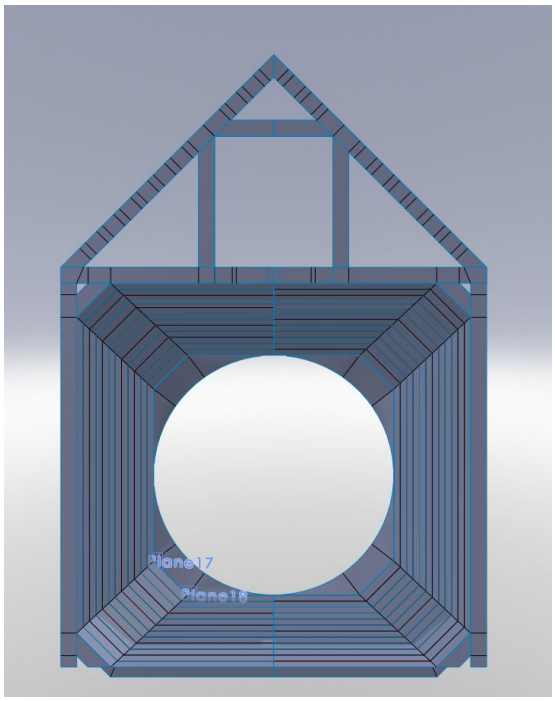

Figure 41: Wind Tunnel Geometry Direct Flow Path View

Figure 42 shown below depicts the final part of the Wind Tunnel, where the propeller will be placed.

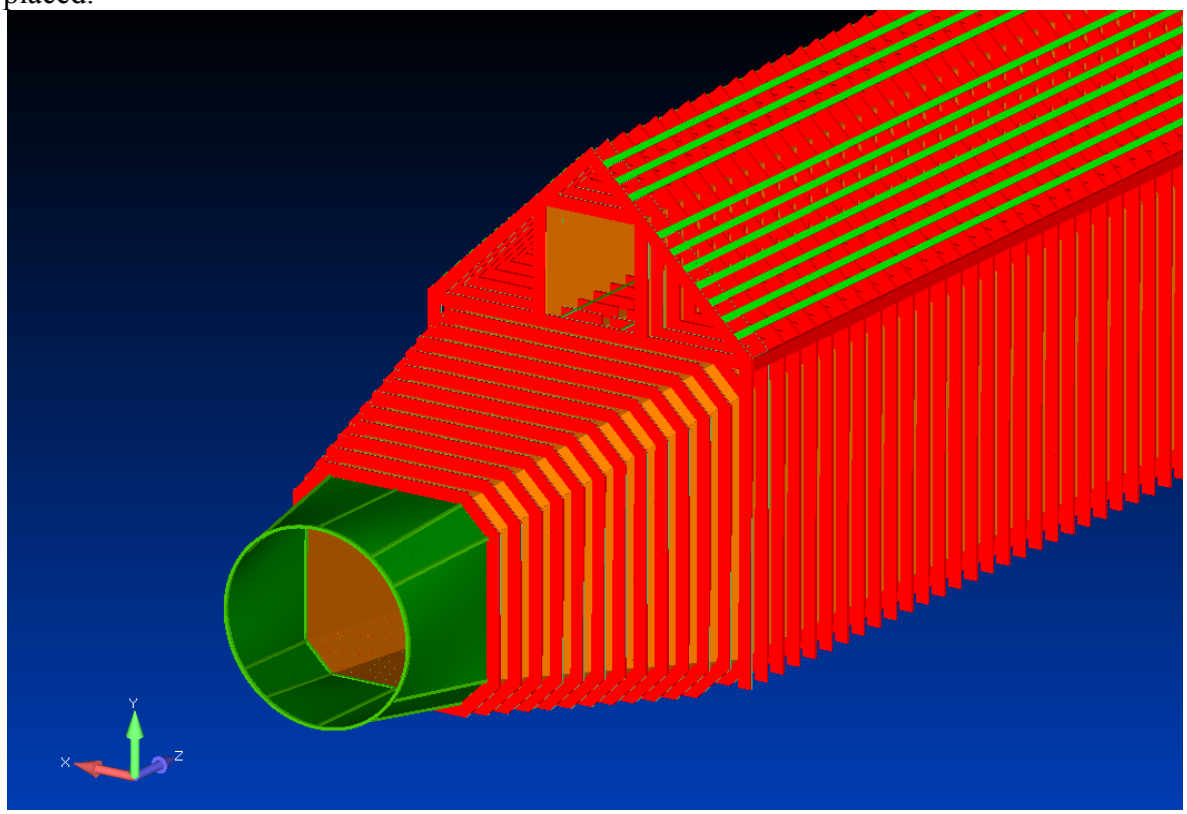

Figure 42: Wind Tunnel Propeller Placement

The following image (Figure 43) shows the corridor built for the cart, including guidance rails. The roof has a double role – to act as both a regular roof, as well as a structural truss member to accommodate the slot for the cart.

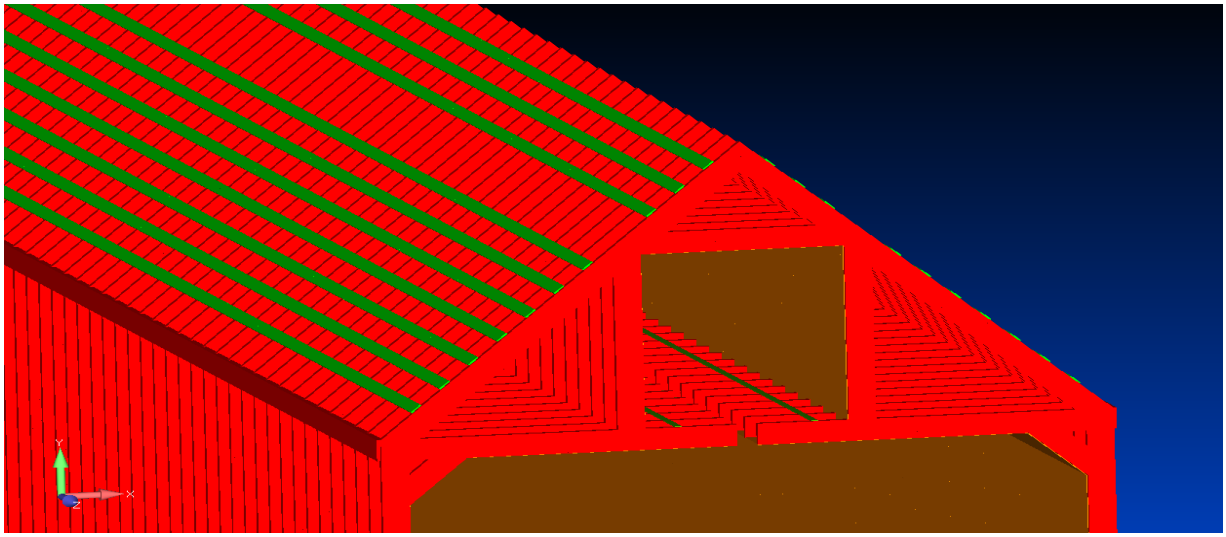

Figure 43: Wind Tunnel Cart Corridor

A standard-size door and a screen, shown in Figure 44, were modeled in order to better understand the concentration of stresses generated by their presence.

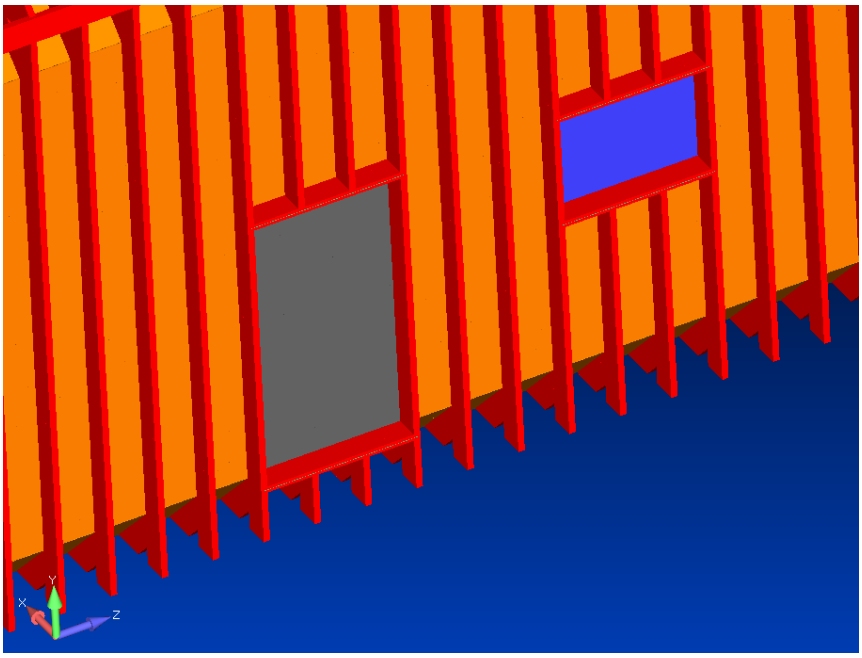

Figure 44: Wind Tunnel Door and Screen

Please note the entrance for truck or maintenance vehicles, shown in Figure 45, will be moving away from the flow straightener in front of the Wind Tunnel, in order to not weaken the structure

and have the largest opening possible. In this structural analysis, the flow straightener has not been considered, because it does not play a structural role in the overall Wind Tunnel.

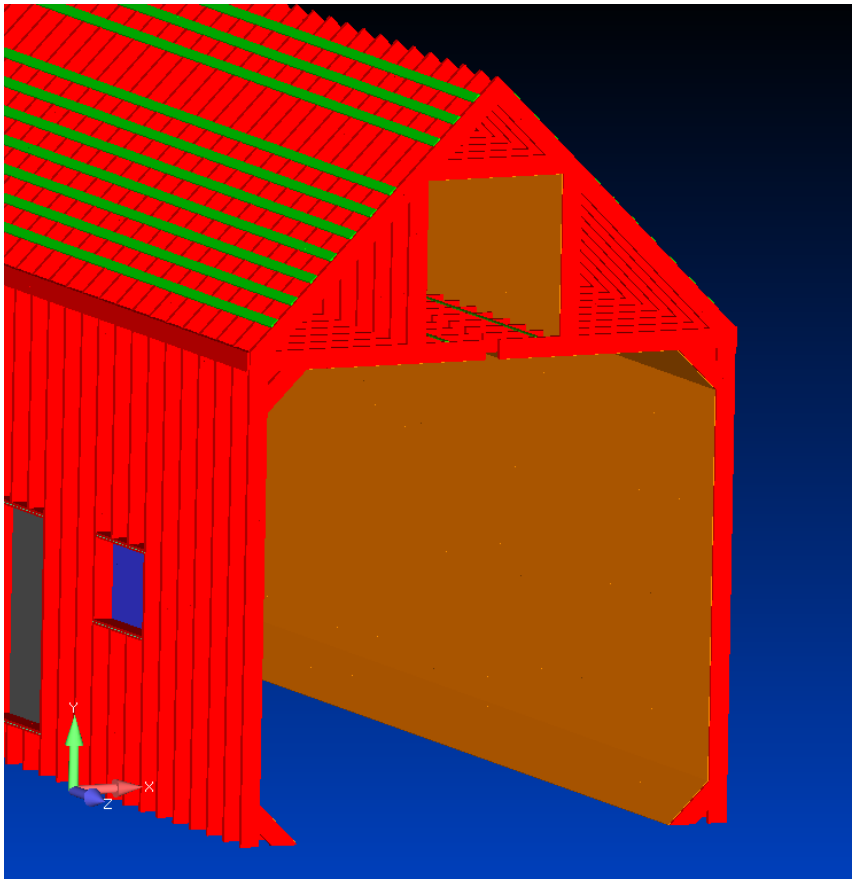

Figure 45: Wind Tunnel Structural Inlet Drawing

Figure 46 below depicts the entire Wind Tunnel geometry.

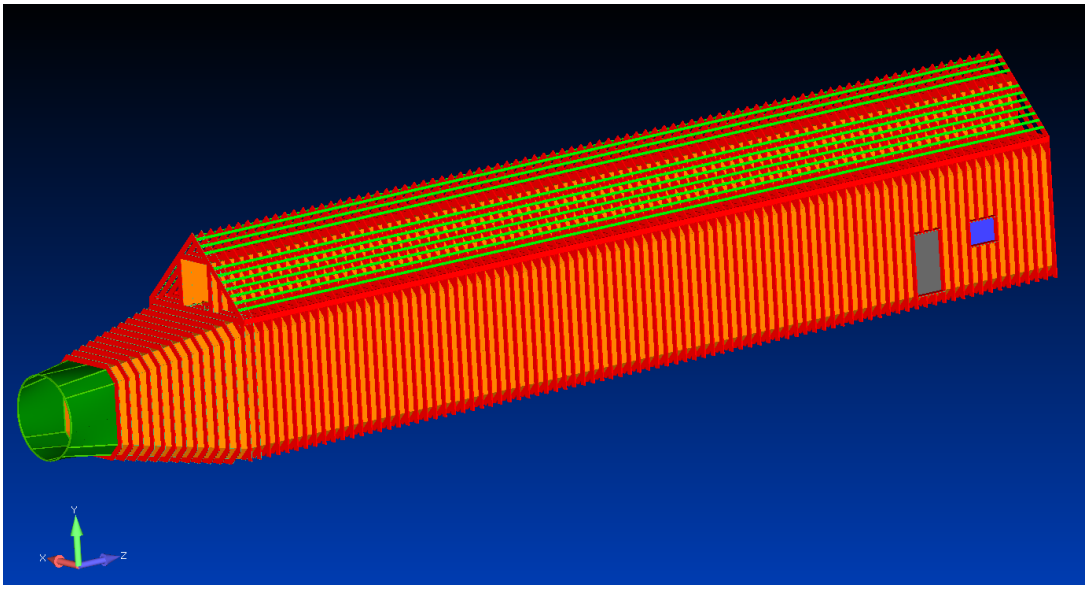

Figure 46: Wind Tunnel Geometry

Material Properties

The first step for the Structural Analysis is to define the materials of the structure. In this case, Structural Steel (Figure 47) for metal parts, Structural Wood (Figure 48) for the entire wind tunnel and acrylic glass (Plexiglas©) for the screen.

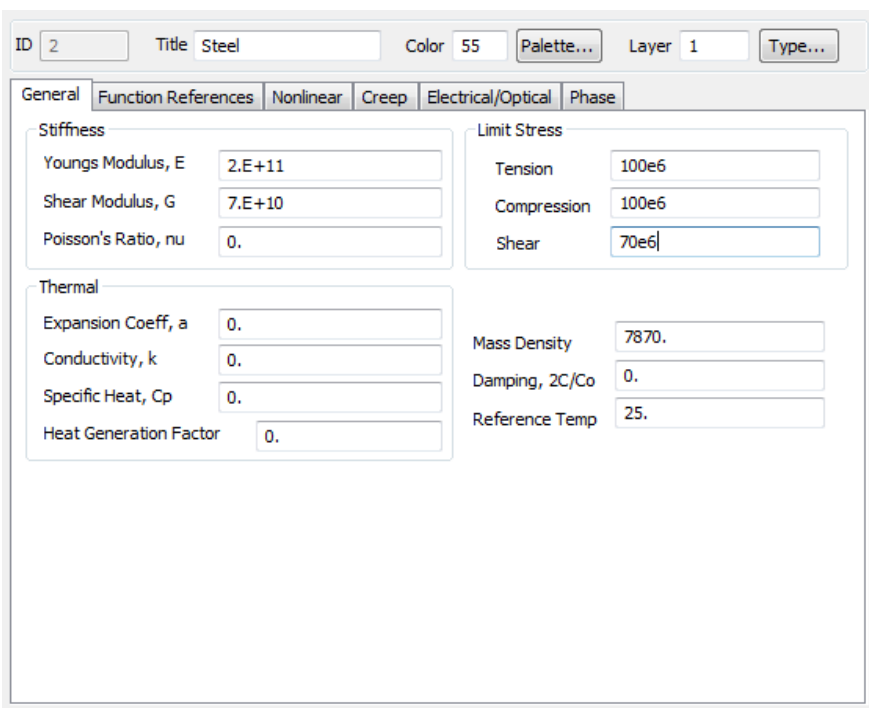

Figure 47: Wind Tunnel Structural Steel Analysis

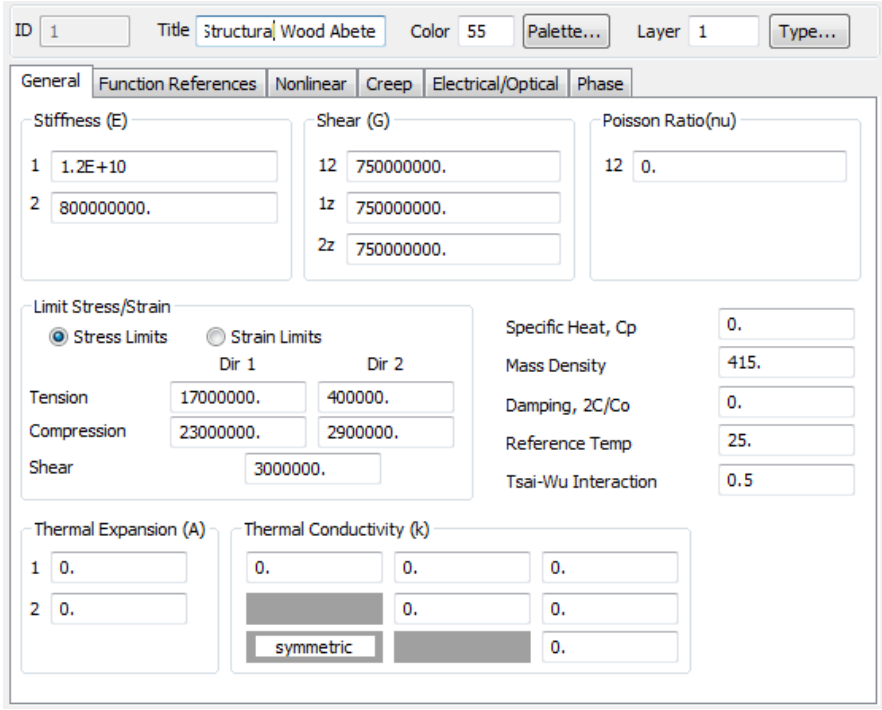

Figure 48: Wind Tunnel Structural Wood Analysis

Element properties

A critical modeling component is the definition of the Element Property. As shown in the previous images, surface elements have been chosen considering mesh quality, computational time and type of problem. Each element has been defined as a laminate element, whereby the Failure Index Method (with Tasi-Wu interaction theory) is more adequate, as opposed to the Von Mises Criterion due to the presence of the wood (an orthotropic material). Although the structure was defined using laminate elements, the substitution of steel plate element (isotropic material) yields qualitative information. In addition this provides for a reduction in computational time, and the quantitative information allows one to assign a Failure Index for stresses modeled for the structure. Due to the nature of the Failure Index, it provides for a PASS or NON-PASS test. The structure is considered safe from failure if the Failure Index remains within the range of 0 and 1. In Figure 49, it is possible to observe the screenshot of a general laminate element.

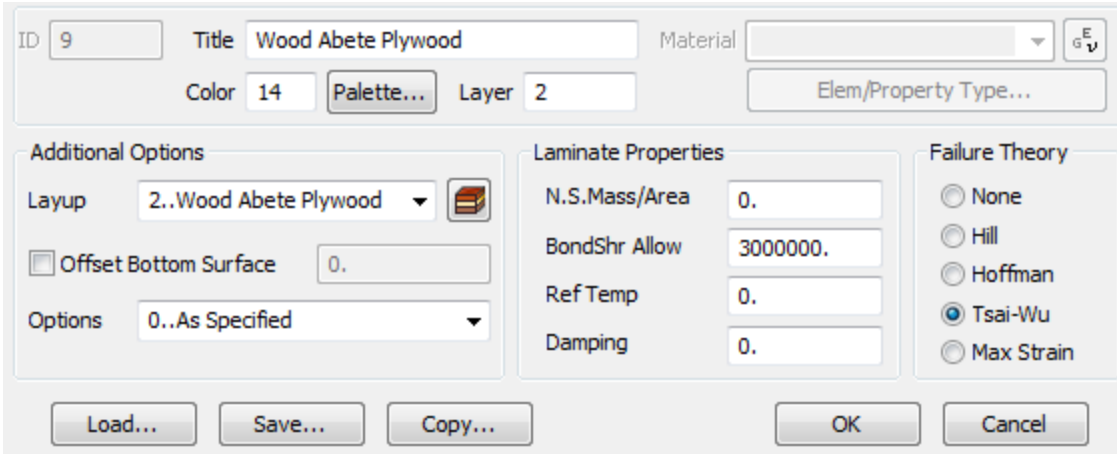

Figure 49: Wind Tunnel Structural General Laminate Element

Mesh Definition

The mesh generated with described parameters present a total number of 282,125 of Laminate Elements, as illustrated in Figure 50. Due to the symmetry of the problem and the regular shape of the structural elements (such as the vertical studs and plywood plate), the mesh results are geometrically simple and well structured, leading to an overall high mesh quality. Reliable results in the structural analysis can be achieved only if quality meets high standards, such as these.

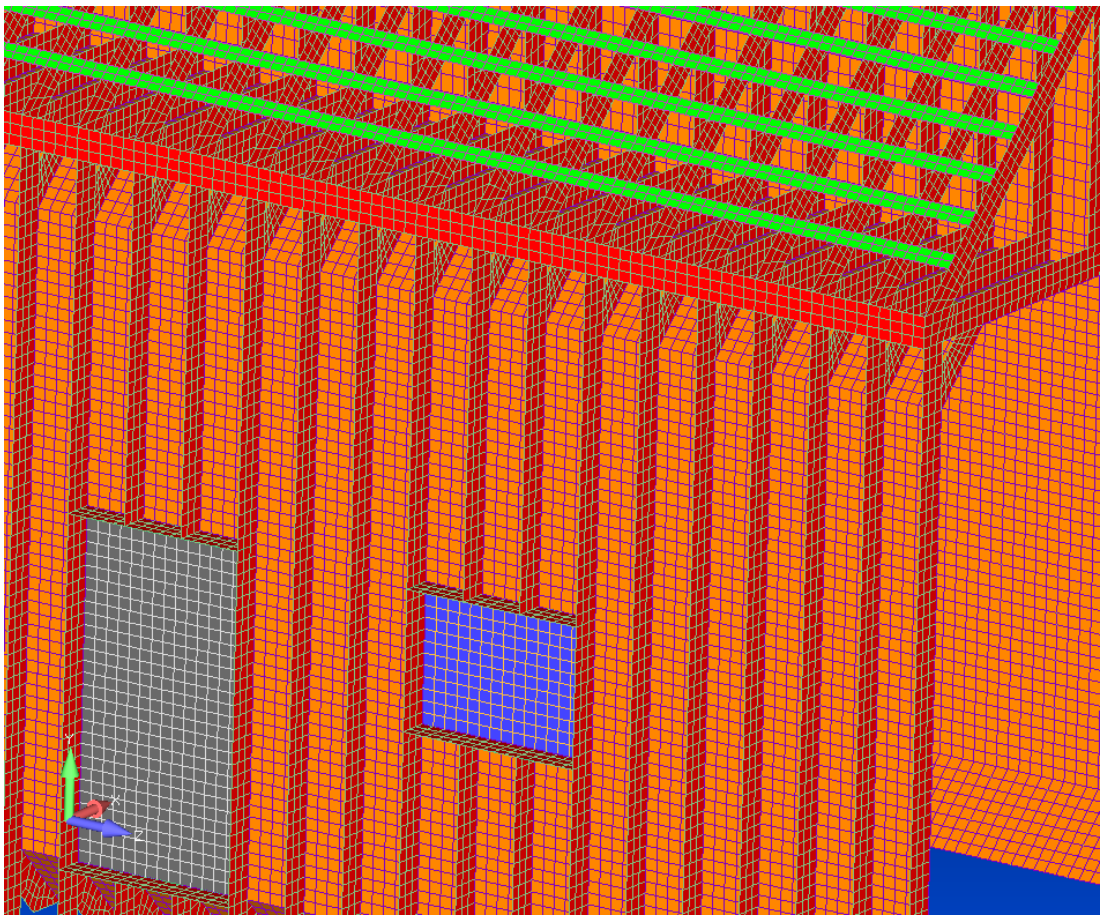

Figure 50: Wind Tunnel Mesh Illustration

Load Sets and Constraint Set

This project represents a combination of different analyses due to the complexity and dimension of the structure itself.

The first Load Set is related to the operational condition of the Wind Tunnel:

- 2,000 Pa Differential Pressure over the internal plate of the Wind Tunnel for the constant section part.
- 2,500 Pa Differential Pressure over the internal plate of the Wind Tunnel for the convergent part (the increase in velocity reflects into and increment of Differential Pressure).
- Gravity (9.81 m/s^2).
- 500 Kg Cart placed in each elemental section of the Wind Tunnel.
- 1,000 N force placed on the first portal, along the longitudinal axis, to replicate the load of the flow straightener and screens.

These loads are defined, thanks to previous CFD Analysis, considering maximum rounded observed values. In addition, they were doubled for safety reasons.

The second Load Set is related to the weather conditions of the Morgantown area. A snow accumulation of 1 m over the entire roof with the heaviest snow possible (500 kg/m^3) was considered. This result in a snow loading with a density range of 100 – 500 kg/m^3 and would represent accumulation during an extraordinary winter. This condition is clearly the worst possible scenario, resulting in a 5,000 Pa loading over the entire roof. Moreover, considering the steep roof pitch, such accumulation would not likely be realized.
The last Load Set is identified by a 50 mph wind on the lateral surface of the Wind Tunnel. The value of the load is calculated considering the entire lateral surface as Stagnation Region for the wind. This hypothesis will be more severe than any real conditions. Such a wind load results in a 300 Pa over the entire exposed lateral surface (roof included).
The base of the entire structure is fixed to the ground.

Structural Results

Operational conditions

This simulation corresponds to the load defined for the operational condition. It is possible to observe in the following images (Figure 51 to Figure 54) that the structure completely satisfies the threshold identified by the Failure Index Method. The presence of the door and the screen does not affect the integrity of the structure. The Failure Index Contour is between 0 and 0.7.

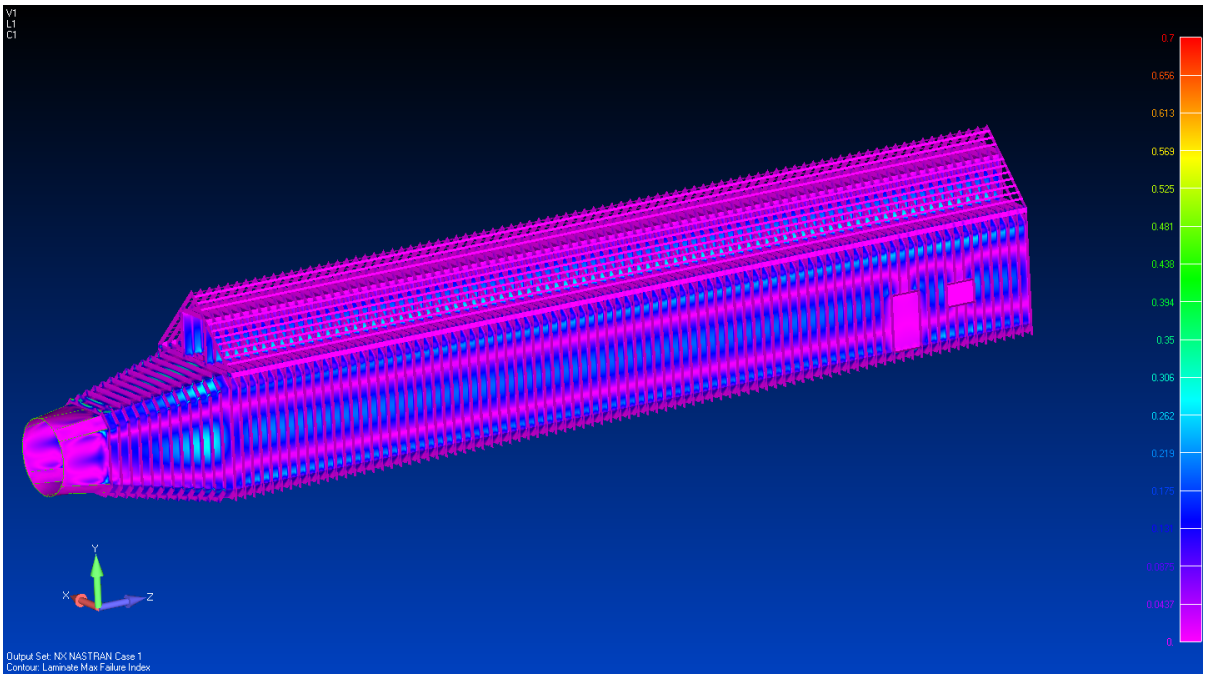

Figure 51: Wind Tunnel Operational Conditions Full Length

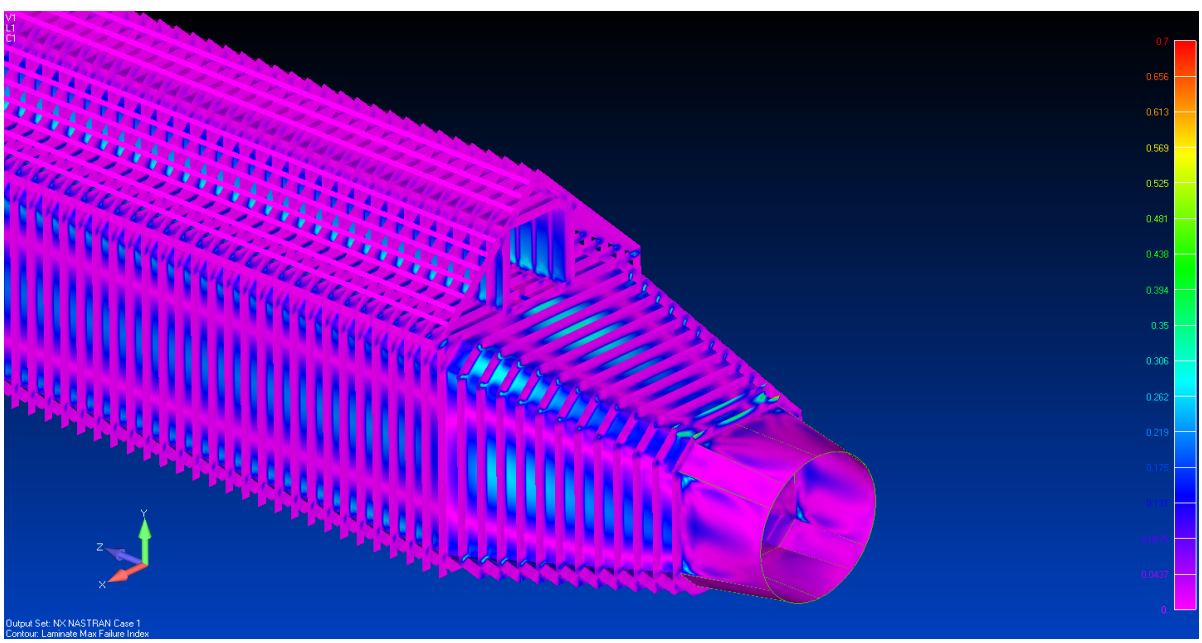

Figure 52: Wind Tunnel Operational Conditions Exit

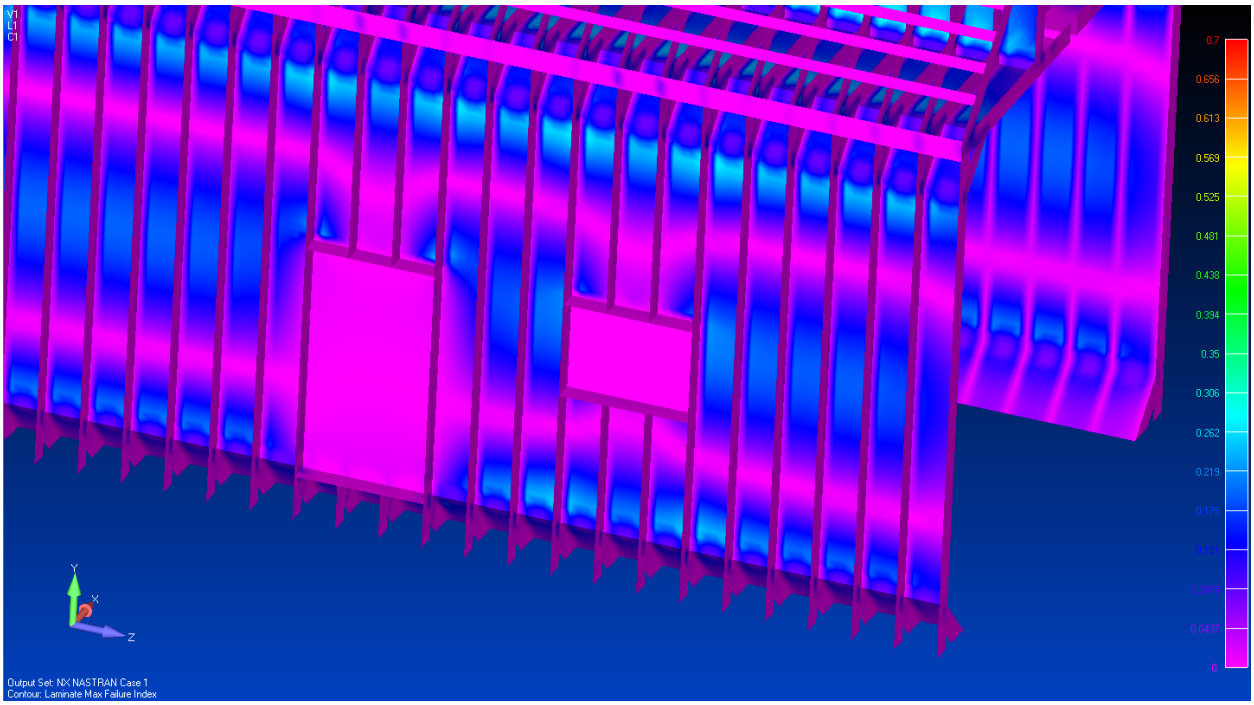

Figure 53: Wind Tunnel Operational Conditions Screen and Door

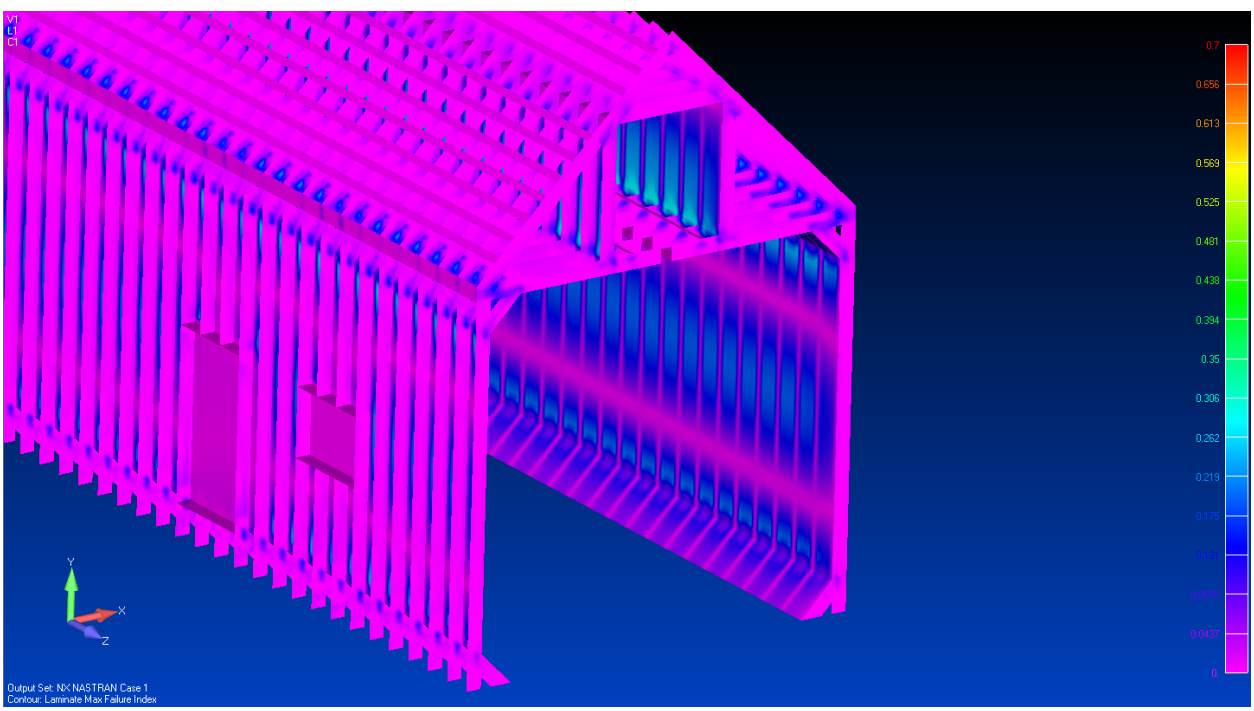

Figure 54: Wind Tunnel Operational Conditions Inlet

Snow Accumulation

Applying the load set described previously for Snow Accumulation Condition, Figure 55 and Figure 56 show that is clear that the structure can withstand these extraordinary conditions with a considerable factor of safety.

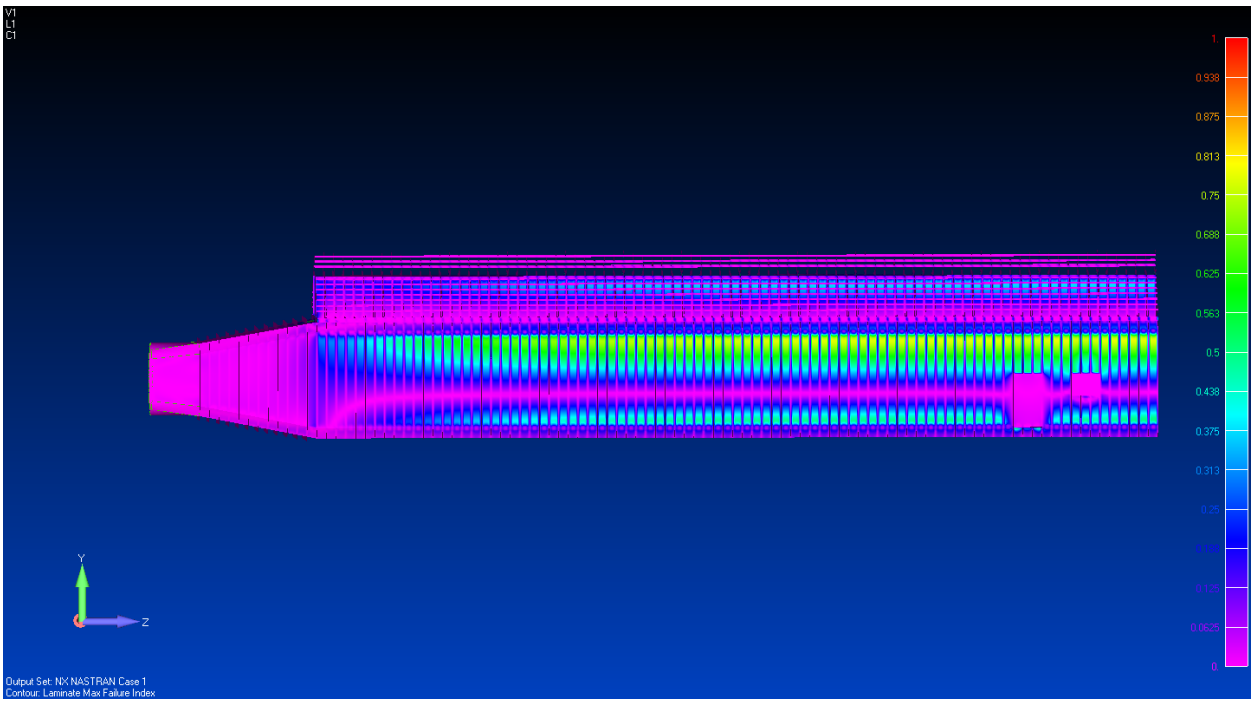

Figure 55: Wind Tunnel Load Conditions Full Length

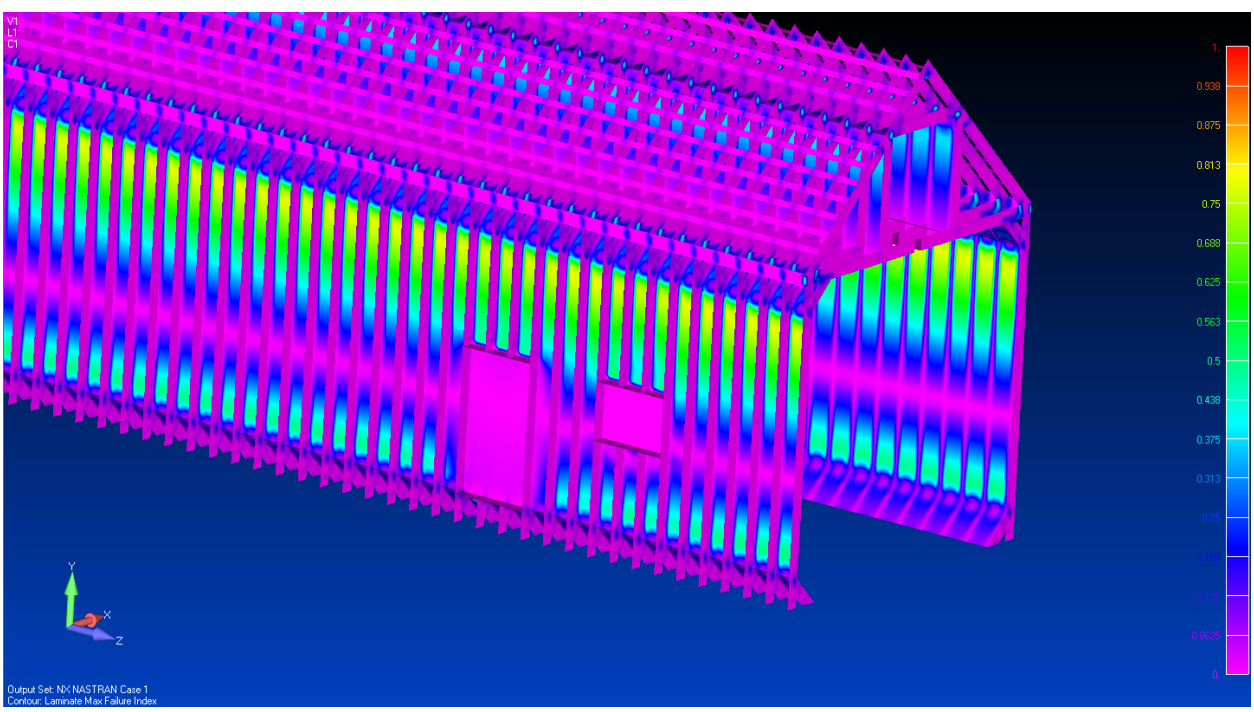

Figure 56: Wind Tunnel Load Conditions Door and Screen

Wind load

Applying the load set described previously for Lateral Wind Condition, Figure 57 and Figure 58 shows it is clear that the structure can withstand these extraordinary conditions with a substantial safety level.

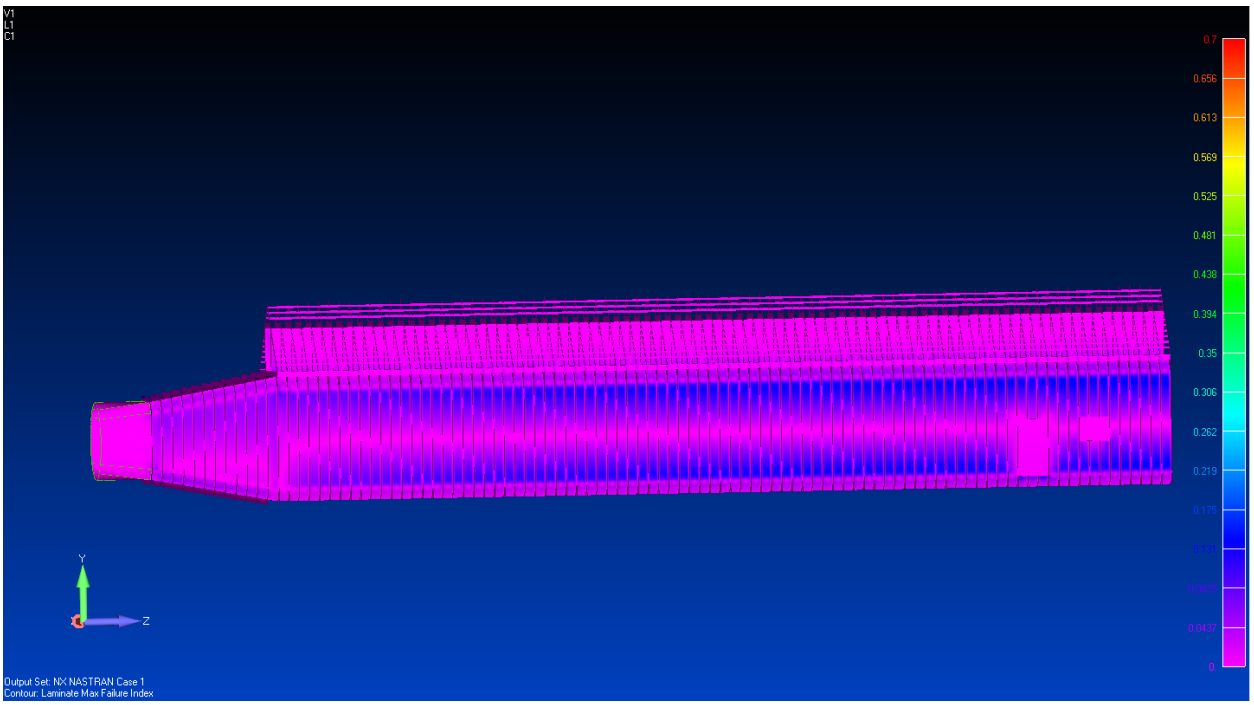

Figure 57: Wind Tunnel Lateral Wind Load Conditions Full Length

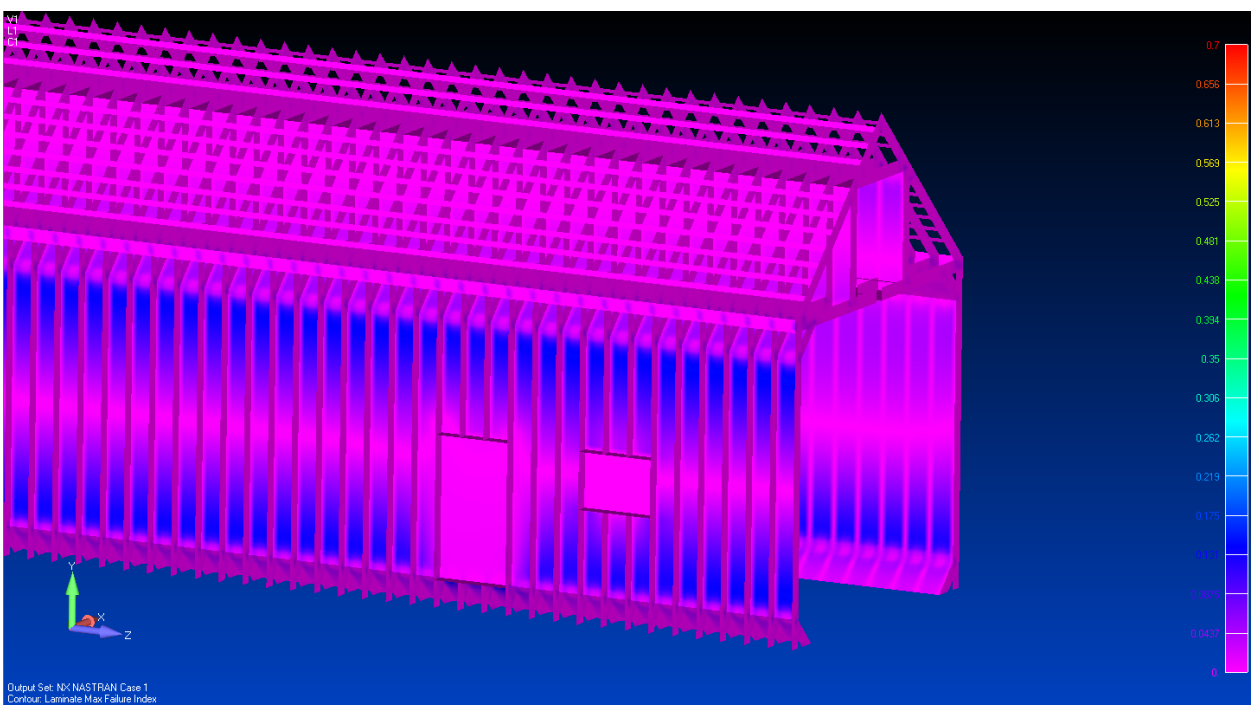

Figure 58: Wind Tunnel Lateral Wind Load Conditions Door and Screen

Natural Modes

Due to the operational conditions of the Wind Tunnel, it is extremely important to verify that no resonance problems occur.
The excitation frequency generated by a 4-blade propeller that is being powered by an engine operating between 1000 and 2000 rpm is in the range of 65-135 Hz. A 5-blade propeller will be in the 85-165 Hz operating range.

Femap is able to indicate the first 10 Natural Frequencies of the model. It is important to remember that only the first 5 values shown in Figure 30 have a physical relevance. The results are collected in the following Table 16: Wind Tunnel Natural Frequencies.

Frequency	Unit
Excitation Frequency (4 blades)	65-135
Excitation Frequency (5 blades)	85-165
1st Natural Frequency	4.45
2nd Natural Frequency	5.88
3rd Natural Frequency	9.06
4th Natural Frequency	11.81
5th Natural Frequency	13.13

Table 16: Wind Tunnel Natural Frequencies

It is clear that no problem of resonance will occur, since the excitation frequencies are higher than the Natural Frequencies with a sensible margin. This image illustrated in Figure 59 the deformed shape of the model for the first Natural Frequency with an amplification factor for the deformation of 30.

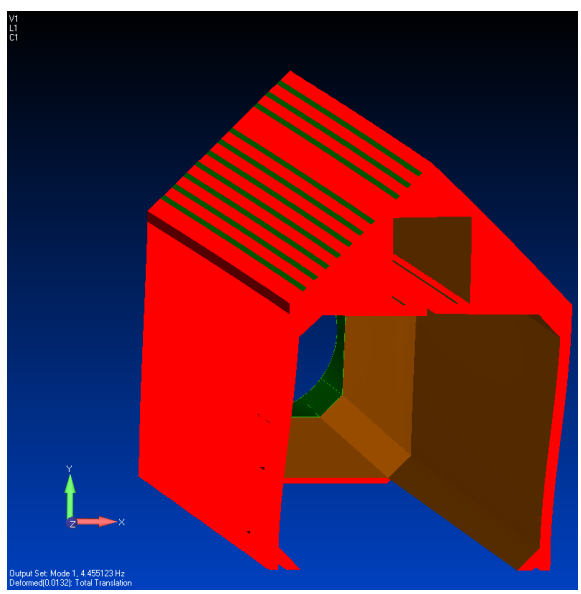

Figure 59: Wind Tunnel Deformed Shape Model

Buckling

Due to compression loading on the structure, it is important to check that no buckling problems could occur during the operational conditions. The result obtained by Femap© and shown in Figure 60, does not reflect the symmetry of the problem. These are only mathematical results (eigenvalue of the load is 8), without physical values. However, it is possible to say that buckling will not occur, given the design inputs and boundary conditions.

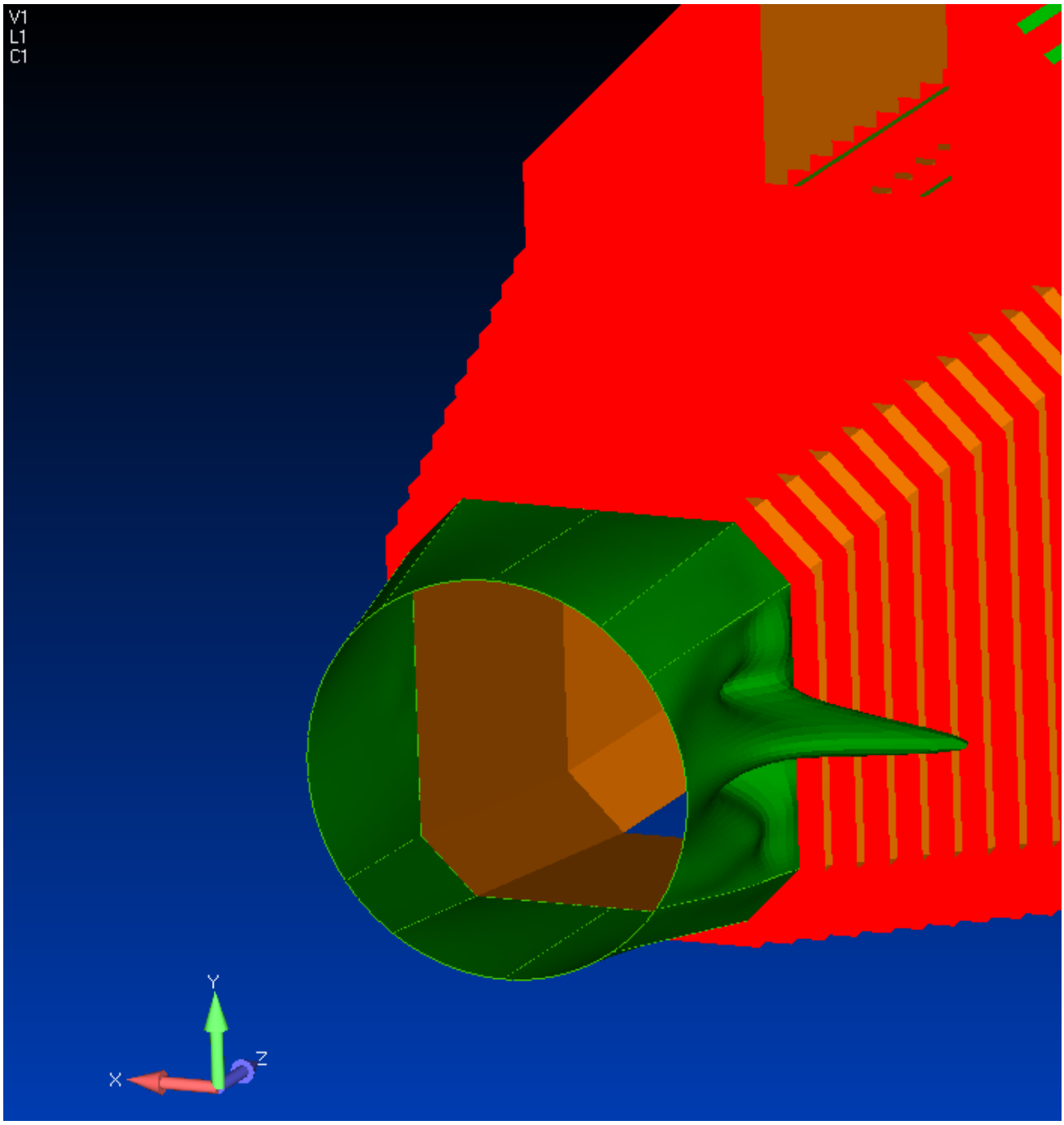

Figure 60: Wind Tunnel Deformed Shape Model

APPENDIX B: Wind Tunnel Construction

The construction of the Wind Tunnel is divided into five major subtasks:

- Main Structure
- Engine and Propeller
- Services (Electric and Compressed Air system)
- Data Acquisition System (DAQ) and Instrumentation
- Movable Platform

Wind Tunnel main structure

The structure of the Wind Tunnel is composed of three main components. The concrete floor and footers provide the foundation for the wood structure, which is the second component. The remaining component is the metal convergent structure in front of the wind tunnel that will stabilize the wind tunnel internal flow, minimizing turbulence intensity, in order to provide for a repeatable, quantifiable flow field. The structural components were chosen upon the FEA results observed in the structural analysis. Table 17 show details the components of the wood structure. Table 18 details the components of the metal structure.

Table 17: Wind Tunnel Wood Structure Components

Component	Qualification
2"x8"x16' Kiln Dried Lumber	Section component
2"x8"x16' Treated Lumber (grade 1)	Base component
1"x4"x16' Kiln Dried Lumber	Roofing fixing
4'x8'x1/2" Plywood BC	Internal covering
4'x8'x1/2" Plywood CC	Gusseting
4'x8'x3/4" Plywood CC	jig section
Metal Roofing	Galvanized Steel
Metal Wall	Galvanized Steel

Several solutions have been put into place to guarantee the best and safest construction result. The side-walls of the Wind Tunnel are composed at the bottom of 7 inch concrete curb, in order to prevent the direct contact in any situation of the wood with stagnant water or snow. Metal siding was fitted all the way into the terrain to protect even more from rain or outside snow accumulation. In addition, French drain and gravel has been used to drain as fast as possible water precipitation. On top of the curb and over its entire length, a pressure treated lumber has been connected with Tapcon® screws and Hurricane straps. The studs of the side-wall are then connected to the pressure treated lumber with screws. At every single joint of two pressure treated lumbers, a king stud has been put into place (see

Figure 64). All the joint of the truss and sidewall has been reinforced with ½ in. gusset (as shown in **Figure 61**). A number of four emergency doors have been placed, two at the center and one for each end of the Wind Tunnel test section. In order to reinforce the door frame a 2''x8'' header has been built with king stud, as shown in

Figure 64.

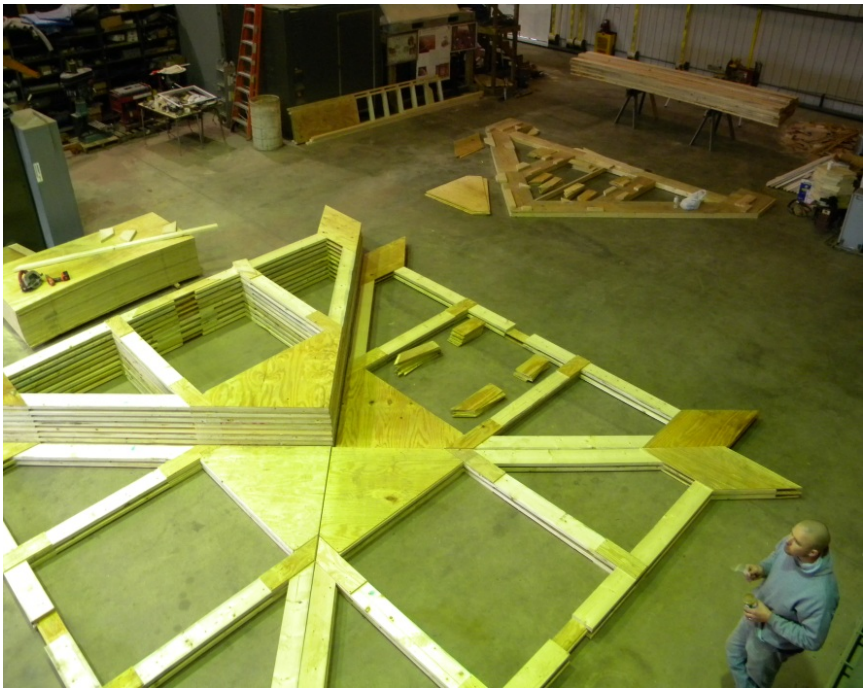

Figure 61: Wind Tunnel Wood Actual Structure Components

Figure 62: Wind Tunnel side-wall construction

Figure 63: Wind Tunnel metal roofing and siding construction

Figure 64: Wind Tunnel Emergency door detail

Table 18: Wind Tunnel Metal Structure Components

Component	Qualification
2''x2''x0.125'' Steel Square Tube	Section component
2mm Steel Plate	Internal covering
Metal Roofing	Galvanized Steel
Metal Wall	Galvanized Steel

Figure 65: Wind Tunnel entrance section with metal frame

Engine and Propeller

A Diesel engine is recognized as the best solution for powering the propeller of the wind tunnel. Based on the wind tunnel power requirement of 1200 HP, a 2200BHP diesel engine was chosen (Table 19).

Table 19: Propeller Engine Specifications

Parameter	Value
Engine Manufacturer	Detroit Diesel Corp.
Model	16v149TiB
Number of Cylinders	16
Cylinders Configuration	V
Displacement [L]	39.18
Max Power[BHP@rpm]	2200@1900
Max Torque [lb-ft@rpm]	6683@1350

Figure 66: Propeller Engine during installation

The propeller chosen is produced by Whirl Wind Propellers Corporation. The following table (Table 20) summarizes the main characteristics.

Table 20: Wind Tunnel Propeller Characteristics

Parameter	Value
Manufacturer	Whirl Wind Propellers
Model	Wind Tunnel
Blade Material	Carbon Fiber
Number of blades	5
Hub Material	Aluminum
Diameter [ft]	10
Max Power [HP]	1500
Max Rotational Speed [rpm]	1500
Noise Level [db@ft]	80@50

An actual noise level for this propeller is not available but, it is available the noise level for a propeller with ¾ diameter. Considering that both have similar blade tip velocities, it is reasonable to assume comparable noise levels.

Auxiliary Services

The fundamental auxiliary services needed to support wind tunnel operation are electric compressed air. Electricity service of approximately 200 amps, 120/240V, single phase will be needed for tunnel lighting, sampling systems, data acquisition, and control. In order to meet the accelerated timeline of the current project, generator power will be provided. Compressed air will be provided from a dedicated compressor with moisture and particulate removal.

Data Acquisition System (DAQ) and Instruments

The varieties of tests that are going to be performed, and the associated types of measurement, require a large number of instruments and significant data management. A customized DAQ, specially developed by CAFEE, was utilized. It is able to acquire the data from emissions instruments (gaseous and particulate matter), placed in different positions, as well as engine sensors and wind tunnel control. Such DAQ acquires contemporary from all the instruments, avoiding the time alignment issues and producing a single collection data file. The data capturing follow a high speed protocol of 10Hz.

APPENDIX C: Plume Panels

Pre-2007 Truck, Idle Test

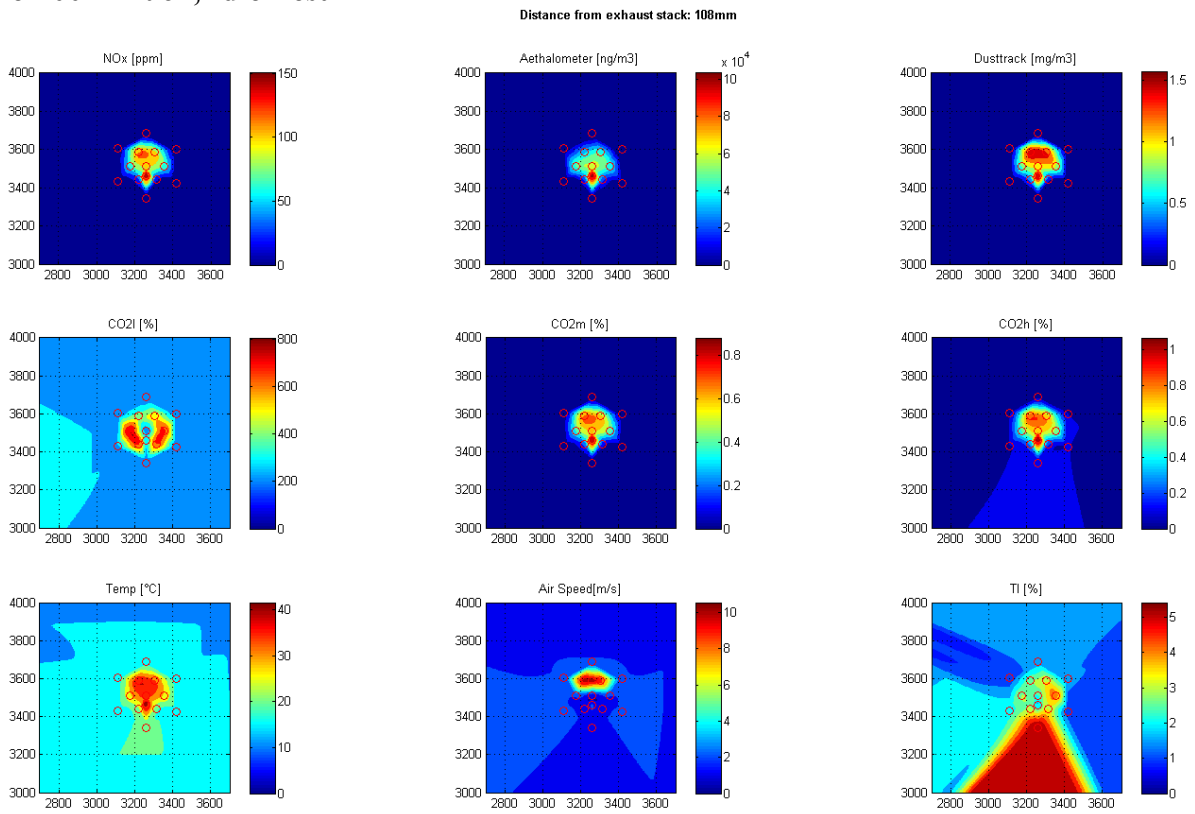

Figure 67: Pre2007 vehicle, Idle Test, Plane 1

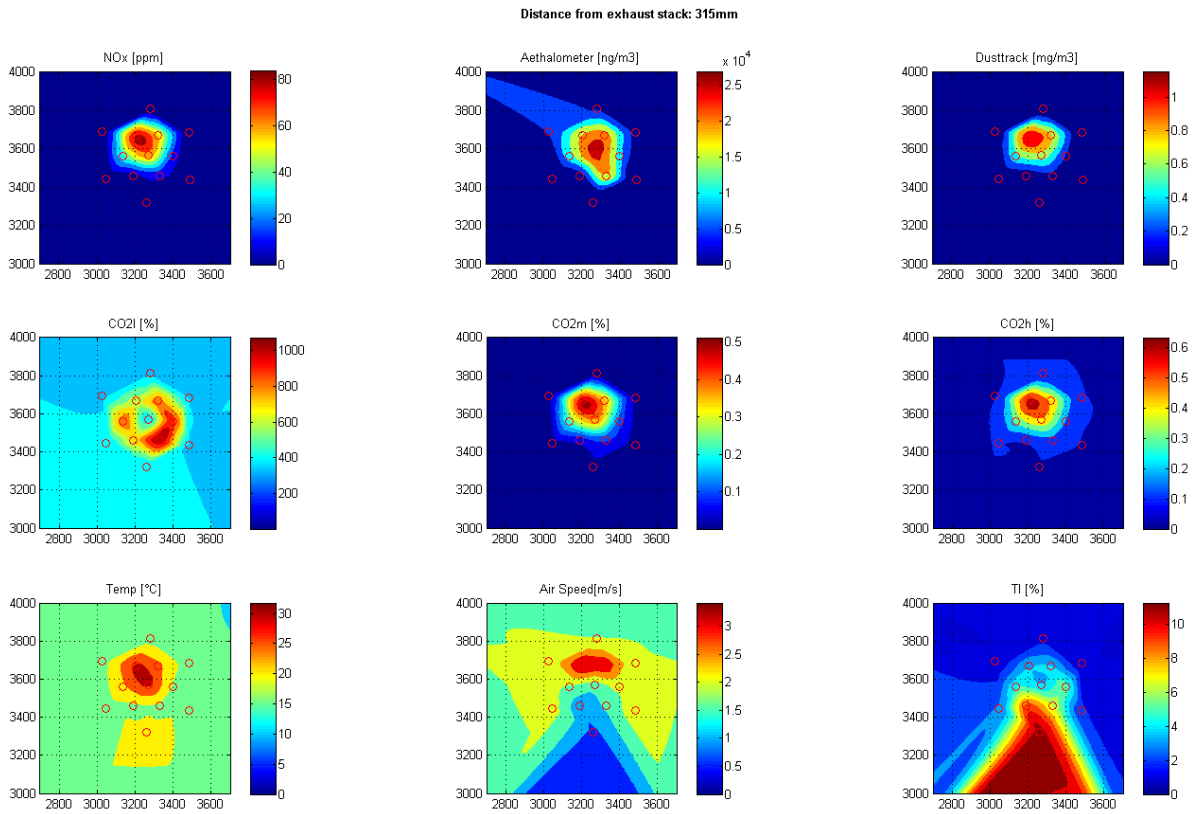

Figure 68: Pre-2007, Idle Test, Plane 2

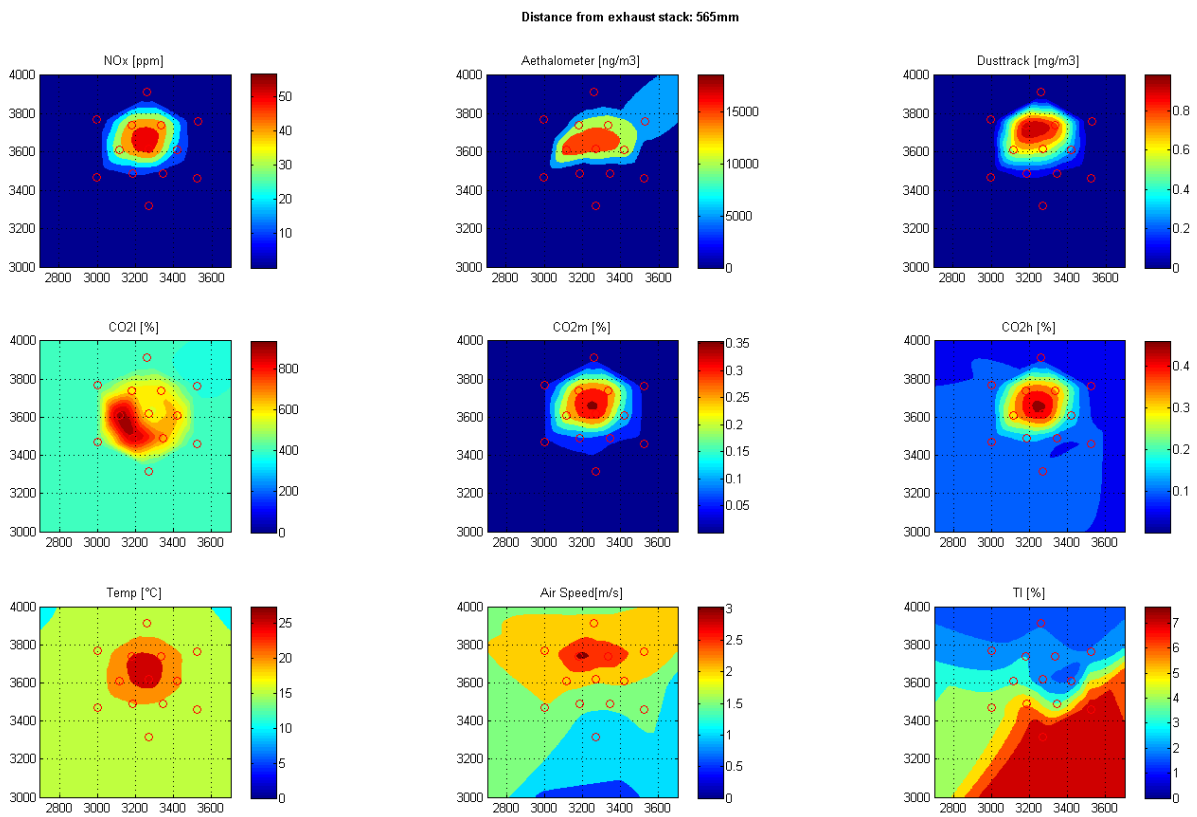

Figure 69: Pre-2007, Idle Test, Plane 3

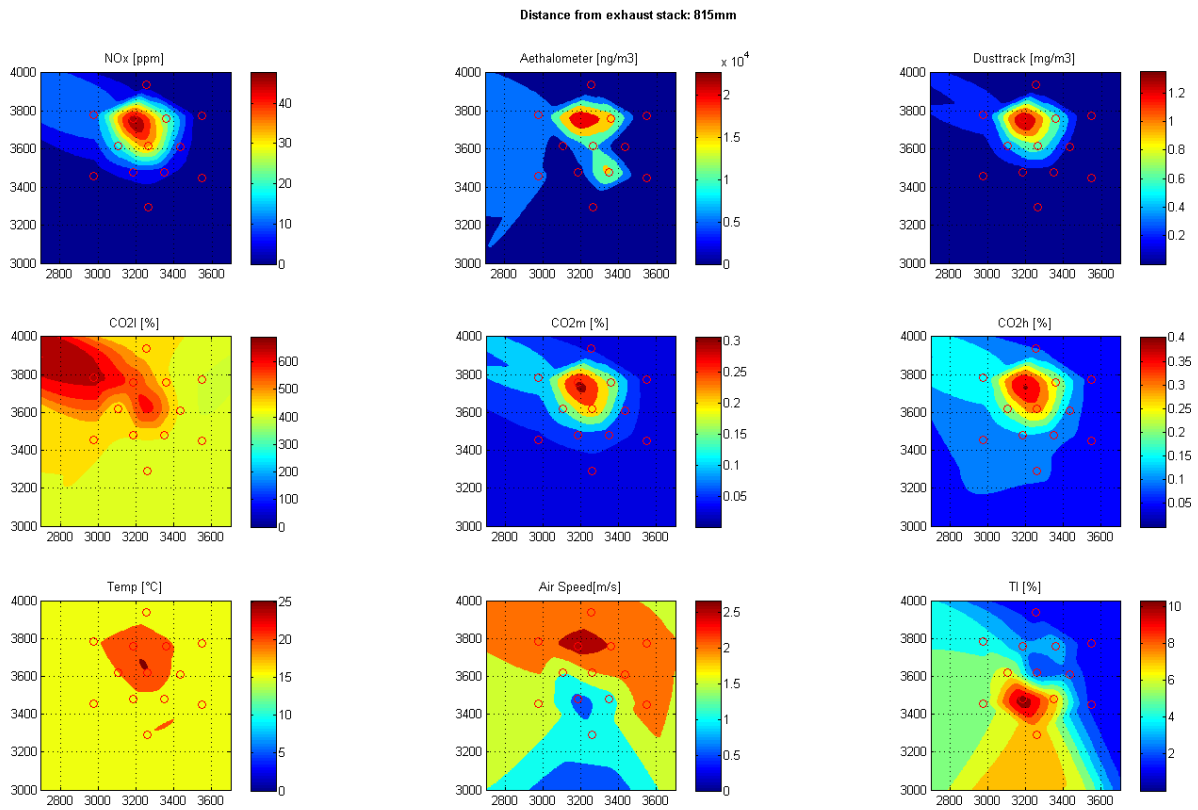

Figure 70: Pre-2007, Idle Test, Plane 4

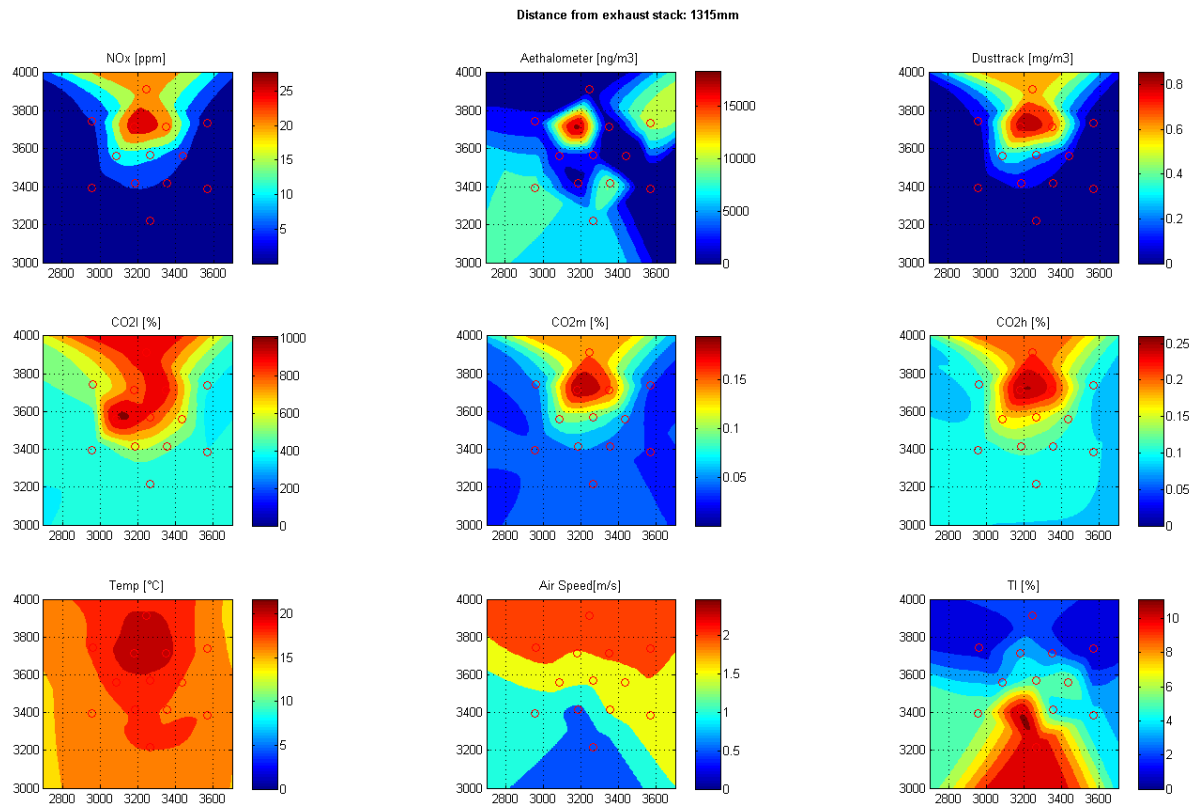

Figure 71: Pre-2007, Idle Test, Plane 5

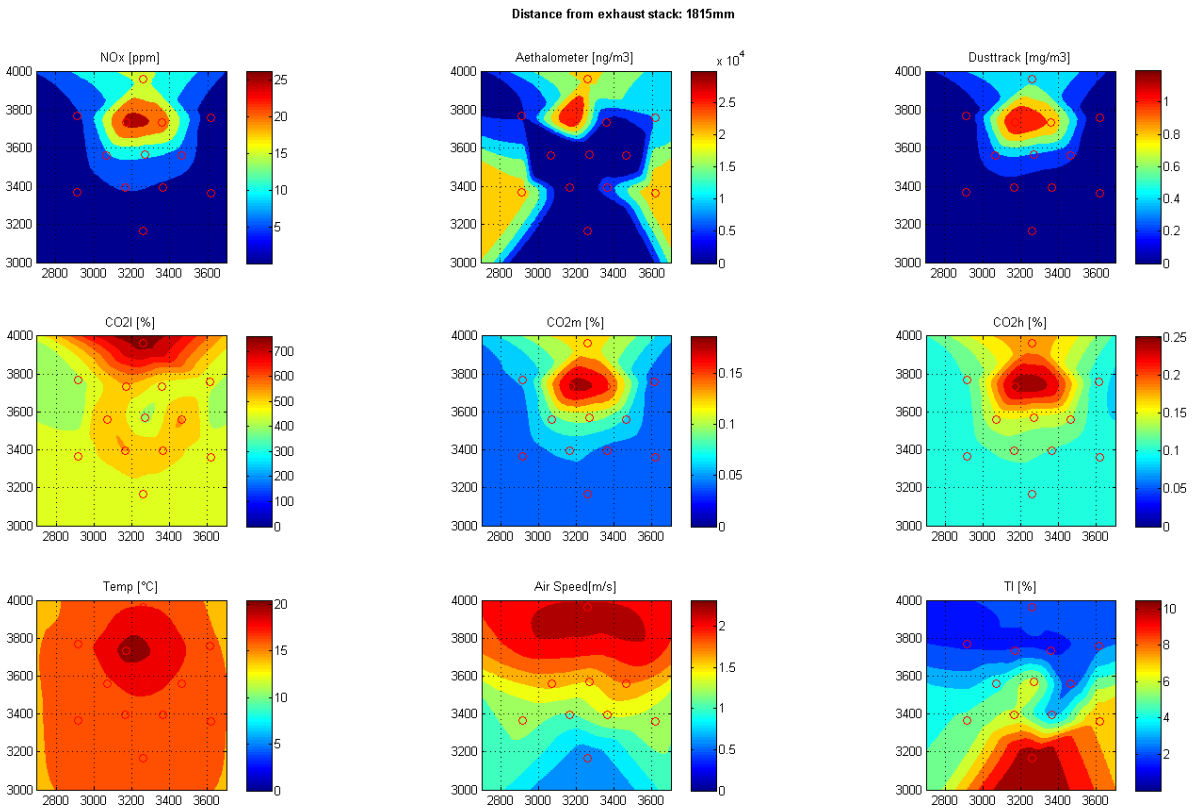

Figure 72: Pre-2007, Idle Test, Plane 6

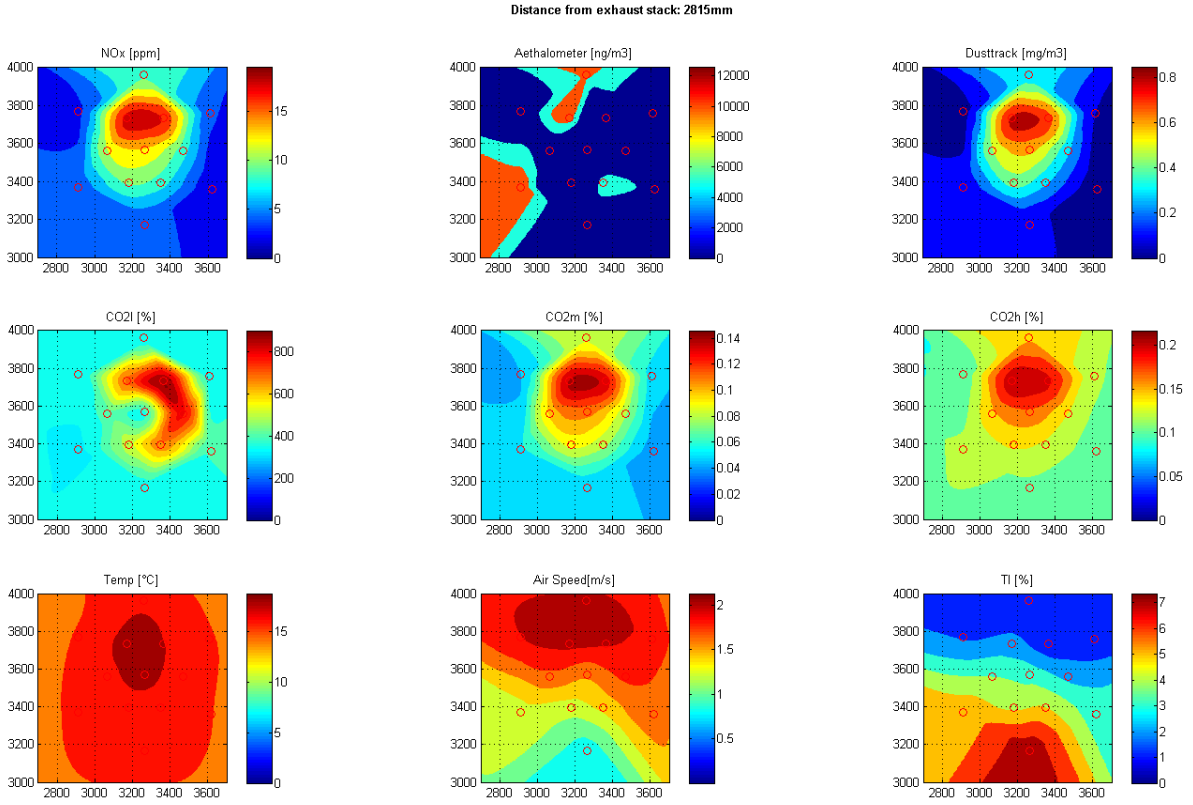

Figure 73: Pre-2007, Idle Test, Plane 7

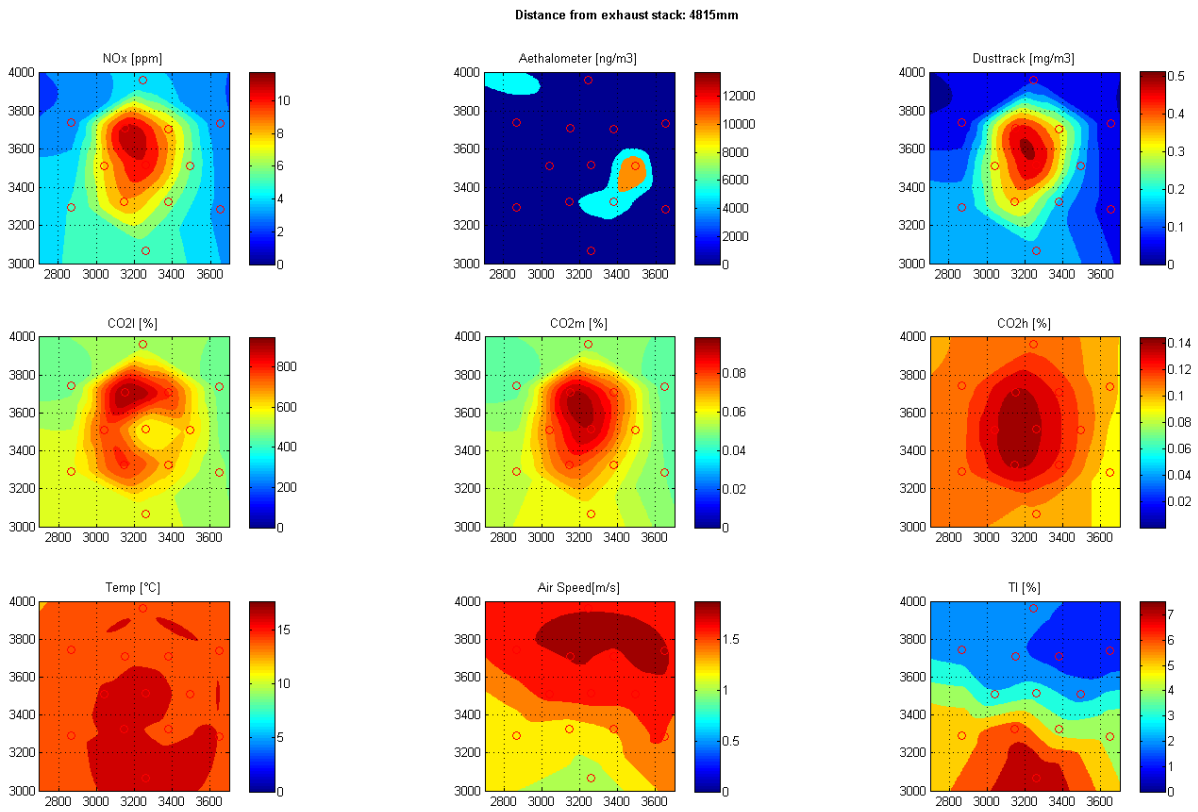

Figure 74: Pre-2007, Idle Test, Plane 8

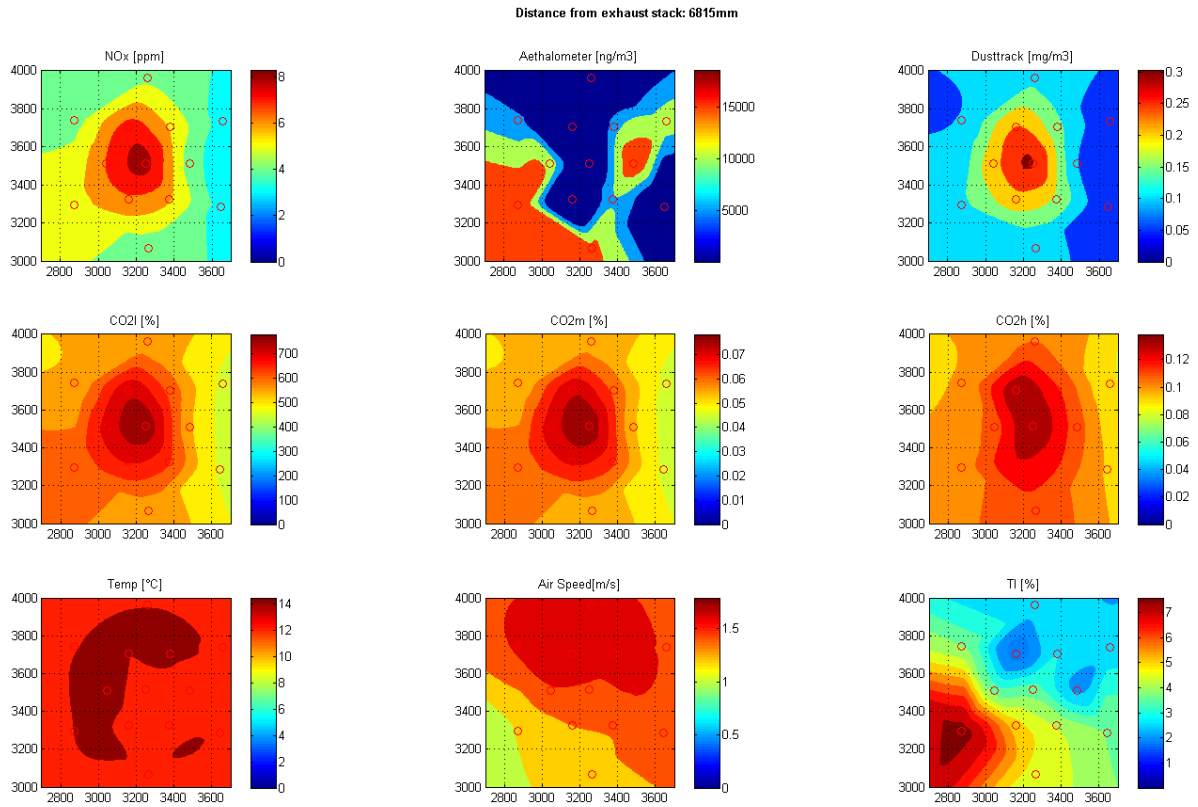

Figure 75: Pre-2007, Idle Test, Plane 9

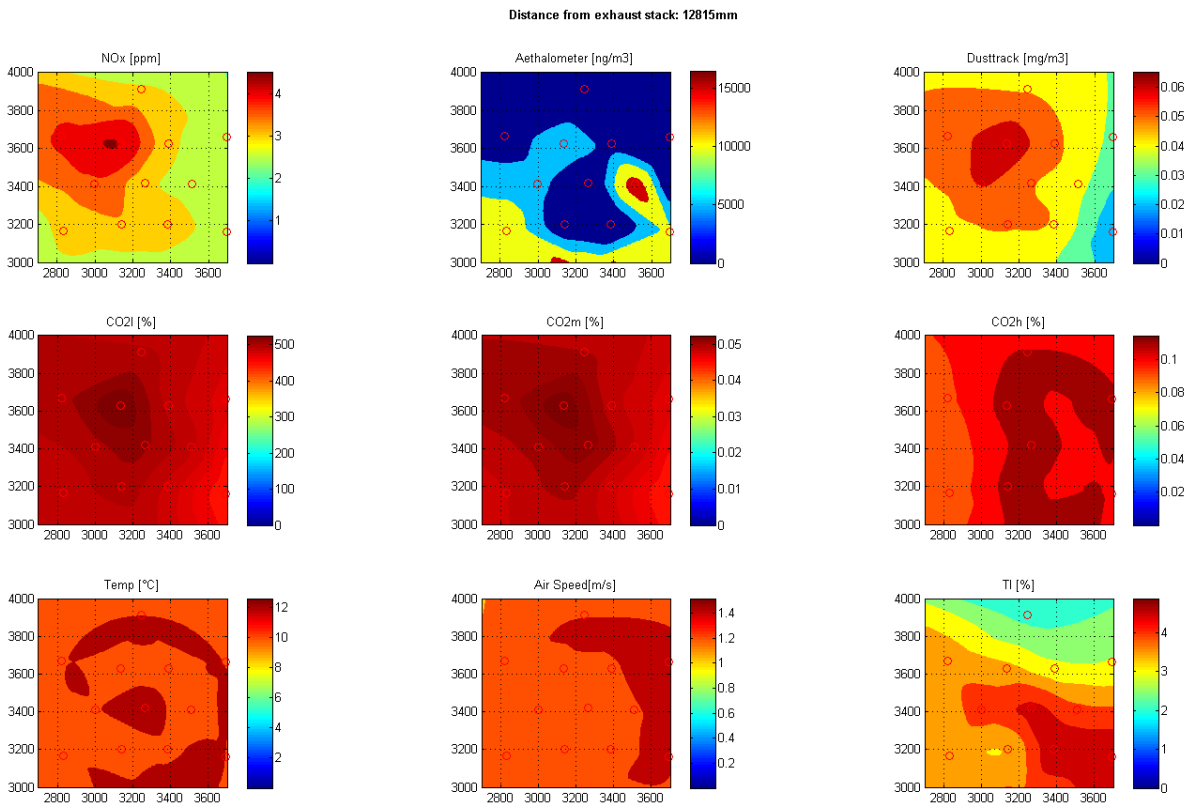

Figure 76: Pre-2007, Idle Test, Plane 10

Pre-2007 Truck, 20mph Test

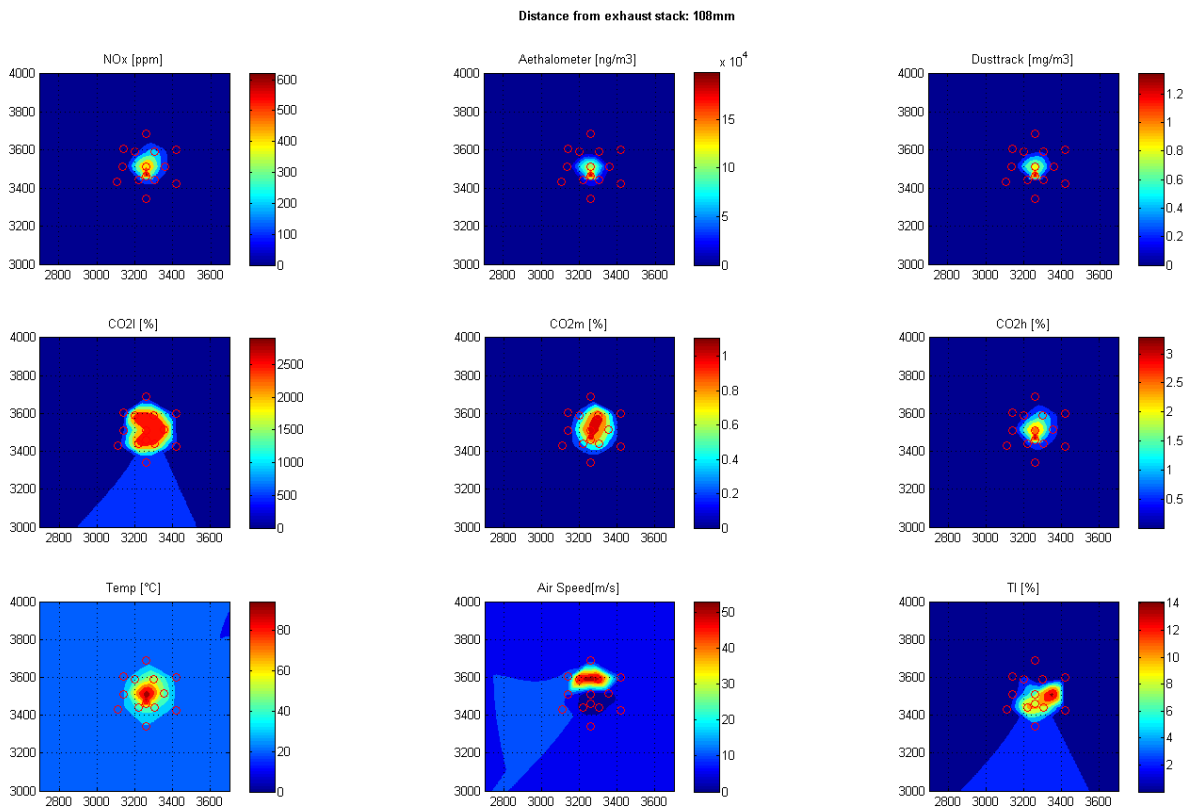

Figure 77: Pre2007 vehicle, 20mph Test, Plane 1

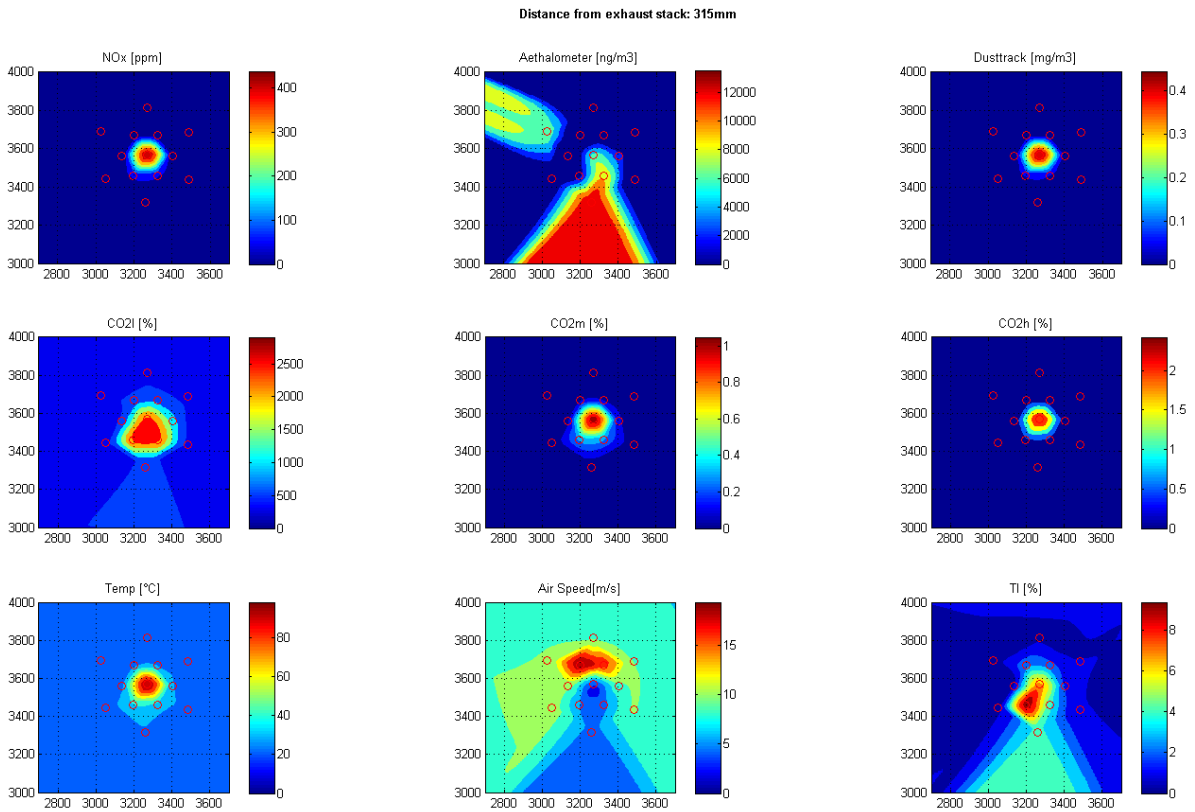

Figure 78: Pre2007 vehicle, 20mph Test, Plane 2

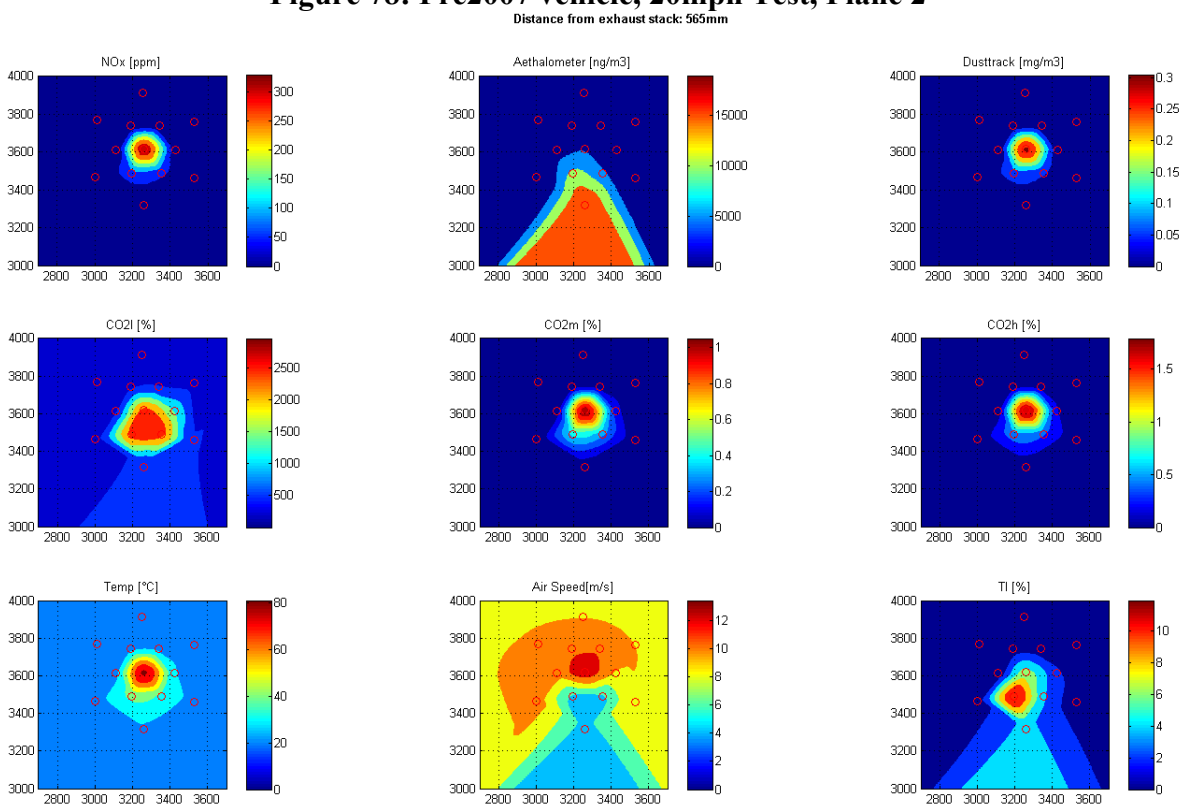

Figure 79: Pre2007 vehicle, 20mph Test, Plane 3

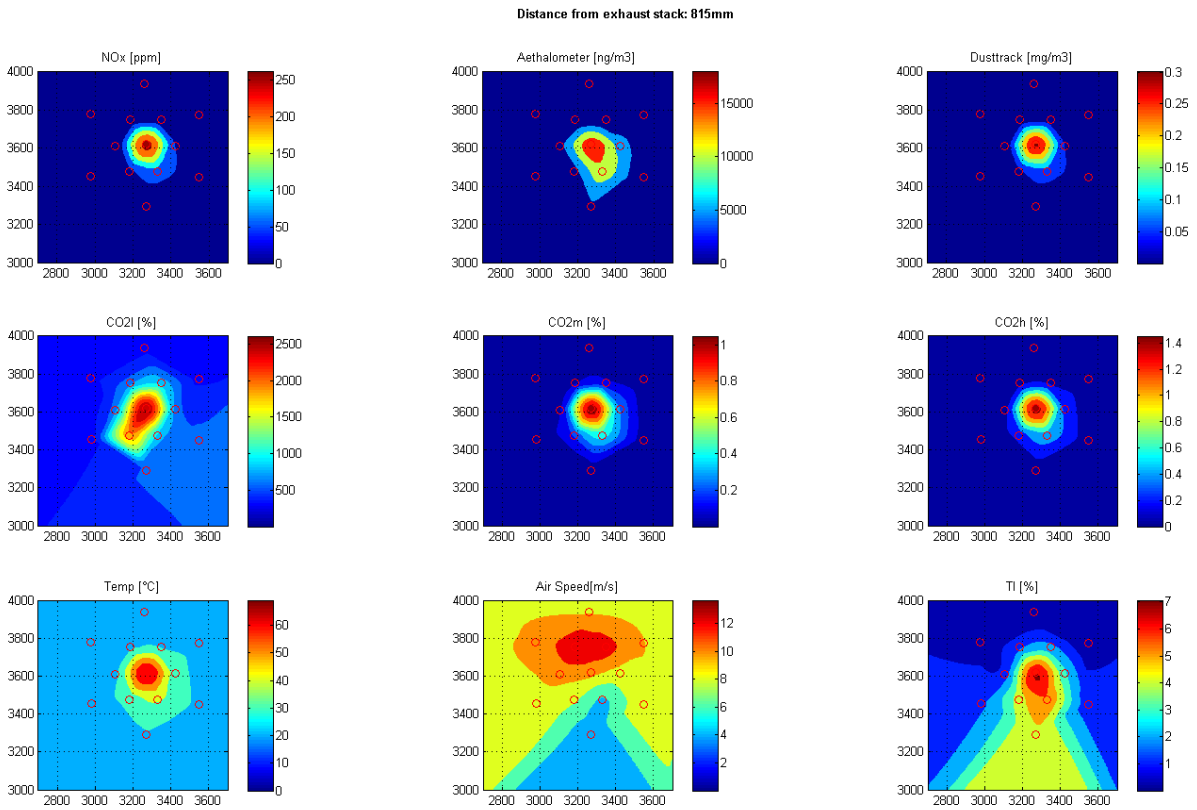

Figure 80: Pre2007 vehicle, 20mph Test, Plane 4

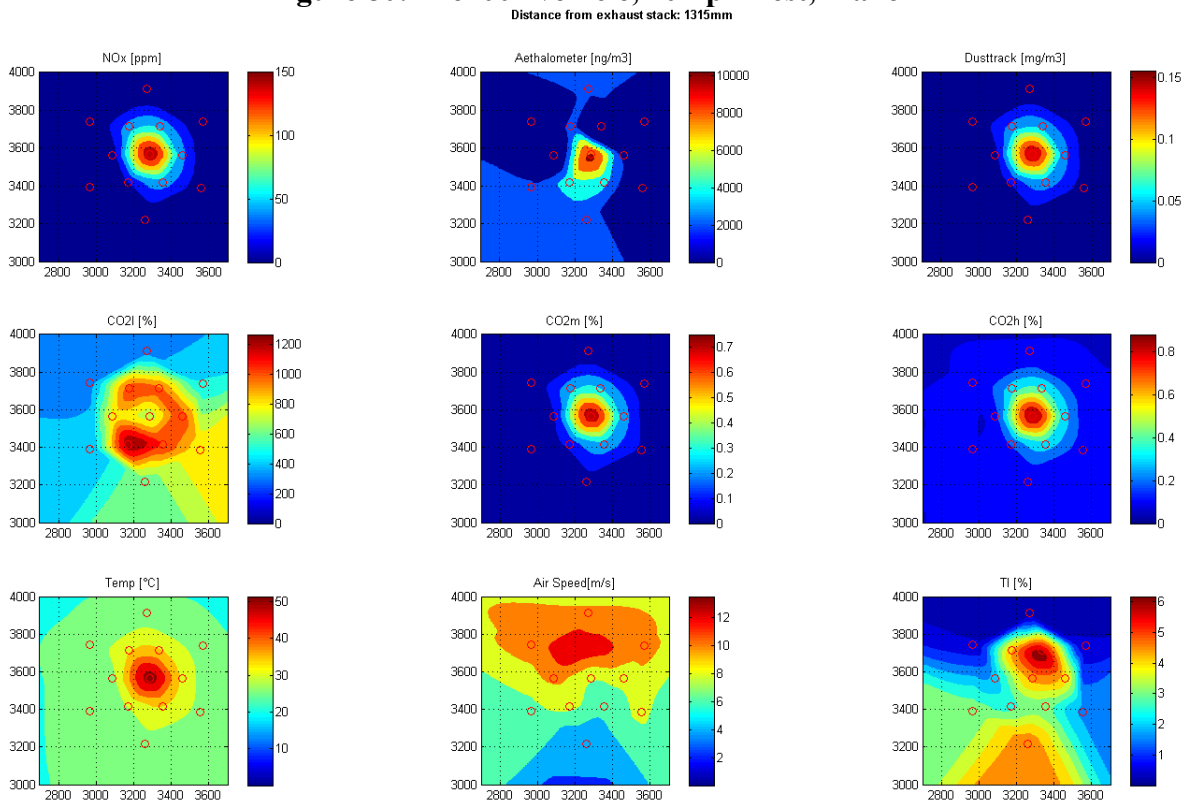

Figure 81: Pre2007 vehicle, 20mph Test, Plane 5

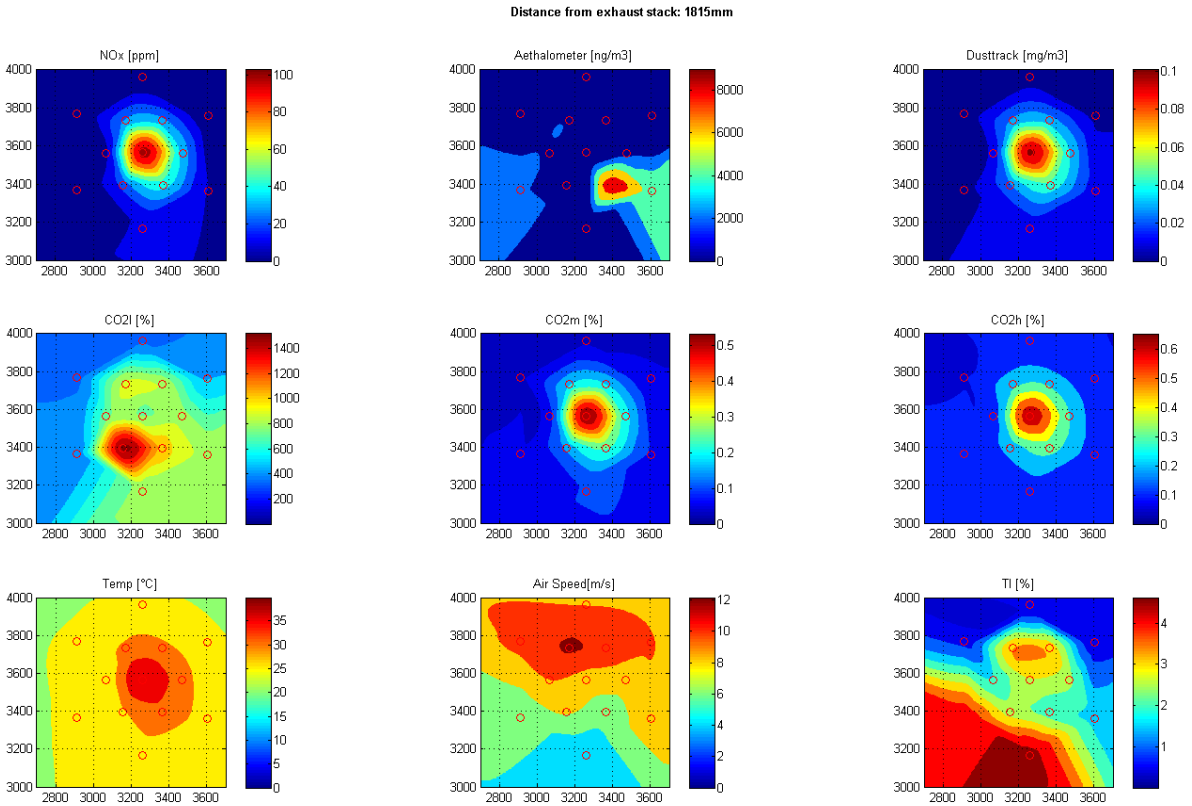

Figure 82: Pre2007 vehicle, 20mph Test, Plane 6

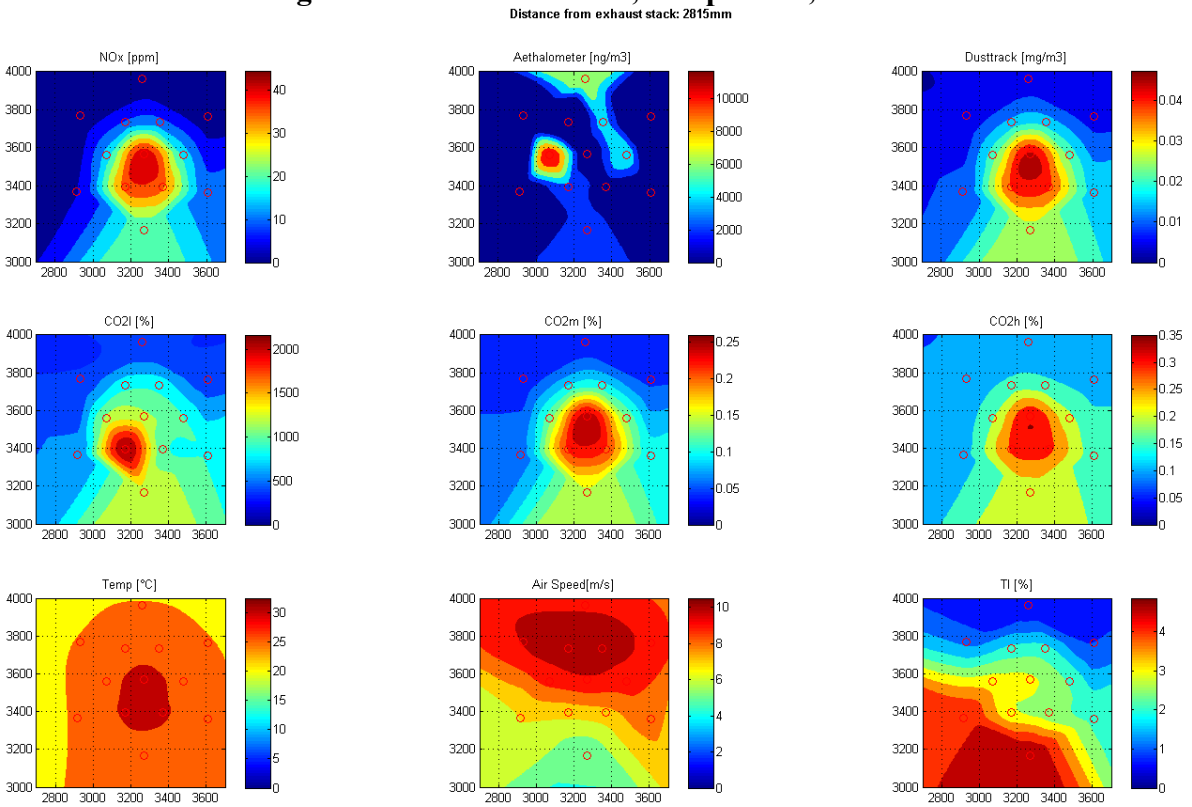

Figure 83: Pre2007 vehicle, 20mph Test, Plane 7

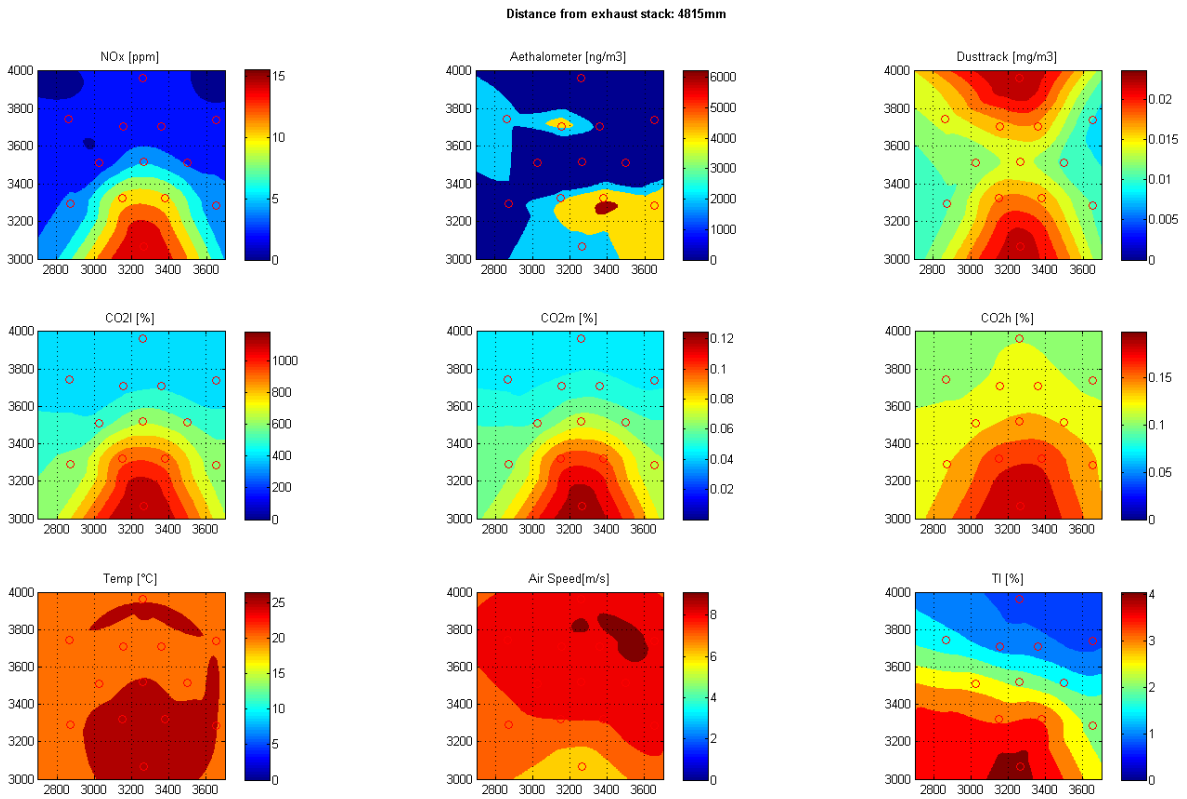

Figure 84: Pre2007 vehicle, 20mph Test, Plane 8

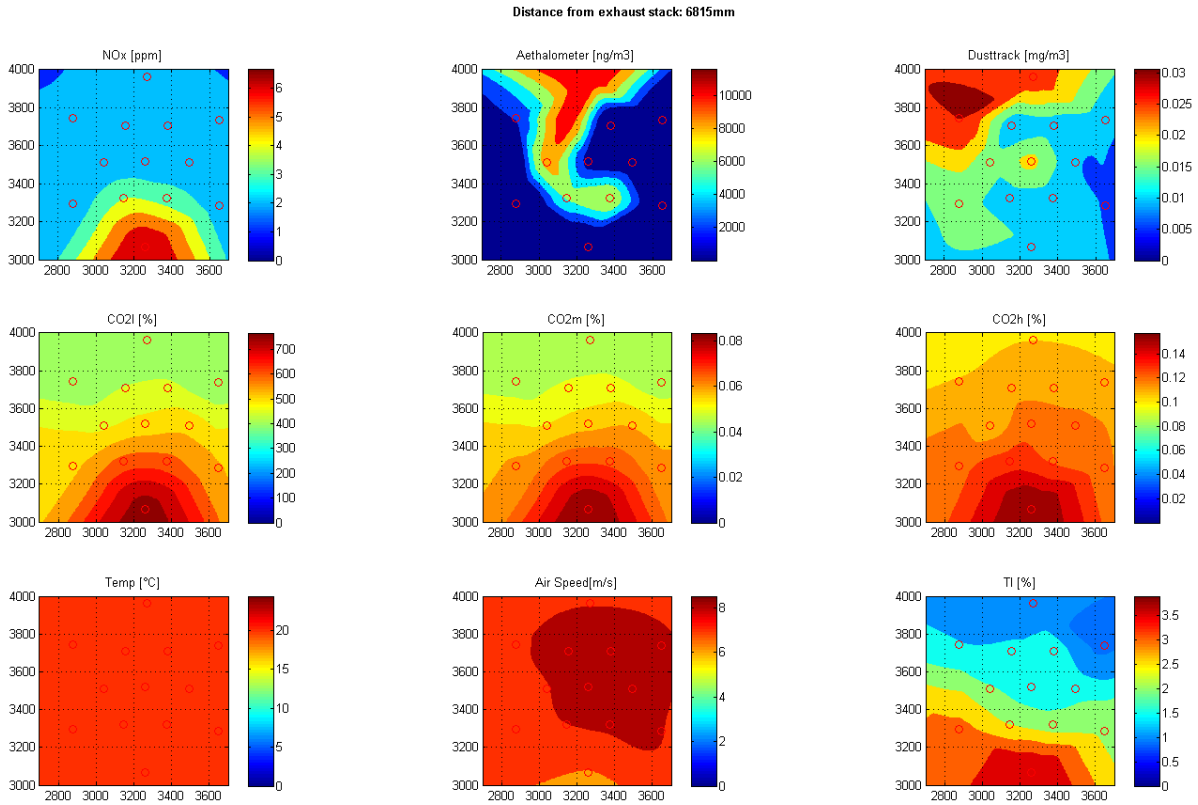

Figure 85: Pre2007 vehicle, 20mph Test, Plane 9

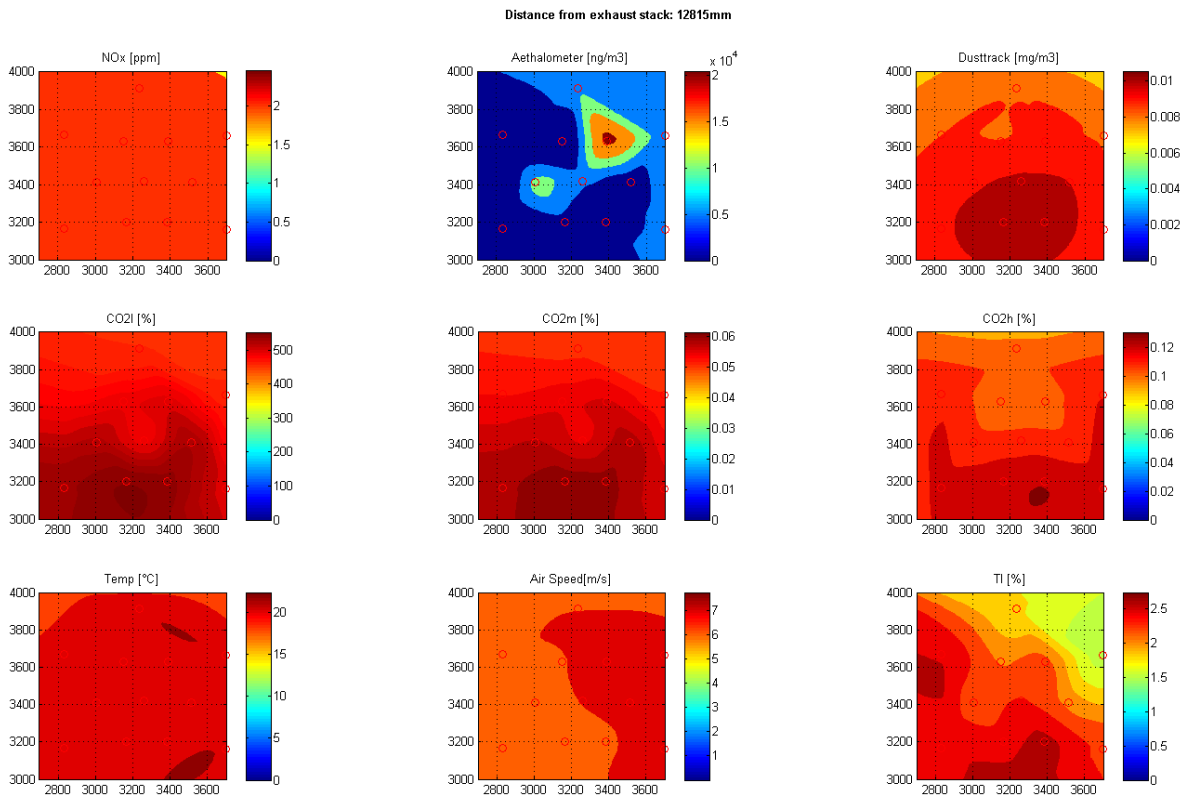

Figure 86: Pre2007 vehicle, 20mph Test, Plane 10

Pre-2007 Truck, 35mph Test

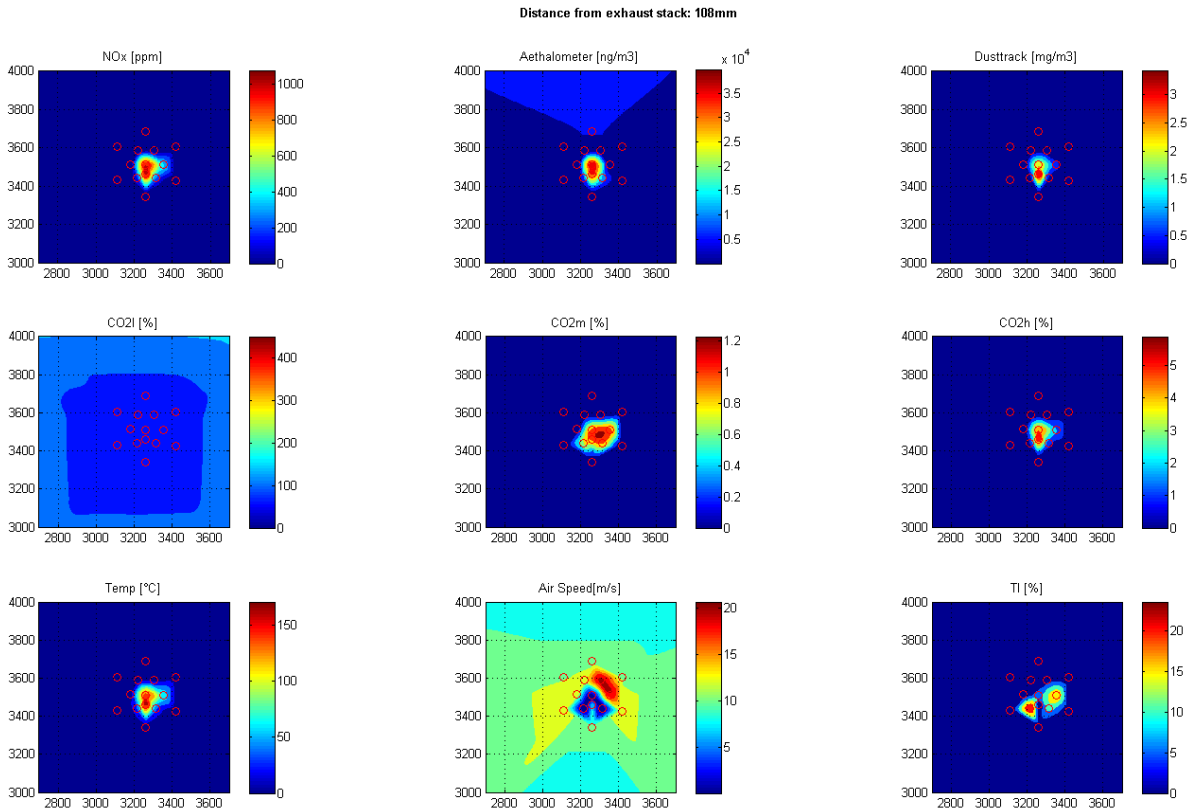

Figure 87: Pre-2007, 35mph Test, Plane1

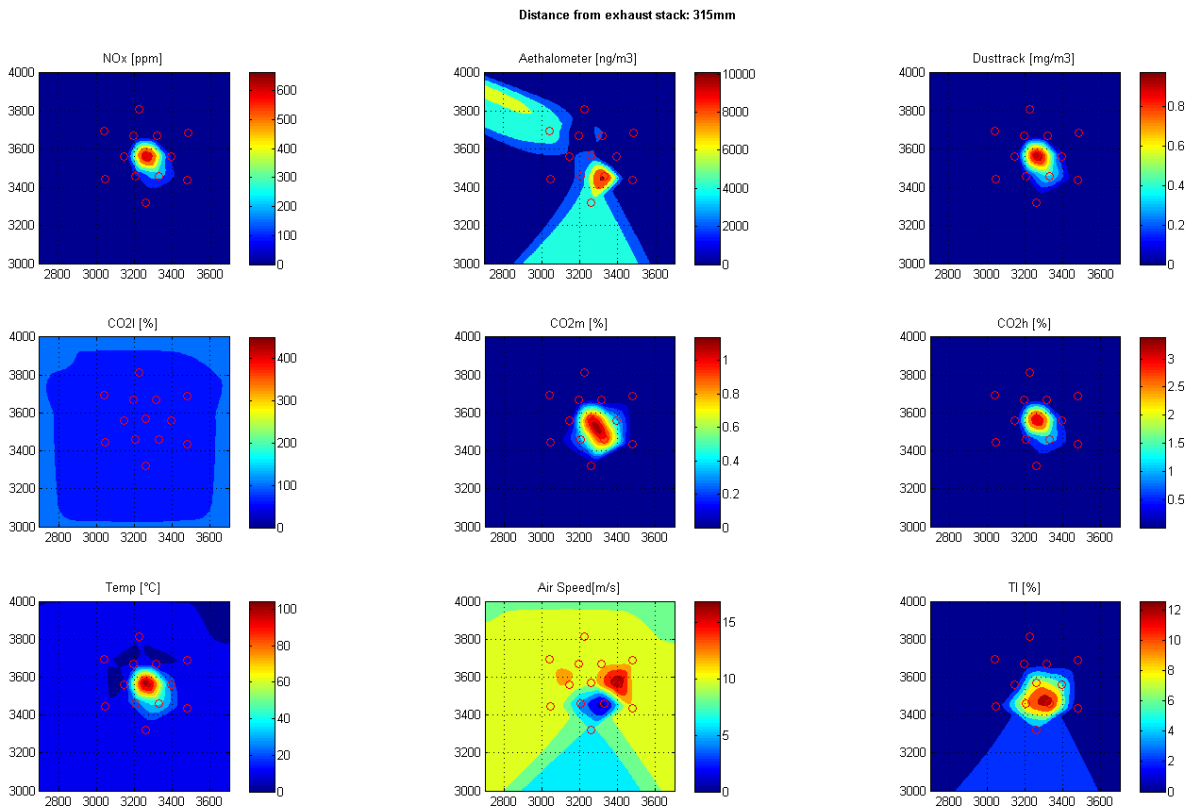

Figure 88: Pre-2007, 35mph Test, Plane 2

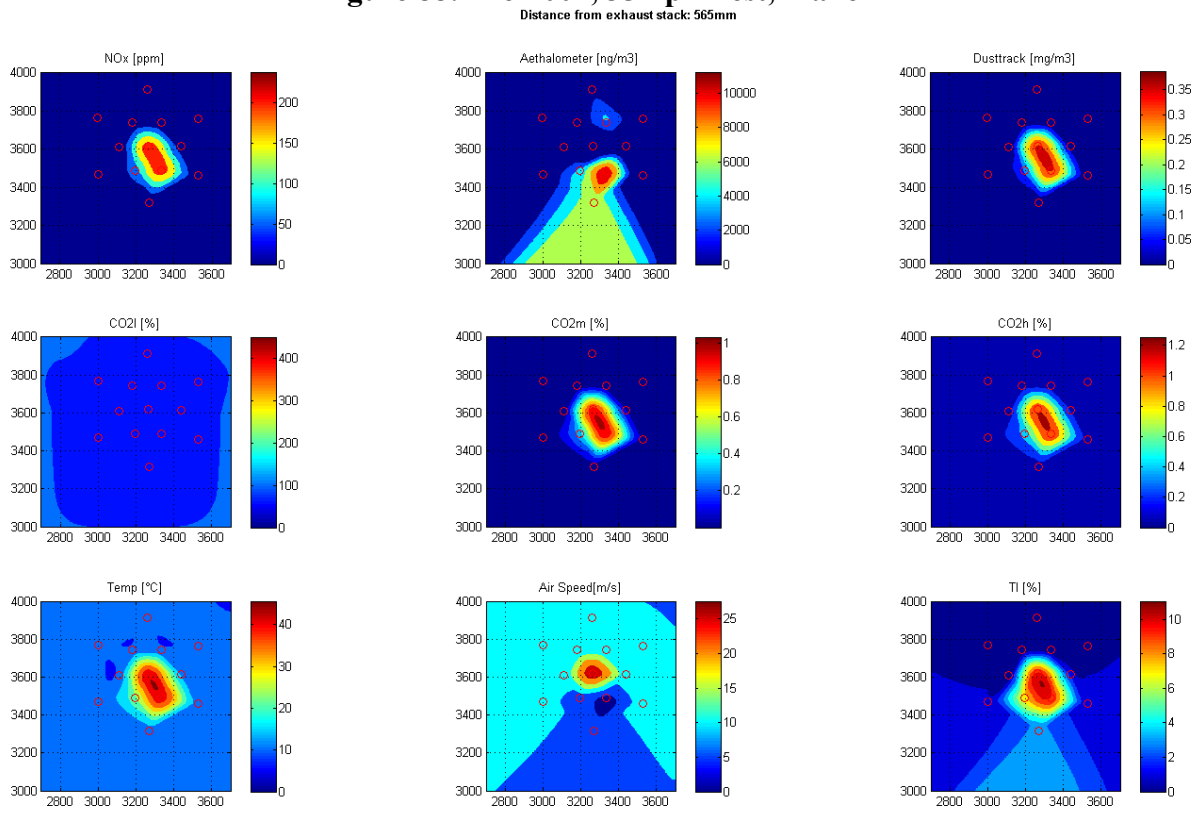

Figure 89: Pre-2007, 35mph Test, Plane 3

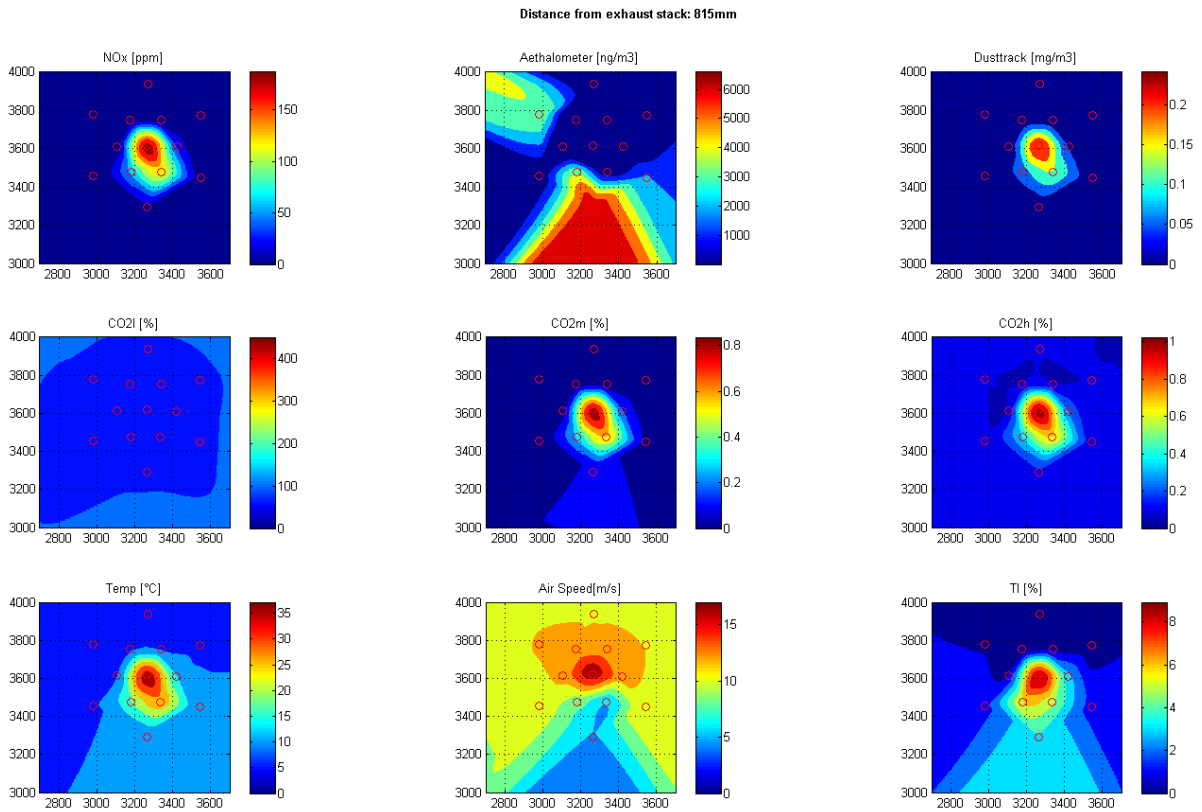

Figure 90: Pre-2007, 35mph Test, Plane 4

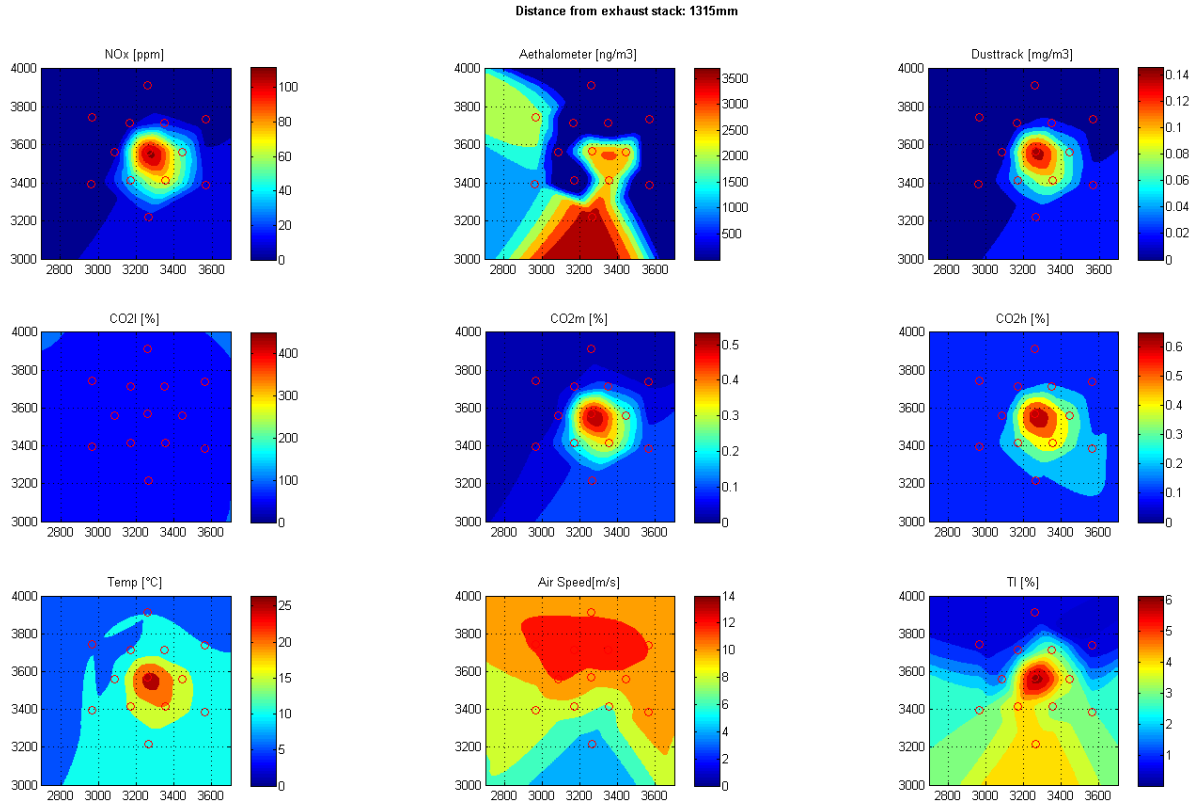

Figure 91: Pre-2007, 35mph Test, Plane 5

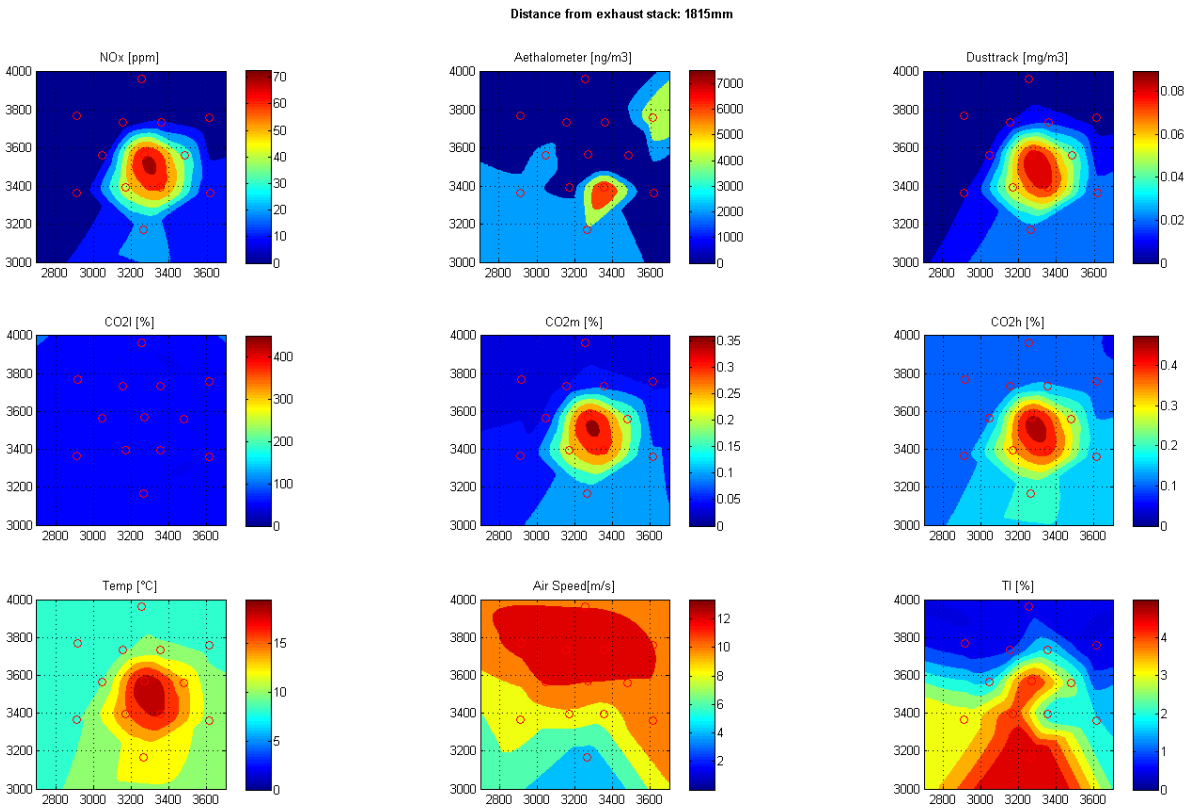

Figure 92: Pre-2007, 35mph Test, Plane 6

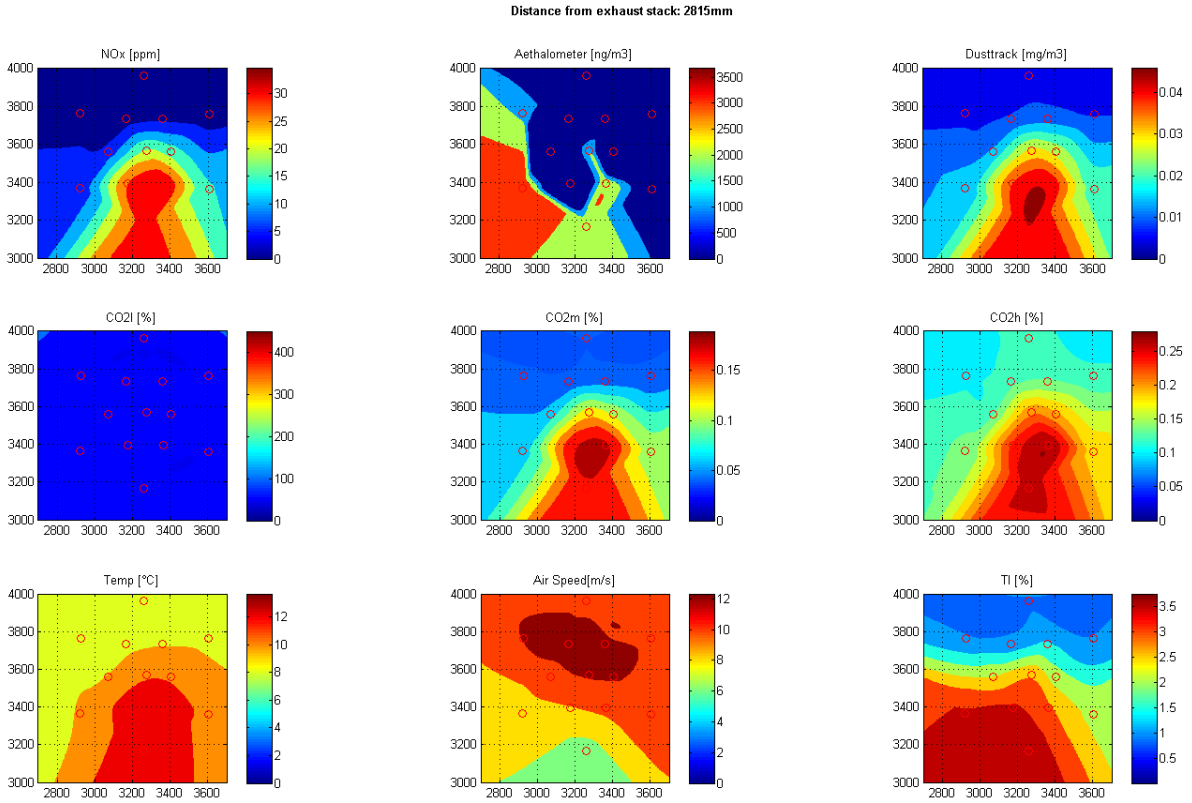

Figure 93: Pre-2007, 35mph Test, Plane 7

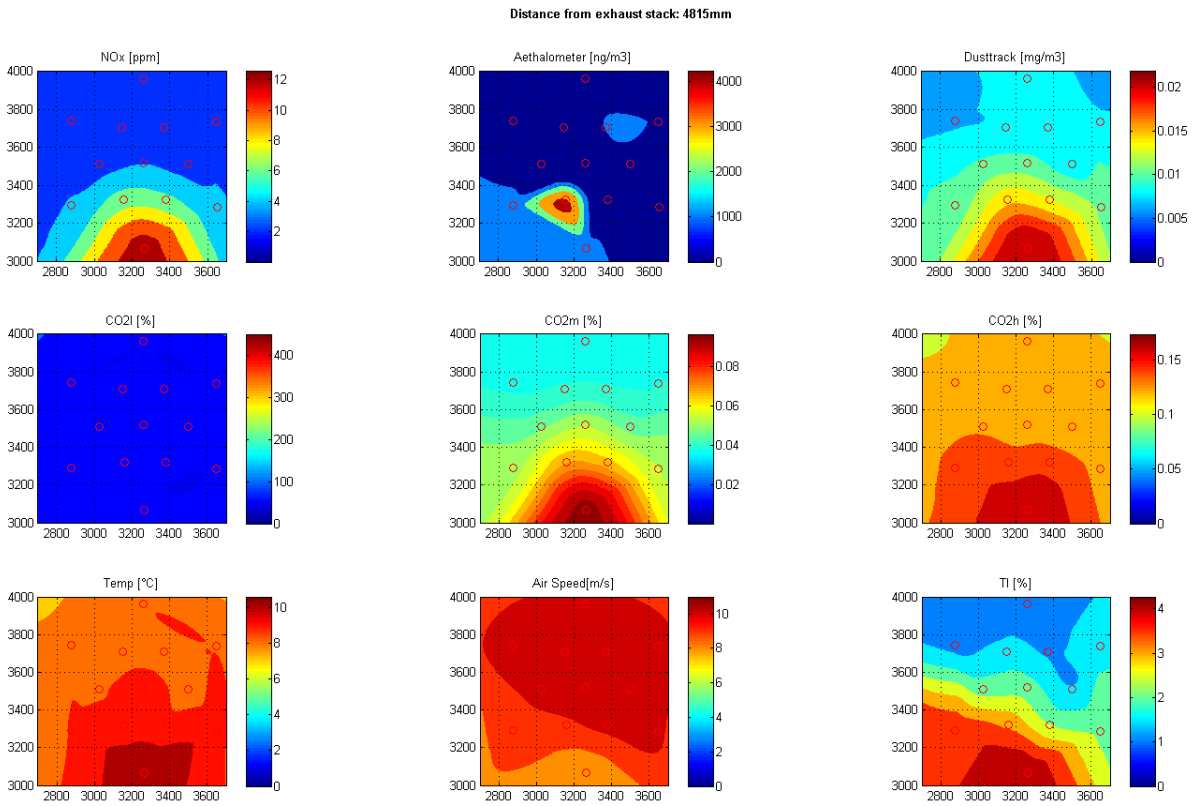

Figure 94: Pre-2007, 35mph Test, Plane 8

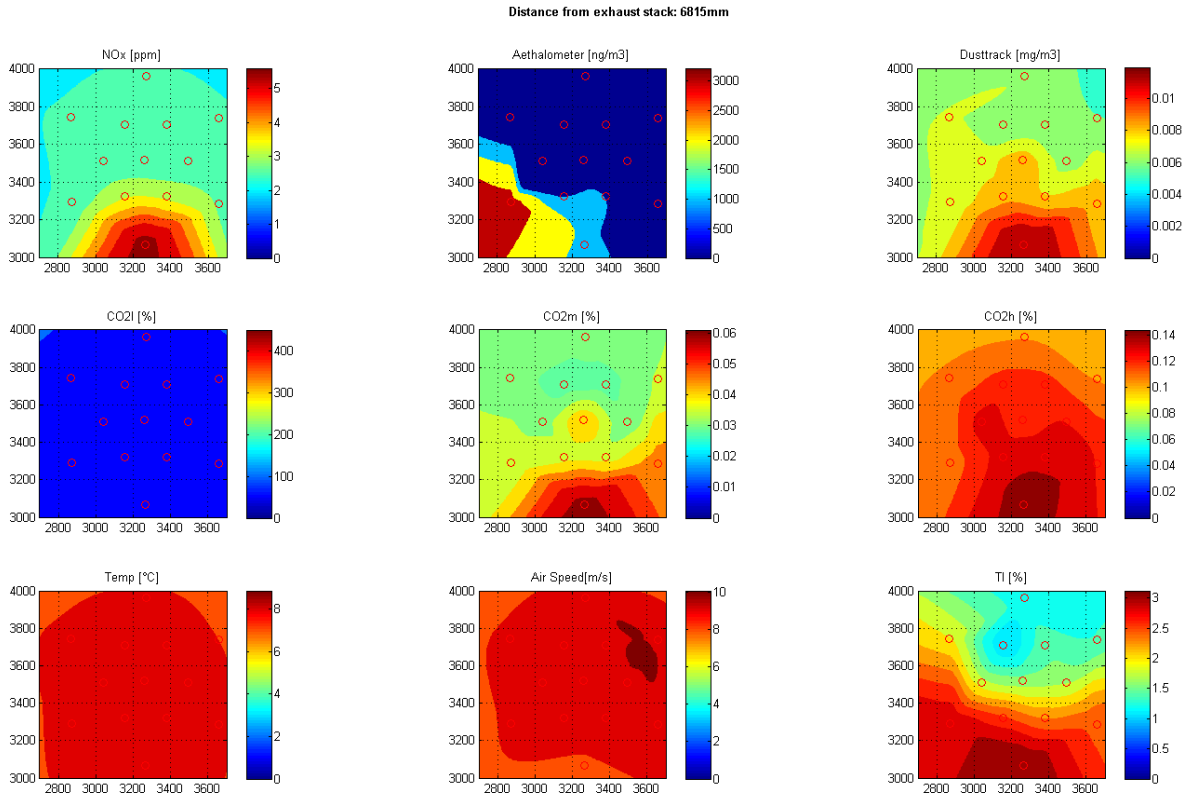

Figure 95: Pre-2007, 35mph Test, Plane 9

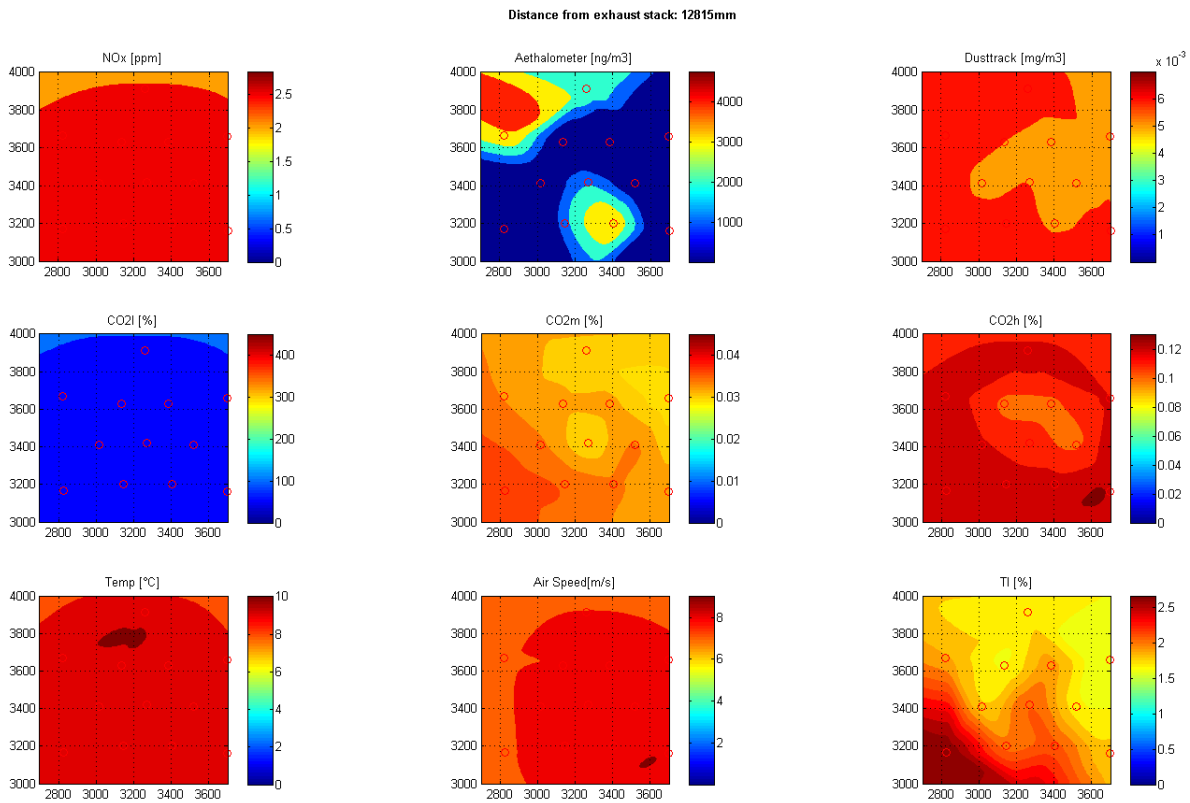

Figure 96: Pre-2007, 35mph Test, Plane 10

Post-2007 truck, Idle Test

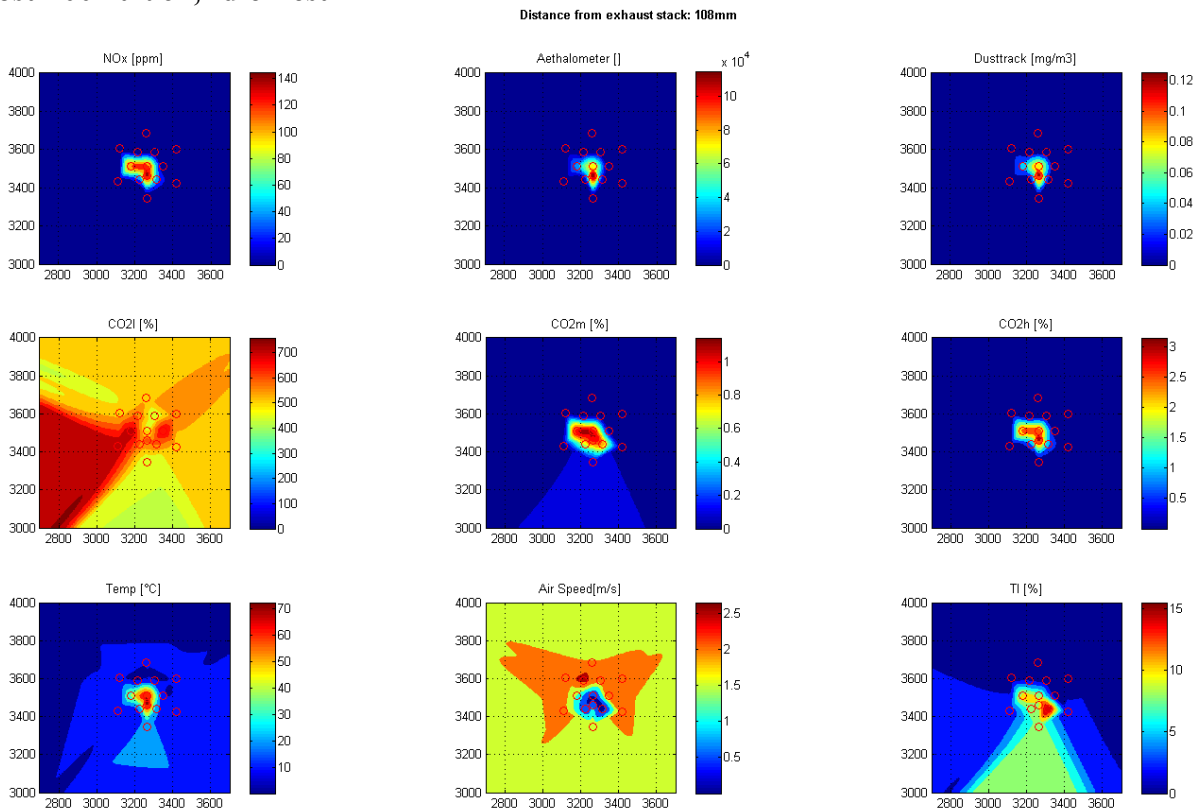

Figure 97: Post-2007, Idle Test, Plane 1

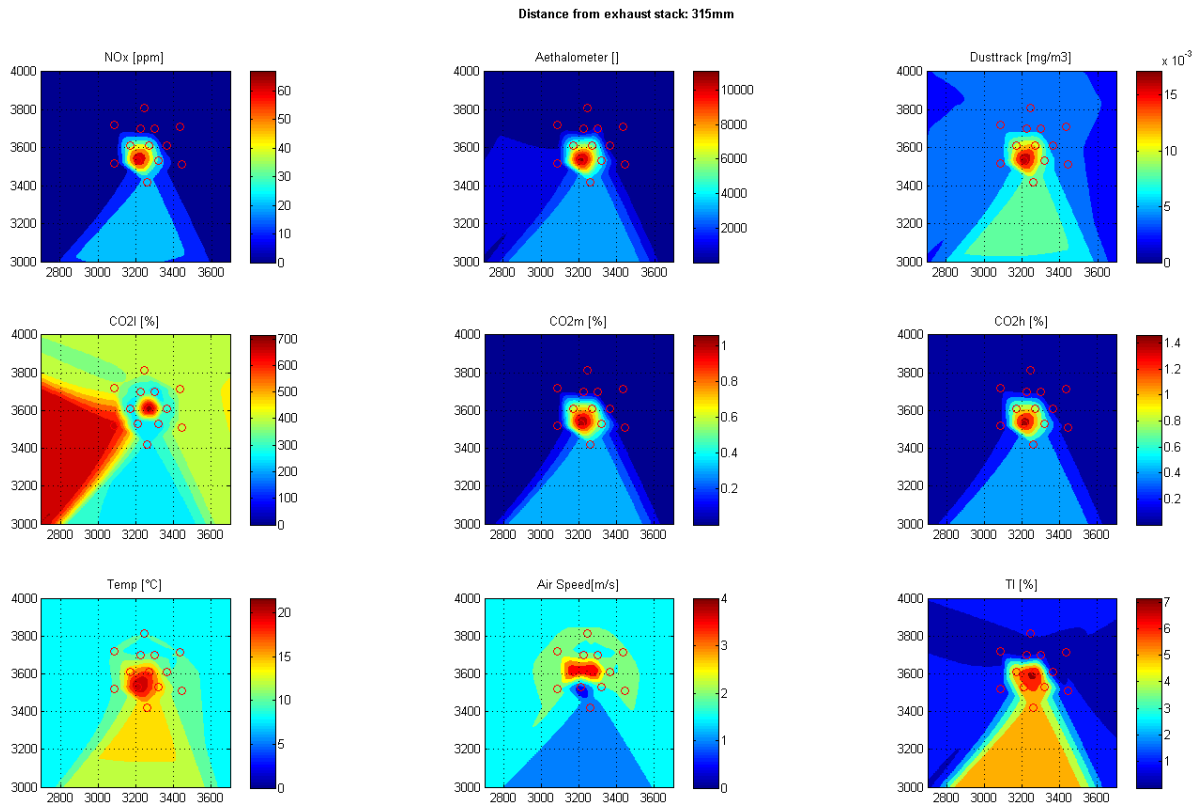

Figure 98: Post-2007, Idle Test, Plane 2

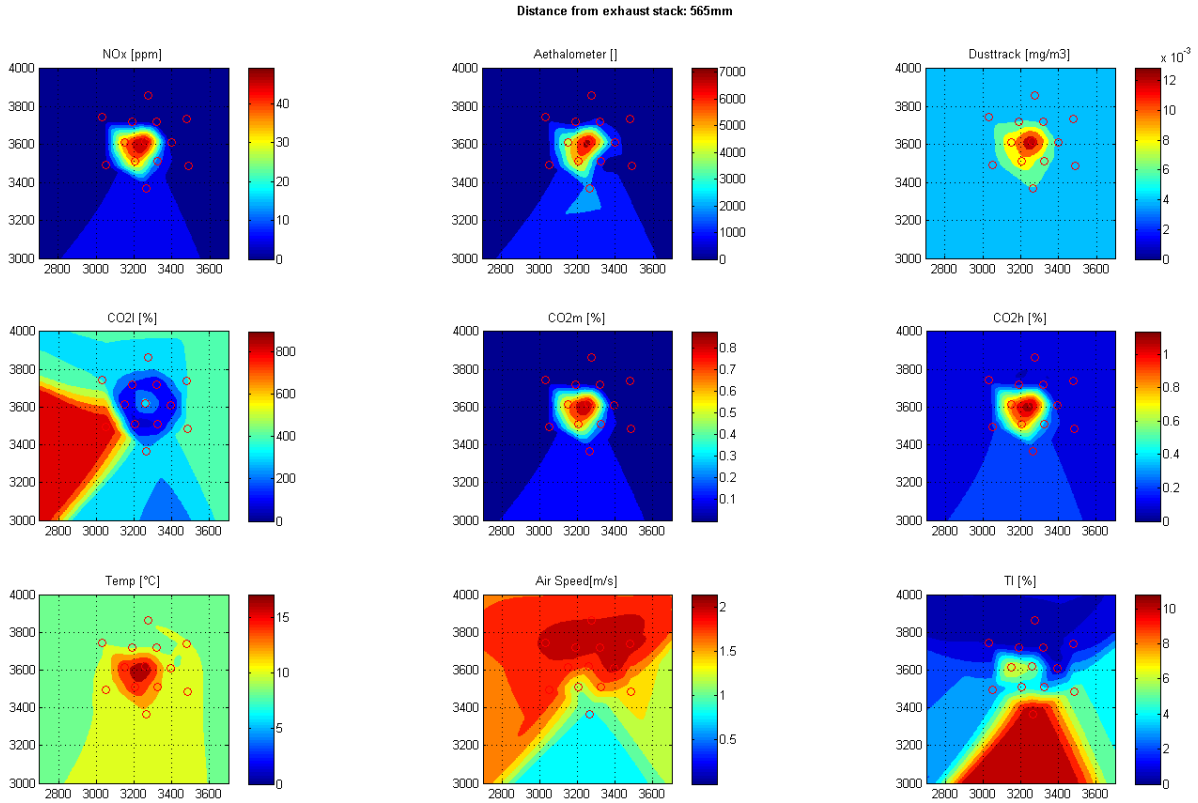

Figure 99: Post-2007, Idle Test, Plane 3

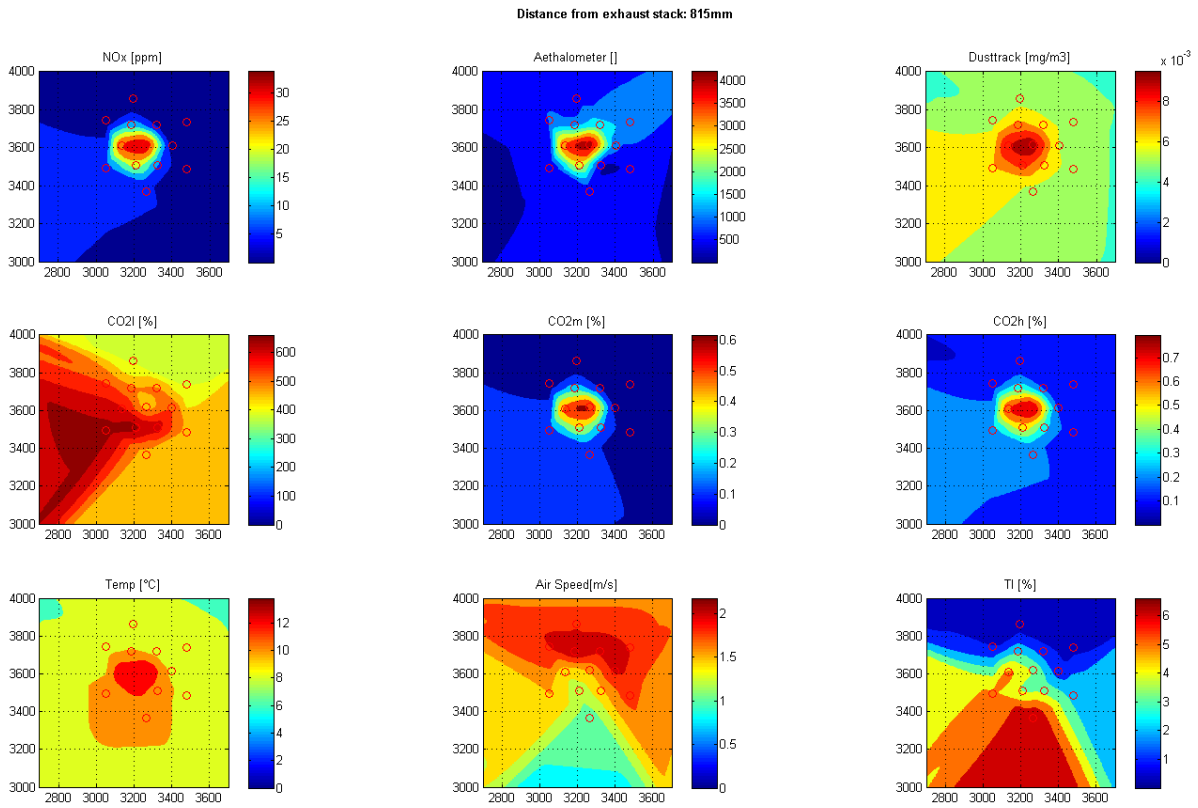

Figure 100: Post-2007, Idle Test, Plane 4

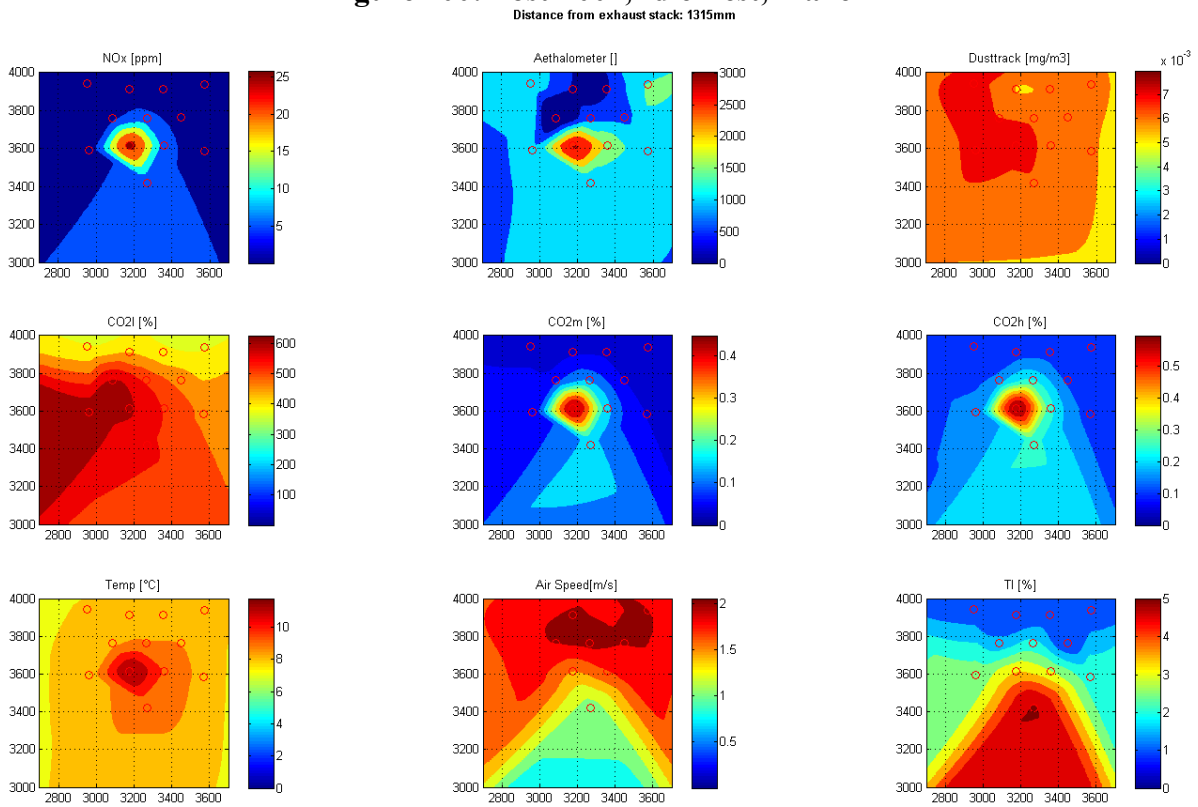

Figure 101: Post-2007, Idle Test, Plane 5

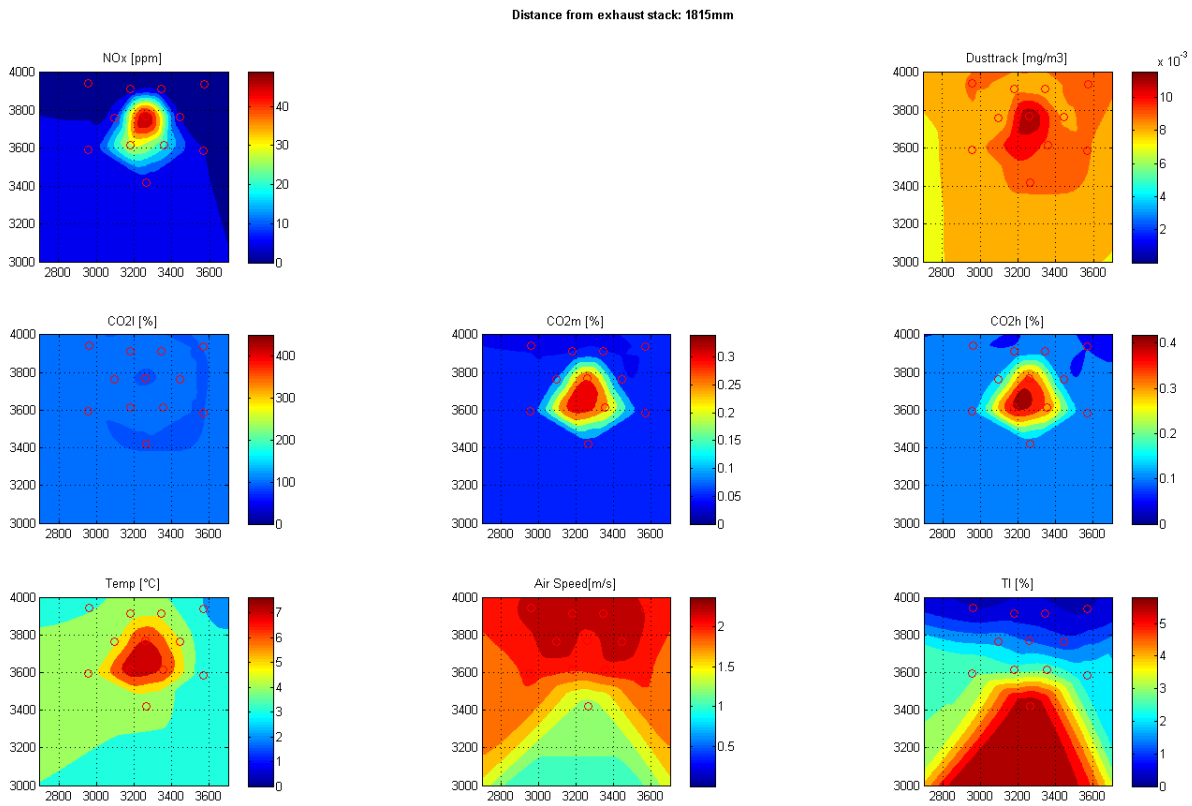

Figure 102: Post-2007, Idle Test, Plane 6

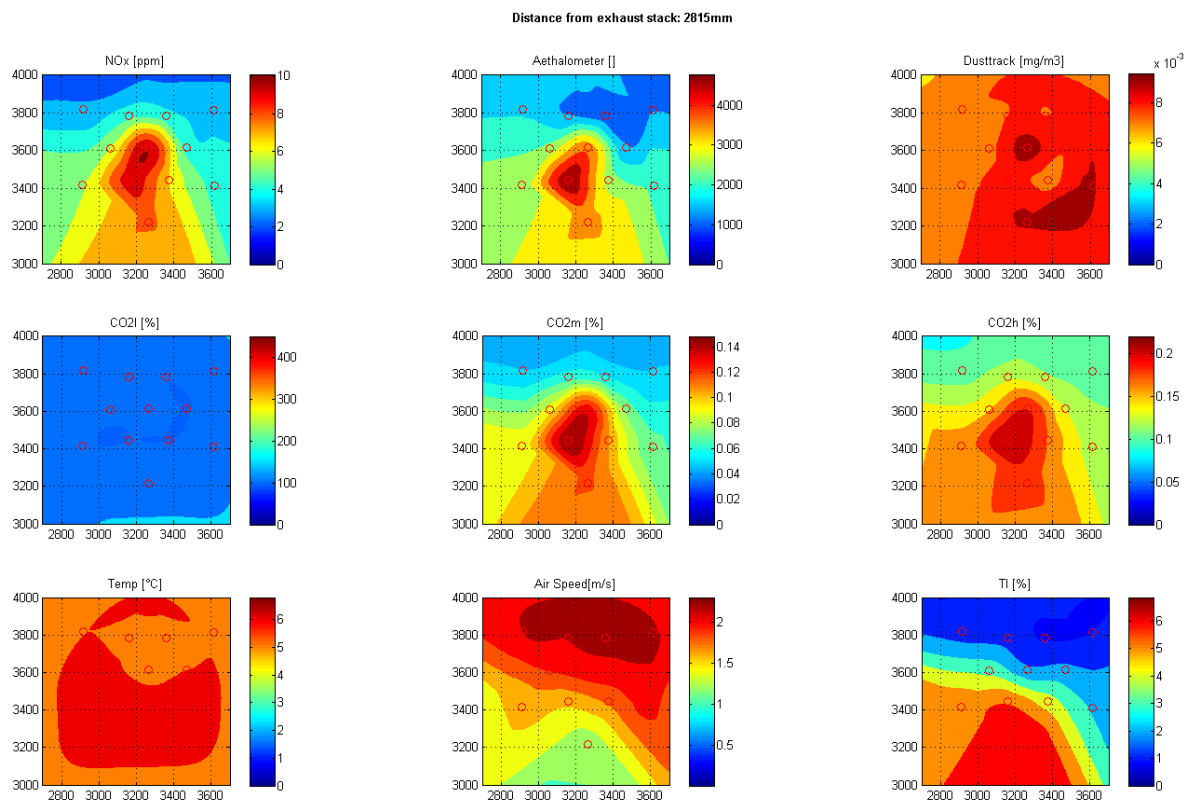

Figure 103: Post-2007, Idle Test, Plane 7

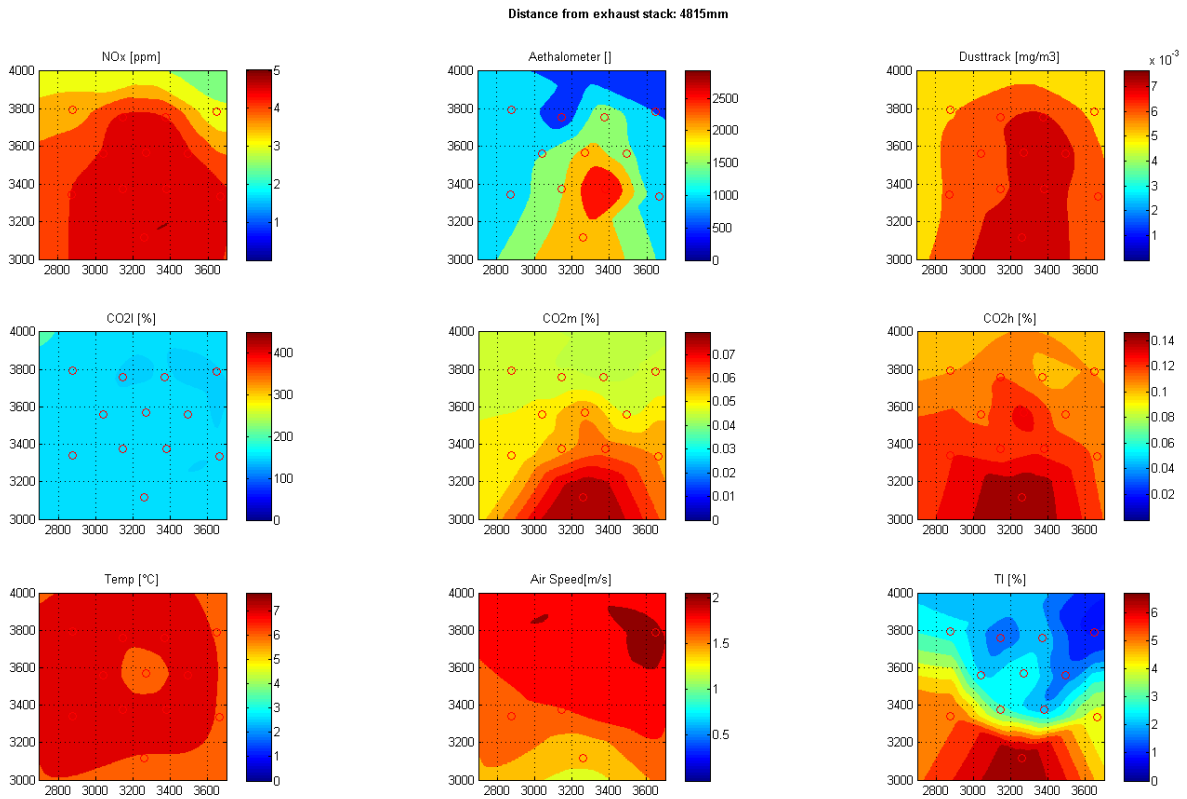

Figure 104: Post-2007, Idle Test, Plane 8

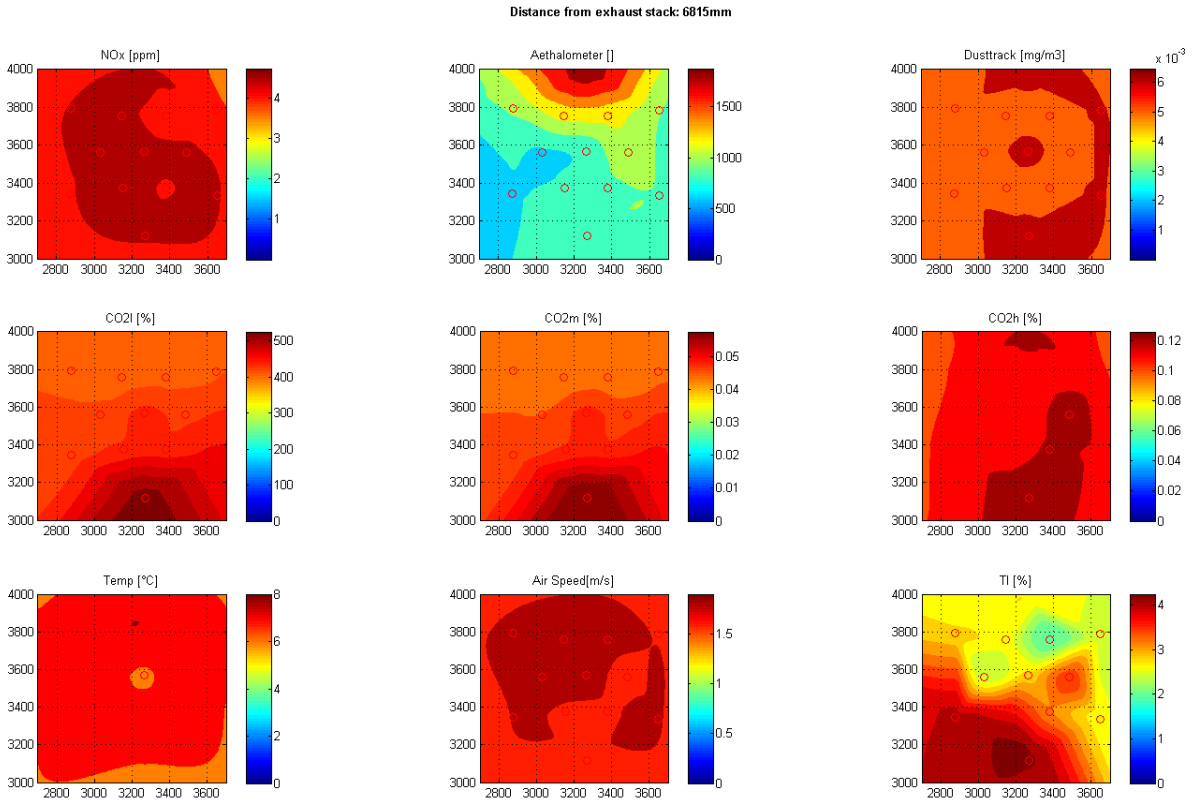

Figure 105: Post-2007, Idle Test, Plane 9

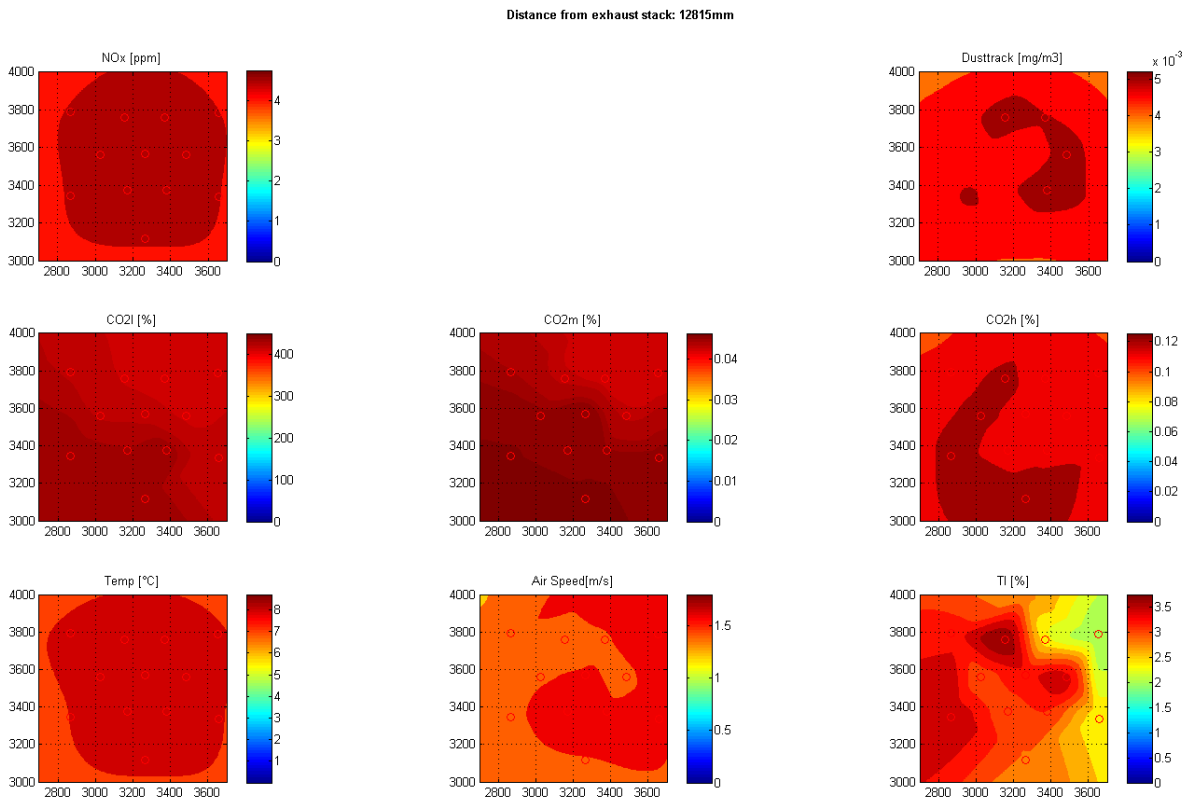

Figure 106: Post-2007, Idle Test, Plane 10

Post-2007 Truck, 20mph Test

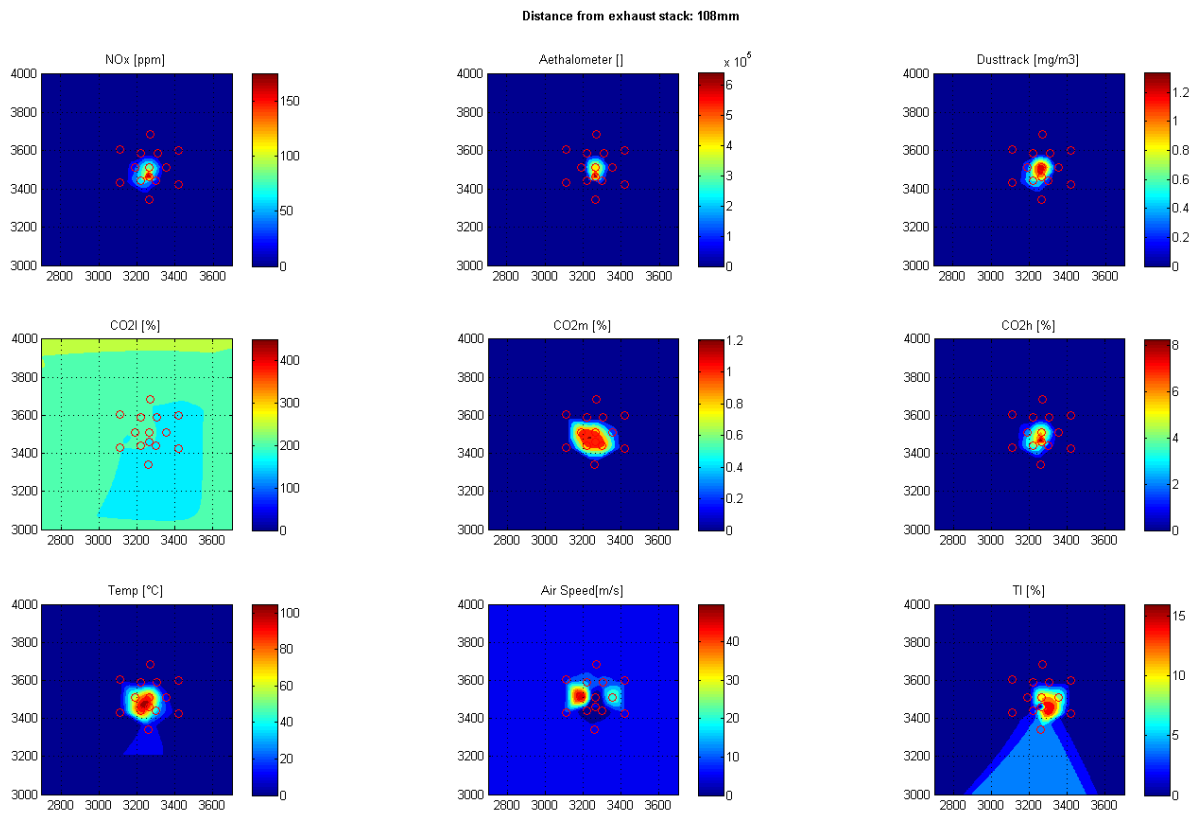

Figure 107: Post-2007, 20mph Test, Plane 1

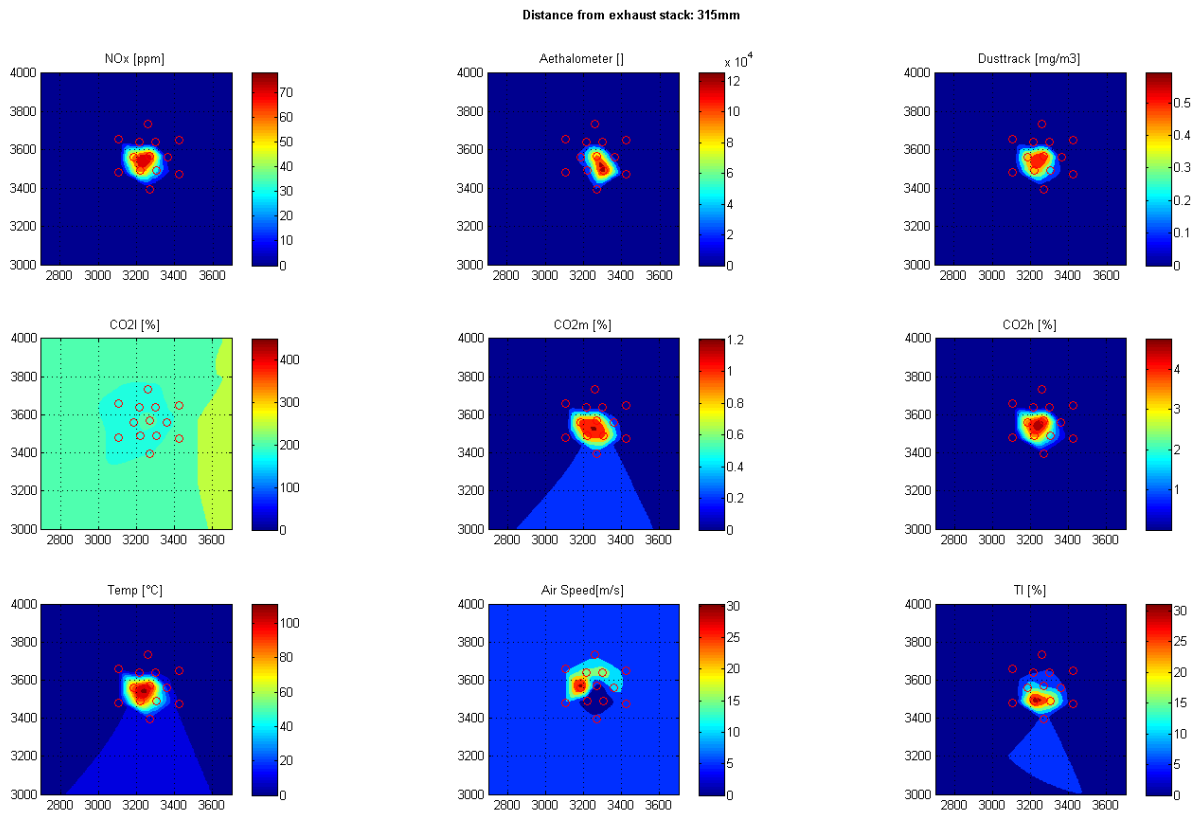

Figure 108: Post-2007, 20mph Test, Plane 2

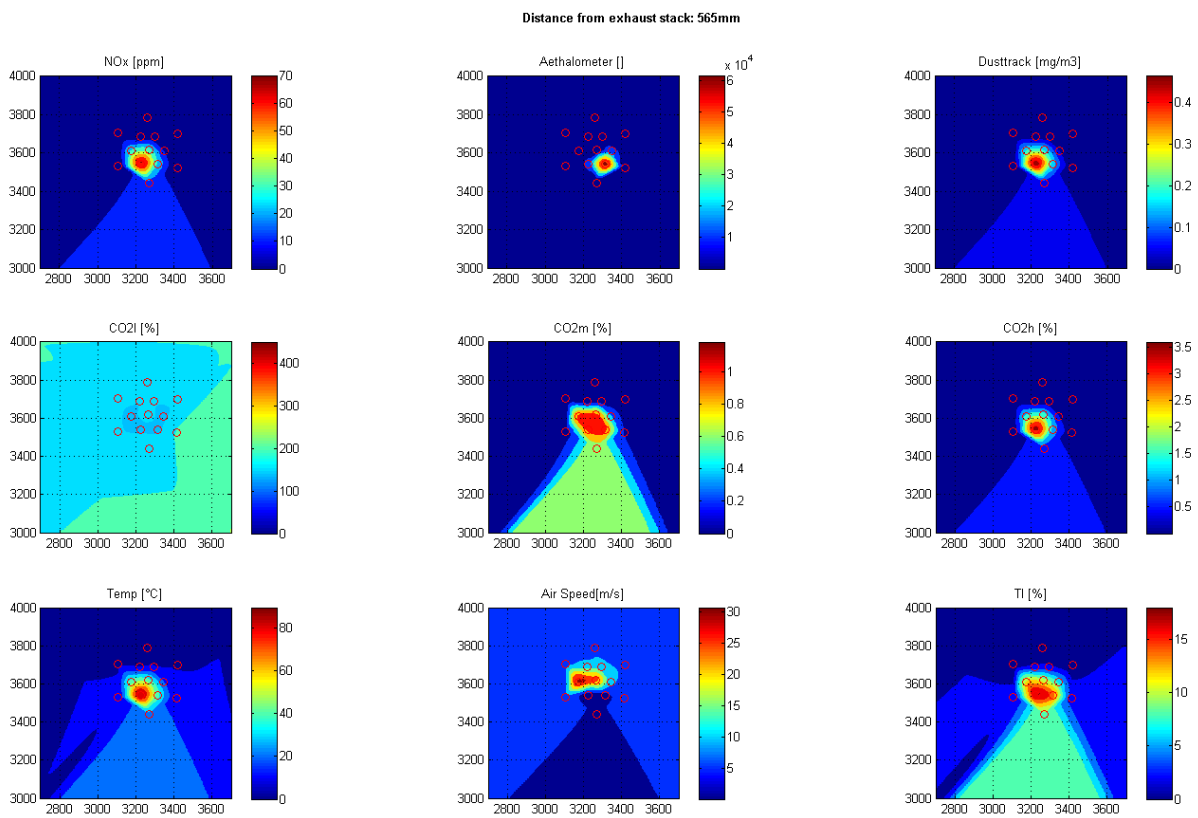

Figure 109: Post-2007, 20mph Test, Plane 3

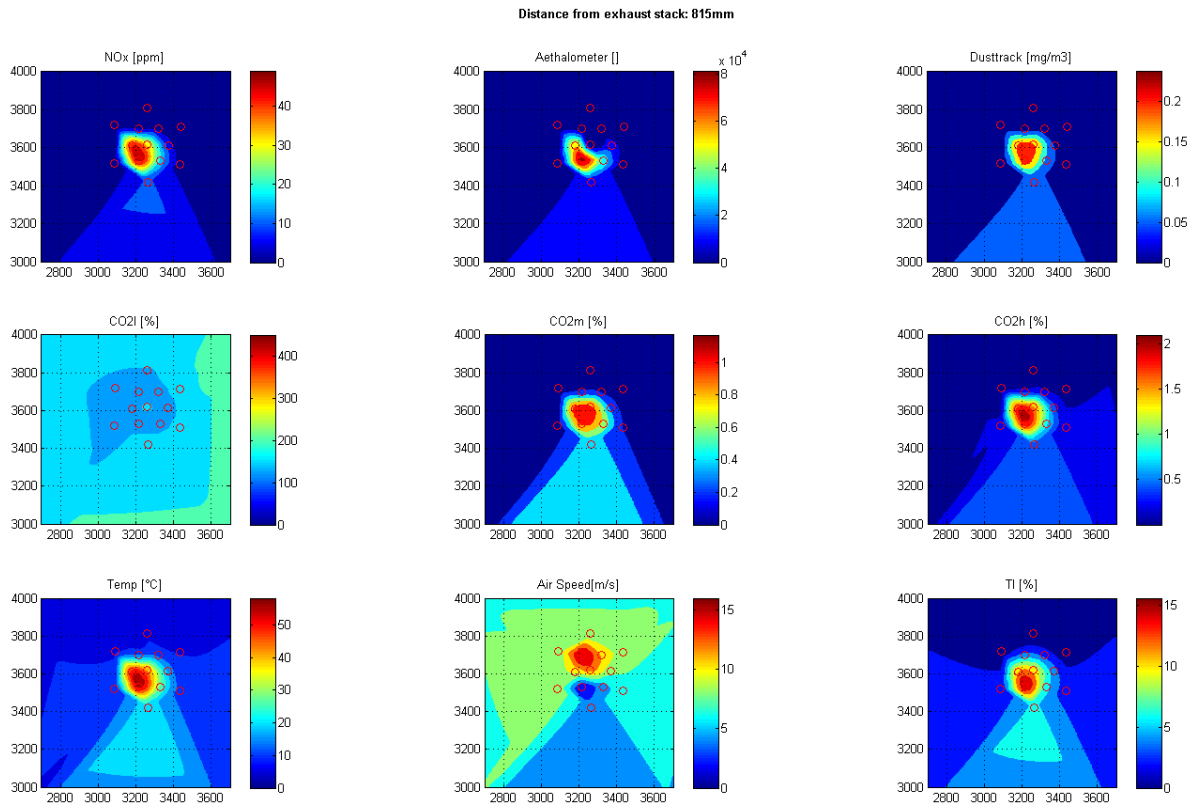

Figure 110: Post-2007, 20mph Test, Plane 4

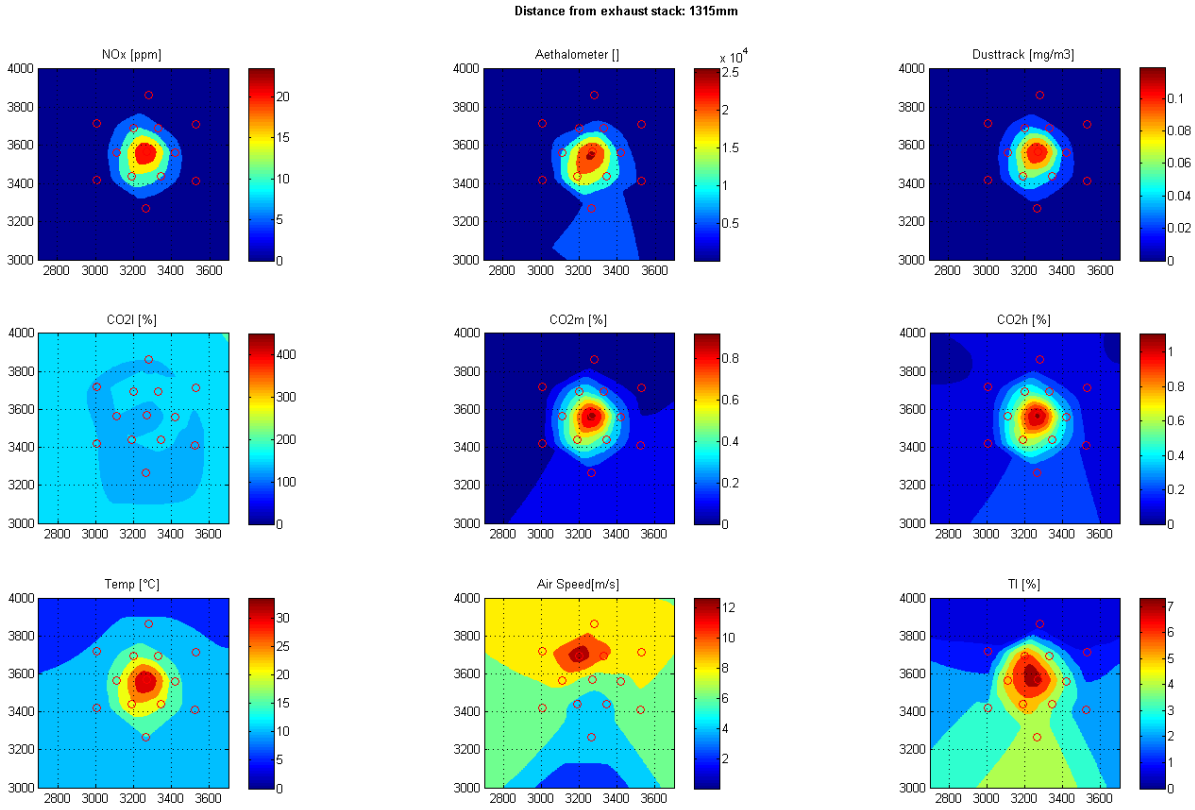

Figure 111: Post-2007, 20mph Test, Plane 5

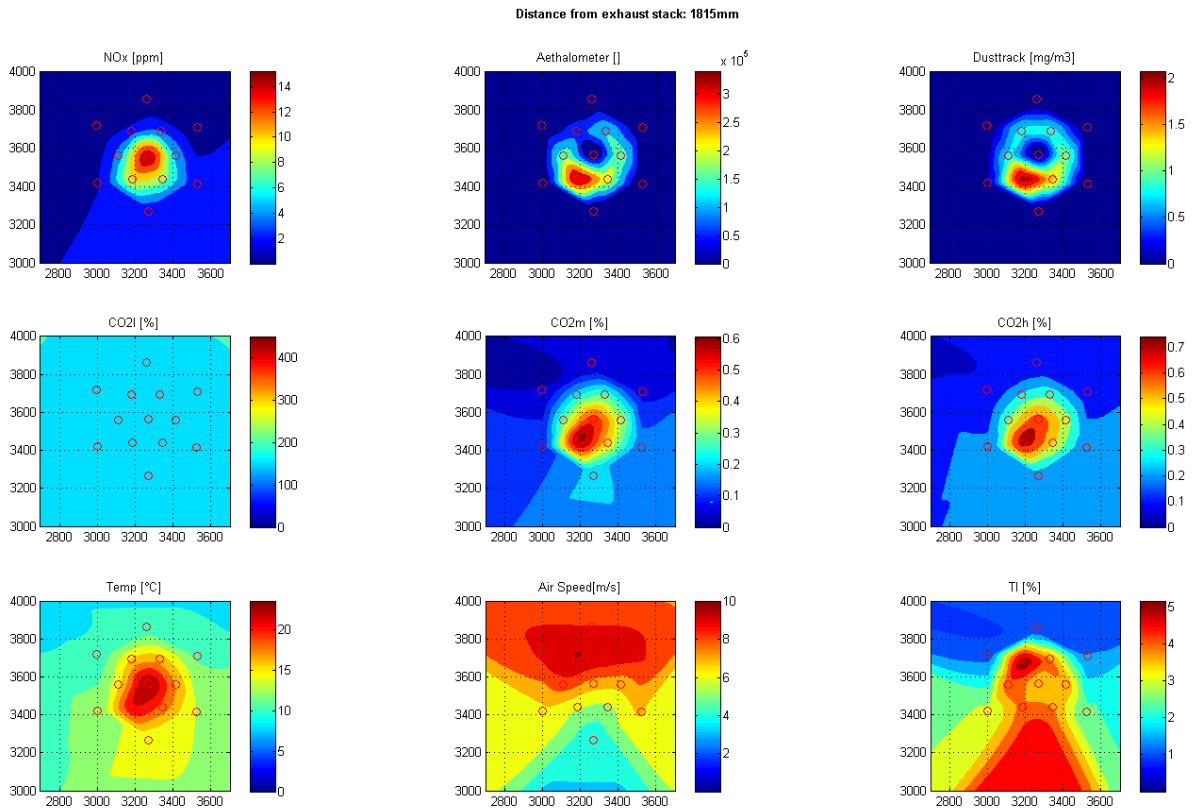

Figure 112: Post-2007, 20mph Test, Plane 6

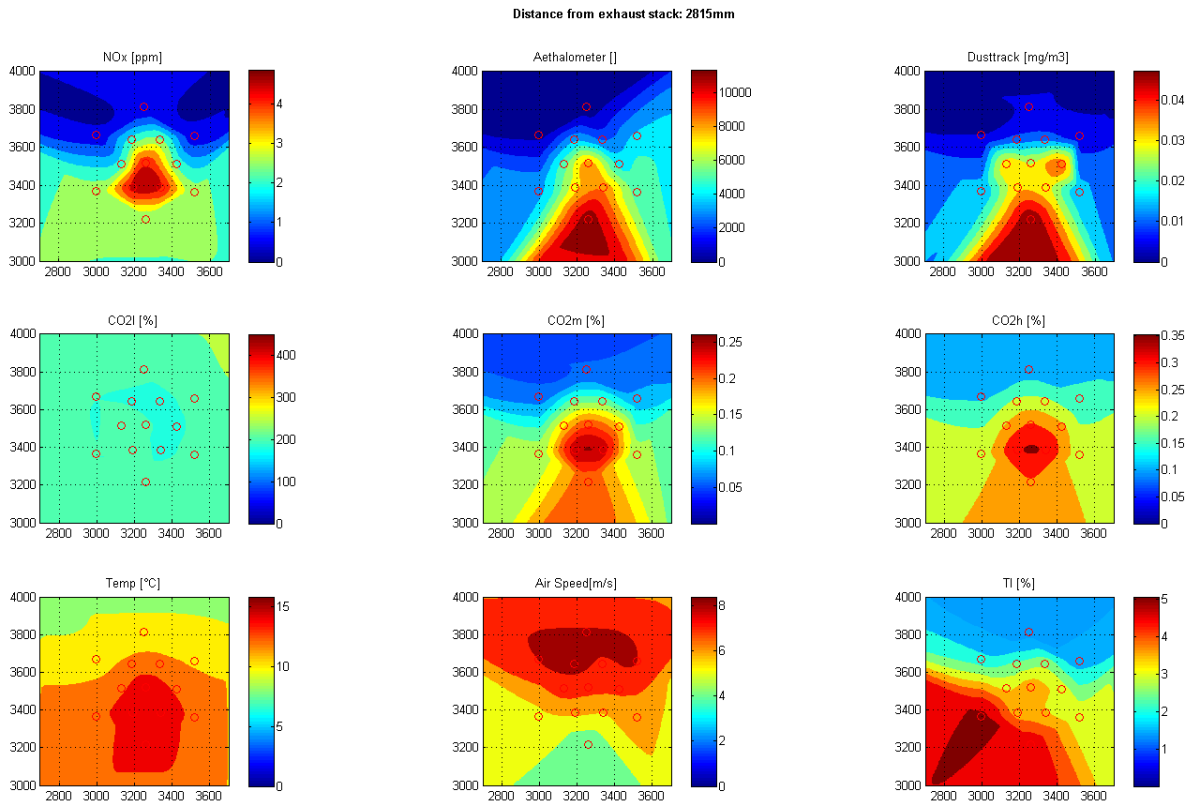

Figure 113: Post-2007, 20mph Test, Plane 7

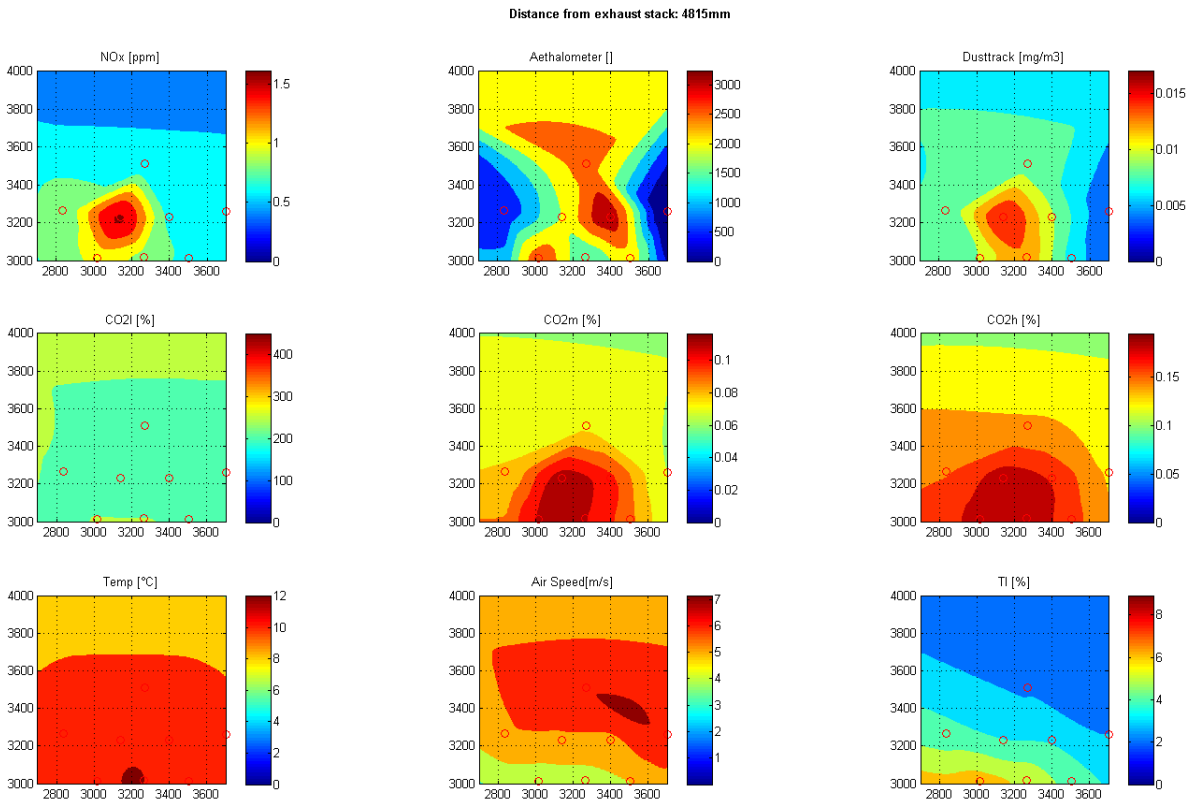

Figure 114: Post-2007, 20mph Test, Plane 8

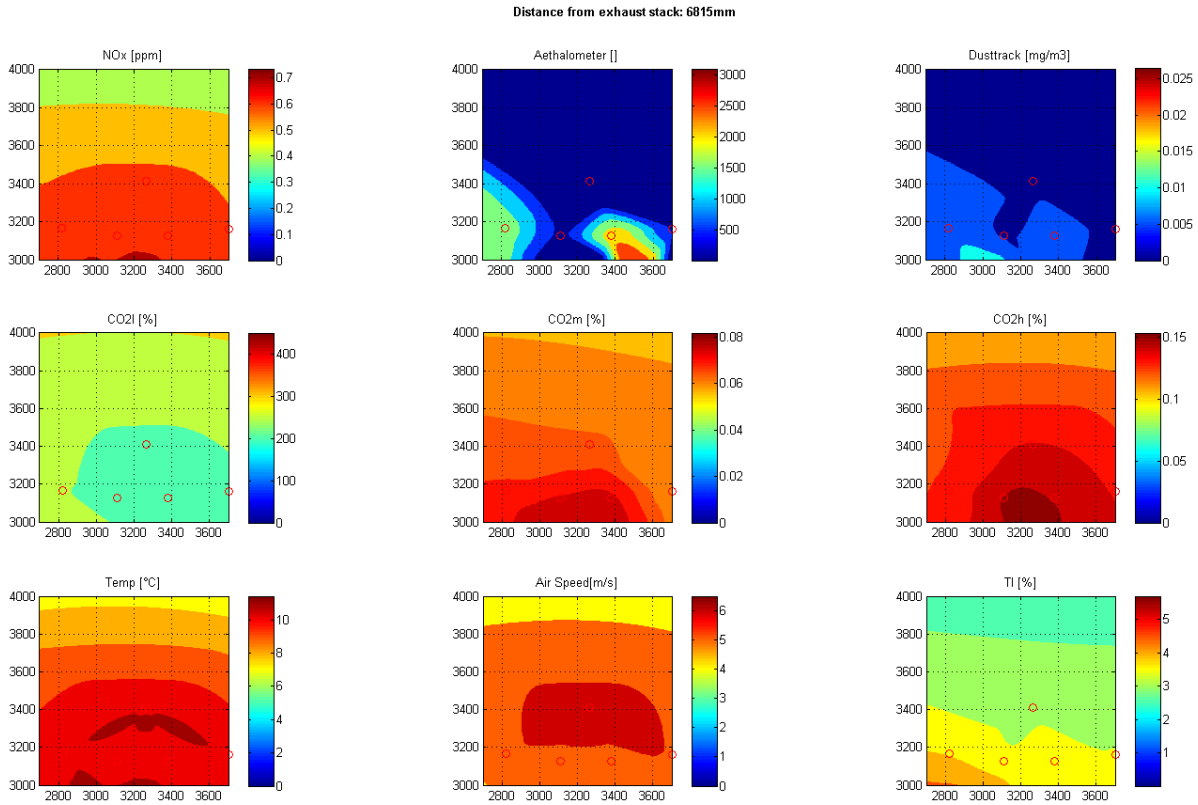

Figure 115: Post-2007, 20mph Test, Plane 9

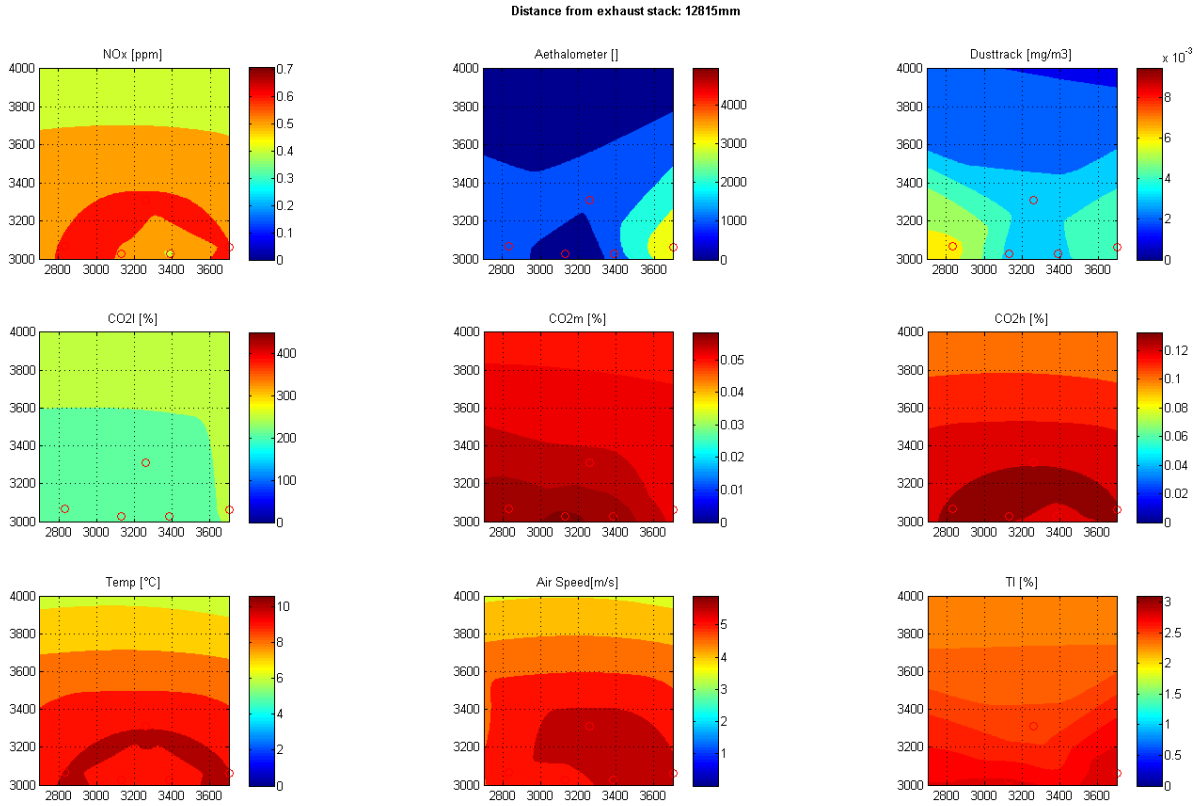

Figure 116: Post-2007, 20mph Test, Plane 10

Post-2007 Truck, 35mph Test

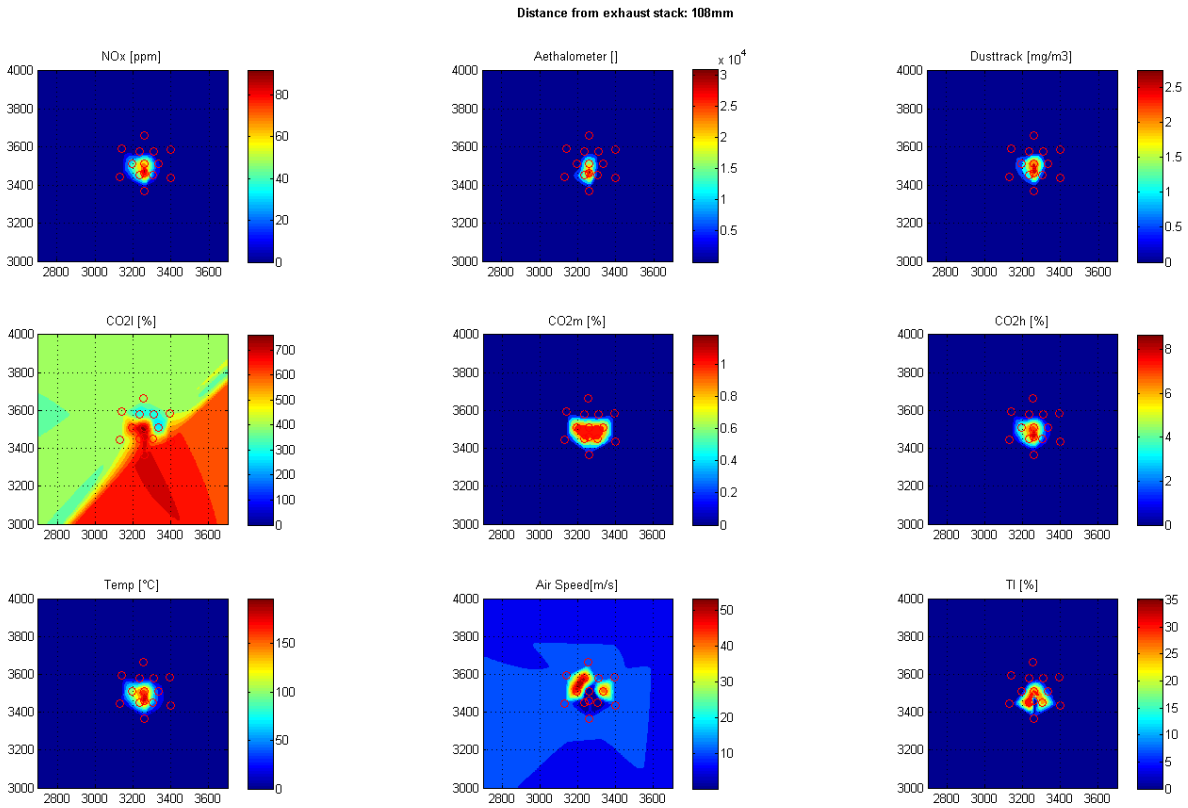

Figure 117: Post-2007, 35mph Test, Plane 1

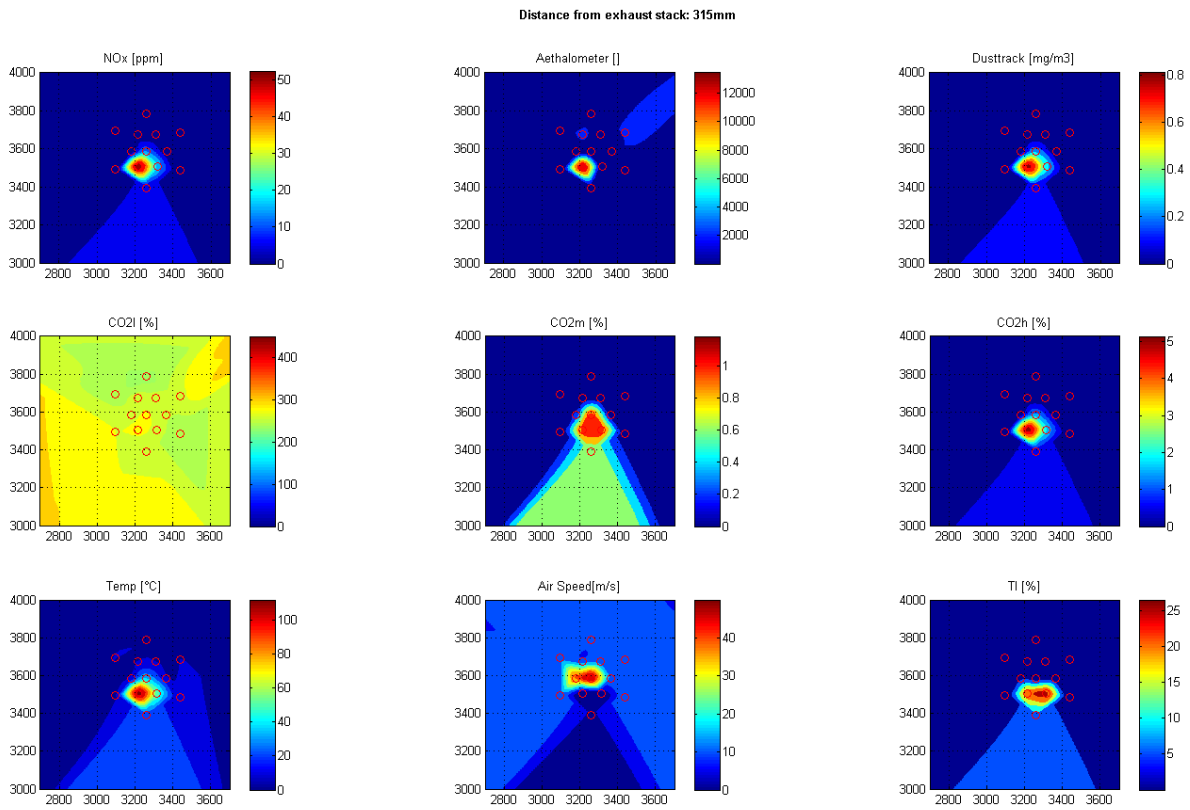

Figure 118: Post-2007, 35mph Test, Plane 2

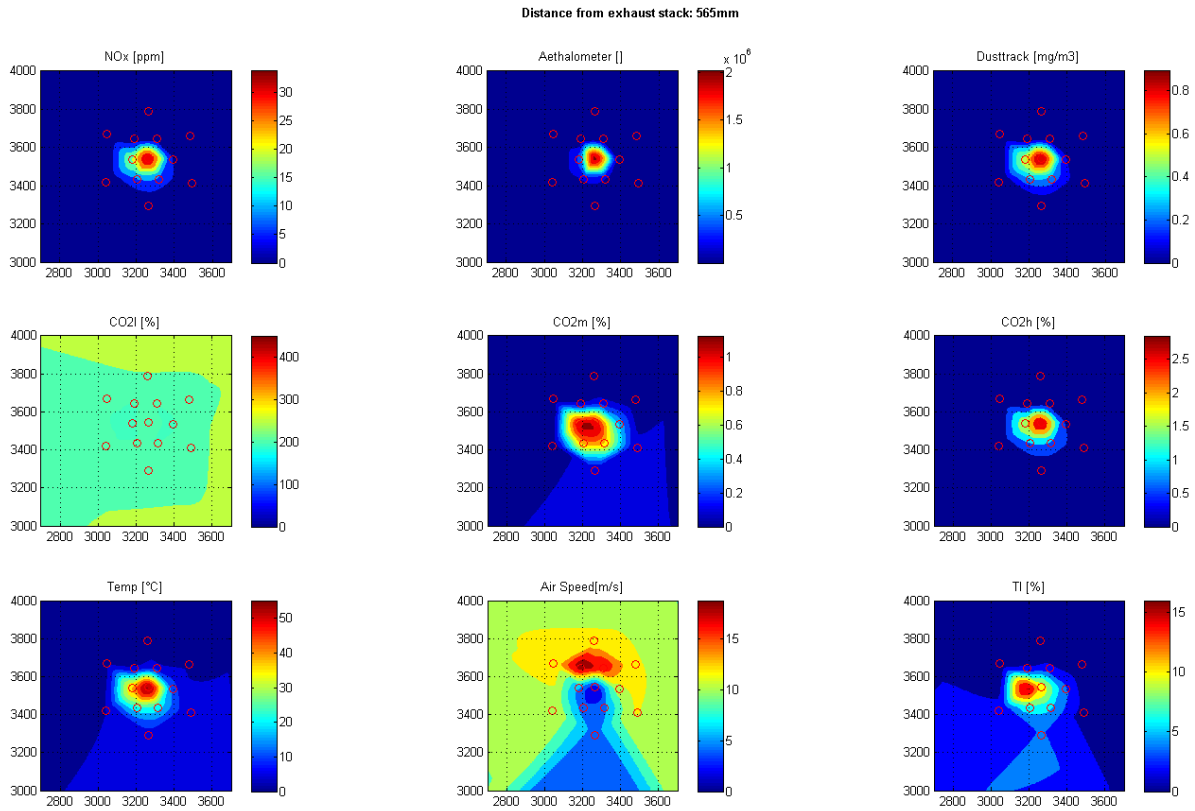

Figure 119: Post-2007, 35mph Test, Plane 3

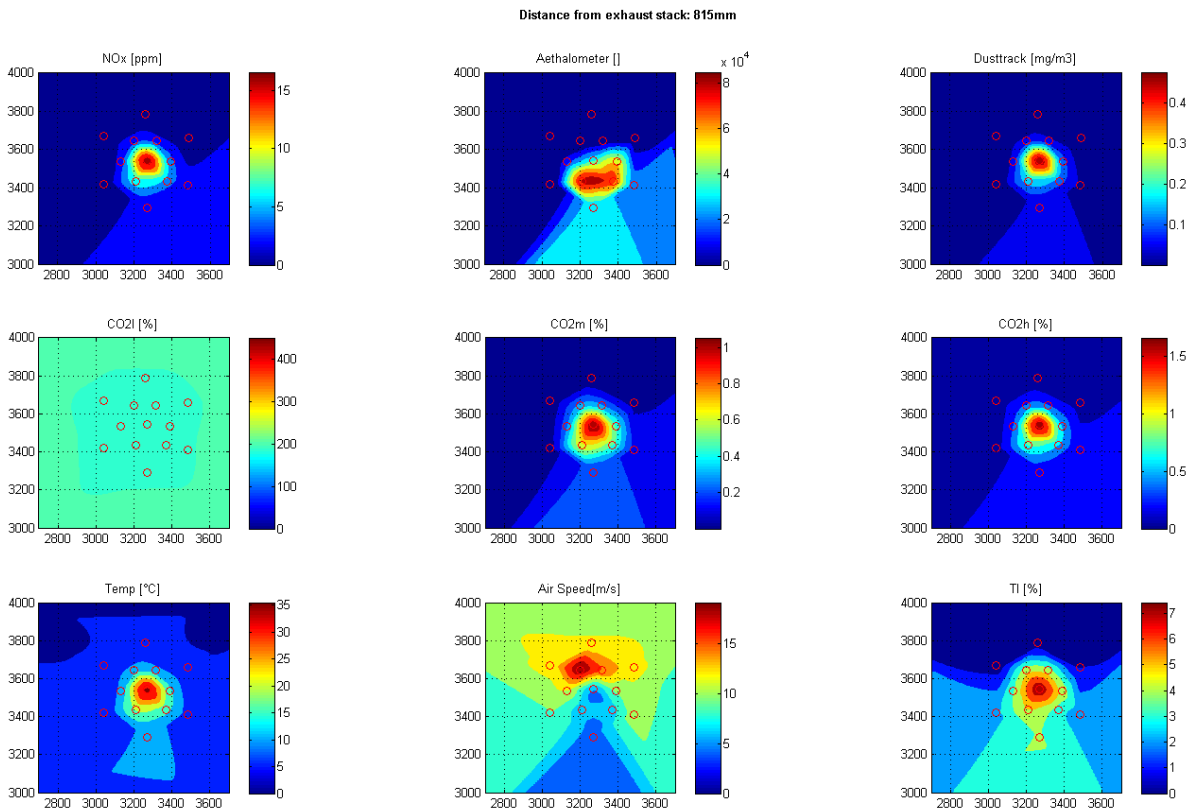

Figure 120: Post-2007, 35mph Test, Plane 4

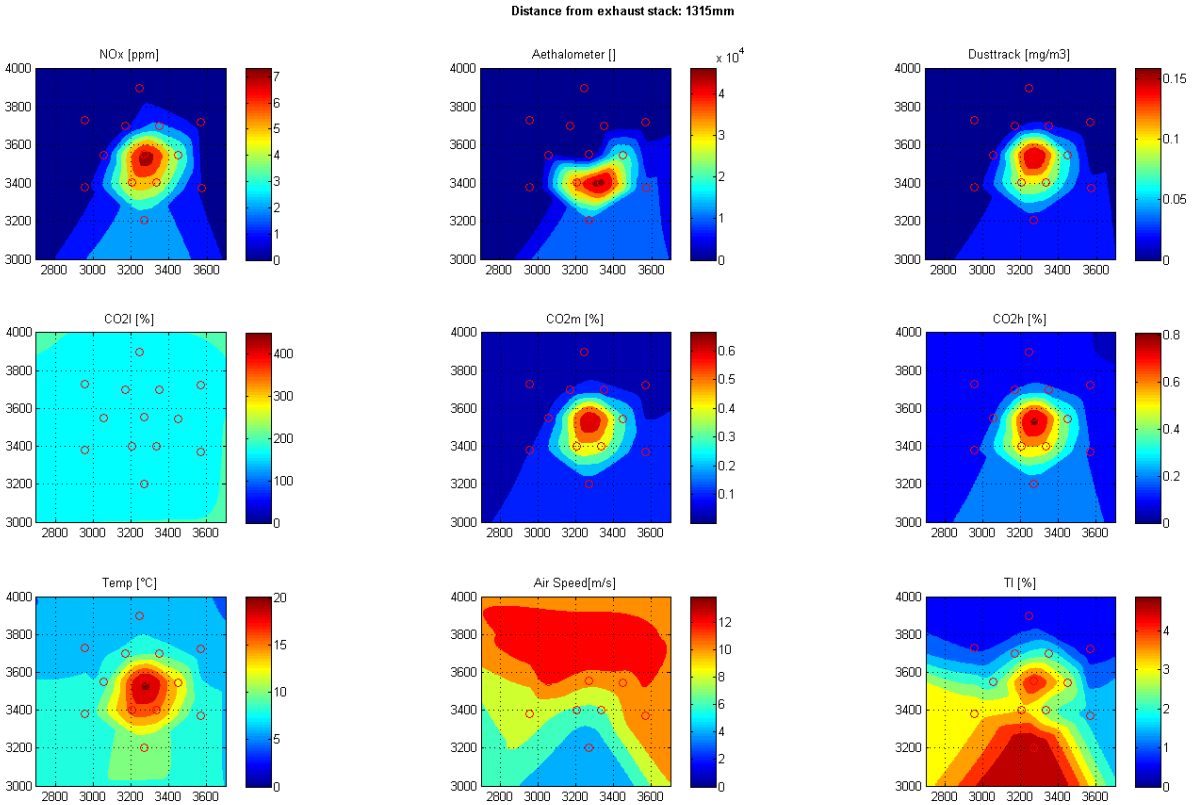

Figure 121: Post-2007, 35mph Test, Plane 5

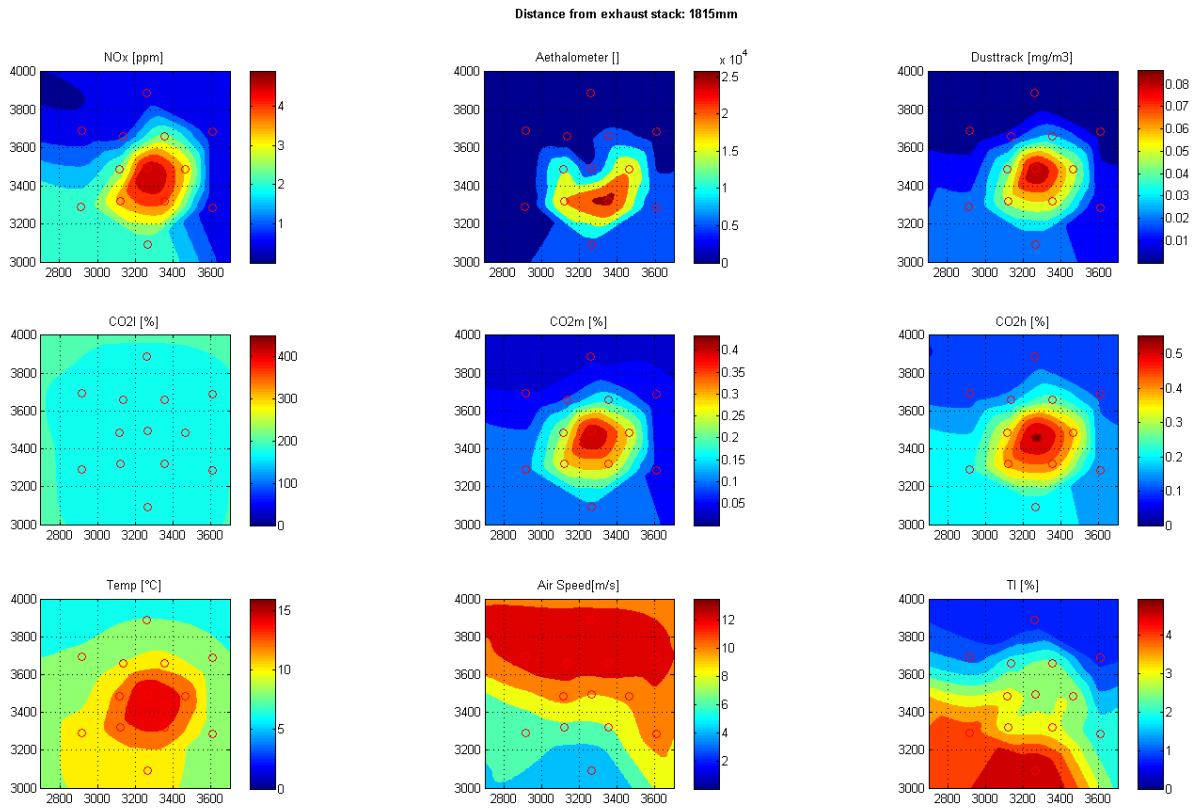

Figure 122: Post-2007, 35mph Test, Plane 6

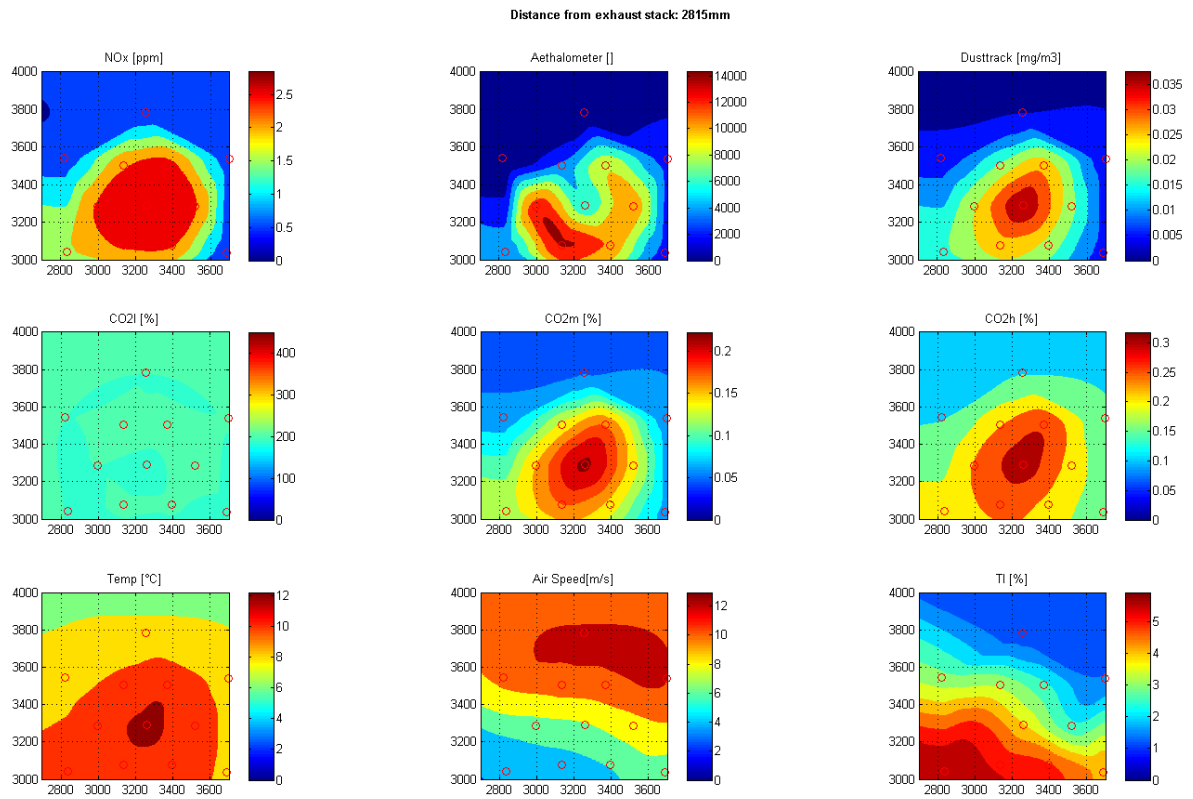

Figure 123: Post-2007, 35mph Test, Plane 7

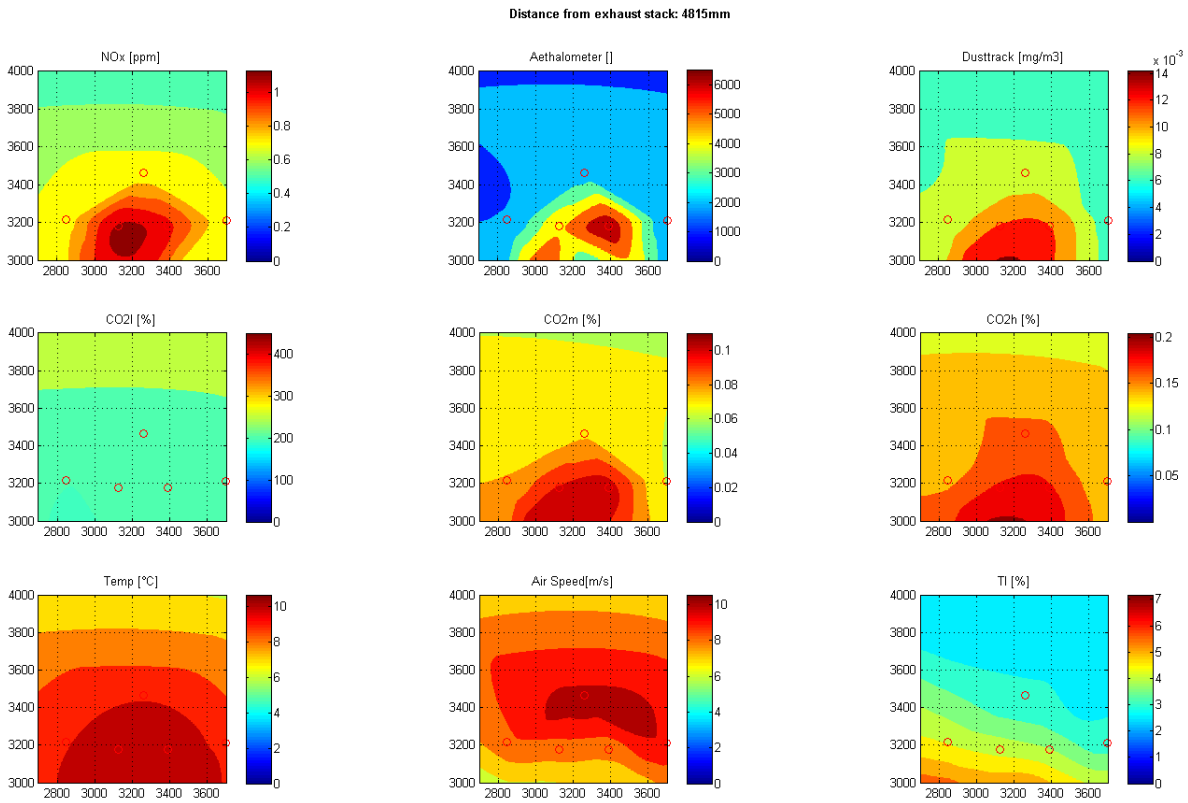

Figure 124: Post-2007, 35mph Test, Plane 8

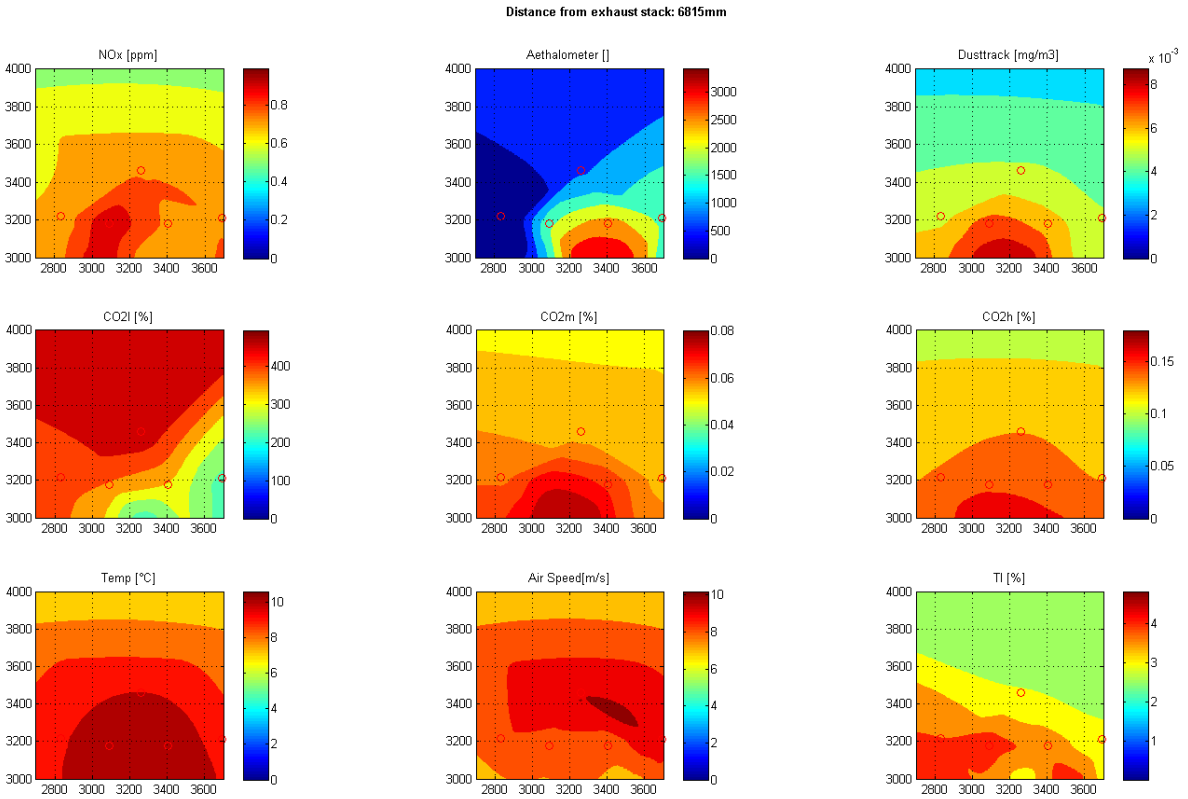

Figure 125: Post-2007, 35mph Test, Plane 9

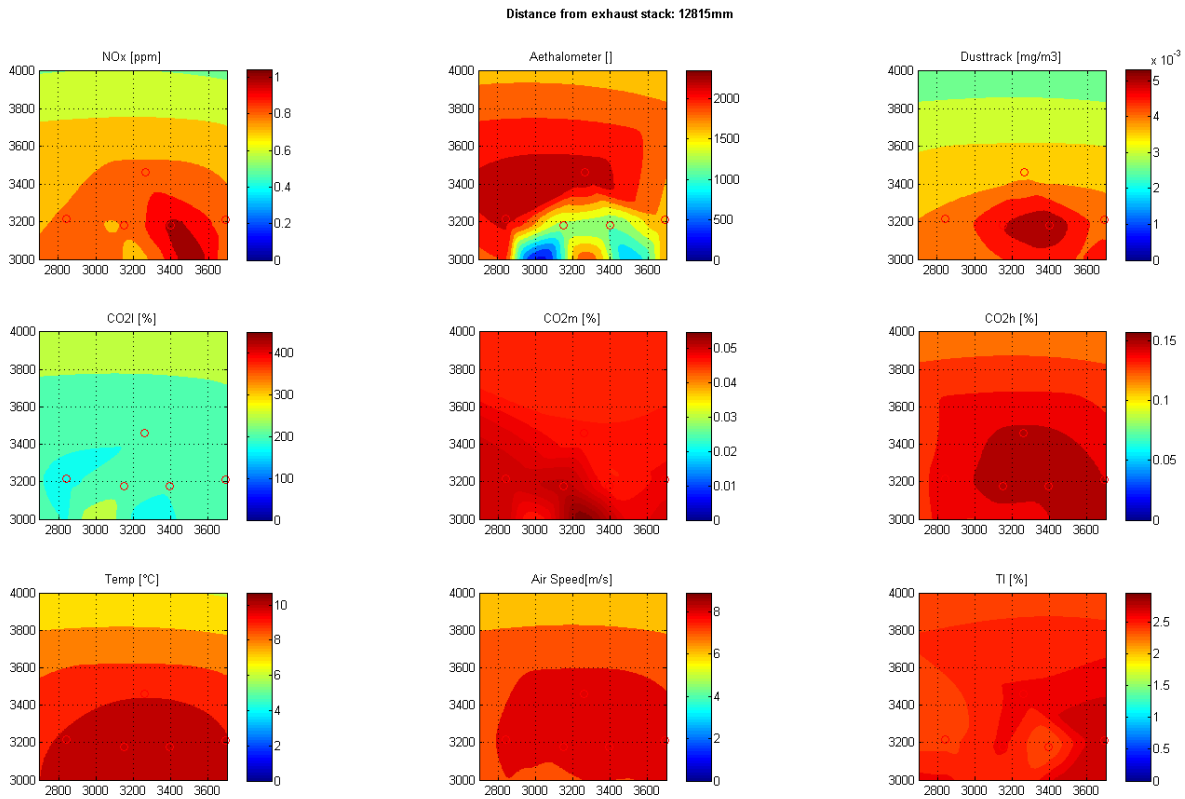

Figure 126: Post-2007, 35mph Test, Plane 10

Post-2010 Truck, Idle Test

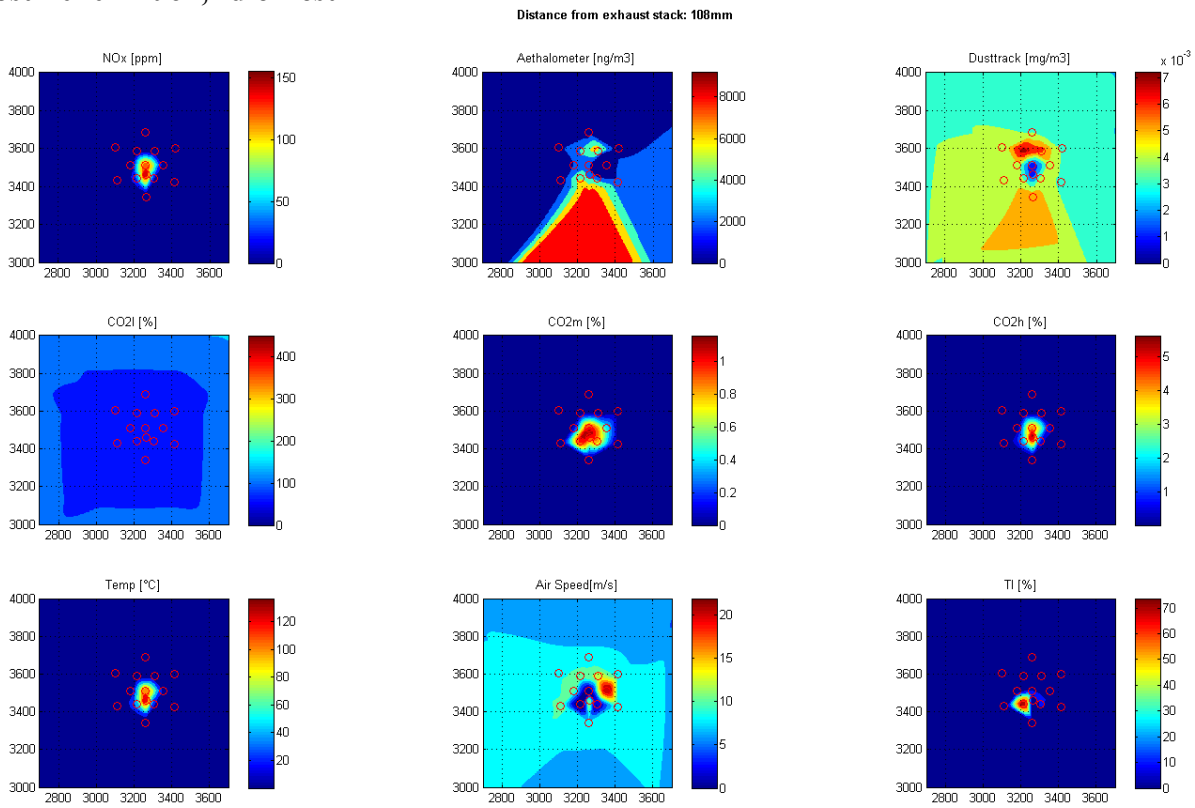

Figure 127: Post-2010, Idle test, Plane 1

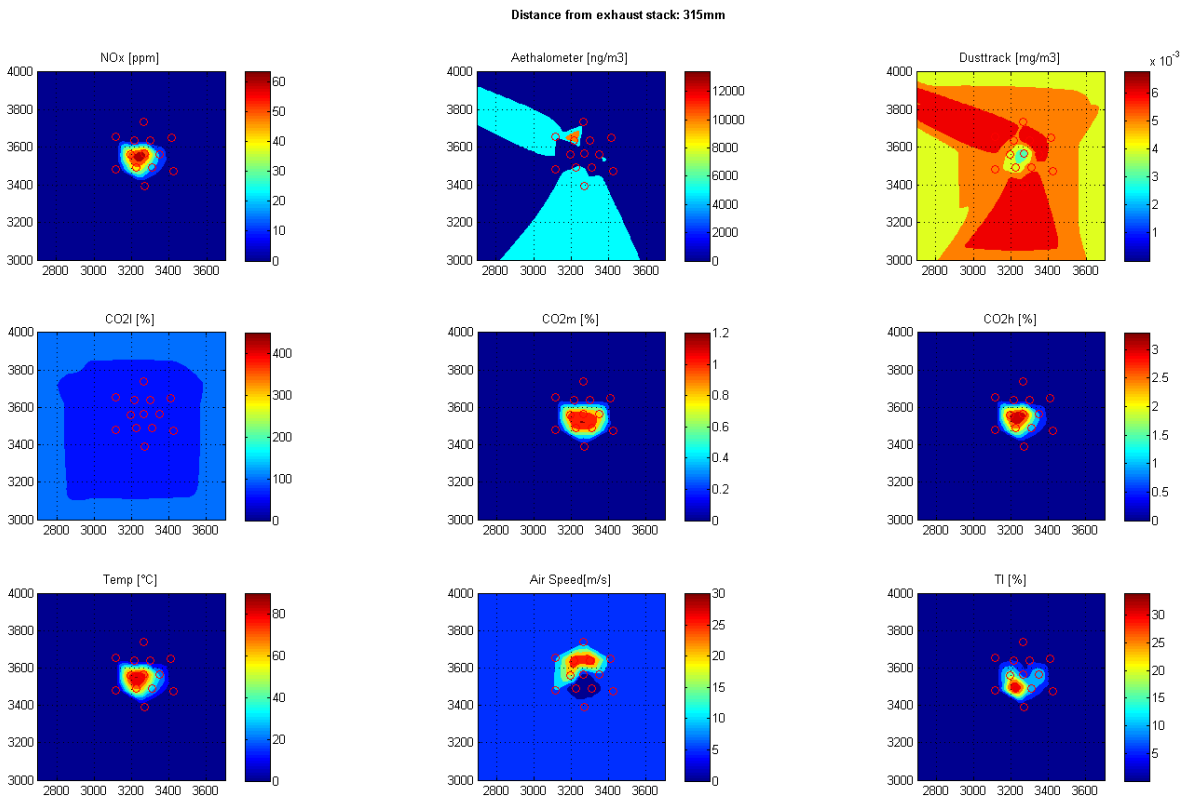

Figure 128: Post-2010, Idle test, Plane 2

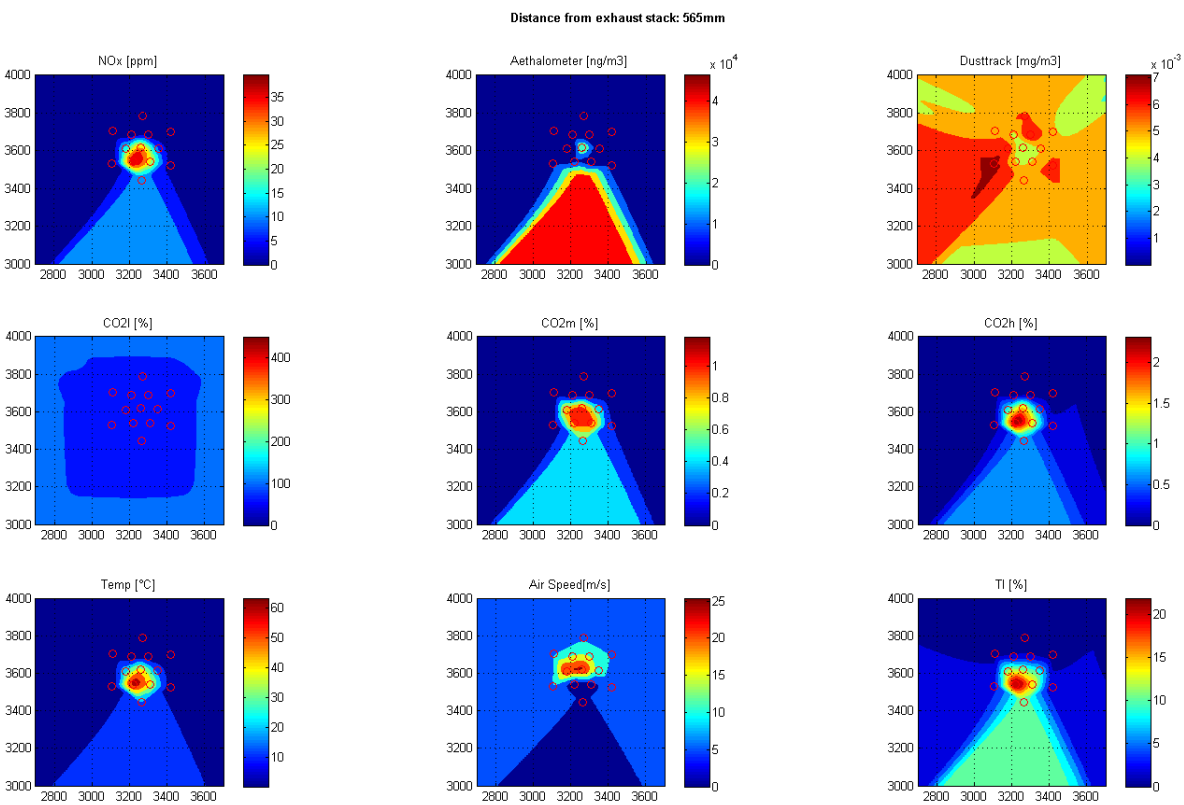

Figure 129: Post-2010, Idle test, Plane 2

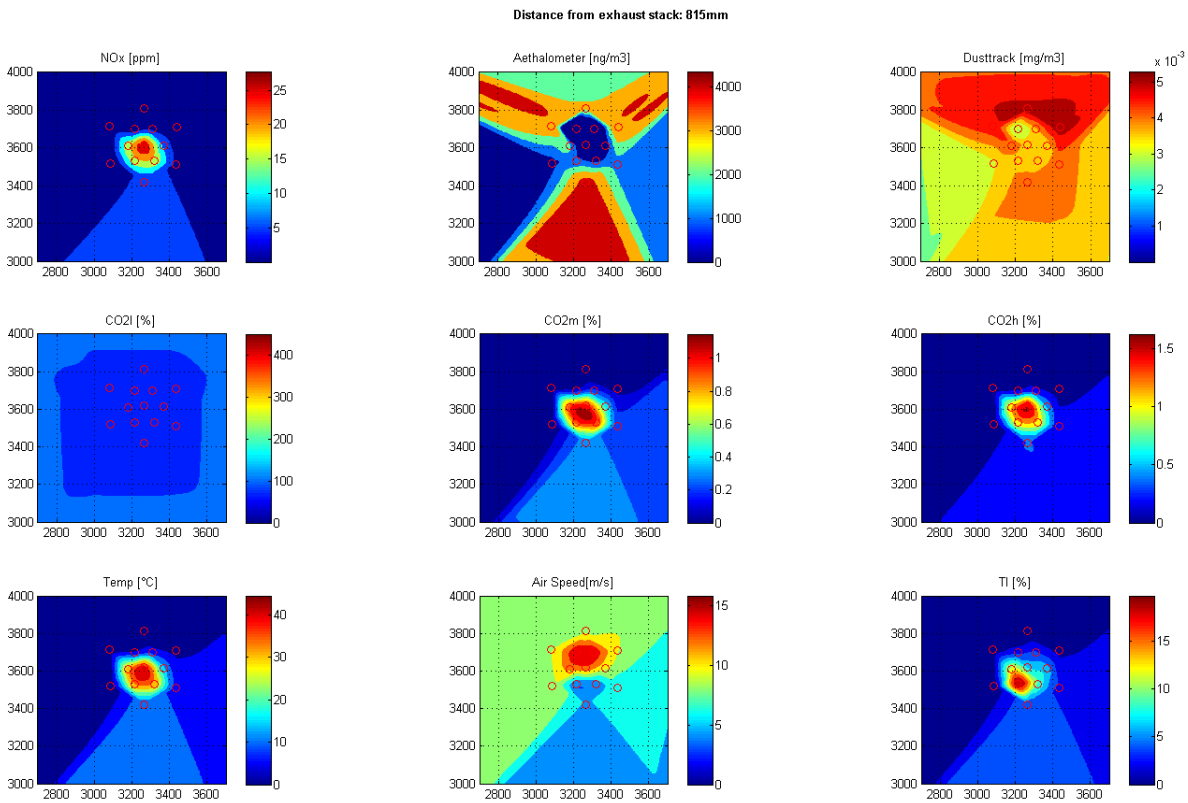

Figure 130: Post-2010, Idle test, Plane 4

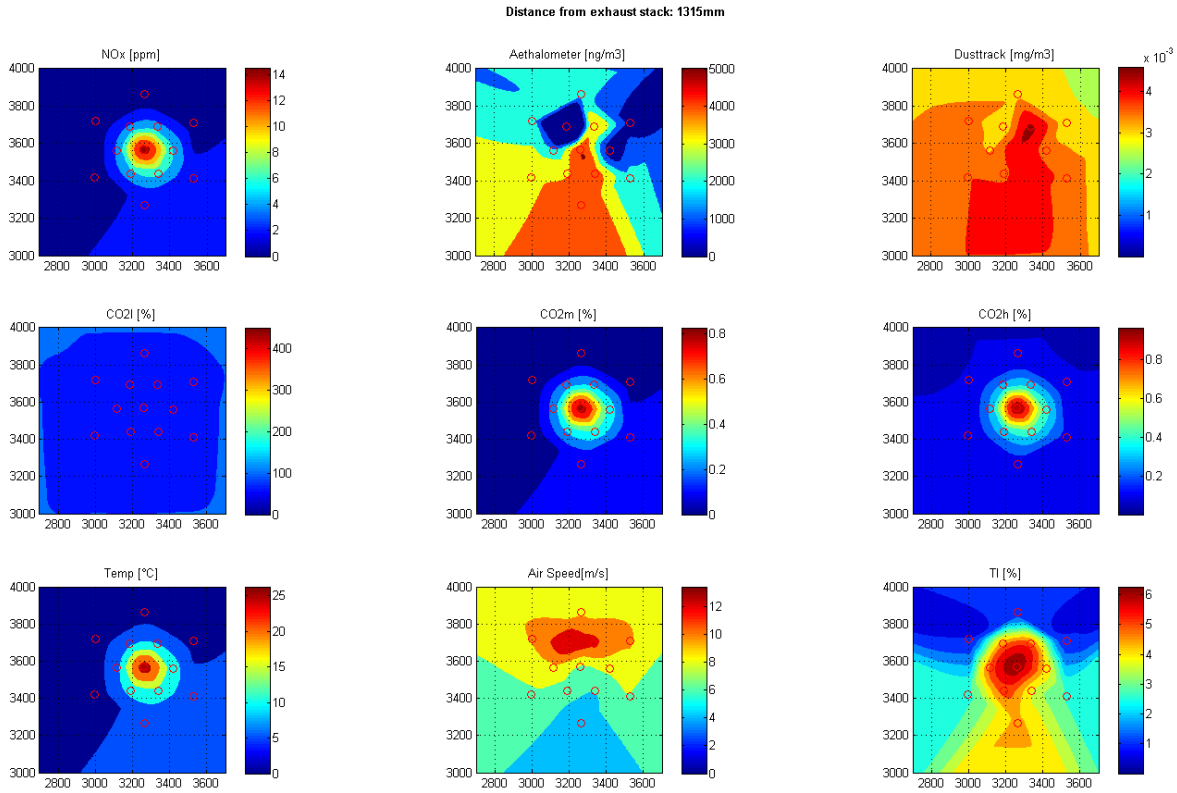

Figure 131: Post-2010, Idle test, Plane 5

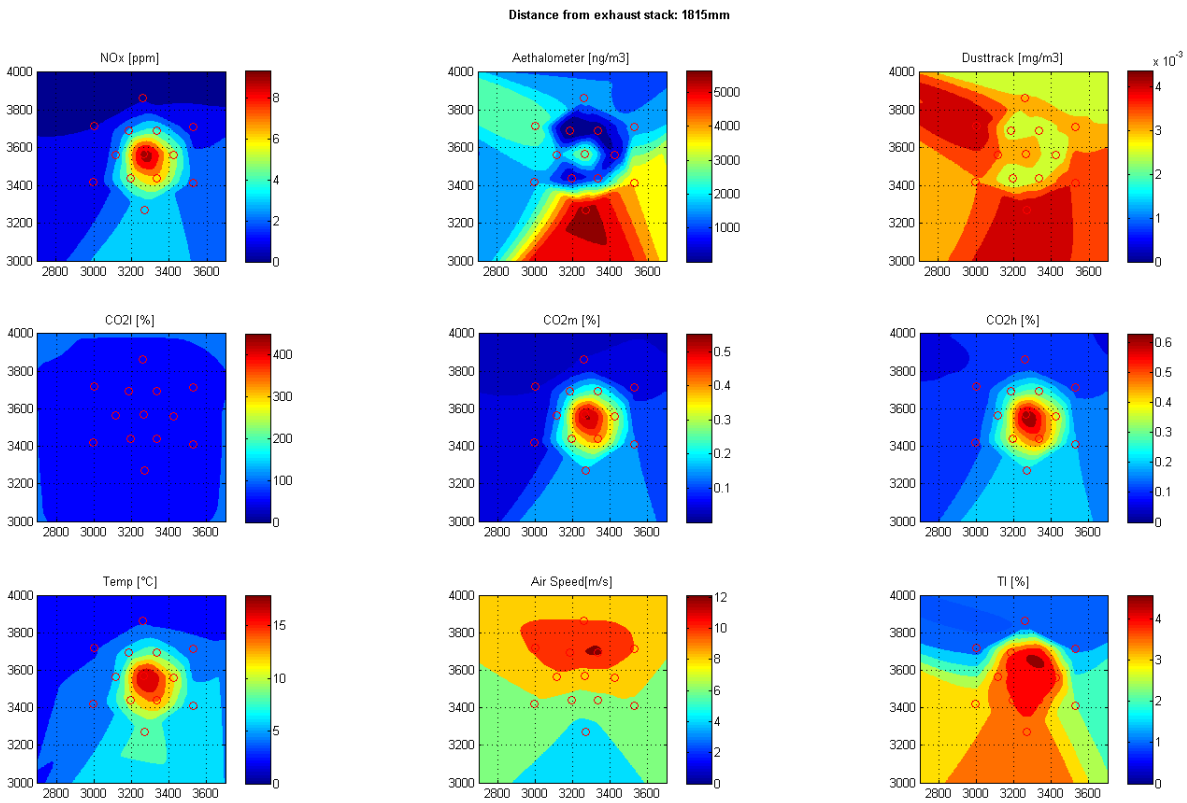

Figure 132: Post-2010, Idle test, Plane 6

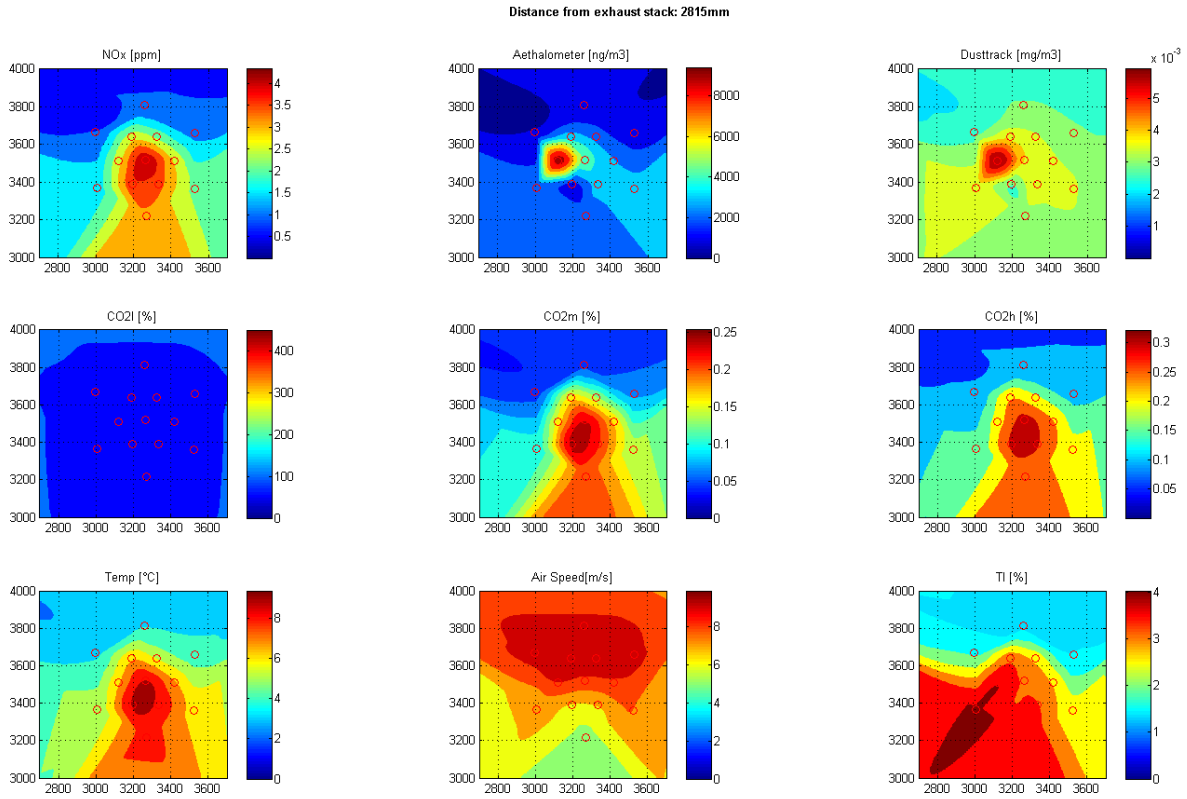

Figure 133: Post-2010, Idle test, Plane 7

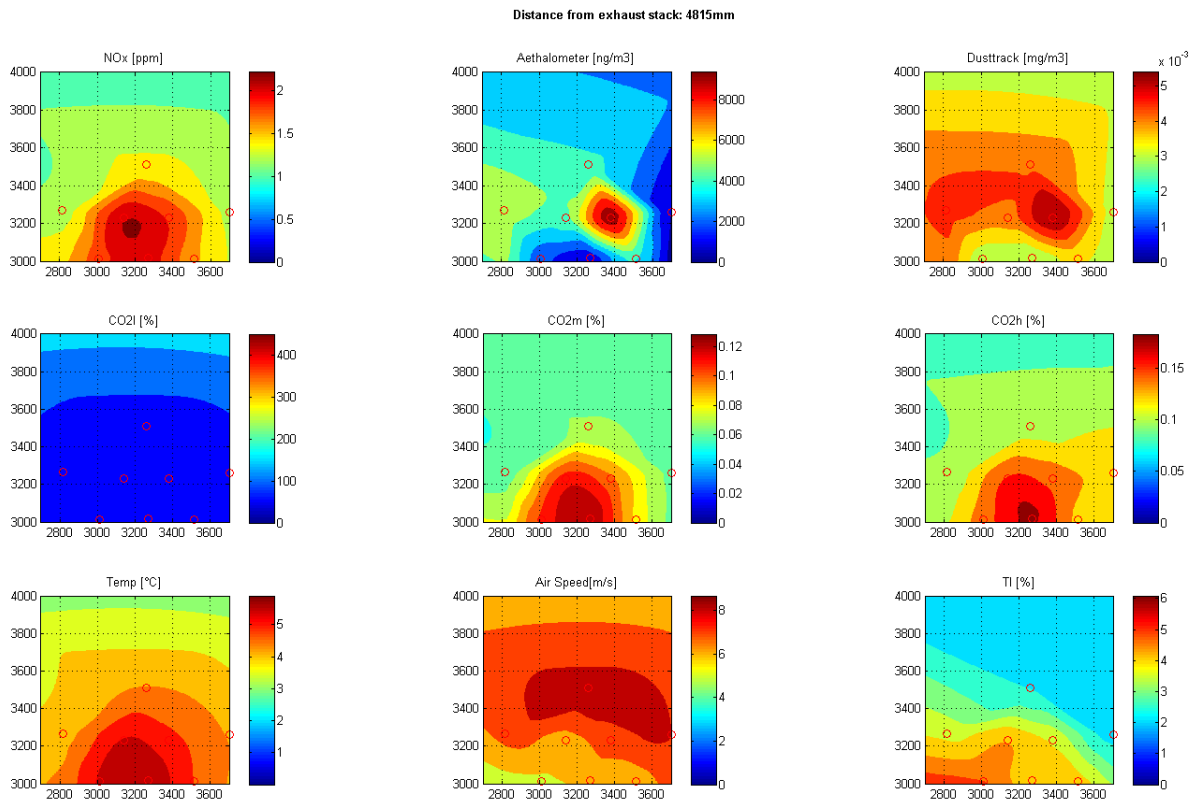

Figure 134: Post-2010, Idle test, Plane 8

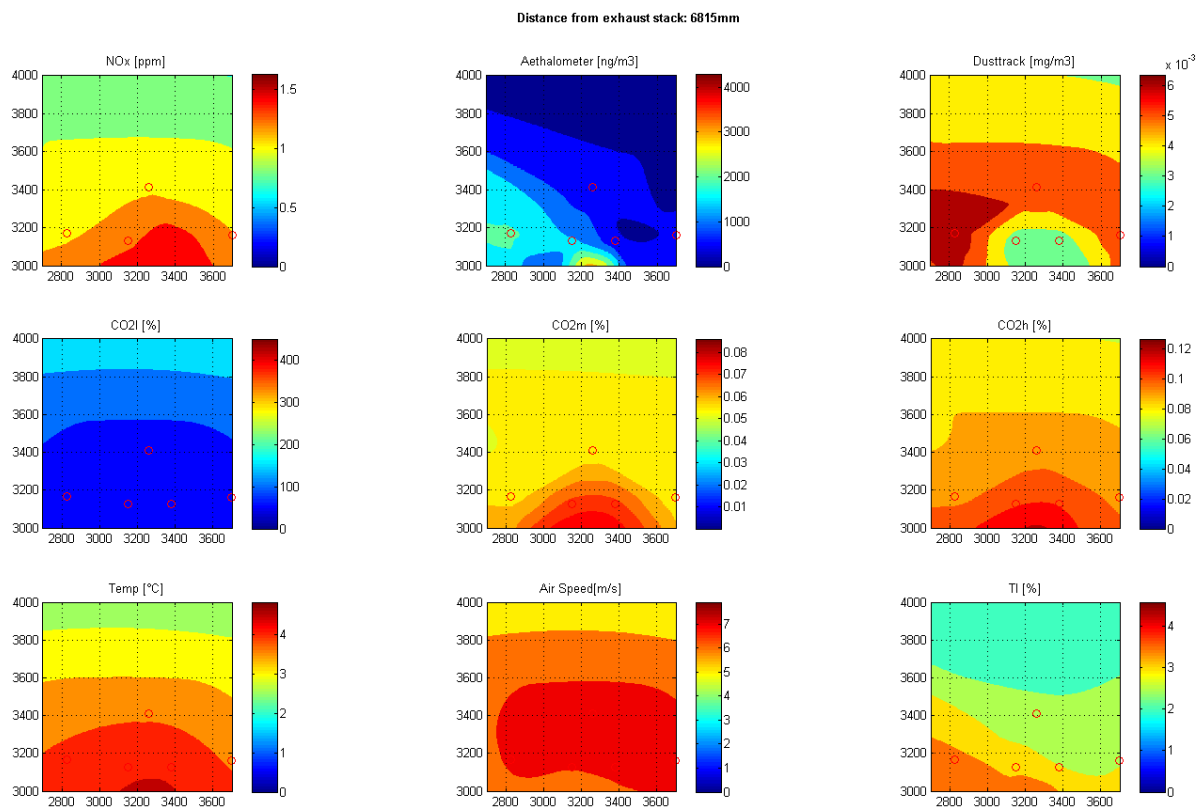

Figure 135: Post-2010, Idle test, Plane 9

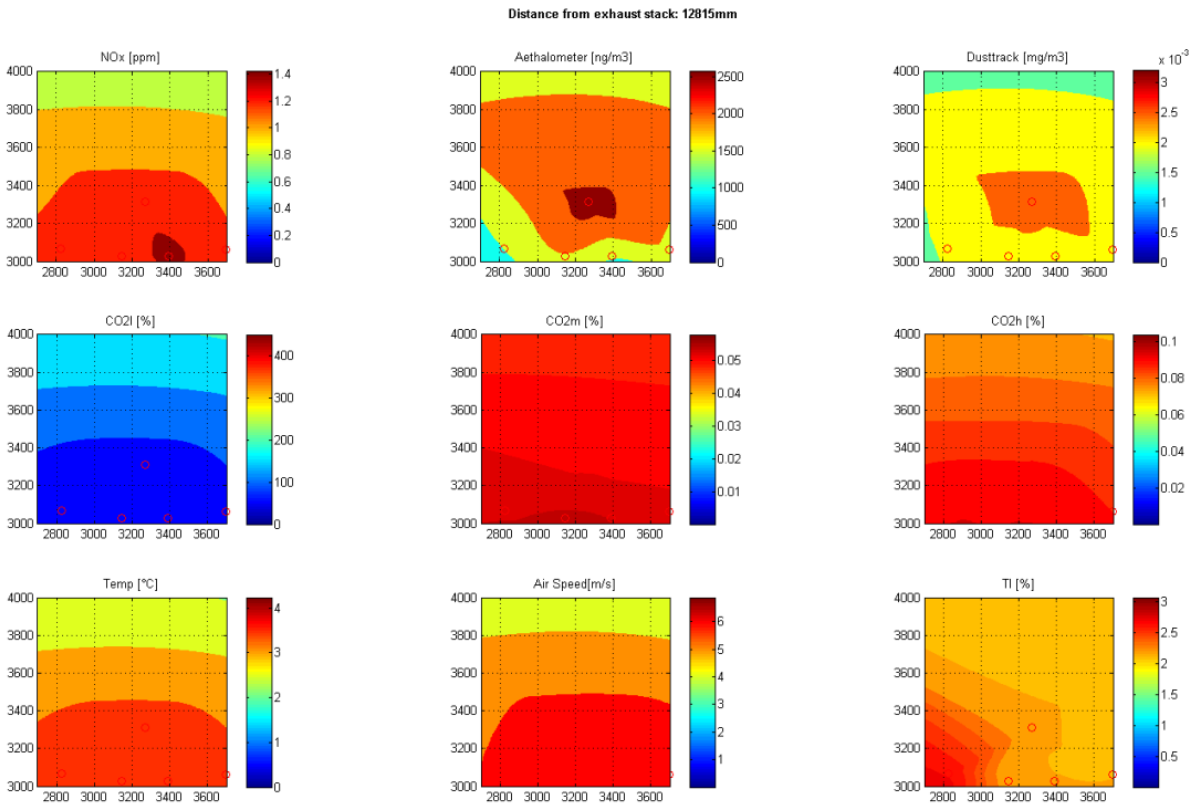

Figure 136: Post-2010, Idle test, Plane 10

Post-201 Truck, 20mph Test

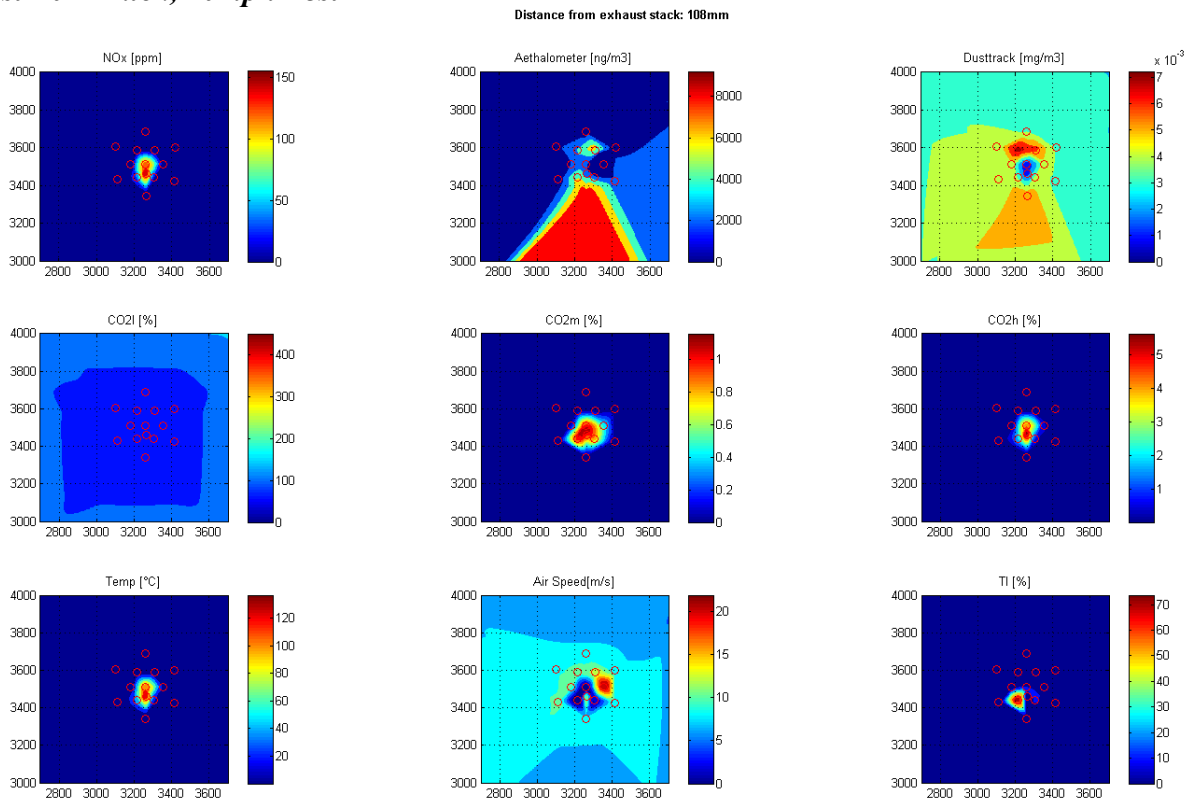

Figure 137: Post2010, 20mph Test, Plane 1

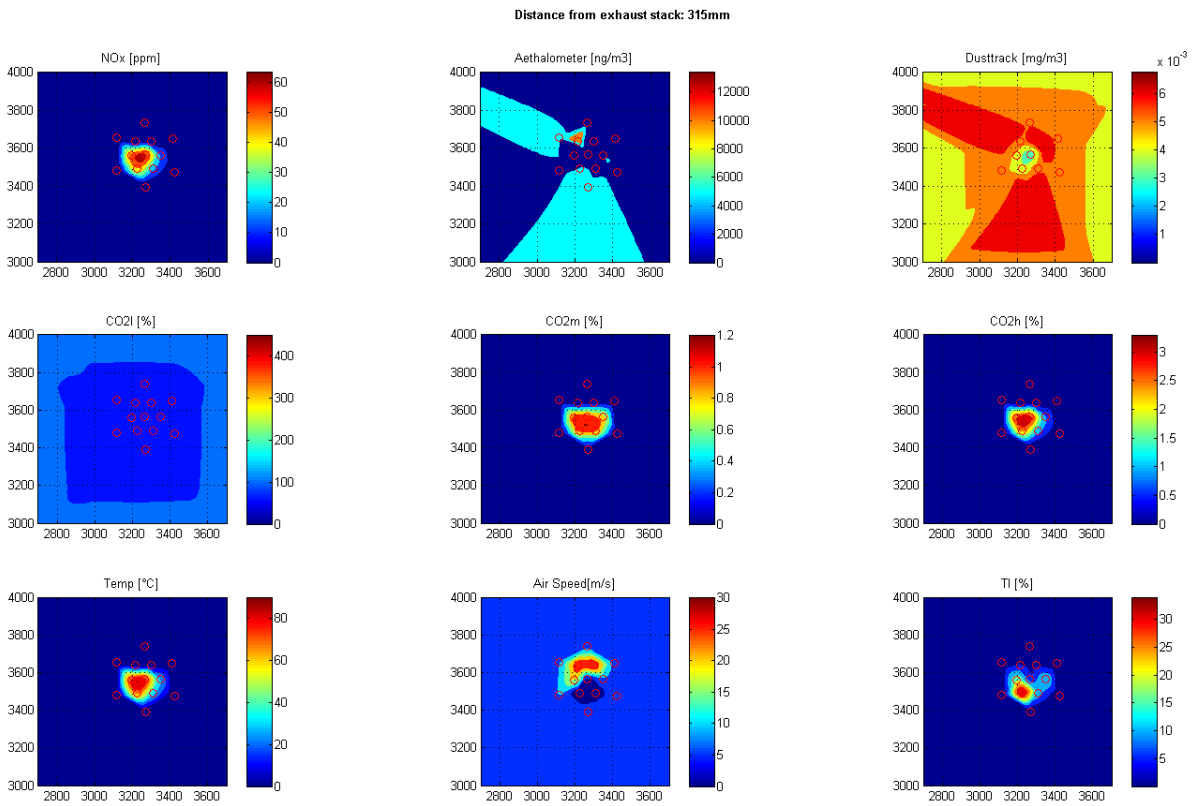

Figure 138: Post2010, 20mph Test, Plane 2

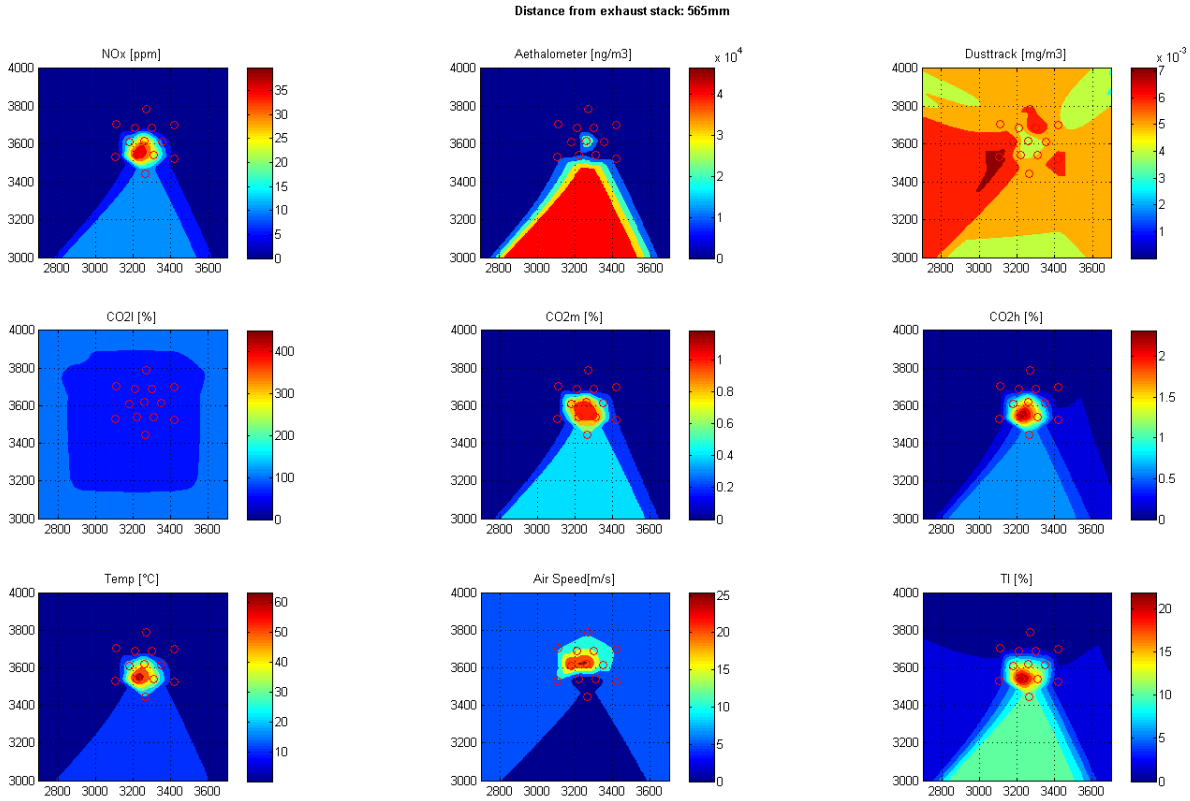

Figure 139: Post2010, 20mph Test, Plane 3

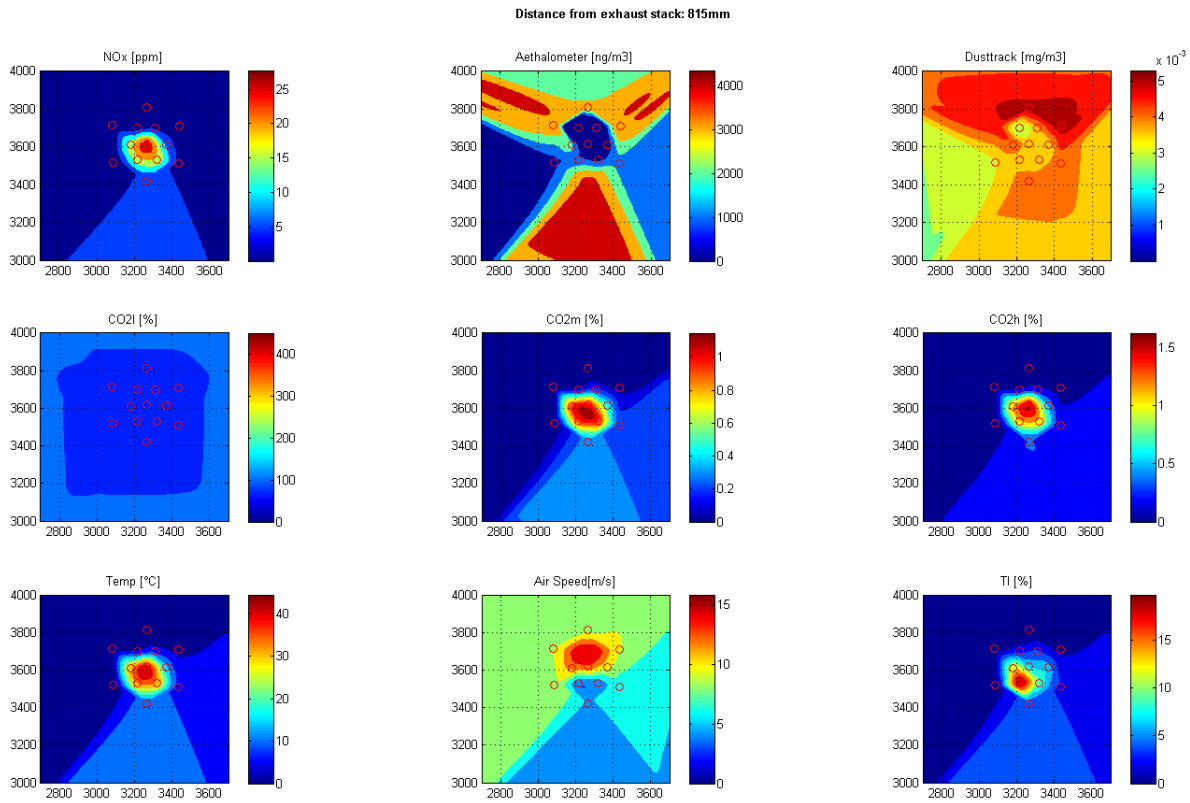

Figure 140: Post2010, 20mph Test, Plane 4

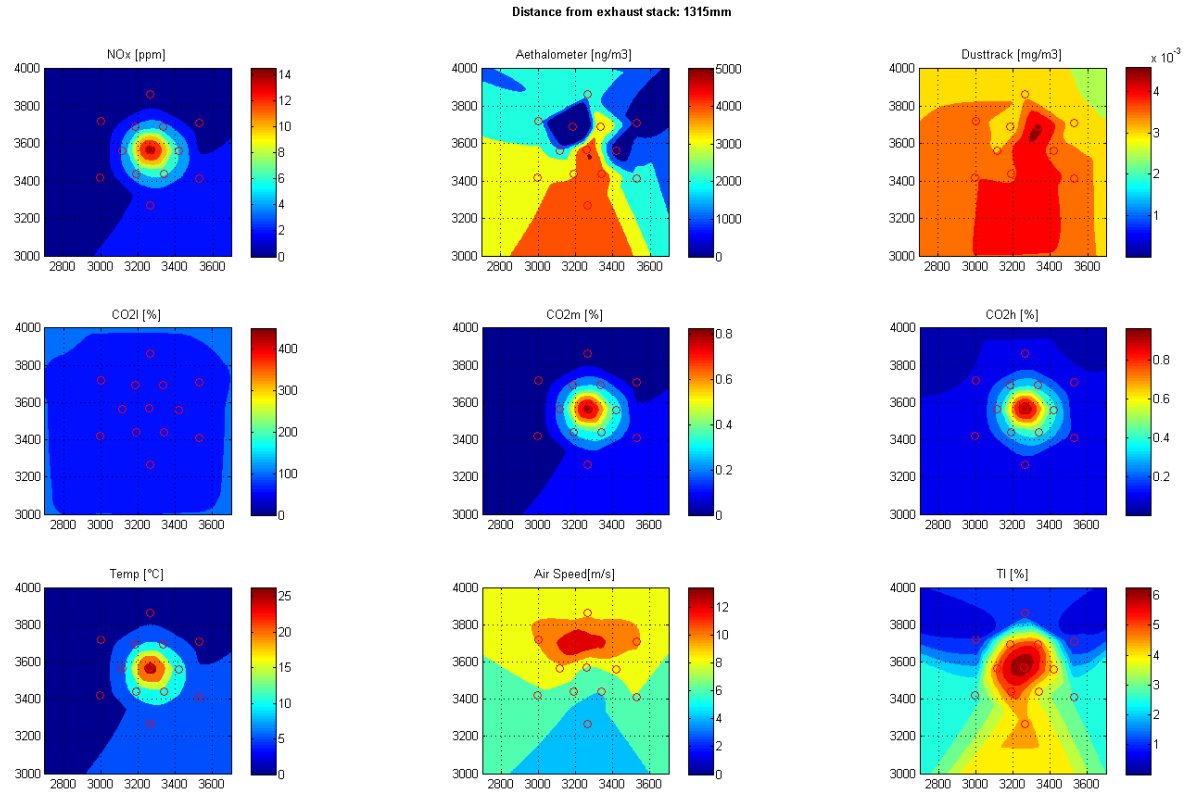

Figure 141: Post2010, 20mph Test, Plane 5

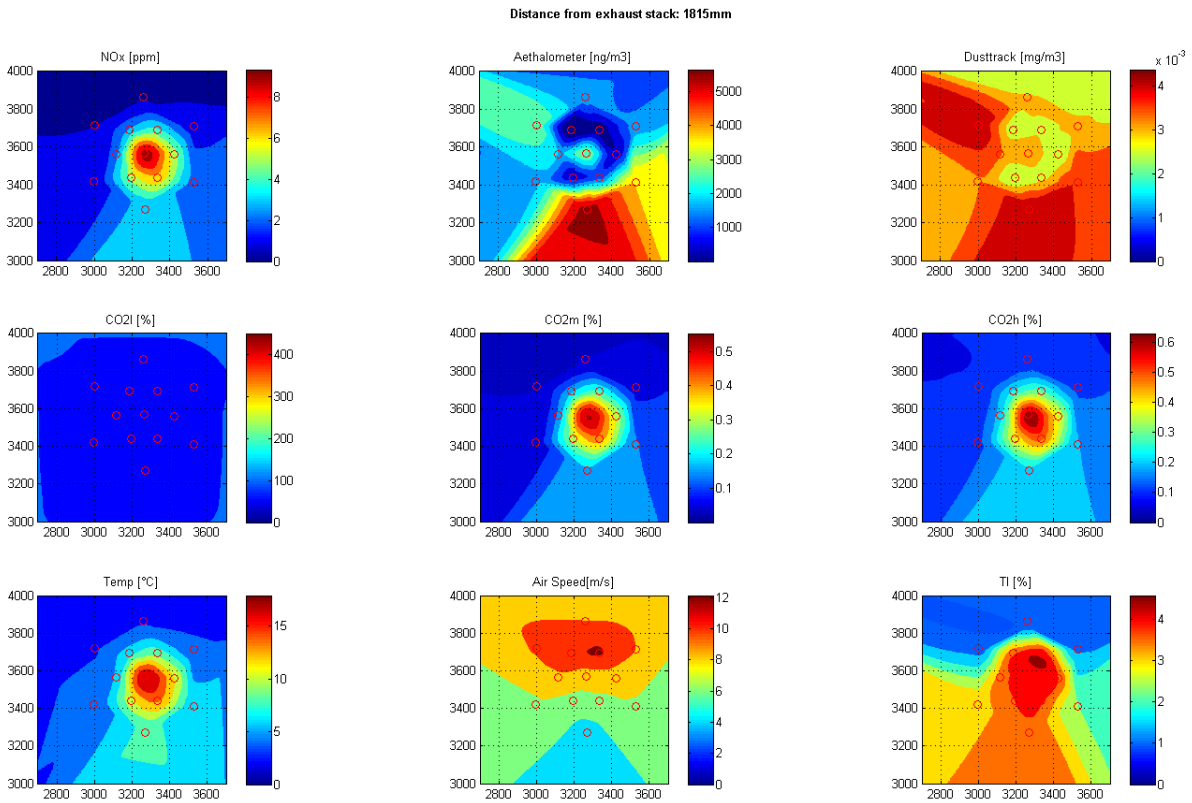

Figure 142: Post2010, 20mph Test, Plane 6

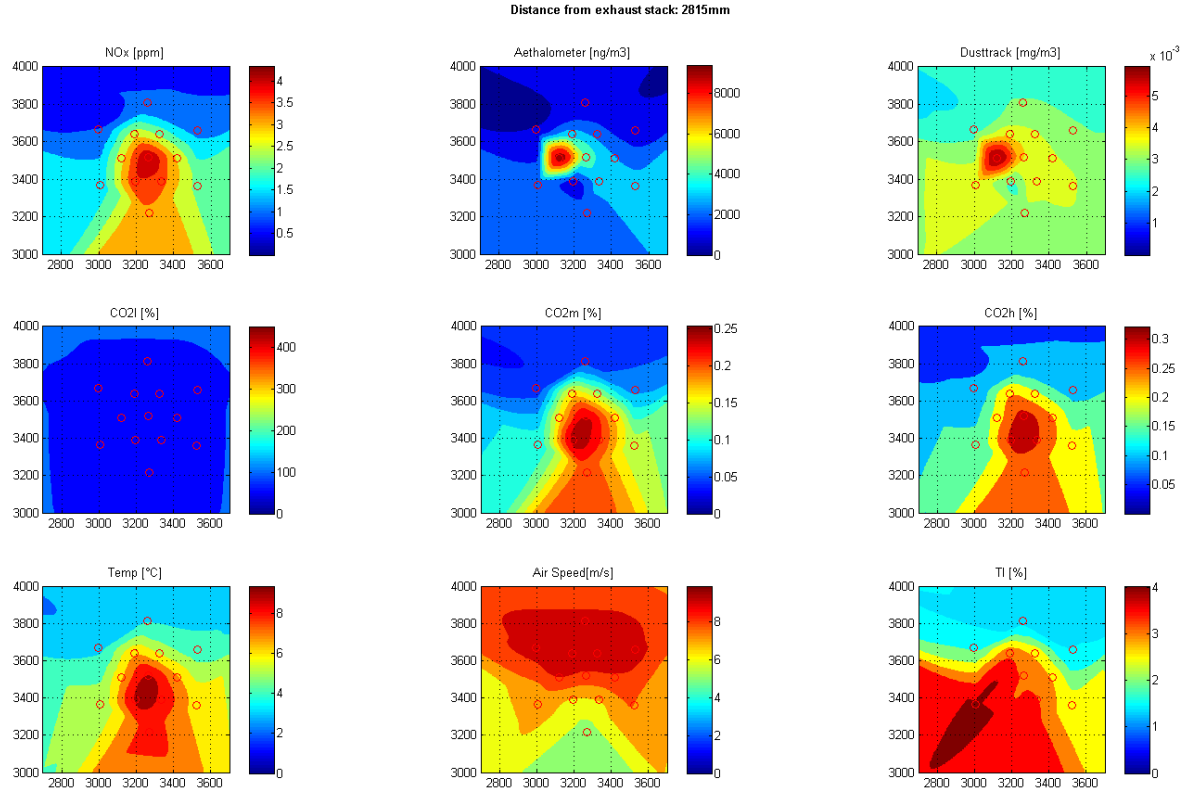

Figure 143: Post2010, 20mph Test, Plane 7

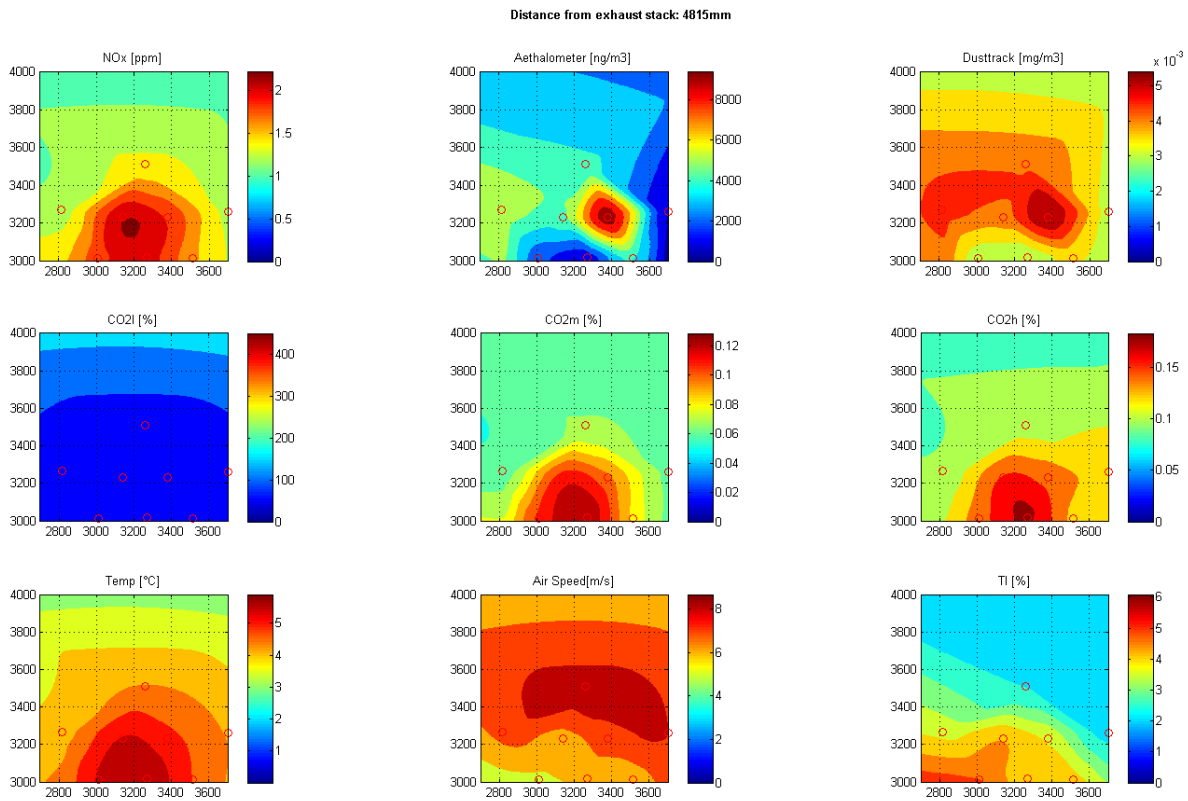

Figure 144: Post2010, 20mph Test, Plane 8

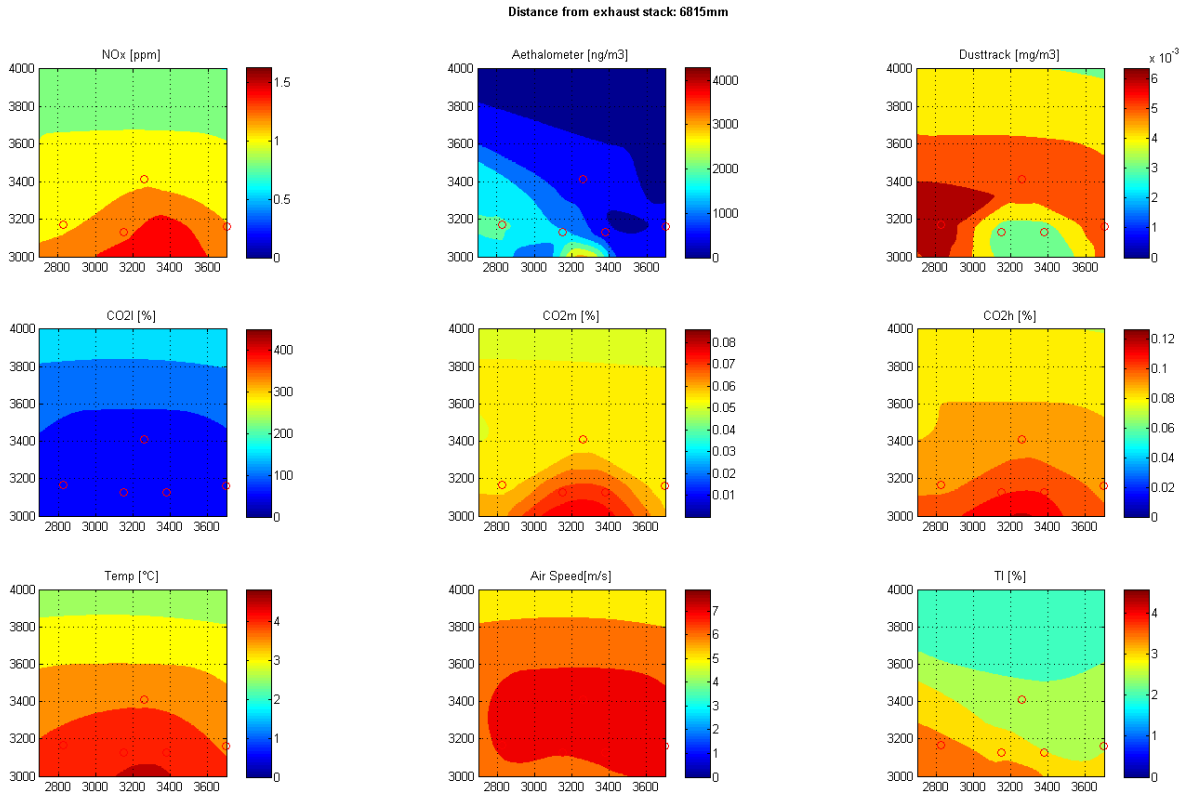

Figure 145: Post2010, 20mph Test, Plane 9

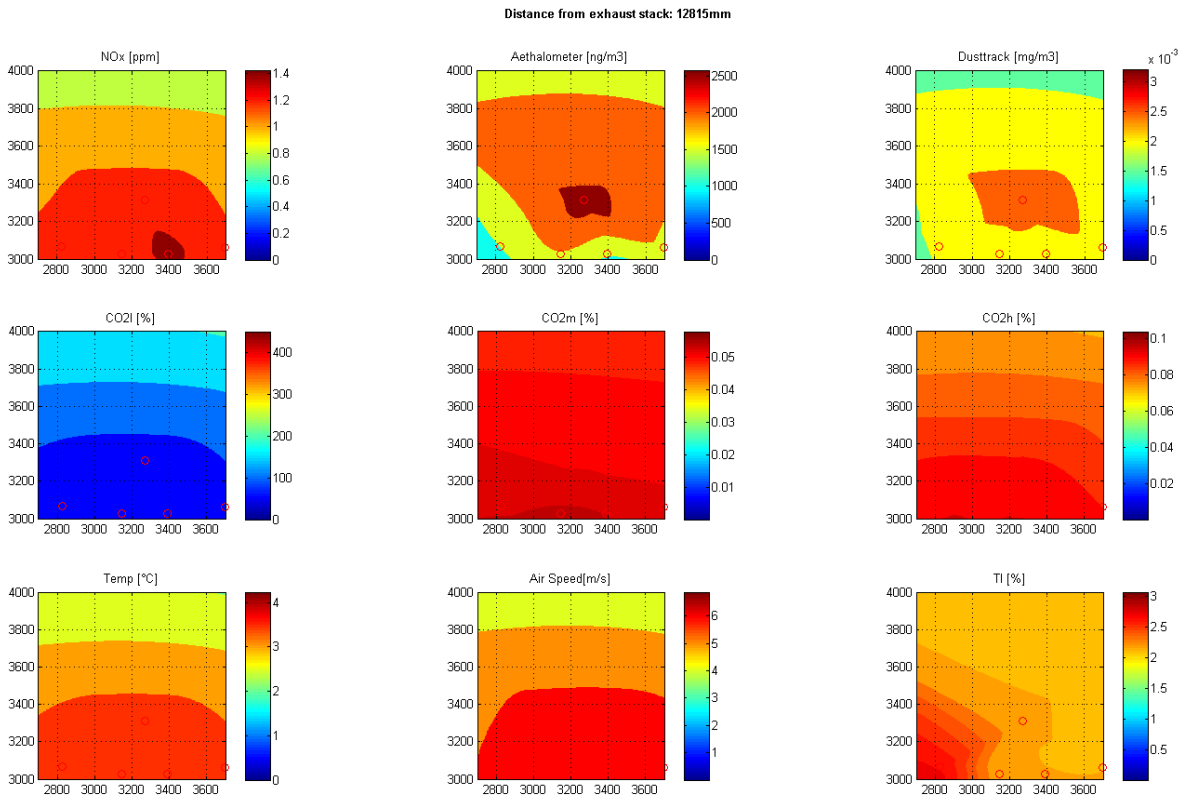

Figure 146: Post2010, 20mph Test, Plane 10

Post-2010, 35mph Test

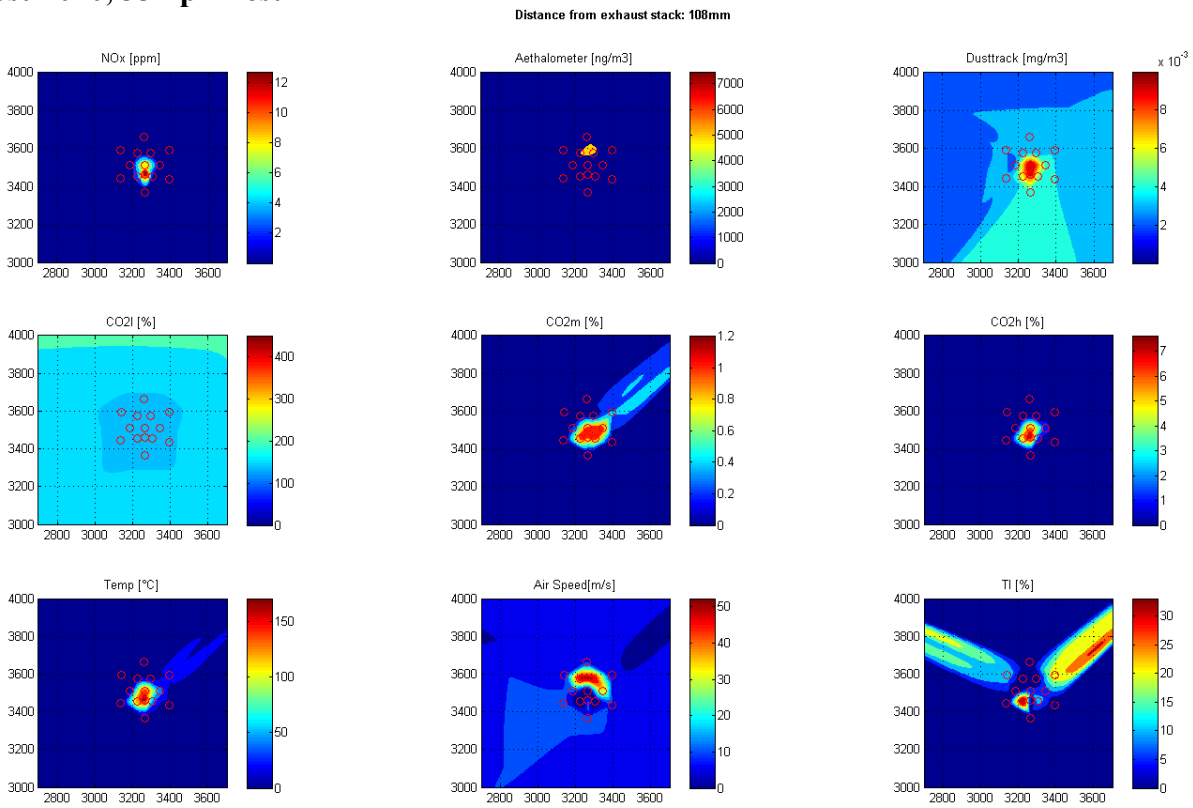

Figure 147: Post2010, 35mph Test, Plane 1

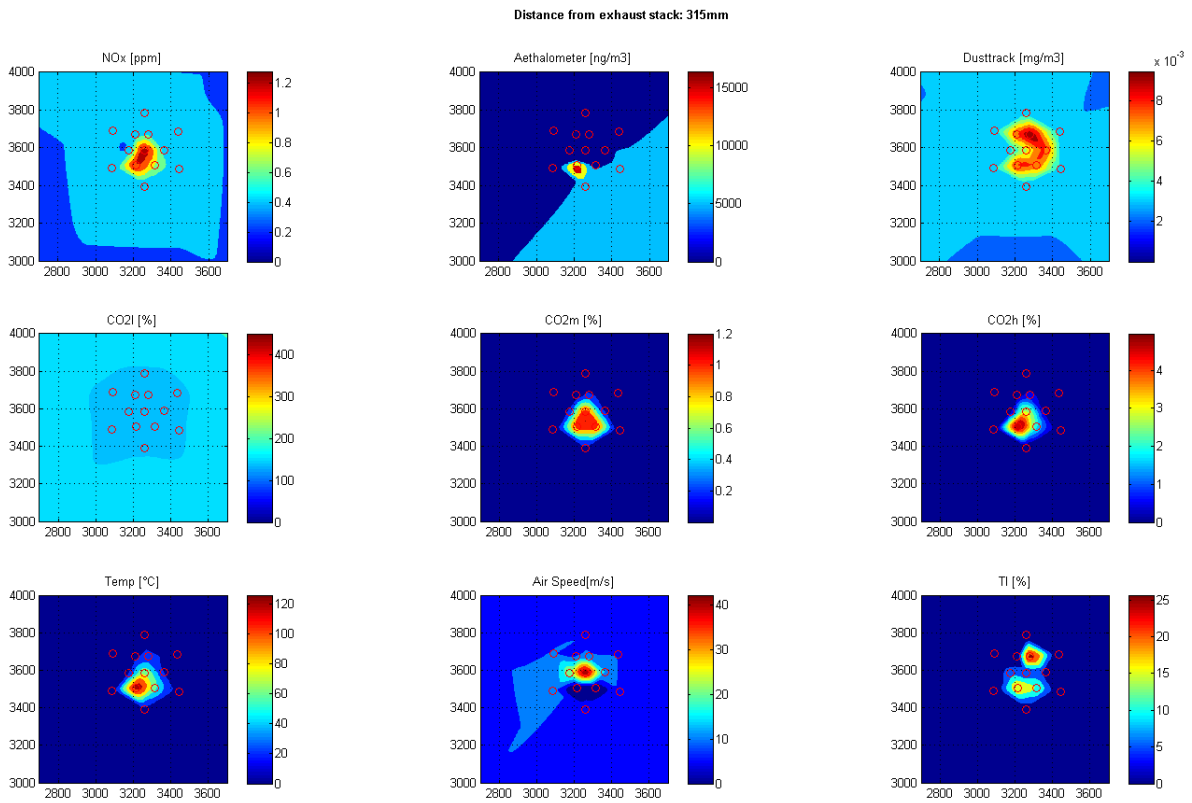

Figure 148: Post2010, 35mph Test, Plane 2

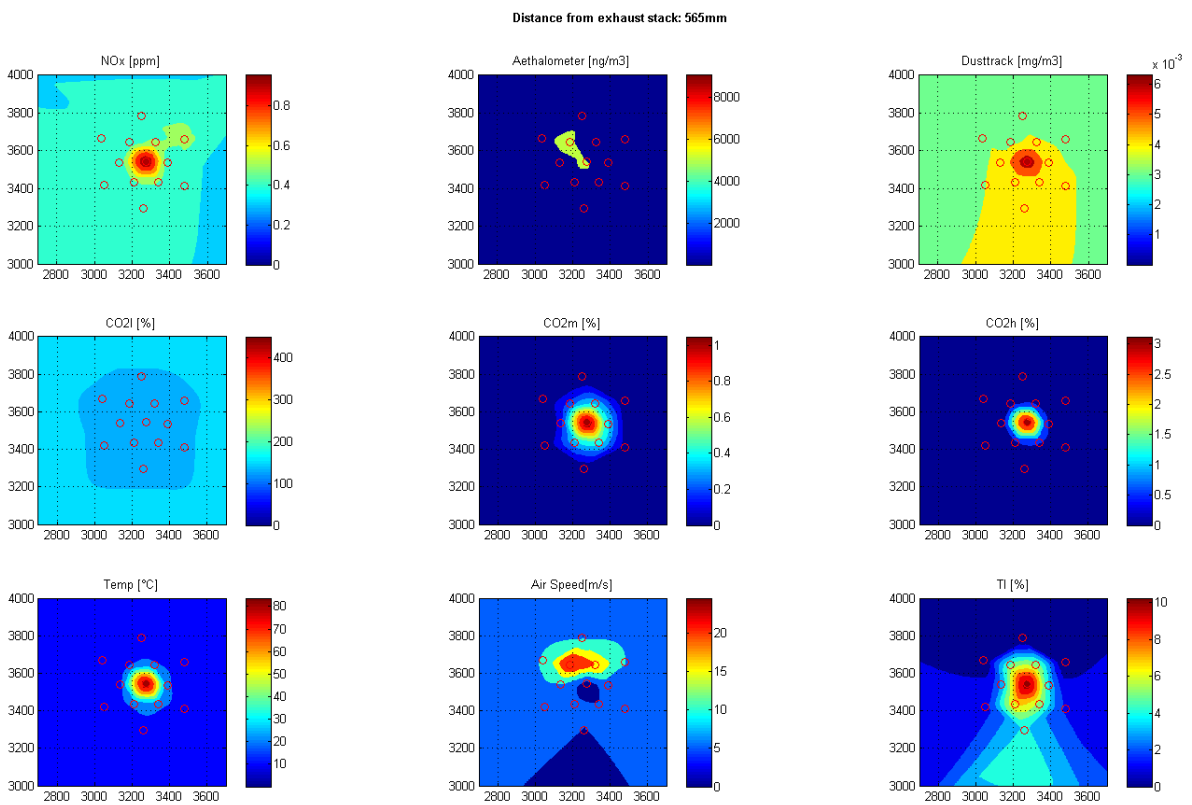

Figure 149: Post2010, 35mph Test, Plane 3

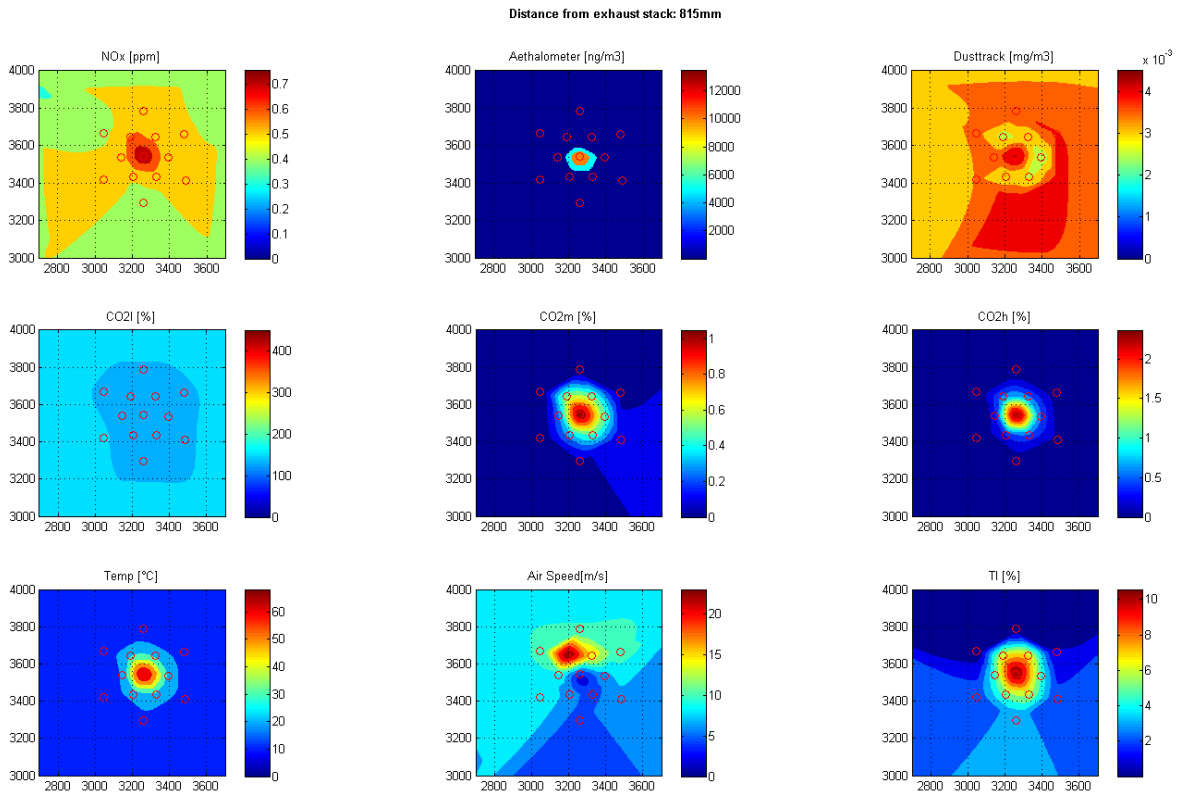

Figure 150: Post2010, 35mph Test, Plane 4

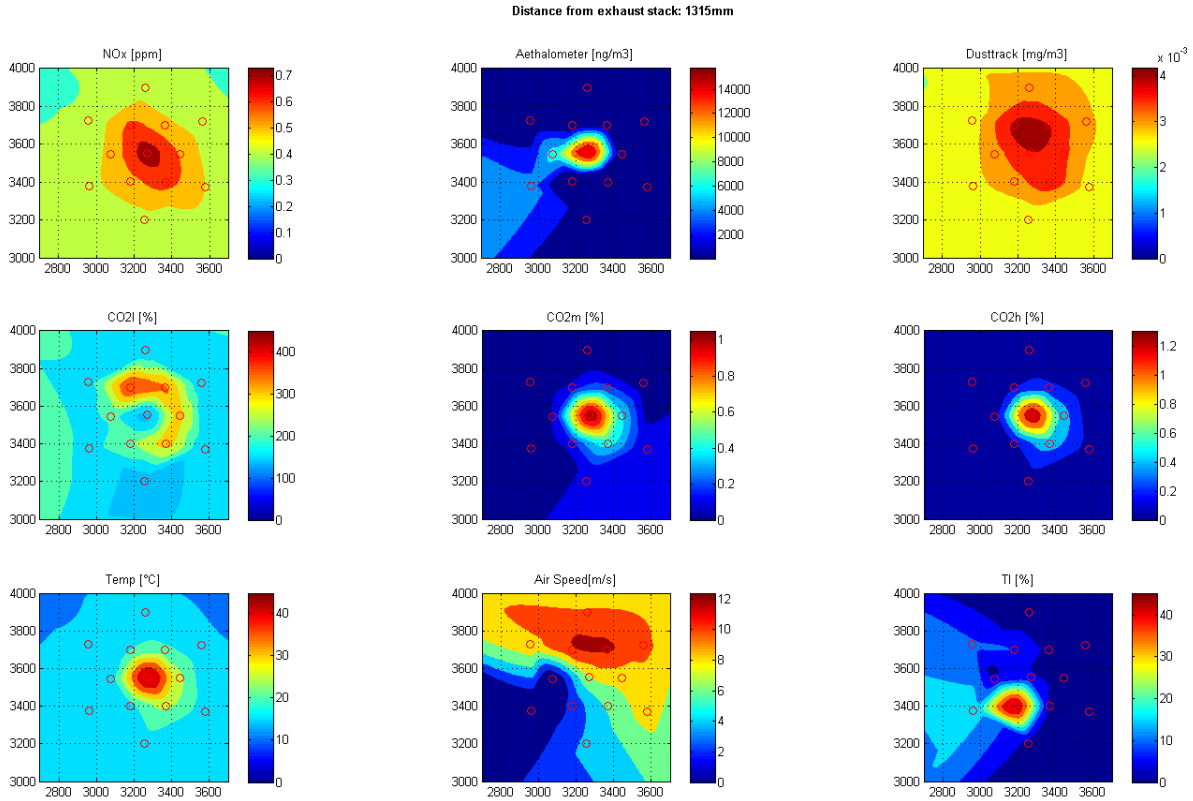

Figure 151: Post2010, 35mph Test, Plane 5

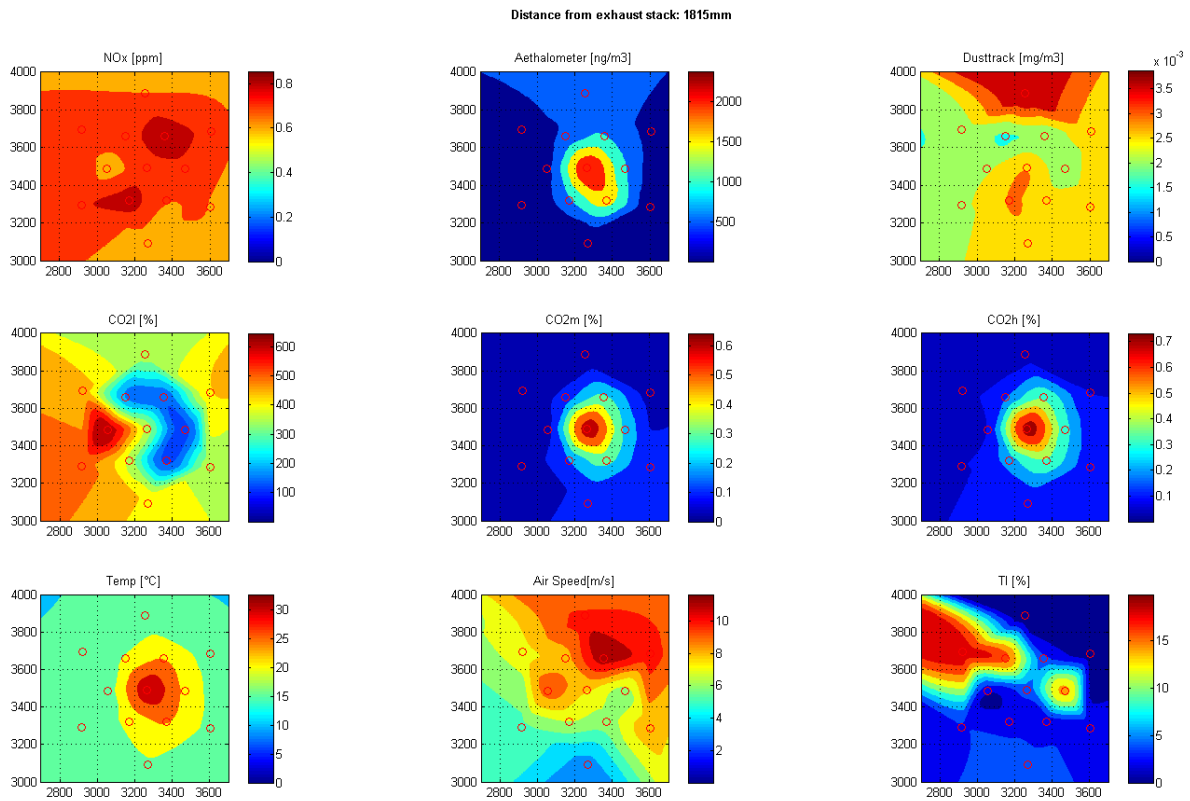

Figure 152: Post2010, 35mph Test, Plane 6

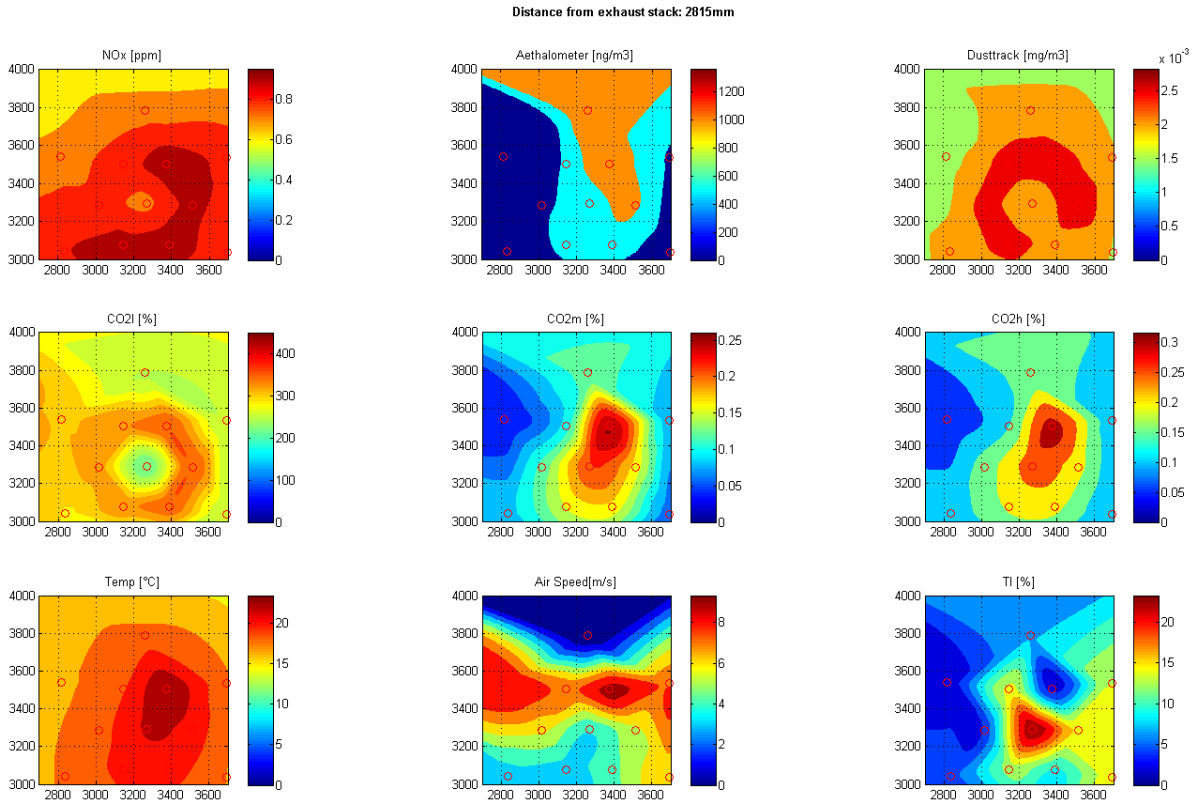

Figure 153: Post2010, 35mph Test, Plane 7

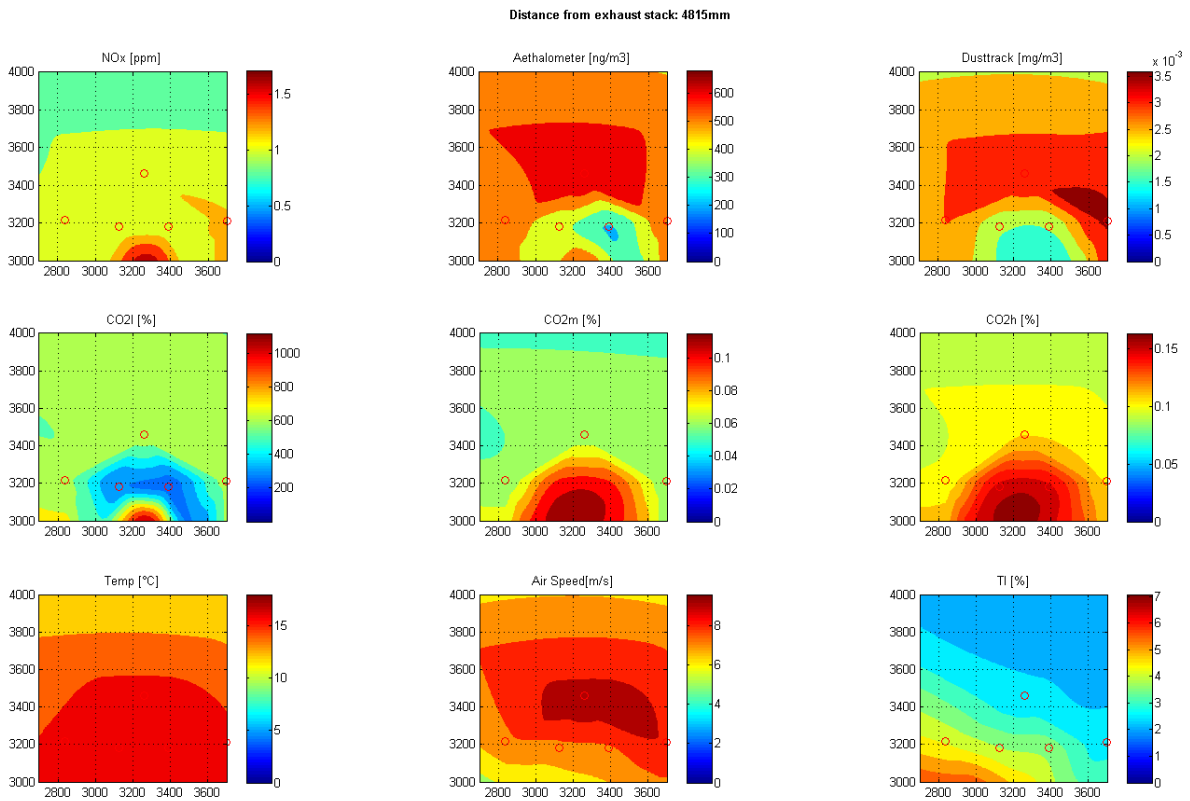

Figure 154: Post2010, 35mph Test, Plane 8

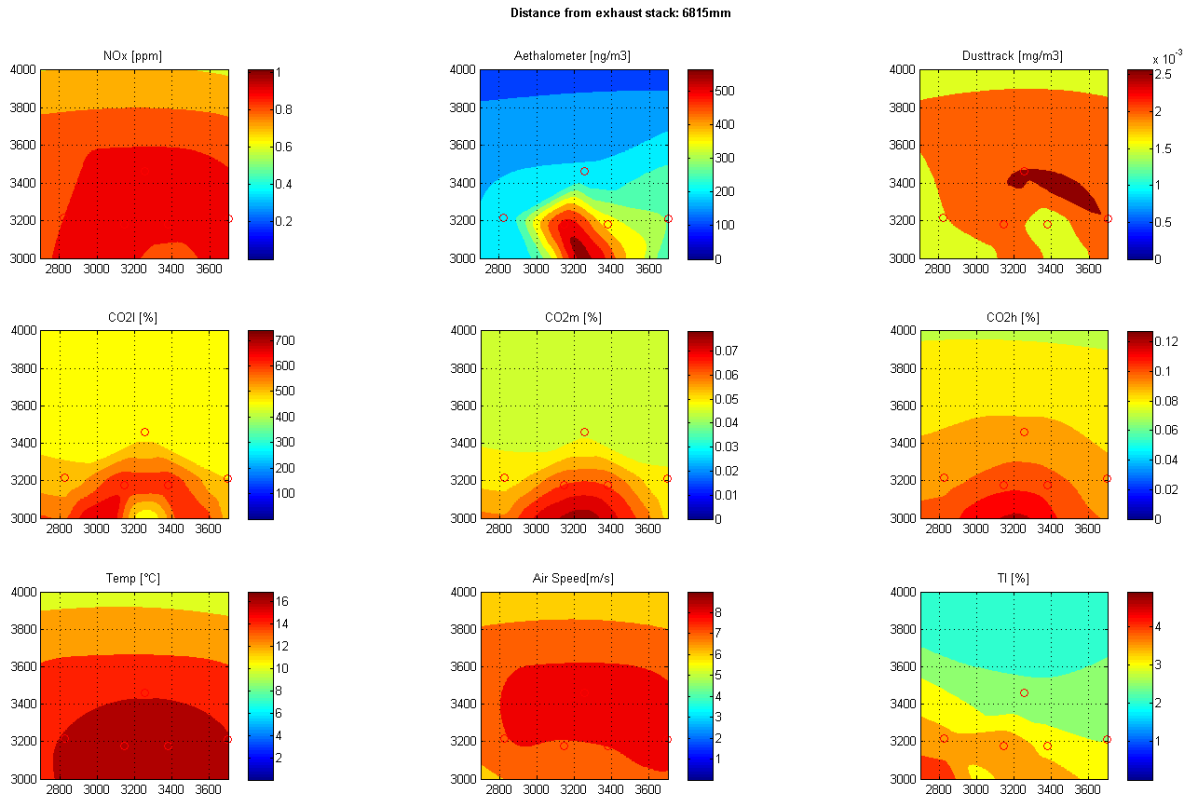

Figure 155: Post2010, 35mph Test, Plane 9

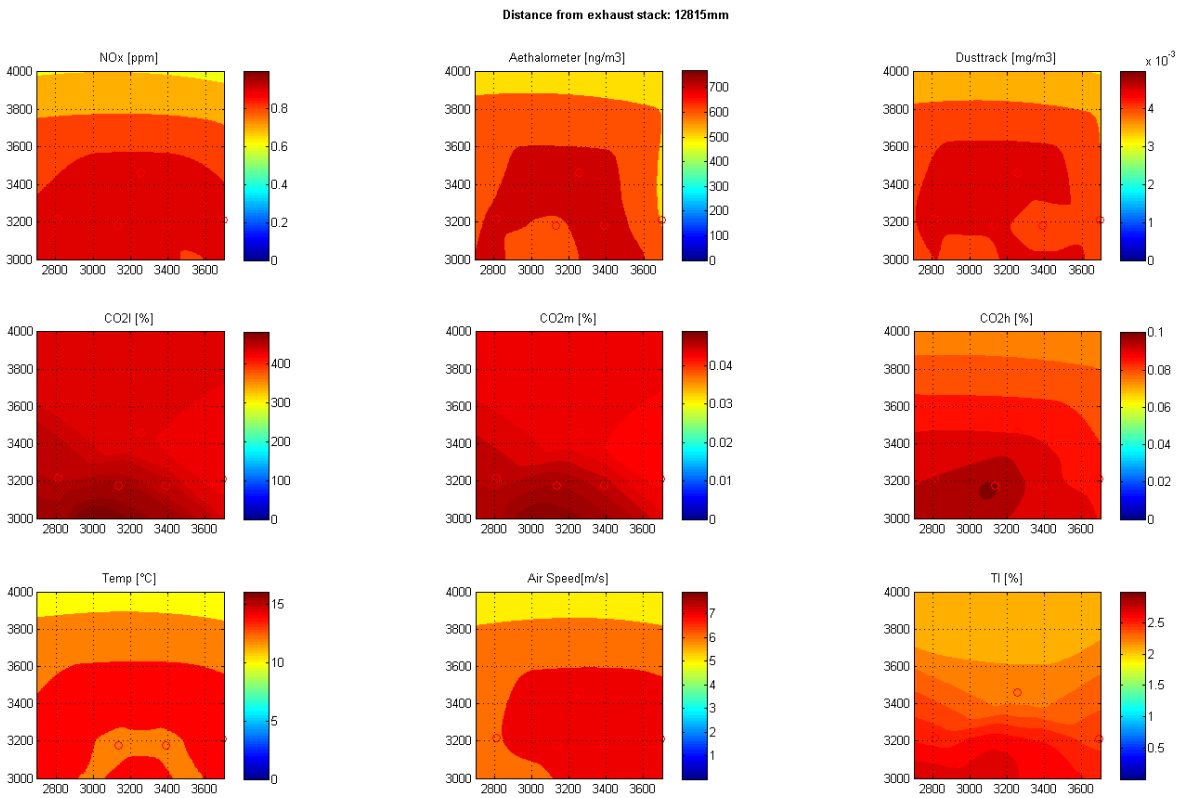

Figure 156: Post2010, 35mph Test, Plane 10

References

[1] M. Gautam, N. Clark, S. Mehta, J. Boyce, F. Rogers and A. Gertler, "Concentrations and Size Distributions of Particulate Matter Emissions from a Class-8 Heavy-duty Diesel Truck Tested in a Wind Tunnel," *SAE Transactions, Journal of Fuels and Lubricants,* pp. 1615-1634, 2004.

[2] E. Zervas and P. Dorlhene, "Comparison of Exhaust Particle Number Measured by," *Aerosol Science and Technology,* pp. 40:11, 977-984, 2012.

[3] J. Rae, H. William and A. Pope, Low-Speed Wind tunnel testing, 1984.